HYPERSPECTRAL IMAGING FOR ESTIMATING NITROGEN USE EFFICIENCY IN MAIZE HYBRIDS

by

Monica B. Olson

A Dissertation

Submitted to the Faculty of Purdue University

In Partial Fulfillment of the Requirements for the degree of

Doctor of Philosophy

Department of Agronomy

West Lafayette, Indiana

May 2021

THE PURDUE UNIVERSITY GRADUATE SCHOOL
STATEMENT OF COMMITTEE APPROVAL

Dr. Tony J. Vyn, Chair

Department of Agronomy

Dr. Melba M. Crawford

School of Civil Engineering and Department of Agronomy

Dr. Mitch R. Tuinstra

Department of Agronomy

Dr. John P. Davies

Department of Agronomy, Adjunct Graduate Faculty

Dr. Christopher Boomsma

Department of Agronomy, Adjunct Graduate Faculty

Approved by:

Dr. Ron Turco

Dedicated to my family.

Without your support and love I would be nowhere.

ACKNOWLEDGMENTS

First, I would like to thank Tony Vyn, my advisor. Thanks for being patient with my school/work situation as I progressed towards my graduate degree while working full-time. I am very appreciative for your time, willingness to teach, and serve as a mentor during my time at Purdue.

Thanks to all my committee members, Melba Crawford, John Davies, Mitch Tuinstra, and Chris Boomsma. Through each of you, I learned and improved many different skills, and am grateful for the time spent guiding me.

I would also like to thank the Cropping Systems lab, especially Alicia West, Sarah Mueller, Martha Winters, Heather Pasley, Lauren Schwarck, Lia Olmedo Pico and the countless others who provided their knowledge and assistance in data collection and sample processing. Without your help, I would not have been able to complete this research. Similarly, I would like to thank Ali Masjedi, Evan Flatt, Behrokh Nazeri, Claudia Aviles Toledo, Karroll Quijano Escalante, Taojun Wang, and many others who assisted in the different aspects of remote sensing – whether image collection, pre-processing, or processing of data. Thanks for answering my endless questions.

I would like to acknowledge Dow AgroSciences, LLC, now Corteva Agriscience, for its financial support of my graduate studies. Thanks to Nathalia Moretti, Bob Hall, and Chris Boomsma for initiating this research. Most importantly, I am indebted to *all* my Corteva colleagues and supervisors who mentored me and provided technical, statistical, intellectual, and motivational support and advice throughout my journey.

Lastly, I am forever grateful to Alyssa Batula, Python programming guru. I appreciate your patience and the valuable knowledge that you passed on to me. Your careful explanations through emails and countless one-on-one meetings really taught me to program. Thank you for taking time out of your day to help me. Who knew, after banging my head against the wall repeatedly, I would eventually be able to write my own code!

Every one of you has influenced and helped me through this adventure. I am deeply appreciative of your advice and friendship.

TABLE OF CONTENTS

LIST OF TABLES

LIST OF FIGURES

ABSTRACT

Increasing the capability of maize hybrids to use nitrogen (N) more efficiently is a common goal that contributes to reducing farmer costs and limiting negative environmental impacts. However, development of such hybrids is costly and arduous due to the repeated need for laborious field and laboratory measurements of whole-plant biomass and N uptake in large early-stage breeding programs. This research evaluated alternative in-season methodologies, including field-based physiological measurements and hyperspectral remote imagery, as surrogate or predictive measures of important end-of-season N efficiency parameters.

Differences in the genetic potential of 285 hybrids (derived from test crosses to a single tester) with respect to N Internal Efficiency (NIE, grain yield per unit of accumulated plant N) were investigated at two Indiana locations in 2015. The hybrids (representing both early and late maturity groups) were grown at one low N rate and a single plant density. Germplasm sources included USDA, Dow AgroSciences, and "control" checks. Various secondary traits (plant height, stalk diameter, LAI, green leaf counts, and SPAD measurements) were evaluated for their potential role as surrogate measurements for N metrics at maturity (R6) such as plant N content or NIE. Four band (RGB, NIR) multispectral airborne remote sensing imagery at R1 and R3/R4 was also collected. The key findings were: 1) identification of the 10 highest and 10 lowest ranked hybrids for each maturity group in both grain yield and NIE categories, 2) the discovery of 5 top performing hybrids which had both high NIE and high yield, 3) strong correlations of leaf SPAD (at R1 and R2/R3) to grain yield or plant N at R6, 4) none of the surrogate measurements were significantly correlated to NIE, and 5) vegetation indices (NDVI and SR) from the remote imaging were not predictive of hybrid differences in yields or whole plant N content at R6. From these results we concluded genetic potential exists among current maize germplasm for NIE breeding improvements, but that more in-depth investigations were needed into other surrogate measures of relevant N efficiency traits in hybrid comparisons.

Next, hyperspectral imaging was investigated as a potential predictor of agronomic parameters related to N Use Efficiency (NUE, understood here as grain yield relative to applied N fertilizer input). Hyperspectral vegetation indices (HSI) were used to extract the image features for

predicting N concentration (whole plant N at R6, %N), Nitrogen Conversion Efficiency (biomass per unit of plant N at R6, NCE), and NIE. Images were collected at V16/V18 and R1/R2 by manned aircraft and unmanned aerial vehicles (UAVs) at 50 cm spatial resolution. Nine maize hybrids, or a subset, were grown under N stress conditions with two plant densities over three site years in either 2014 or 2017. Forty HSI-based mixed models were analyzed for their predictability relative to the ground reference values of %N, NCE, and NIE. Two biomass and structural indices ($HBSI1_{682,855}$ and $HBSI2_{682,910}$ at R1) were predictive of NCE values and capably differentiated the highest and lowest ranked NCE hybrids. The highest prediction accuracy for NIE was achieved by two biochemical indices ($HBCI8_{515,550}$ at both V16 and R1, and $HBCI9_{490,550}$ at R1). These also allowed for hybrid differentiation of the highest and lowest ranked NIE hybrids. From these results, we concluded that accurate end-season prediction of hybrid differences in NCE and NIE was possible from mid-season hyperspectral imaging (yet not for %N). Furthermore, the quality of the predictions was dependent on image timing, actual HSI, and the targeted N parameter at maturity.

One benefit to hyperspectral imaging is that it can provide greater discrimination of imaged materials through its narrow, contiguous bands. However, the data are highly correlated in some ranges. This problem was mitigated through the use of partial least squares regressions (PLSR) to predict the three N parameters from the field data described previously. Data were divided into train and test; then ten-fold cross validation was performed. The twelve models evaluated included those with 89 image bands of 5 nm widths and a selected, reduced set of hyperspectral bands as predictors. The key findings were that PLSR models based on V16 and R1 images provided accurate predictions for final whole-plant %N ($R^2 = 0.73$, CV = 11%; $R^2 = 0.68$, CV = 10%) and NCE at R6 ($R^2 = 0.71$, CV = 10%; $R^2 = 0.73$, CV = 12%) but not NIE. Additionally, accurate hybrid differentiation was possible with the combination of hyperspectral imaging and PLSR at R1 to predict %N and NCE values at R6 stage.

The PLSR and HSI results from this research showed that hyperspectral imaging has the potential for prediction of NUE parameters through non-destructive remote sensing at a broad scale. Additional validation is needed through the study of other genotypes and locations. Nevertheless, practical application of these methods through the integration into early stage breeding programs

may allow the early identification of the highest and lowest ranked hybrids providing data-driven decisions for selecting genotypes. Implementation of improved imaging approaches may drive the increased development of maize hybrids with superior NUE.

CHAPTER 1. DETECTION OF NITROGEN USE EFFICIENCY IN MAIZE HYBRIDS THROUGH TRADITIONAL AND NON-TRADITIONAL PHENOTYPING METHODOLOGIES

1.1 Introduction

Nitrogen (N) is an essential nutrient for plants and is commonly used in fertilizer in order to support agricultural production (Ribaudo et al., 2011). World consumption of N has increased since the 1960s ("IFA Statistics," 2016). In the United States, 97% of all acres planted in maize, the single most common crop in the United States, receive N as manure or chemical fertilizer (Ribaudo et al., 2012). Unfortunately, the amount of N available to maize plants is often much less than the amount of fertilizer applied since mineral N availability is affected by a multitude of factors such as precipitation, temperature, microbial effects, soil type, rate of application, placement, timing, fertilizer source, etc. (Ribaudo et al., 2011). Though higher than other crops, the percentage of applied N fertilizer recovered by maize plants in the United States was calculated to be only 37% (Cassman et al., 2002). More recently, Ciampitti and Vyn (2012) found a 44% N recovery efficiency (NRE, percent of N fertilizer in aboveground plant biomass) for maize hybrids commercialized after 1990 and Mueller et al. (2019) found NRE values greater than 50% for hybrids from 2003 and 2015. Though NRE values have improved these excessive losses are an economic as well as environmental cost negatively affecting air and water quality as well as human health (Doering et al., 2011; Ribaudo et al., 2011). Thus, a large opportunity exists to decrease N use and loss by increasing maize's efficiency in using this important nutrient.

In the 1960s, in order to increase the utilization of resources, scientists introduced the concept of breeding for high resource efficiency (i.e. increasing the percent of resource used per unit of dry matter) (Donald, 1968). Plant breeding efforts have focused on yield; however, research has shown that a plant's ability to use N has been improved indirectly (Ciampitti & Vyn, 2012; Moose et al., 2009). Nevertheless, more research into increasing crop N efficiency is encouraged by experts (Doering et al., 2011). Such physiological research requires extensive phenotyping work to investigate the plant N levels and develop a greater understanding of plant N use and NUE parameters. Unfortunately, the current accepted methods for determination of plant N content such as Dumas combustion consists of destructive tissue sampling which requires considerable

levels of time and effort in both the field and laboratory (Muñoz-Huerta et al., 2013; Unkovich et al., 2008; Zhao et al., 2003).

During the last 20 years there have been extensive advancements in the field of genotyping; however, the current bottleneck to breeding and genetic advancement is in the field of phenotyping (Araus & Cairns, 2014; Cobb et al., 2013; Jin et al., 2020). The use of field spectrometers such as the Minolta SPAD-502 chlorophyll meter have been an attempt to improve phenotyping methods and decrease labor associated with leaf N content estimation. However, though positively correlated to leaf N and chlorophyll levels in maize and other plants (Bullock & Anderson, 1998; Schepers et al., 1992; Yoder & Pettigrew-Crosby, 1995), the SPAD chlorophyll meter still requires hands-on sampling of each plant and thus is only a slight improvement over traditional phenotyping methods.

Delineated below is a brief review of the current literature of hyperspectral-based remote sensing of N in maize and studies into the prediction of relevant physiological traits such as grain yield, biomass, N uptake, chlorophyll, and the N nutrition index. Objectives, with detailed hypotheses, and methodology then follow.

1.2 Hyperspectral Remote Sensing

Remote sensing is the process of observing, collecting, and analyzing data without direct contact with the object or phenomenon in order to garner information about said object or phenomenon (Lillesand et al., 2014). Red, green, blue (RGB) cameras are traditional instruments of remote sensing data collection; other technologies include hyperspectral, radar, and thermal sensors (Lillesand et al., 2014). Cameras or sensors are placed on platforms which are space borne (on satellites), airborne (on planes or unmanned aerial vehicles such as drones), or fixed at ground level (Lillesand et al., 2014). A major benefit to remote sensing is its non-destructive aspect. Also, in the long term it is expected that once methods are standardized, remote sensing can also decrease labor costs inherent to today's hands-on phenotyping methods (Araus & Cairns, 2014; Cobb et al., 2013; Rodrigues Junior et al., 2014; White et al., 2012).

Hyperspectral instruments collect data with a continuous and extremely wide spectral range (usually 300nm to 2500nm) and narrow bandwidths resulting in datasets with hundreds of bands

(widths range from 1nm per band to broader bandwidths, such as 40 or 70nm). The benefit to hyperspectral data is greater differentiation between materials with absorbance or reflectance characteristics in very narrow wavelength intervals (Lillesand et al., 2014). However the enhanced spectral and spatial resolution results in multicollinearity in the data because spatially neighboring pixels and neighboring spectra are likely characterizing similar materials (Bioucas-Dias et al., 2013). This multicollinearity presents an issue when using narrow-band vegetation indices for analysis and prediction of physiologically relevant data such as yield and plant N levels (Quemada et al., 2014). It also presents an issue known as the Hughes phenomenon or the 'curse of dimensionality' (Thenkabail et al., 2014). Due to the multicollinearity inherent in hyperspectral data, as the number of bands used in a model increases the number of pixels needed to train the model grows exponentially in order to maintain statistical confidence in the model (Thenkabail et al., 2014). As discussed by Bajwa and Kulkamini in Thenkabail et al. (2012) this phenomenon can only be overcome by decreasing data redundancy (i.e. incorporating some type of dimensionality reduction process such as principle component analysis to obtain the true lower dimensional data space) and increasing the number of training pixels. Due to the difficulty and expense in acquiring more training data which often means additional hands-on phenotyping field work, increasing the number of training pixels can be a very difficult option thus dimensionality reduction is critical and often the only solution for hyperspectral data analysis (Thenkabail et al., 2012). In addition to complicating data analysis the substantial amount of data in hyperspectral images necessitates large amounts of computing power for analysis (Bioucas-Dias et al., 2013).

1.3 Remote Sensing Of Plants: Leaf and Canopy Level

When light hits a leaf, the light is absorbed, transmitted, or reflected (Campbell & Wynne, 2011). The biochemical characteristics of the leaf such as the internal pigments, water content, and internal cellular structures affect the light response (Campbell & Wynne, 2011; Thenkabail et al., 2012). Studies have shown that leaf components such as cell walls and nuclei reflect light differently depending on the wavelength of the light (Gausman, 1977). Also, the chemical bond vibrations of the leaf constituents, such as the N-H or C-H bonds of proteins, are known to produce observable absorption features at specific wavebands (Curran, 1989). According to Campbell and Wynne (2011), changes in leaf reflectance can indicate changes in plant vigor, plant maturation or plant stress. However, though spectral changes occur and are observed in plants under stress,

different nutritional stresses do not produce unique fingerprint-like spectral responses for identifying the specific nutritional deficiency (Masoni et al., 1996). Just as the biochemistry of the leaf can be sensed, so, too, can the physical characteristics of the leaf, such as the leaf thickness and cuticle, affect the light response and thus the absorption and reflectance observed through remote sensing (Gausman & Allen, 1973).

Complicating matters is that aerial or satellite remote sensing consists of measuring canopy reflectance and not just leaf reflectance. At the canopy level, the remote sensing image represents the photon scattering from the leaves, but also stems and soil (Campbell & Wynne, 2011; Hatfield et al., 2008). Additionally, the horizontal and vertical distribution of the canopy, foliage orientation, and foliage density all impact canopy structure and thus measured reflectance (Hatfield et al., 2008). Furthermore, the wavelengths and bandwidths used for sensing, solar illumination and shadowing, sensor characteristics, and sensor geometry all impact the remote sensing imagery (Campbell & Wynne, 2011; Hatfield et al., 2008).

1.4 Remote Sensing of Plants: Impact of Spatial Resolution

The impact of spatial resolution has been examined by researchers, but often the interest is on the impact on classification results as opposed to evaluating the effect on the vegetation index (VI) itself. Additionally, in these studies the classification methods and image processing methods have varied greatly and thus are difficult to compare. Huanxue et al. (2014) found that crop acreage accuracy estimations decreased as resolution decreased when imaging maize at 20m to 160m due to a higher proportion of mixed pixels at the low resolution; thus, crop proportion had a large impact on the effects of spatial resolution. For imaging and mapping of rangelands, Thorp et al. (2013) realized that fine spectral resolution was more important than the image spatial resolution when considering resolution from 15m to 150m. However, the mapping was based on multiple endmember spectral mixture analysis (MESMA) and thus they were assessing the sensitivity of this technique to the resolution differences. Analysis of images with higher resolution (0.025m to 2.5m) across widely varied agricultural vegetation (containing sugarcane, eucalyptus, citrus, etc.) by Liu et al. (2020) showed that the highest classification accuracy occurred at intermediate spatial resolution (0.05-0.25m). Their research included VI as some of the features extracted from the images to use for classification, but also included spectral, shape and texture features which were

then inputted into two supervised classification methods (random forest and support vector machines) assessed for accuracy. The analysis indicated a higher importance of spectral and VI information for classification at all spatial resolutions, yet this study did not assess the direct impact of resolution on VI themselves.

In a study more focused on VI by Zhou et al. (2018) studying the effects of N on rice the authors discovered that as spatial resolution decreased (from 0.13cm to 45cm) the correlations between VI and leaf N concentration also decreased. Furthermore, VI were more stable at the finer resolutions (<1.4cm) at early growth stages (early tillering) but equally stable at later developmental stages for coarser resolutions (<5.6cm). With a continued focus on the direct impact of spatial resolution on VI, Jiang et al. (2005) conducted a mathematical analysis on the impact on NDVI from their interest in spatial resolution from satellite imaging. Their theoretical discussion concluded that the NDVI based on coarse or low resolution would be greater than the NDVI based on fine or high resolution as soil had lower levels of red reflectance and as the proportion of vegetation approached 20-50% and thus became more heterogenous.

Consensus exists that spatial resolution decisions should also be driven by the species' physiological characteristics, crop proportion or distribution and ecosystem being imaged plus the main focus of the research-whether it be classification of large vegetative areas or predicting biochemical concentrations at leaf level (Huanxue et al., 2014; Liu et al., 2020; Zhou et al., 2018).

1.5 Physical and Biochemical Response of Maize to Nitrogen Stress

N stress has both biochemical and physical effects on maize plant growth. Pigment concentrations in the maize leaves (such as those of chlorophyll a, chlorophyll b, and carotenoids) decrease as plants experience N stress (Zhao et al., 2003) while those of other pigments (e.g. anthocyanins) increase under N stress (Lawanson et al., 1972). Though maize plants accumulate higher N content levels in the leaves above the ear leaf (DeBruin et al., 2013) photosynthesis rates in the top leaf of a maize plant decrease under N stress (Zhao et al., 2003). Overall canopy photosynthesis rates per unit leaf area decrease for both N sufficient and N stressed plants with lower positions in the canopy (Zhao et al., 2003) likely due to the N dilution effect that occurs as maize plants increase mass quickly (Greenwood et al., 1986; Lemaire & Gastal, 1997). However, rates of canopy photosynthesis per leaf area for the low N plants decrease more quickly (Zhao et al., 2003).

Canopy photosynthesis per unit ground area rates increase over time at both high and low N treatments as the maize canopy develops covering more of the ground surface area (Zhao et al., 2003). However, the N stressed plants have a much lower (nearly flat) rate of increase in the canopy photosynthesis per ground area rate (Zhao et al., 2003).

The physical responses of maize plants to N stress are just as pronounced as the biochemical responses described above. Both leaf area per plant and plant height decrease with N stress (Zhao et al., 2003). Additionally, lower leaves senesce more quickly and the plants produce lower amounts of total root mass, even though at low N levels plants have a higher root: shoot ratio (Banziger et al., 2000; Gastal et al., 2015). N stress impacts maize reproduction development, though the timing of the N stress influences its final impact on the plant's reproductive success (Sadras & Calderini, 2015). Both number of kernel rows and number of pollinated kernels per row can be negatively impacted by N stress (Andrade et al., 1999; Uhart & Andrade, 1995a). N stress also decreases kernel weights (Ciampitti et al., 2013; Uhart & Andrade, 1995b). Delays in pollen shed and silk emergence, and particularly a lengthening of the anthesis-silking interval with low N, also negatively affect grain yields (Banziger et al., 2000). The number of successfully established kernels can be reduced further thru increased kernel abortion in early grain fill (Banziger et al., 2000).

1.6 Reflectance Characteristics of Maize under Nitrogen Stress

Many of the physical and biochemical changes that plants experience due to N stress described above are perceived by the remote imaging which measures the integrated N stress response. As early as 1974, Al-Abbas, Barr, Hall, Crane and Baumgardner (1974) found differences in the spectra of normal and N-deficient leaves when examining individual leaves with a spectro-reflectometer. Under N stress both field grown and chamber grown plants have higher reflectance values in the green and red portions of the spectrum and lower reflectance in the NIR portion than those provided with sufficient N (Walburg et al., 1982; Zhao et al., 2003). These changes in reflectance under differing N conditions were also evident for other maize hybrids with repeated imaging and multiple growing seasons (Walburg et al., 1982). Conceptually, as N stress increases the spectral response flattens out in the VNIR. Clay et al. (2006) witnessed similar results in their multispectral N fertilization field experiment with a consistent response across the three

developmental growth stages examined (V8-V9, V11-VT, and R1-R2). Analogous results were found with hyperspectral imaging of maize at R3 which showed an increase in reflectance and broadening of the spectral signature in the green region (525-625nm) under N stress (Campbell et al., 2007). Additionally, a left-ward shift in the reflectance curve in the red/far-red region (690-740nm) occurred under N stress conditions (Campbell et al., 2007). This difference was clearly detectable using the 1st derivative of the reflectance and is often described as the red-edge (Campbell et al., 2007).

1.7 Hyperspectral Data Analysis

Research on remote sensing and spectral absorbance or reflectance of leaves or canopies is ongoing especially for determining correlations between remote sensing spectral measures and in-field measured physiological attributes (Campbell & Wynne, 2011). Multiple methods exist to deal with the multi-collinearity issues inherent to hyperspectral data previously described and yet not lose valuable pieces of information. Solutions include vegetation indices, linear and non-linear regression, principal component analysis, various machine learning methods, crop models, or combinations of these.

1.7.1 Vegetation Indices

Vegetation Indices (VI) are ratios or functions of reflectance values across various spectral bands developed to emphasize chemistry-based characteristics and often used to predict specific physiological measures (Campbell & Wynne, 2011) or to assess canopy attributes such as Leaf Area Index (LAI) or biomass (Mulla, 2013). By selecting specific hyperspectral bands to use, the multi-collinearity issue within hyperspectral data is avoided. Hundreds of vegetation indices exist, consisting of both broad and narrow bands, to predict phenotypic factors. However, the utility of these VIs is dependent on crop, leaf density (LAI), and other agricultural conditions (Campbell & Wynne, 2011). Sims and Gamon (2002), in their analysis of 53 species, showed that due to differences in leaf surface reflectance properties most VIs did not predict chlorophyll levels across crop types; the most broadly predictive VIs in their analysis were mSR705 and mND705. Another drawback to VIs is that they use only a few bands and thus a lot of information from the hyperspectral imaging can be lost (Mulla, 2013). Another known limitation of VIs is their

propensity to become saturated at higher leaf densities (i.e. LAI values greater than 2 or 3) (Carlson & Ripley, 1997; Thenkabail, Smith & De Pauw, 2000). An example is the Normalized Difference Vegetation Index (NDVI = (NIR-red)/(NIR +red)) which will level off (i.e. saturate) at complete canopy cover in the middle of the growing phase, while plants are still continuing to add biomass (Carlson & Ripley, 1997; Thenkabail et al., 2000). Campbell and Wynne (2011) describe the quantitative and qualitative use of VIs. However, many authors caution readers concerning quantitative use of VIs due to the indices' ability to be influenced by factors external to those experienced by the plants such as viewing angles, plant spacing, row direction, atmospheric effects, and soils (Campbell & Wynne, 2011; Haboudane et al., 2008).

The bands used in vegetation indices are usually selected or specific to the physical or biochemical characteristics that the VI is attempting to measure and predict and this knowledge-based selection limits the VI to specific wavelengths or regions. For example, Thenkabail et al. (2000) evaluated maize, cotton, potatoes, sunflower, and soybeans at multiple agronomic stages over multiple soil types and nearly 200 locations with a spectroradiometer. From their research, Thenkabail et al. (2000) determined the optimal bands for general agricultural information, i.e. those bands containing the most information for predicting biomass or leaf area index as the following: Blue at 495nm; Green at 525, 550, and 568nm; Red at 668, 682, and 696nm; Red-edge at 720nm; and NIR at 920, 982 (for moisture) and 1025nm. However, another useful method is to select wavebands based on the coefficient of determination to a specific physiological variable and simply calculate reflectance ratios relative to all other wavebands (Zhao et al., 2003). Still other researchers calculate normalized indices or ratios for every band using the actual reflectance or 1st derivative values developing contour maps of the coefficient of determination (r2) between the target physiological measure, e.g. chlorophyll, and the vegetation index (Inoue et al., 2016). Then point(s) on the map with the highest r2 value are selected as the most predictive combination of wavelengths (Inoue et al., 2016).

1.7.2 New Vegetation Indices

A fourth method based on VIs is to develop a completely new index based on knowledge of biochemical parameters and the data set in hand (Chen et al., 2010). Researchers then use virtual modeling, and validation of the new index with a test data set (Chen et al., 2010). Such vegetative

indices are based on wavebands identified to be most important in those specific data and must be evaluated with a multitude of data sets by other researchers to determine if broadly applicable.

1.7.3 Bandwidths of Vegetation Indices

Another way to vary vegetation or spectral indices is to vary the bandwidths used. With hyperspectral data bandwidths can be modulated by pooling and the effects studied. Thenkabail et al. (2000) evaluated the optimal bandwidths and determined that the most predictive VI had narrow or very narrow bands from 1-30nm concluding that narrowband VIs had higher predictive accuracy for characterizing agricultural characteristics. Recommended bandwidths depended on the band center with widths of 30nm for blue bands as opposed to 10 and 20nm widths in the green portion of the spectrum. Interestingly, the suggested widths for red bands were only 4nm wide, red-edge widths were 10nm while in the NIR portion widths were much greater (70nm) (Thenkabail et al., 2000). Many studies have shown the utility and value of narrow-band indices (Thenkabail et al., 2012) such as by finding stronger correlations to chlorophyll plant pigments and carbon and N levels than broadband indices (Campbell et al. (2007).

1.7.4 Transformations and Regression Models

Using regression models combinations of spectral indices have been evaluated for their ability to predict N status (Li et al., 2014). Also, combinations of wavebands themselves have been evaluated to predict various physiological attributes (Osborne et al., 2002b). It is useful to note that comparisons for index sensitivity across varying scales can be done using the Noise Equivalent method (Li et al., 2014; Viña et al., 2011). Another method to reduce the dimensionality of the hyperspectral data is to apply principal component analysis projecting the bands onto lower dimensional space while maximizing the variance within the data (Bioucas-Dias et al., 2013). Artificial neural networks and support vector machines are machine learning approaches which can also be used for complex data sets (Karimi et al., 2008). Combinations of these methods have also been used for hyperspectral data analysis (Thenkabail et al., 2012).

1.7.5 Crop Models

Finally, remote sensing has been used to predict certain variables for inputting into a crop model rather than inputting the actual measurements (Baret et al., 2007; Pinter et al., 2003). Since crop models are based on physical and physiological knowledge of specific environmental and/or biological systems, using remote sensing for inputting into these models is a way to leverage this new technology and potentially increases its predictive value. There will be no further elaboration on the use of crop models with hyperspectral data in this dissertation.

Table 1.1. Waveband regions and centers (nm) identified for predicting physiological traits. Note: Results presented only up to 1400nm

Predicting	Blue	Green	Red	Red-Edge	NIR (800-1300)	FNIR (to 1400nm)	Reference
Grain yield		530, 585	655, 660, 685, 675	705, 715	935, 940	1025, 1097	(Osborne et al., 2002c)
		531	682		855	1075	(Thenkabail et al., 2014)
		550		710			(Blackmer, Schepers, Varvel, & Walter-Shea, 1996)
					880, 900, 920, 970		(Elsayed & Darwish, 2017)
				701	839		(Goel, Prasher, Landry, Patel, Viau, et al., 2003)
Plant Biomass		505, 515, 545					(Osborne et al., 2002c)
		550	682		855, 910	1075, 1245	(Thenkabail et al., 2014)
	439	511	625		954		(Thenkabail et al., 2000)
	409, 416, 490		626, 656	701, 778, 785, 793	824, 839		(Goel, Prasher, Landry, Patel, Bonnell, et al., 2003)
Plant nitrogen or chlorophyll		550-600					(Osborne et al., 2002c)
	405, 490	515, 550, 570		705, 720, 700-740			(Thenkabail et al., 2014)
	453, 498	505, 588	603				(Goel, Prasher, Landry, Patel, Bonnell, et al., 2003)
		550		710			(Blackmer, Schepers, Varvel, & Walter-Shea, 1996)
		554, 575		702, 712			(Zhao et al., 2003)
				700, 715, 726, 735, 745, 750			(Campbell et al., 2007)
		510, 540-560		700-720	>760		A. Gitelson in (Thenkabail et al., 2012)
		525, 570	600, 630, 680	705			(Schlemmer et al., 2005)

1.8 Predicting Biomass with Hyperspectral Sensing

A summary of bands useful for predicting biomass according to the literature are shown in Table 1.1. The zones include the blue region and lower bands in the green region which are different from those bands useful for predicting grain yield. Not surprisingly, the bands in the literature described as useful in predicting biomass are more similar to those for predicting plant N content than those for grain yield.

Vegetation indices based on hyperspectral remote sensing have been extensively studied for evaluating biomass in maize. Experiments have evaluated crop biomass at single as well as multiple timepoints. Thenkabail et al. (2000) evaluated the relationship between multiple narrow band vegetation indices of late vegetative or critical developmental stage (R1/R2) maize to whole plant biomass at the same corresponding phenological stage. In their analysis, the authors found that the 4-variable Optimum Multiple Narrow Band Reflectivity (OMNBR) model, through stepwise linear regression, had a similar coefficient of determination (0.78) as the narrow band NDVI model (0.71) for predicting maize biomass at their respective developmental stages. In the publication the OMNBR VI was a multiple linear regression model including a soil line offset with narrow bands selected for the highest R^2 values. Interestingly the 2-variable OMNBR had a lower coefficient of determination than the 2-band NDVI (Thenkabail et al., 2000). The soil adjusted index TSAVI provided a positive increase in R^2 value over the broad-band NDVI for biomass; however, there was no improvement over the 4-variable OMNBR or narrow-band NDVI models mentioned above (Thenkabail et al., 2000). In agreement with Goel, Prasher, Landry, Patel, Viau, et al. (2003), Thenkabail et al. (2014) recommended using variations on NDVI [(band 1- band 2)/(band 1 + band 2)] for estimating biomass with band 1 in the NIR region (at 855, 910, 1075, or 1245nm), green region (at 550nm), or the SWIR (at 1650 or 2205nm) and red, always as band 2 at 682nm. Similar conclusions were obtained by Quemada et al. (2014) when they found that various xanthophyll (such as PRI based in the green region only) or other chlorophyll indices (TCARI, OSAVI, or combinations thereof, based on lower portions of the red regions) were not linearly related to biomass.

Many studies found that the closer the imaging was to the desired prediction stage the strength of the relationship between imaging and ground reference data generally increased. In a study conducted by Goel, Prasher, Landry, Patel, Viau, et al. (2003) the researchers determined that the

NDVI model based on VT data was best at predicting whole plant R6 biomass than the NDVI models based on V4 or R6 images. The authors also reported that the 2-band NDVI VT model was better than any 5-band model (regardless of imaging date). The poor relationship between R6 images and R6 physiological data may be due to leaf senescence effects on reflectance. The authors reported that the 5-band models tended to underestimate values in the validation test set and have poor predictive values while the VT NDVI-based model only had a 2% overestimation and a high coefficient of efficiency (0.349) value, indicating good prediction. However, when comparing the three best NDVI models for predicting R6 whole plant biomass those based on VT images only explained 27% of the variance in biomass while those based on R5/R6 images accounted for 40% of the biomass variance (Goel, Prasher, Landry, Patel, Viau, et al., 2003). In a study of imaging at approximately ~V8 by Quemada et al. (2014) none of the indices predicted R6 whole plant biomass and Pearson correlation coefficients were less than 0.55, while 3 R1 indices, [2 greenness (NDVI and RDVI) and 1 chlorophyll index (Red-Edge index, R750/R710)] had high correlation coefficients (>0.55) to R6 above-ground biomass.

Regression models based on imaging at vegetative stages of V6/V7 or V14/R1 were unable (R^2 <0.60) to accurately predict biomass levels by Osborne et al. (2002c). This may be explained by the fact that there were one or 2 months between the imaging date and the later biomass sampling date. Maize plant growth is very rapid from V6 thus the plants imaged were quite different from those sampled later, especially since they did not experience drought stress. In the same report Osborne et al. (2002c) described strong biomass predictions (R^2 =0.87) with image based regression equations with only a two day difference between imaging and sampling dates at V13-V16 for well-watered and drought conditions Evaluating plants under well-watered conditions only showed an even better fit (R^2 =0.94) for estimating biomass at V13-V16 suggesting there is interplay between plant stress, plant growth and reflectance (Osborne et al., 2002c). That interaction was also evident in a study evaluating salinity, water stress and remote sensing of maize conducted by Elsayed and Darwish (2017). The scientists found that there was a statistically significant linear relationship between biomass (as dry weight) and a VI index centered at 970 and 900nm (R^2 =0.56). However, the proportion of variance in the index predictable from canopy water content, water mass, and biomass fresh weight was higher than for dry weight biomass (Elsayed & Darwish, 2017). The negative impact of timing between imaging and sample collection was less pronounced for N concentration. Using bands from the NIR and mid-IR range

from images of maize taken at V6/V7 or V14/R1, Osborne et al. (2002c) were able to accurately predict ($R^2 \geq 0.80$) N concentration levels one or two months later.

In summary, the literature points to the broad utility of the narrow-band NDVI index for estimating biomass. However, there is no index that works for all data sets. It is important to note that though index categorization (greenness, chlorophyll, etc.) provides suggestions on use, this categorization is no guarantee on an indices' utility and predictive ability thus it is best to evaluate indices across categories. Another factor to consider is that since index utility is based on the data set, it is critical to use a validation test set (if possible) in the analysis to ensure that the experiment conclusion has not been overly skewed by the data set itself. And, finally, in the analysis it is important to factor in growth stage and, of course, obtain the imaging as close to the actual phenotyping date as possible.

1.9 Predicting Nitrogen Uptake with Hyperspectral Sensing

Prediction of plant N uptake levels based on remote sensing are extremely common throughout the literature. The goal of most remote sensing studies is to obtain in-season measurement of N levels to guide precise and site-specific fertilizer applications in order to decrease overall N fertilizer rates or to allow in-season N applications in order to increase NUE while still maintaining high grain yields. Throughout the multitude of studies there are differences in how N uptake is defined and how the reference N content is measured. Some studies define N uptake as N concentration (i.e. percent nitrogen or mg N/gram dry matter) while other studies define it as N content (i.e. nitrogen per area or kg N/ha) basing the analysis on reference data obtained from N combustion methods such as the Kjeldahl method. Care must be taken when comparing the experiments since in wheat it has been shown that regression models based on VIs for N content (N/unit area) differ and are more predictive than those for N concentration (N/weight) (Mahajan et al., 2014; Sahoo et al., 2015). Other factors that can impact measured N levels relative to imaging are the plant component sampled (leaf, leaf location, stem, husk, etc.) since studies have clearly shown that N levels in the various plant components change over time (Bender et al., 2013; DeBruin et al., 2013).

Many studies characterize N levels based on Minolta Chlorophyll meters which provide SPAD values (Bullock et al., 1995; Bullock & Anderson, 1998; C. Bausch & R. Duke, 1996; Sawyer et

al., 2011). This active meter emits light at 650 and 940nm then measures light transmission through the leaf (Markwell et al., 1995); thus, it is actually a proxy for actual plant N levels. One often cited N-related VI is the N Sufficiency Index which is the ratio of the SPAD values for the N stressed plants normalized by the SPAD values for the N sufficient plants (SPAD for low N/SPAD for high N) (Blackmer & Schepers, 1995). However, since this index is based on direct plant measurements and requires a high N control treatment, it will not be considered as a remote sensing vegetation index in this report.

At the leaf level Blackmer et al. (1994) found that reflectance at 550nm had a strong correlation to leaf N in the laboratory. Similar results were found when linear correlations ($r2 \geq 0.47$) to leaf N, by area or weight, were highest for a chamber grown N stressed hybrid (Zhao et al., 2003). However, the strongest correlations were found utilizing *ratios* of these wavelengths, 554, 575, 702, and 712nm, divided by reflectance in the near infrared range, rather than single wavelengths, supporting the utility of VI for N prediction (Zhao et al., 2003).

Initial field studies evaluated whether imaging could detect changes in the plants when grown under various N conditions. Field results were similar to lab results. From imaging canopies at R5, Blackmer, Schepers, Varvel and Walter-Shea (1996) found that wavelengths at 550 and 710nm and related ratios were most useful for detecting N treatment differences. However, their analysis did not confirm actual plant N levels through plant N analysis but assumed that plants under different N treatments producing different grain yields had different N plant levels. In research on maize, soybean, and maple trees by Campbell et al. (2007), the reflectance based vegetation indices providing the most granularity and differentiation between N levels across plant types were those at the following wavelength ratios or combinations: 750/700, (735-745)/(715+726), and $REIP_w$ as well as the reflectance derivative index at 715/705. Different results were found by Alchanatis et al. (2005) who only evaluated the N-content of maize leaves in the field. Regions correlated to leaf N content ranged from 530-780nm (green and red) and 1000-1070nm (NIR) (Alchanatis et al., 2005). For N content the wavebands of interest from Osborne et al. (2002c) were the green and NIR regions. See Table 1.1 for a summary of specific wavebands presented here.

Indices, both broad and narrow band, have been investigated extensively for prediction of N uptake. So much development has been targeting N that many indices, such as NDNI (Normalized

Difference N Index), CCCI (Canopy Chlorophyll Content Index), CARI (Chlorophyll Absorption Ratio Index), etc., have been built specifically for N and chlorophyll prediction and are named as such. For N or chlorophyll detection Thenkabail et al. (2014) recommended 6 normalized indices similar to NDVI [i.e. (band 1 – band 2)/(band 1 + band2)] with band 1 as 550, 855, or 920nm and band 2 in the lower spectral range of UV (375nm), blue (490nm), green (515 or 550nm) or red (682nm). Other researchers considered a new index, DCNI (double – peak canopy N index), for predicting N concentrations (P. Chen et al., 2010). They found that DCNI predicted N concentration levels in the validation data set with an R^2 of 0.62 and RMSE = 2.7 mg N/g dry matter. This index is based off reflectance values from three bands, 670, 700, and 720nm but was validated with data from only one genotype (P. Chen et al., 2010). Later studies by other research groups evaluated this index with additional maize hybrids and found poor predictability for plant N (Zhao et al., 2018).

Though not specifically N focused Thenkabail et al. (2014) also described three red-edge indices for studying plant stress: 1st order derivative integration over 700-740nm, and 2 normalized indices with band 1 = 855 or 910 and band 2 = 720 or 705. A lack of N can induce a stress response in maize thus these VIs may be predictive of N. Schlemmer et al. (2013) found that of the 6 VIs they evaluated by imaging the canopy from V6 to R1 three red-edge indices [REP, MTCI, or $CI_{rededge}$; R^2 = 0.91, 0.80, and 0.78, respectively] were best at predicting maize leaf N content levels below 6mg/m^2 while CI_{green} was best for predicting higher leaf N content levels (R^2 =0.79) of equivalent sampling dates. In a different study, to avoid the biomass saturation effect common to vegetation indices such as NDVI, Li et al. (2014) also proposed using red edge based vegetation indices for predicting N. The red edge is defined as the inflection point in the transition from red to near infrared in the electromagnetic spectrum which usually occurs in the 705nm region (Schlemmer et al., 2005). Two such indices, CCCI and MTCI, were most consistent at predicting N content (kilograms of N per hectare) across the plant development stages evaluated (V6 – V7 and V10 – V12) (Li et al., 2014). However N concentrations at V10 – V12 could not be predicted accurately by any of the 12 vegetation indices evaluated when they pooled the imaging data across time points (Li et al., 2014). The authors proposed that this lack of fit may be due to the extremely fast plant growth that occurs between V6 and V12 and the reflectance being overwhelmed by the biomass.

Another study in which plant growth stage impacted results was when Bausch and Diker (2001) examined maize canopy crop reflectance of 2 hybrids and determined that their index of interest, N Reflectance Index at V6 was not representative of whole plant N concentration at equivalent sampling times. The authors theorized that at the early growth stages the soil background was affecting reflectance levels measured. However, at later growth stages (V9 and V12) both NRI and plant N Spectral Index (NSI = |1/NDVI|) had a strong positive linear relationship ($r^2 \geq 0.65$) with whole plant N concentration (Bausch & Diker, 2001). Similar results, but for N content, were found by Quemada et al. (2014) who reported weak correlations between spectral indices and total plant N content at around V8 yet strong correlations (correlation coefficient = 0.61) for the R750/R710 index at R1.

Osborne et al. (2002c) were able to predict maize whole plant N concentration at V13-V16 growth stage under high water conditions (R^2 =0.95) or all irrigation levels (R^2 =0.87) with regression equations based on imaging data collected within 2 days of field sampling. Both equations contained reflectance data from at least 5 bands. Though there were no common bands, common regions included: 550-600nm, 1425-1475nm, 1490-1515nm, and 2115-2165nm (Osborne et al., 2002c). In another study focusing on phosphorus and N deficiency using a different maize hybrid Osborne et al. (2002b) found that image based models (from V14 to R1) predict whole plant N concentration at equivalent timings (coefficient of determination, $R^2 > 0.60$). The regression models from the 2 different years were either 8-band or 3-band models with only one waveband region in common, 975nm (Osborne et al., 2002b). In another experiment, 2 to 5-band regression models developed by Goel, Prasher, Landry, Patel, Viau, et al. (2003) based on imaging at tasseling explained more than 75% of the variability in leaf N concentration. Validation of the 5-band model by the researchers indicated a low overestimation and high predictive power. They also found that the NDVI-based model had a smaller overestimation error but lower predictability and explained less than 20% of the variability in N concentration. Yendrek et al. (2017) measured leaf-level reflectance in greenhouse and field-grown maize plants from V7-V10 and found that a PLSR model based on reflectance data from the SWIR region, 1500-2400nm, predicted plant leaf N concentration well (R^2 =0.92-0.96). This portion of the spectrum is known to be the spectroscopic absorption region of N (Curran, 1989). The PLSR model was a much better predictor than the three vegetation indices (NRI_{1510}, $MCARI_{1510}$, and NDNI) evaluated which all had R^2 values less than 0.50 (Yendrek et al., 2017). From a machine learning approach, radial basis function neural

networks built off the Green Vegetation Index (GVI) were found to reliably predict leaf N concentrations of field maize at mid-vegetative growth (Gautam & Panigrahi, 2007). Conversely, Karimi et al. (2008) found no relationship between reflectance data and maize leaf N concentration or chlorophyll content when using support vector machine technology and comparing equivalent imaging and sampling time points at either approximately V4 or VT.

In summary, prediction of N uptake in maize has been investigated extensively but there is little agreement on which VI is best, though red-edge indices are commonly at the top of the list (Thenkabail et al., 2012). Though many studies cite the benefits of partial least squares regression (PLSR) as encompassing a broader portion of the collected spectral data there is no concrete consensus that regression is "better than" vegetation indices since results often vary depending on the data set. Finally, much of the N research points to regions of the spectrum which are in the upper portion of the NIR (>1000nm), most likely due to the spectroscopic absorption characteristics of N itself.

1.10 Predicting Chlorophyll with Hyperspectral Sensing

The photosynthesis biochemical machinery in plants (chlorophyll, rubisco, ATP, NADPH, etc.) contains large amounts of N and is responsible for more than 50% of the N in the leaf (Pons et al., 2008). Thus, a close relationship has been established between N and chlorophyll levels in the plant at both leaf and canopy levels (Schlemmer et al., 2013; Walters, 2003). At the leaf level, Schlemmer et al. (2005) found several ratios (OCAR, YCAR and GGFN) and the red edge predicted leaf chlorophyll content, though water stress did confound estimation by increasing reflectance. As plants become N stressed, chlorophyll content decreased and the red edge wavelength decreased (Schlemmer et al., 2005).

Initial maize field studies by Daughtry et al. (2000) investigating the relationship between reflectance data and leaf chlorophyll identified that wavebands at 550 and 715nm are related to chlorophyll concentration. These wavebands are the same as those identified by Blackmer, Schepers, Varvel and Meyer (1996) as being related to N treatment differences in maize. Those wavebands are also similar to the regions identified by A. Gitelson in Thenkabail et al. (2012) as being related to chlorophylls, carotenoids, and anthocyanins (see Table 1.1).

Besides identification of specific spectral regions as more predictive of chlorophyll levels, multiple vegetation indices or ratios of VIs have been evaluated in relation to chlorophyll. In a study comparing 11 individual VIs and their respective combinations, Haboudane et al. (2008) found that the individual VIs, MTCI and R-M, had the highest R^2 values (≥ 0.77) for estimating chlorophyll content. However, combinations of the VIs were more stable than the individual indices and were quite predictive in their own right with, R^2 values ≥ 0.78 for TCARI/OSAVI, DD/MSAVI, and R-M/MSAVI (Haboudane et al., 2008). In contrast, when Gitelson summarized a large number of crop studies, the author recommended different VIs, ECI and $NDVI_{RE}$, for total chlorophyll detection across a broad range of chlorophyll levels and plant types (Thenkabail et al., 2012). In the same review Gitelson described CI-RE and CI-G as two VIs with the lowest RMSE for chlorophyll detection (Thenkabail et al., 2012). This close relationship of CI-RE and CI-G to chlorophyll was supported by Hunt Jr et al. (2013) who found in their experiment that 6 vegetation indices (CVI, gNDVI, CI-G, NDREI, CI-RE, and MTCI) were strongly positively correlated (correlation coefficient > 0.75) in maize field studies. The latter authors also reported an additional 9 VIs (NGRDI, GLI, VARI, MCARI, TCARI, TCI, TCARI/OSAVI, MCARI/MTVI2, AND TGI) were strongly negatively correlated to chlorophyll content ($r < -0.83$).

Instead of using only specific portions of the spectrum as found in VIs, analysis can also consist of identification of the most useful wavebands or employing the entire spectral region. Goel, Prasher, Landry, Patel, Viau, et al. (2003) found that an NDVI-based model outperformed a 5-parameter (5 spectral region) regression model for predicting chlorophyll content in field studies. However the three best NDVI models only explained less than 25% of the variability in chlorophyll content suggesting that other unrecognized variables were impacting chlorophyll (Goel, Prasher, Landry, Patel, Viau, et al., 2003). Focusing on a broader use of the spectrum, Atzberger et al. (2010) compared statistical models using all bands simultaneously (PLSR and principal component regression) versus a model selecting the most useful wavebands (stepwise multiple linear regression). The authors found that the PLSR model was best for predicting chlorophyll in wheat based on cross validated statistics (R squared and RMSE) successfully dealing with the multicollinearity issue often found in hyperspectral data. Conversely, in an expansive analysis of VIs, PLSR, and interval PLSR models of both crop and non-crop vegetation data over a 22 year period, Inoue et al. (2016) established that the vegetation index RSI (R815/R704) was best for predicting chlorophyll content ($r^2 = 0.891$).

Another method expected by V. Alchanatis and Y. Cohen to make greater use of the information within hyperspectral data are wavelet-based models (Thenkabail et al., 2012). Wavelets, mathematical functions that cut the data into sections with different frequency components for analysis, have also been used to study hyperspectral data for predicting chlorophyll (Blackburn & Ferwerda, 2008). Researchers found that this method outperformed simple linear regression in non-maize studies (Kempeneers et al., 2005) and did not saturate at high chlorophyll content levels (Blackburn & Ferwerda, 2008).

Many VIs have been found to be predictive of chlorophyll plant levels in maize. Overall, vegetation indices with green and red-edge bands avoid saturation and thus result in decreased sensitivity to chlorophyll (Thenkabail et al., 2012). In summary, review of literature above has shown that both VIs and multivariate statistics are useful for predicting chlorophyll plant levels. Further study of various multivariate methods such as PLSR and wavelets remains.

1.11 Predicting Grain Yield with Hyperspectral Imaging

Maize grain yield is one of the physiological attributes that has been studied extensively for its relationship to hyperspectral imaging due to its economic importance. Band regions commonly found to correlate to (or increase) prediction accuracy for grain yield are shown in Table 1.1. The bands for estimating grain yield differ from those predicting other physiological attributes by including near infrared (NIR at 900nm), far near infrared (FNIR) and short-wave infrared (SWIR at 1700nm) bands (Table 1.1). In addition to these spectral regions various models have been identified as predictive of grain yield. Input to these models range from those models built on reflectance data of selected wavebands or features while others are based on specific VIs as the independent variables. Additional models are PLSR models based on reflectance data to more complex models such as artificial neural networks.

Initial studies evaluated whether imaging reflectance at late growth stages (R5) were correlated to grain yields. Blackmer, Schepers, Varvel and Walter-Shea (1996) found that *relative reflectances* (at 550nm and at 710nm) and ratios (at (550-600)/(800-900)) were most closely correlated with grain yield (R^2 =0.74, R^2 =0.76, R^2 =0.86, respectively). To compensate for lighting differences between images the authors normalized the data by calculating relative reflectance as the reflected radiation of the plot relative to a non-N limited plot which unfortunately imposed a requirement

for a reference plot with zero N in every field trial. In maize irrigation and salinity trials, researchers found three hyperspectral vegetation indices significantly correlated (p</= 0.001) to grain yield with coefficients of determination values greater than 0.5 (Elsayed & Darwish, 2017). Because of their emphasis on water the authors largely focused on water indices. The indices Elsayed and Darwish (2017) identified as correlated to grain had waveband regions quite different from the previously mentioned regions: (970-880)/(970+880), (970-900)/(970+900), and (970-920)/(970+920). Goel, Prasher, Landry, Patel, Viau, et al. (2003) evaluated five waveband and NDVI models for predicting various biophysical components of maize grown under various N and weed treatments. The researchers found that although the multiple parameter regression waveband models had R^2 values > 0.91 across all three flights for predicting grain, additional analysis with validation data indicated that these models had poor predictive values. Instead, the NDVI models were better at predicting grain yield than the waveband models. They hypothesized this might be due to the normalization that is inherent to the definition of NDVI resulting in a more broadly applicable model. The most common NDVI waveband in the models for predicting yield was 701nm for the red and 839nm for the NIR (Goel, Prasher, Landry, Patel, Viau, et al., 2003).

Uno et al. (2005) developed 7 different models to predict maize grain yields using a subset (tasseling-only) of the imaging data from Goel, Prasher, Landry, Patel, Viau, et al. (2003). The first 5 models used the reflectance data as inputs for the variables of 3 vegetation indices (PRI, NDVI, and SR), a stepwise linear regression model (SLR), and an artificial neural network (ANN). The last 2 models also used principal component analysis to remove the correlations between the bands. The top five components which contained 94% of the variance were used as inputs into two additional models based on SLR and ANN (Uno et al., 2005). Both SLR and ANN models predicted grain yields with average yield differences of 3.4% or less and had the highest correlation coefficients (0.75-0.76) amongst all models (Uno et al., 2005). However, full consideration of the best models determined that the RMSE was still 20%, (over 1000 kg grain/ha), too high for applied yield predictions according to the researchers (Uno et al., 2005). In the discussion by Uno et al. (2005) the authors pointed out the different results between the predictive ability of their models versus the study by Goel, Prasher, Landry, Patel, Viau, et al. (2003) which were both based on the same imaging data. The researchers noted that plot reflectance values had different definitions. Goel, Prasher, Landry, Patel, Viau, et al. (2003) defined the plot reflectance values as the mean reflectance values of *all* the pixels within the polygon. No mention was made of how soil or non-

maize pixels were filtered out. As an alternative, to remove the potential of non-maize pixels affecting results, Uno et al. (2005) manually selected five plant-only pixels within each polygon plot and used those values as the plot reflectance values in their models. This seemingly small change had a large impact on the fit and prediction capability of their models. In summary, hyperspectral imaging can be used to predict grain yield but with varying degrees of success, much of it dependent upon fine details in spectral and spatial pre-processing and analysis of the imaging data.

Remote sensing of maize has been done at various growth stages to determine whether imaging at a specific growth stage is more predictive of final season grain yields. In a study which evaluated imaging at both early and late development stages (Osborne et al., 2002c) found that grain yield was best predicted (R^2 values 0.88 or greater) with reflectance data from V13 or later when using stepwise linear regression. However, each maize growth stage had a different model. Additionally, not only did each of the models differ by year but there were few or no common wavebands across the growth stages (Osborne et al., 2002c). Another study evaluating NDVI models based on imaging at tasseling versus R6 resulted in higher R^2 values (~0.89) for the R6 image versus the tasseling image (~0.56) (Goel, Prasher, Landry, Patel, Viau, et al., 2003). CIMMYT researchers investigated the maize grain yield prediction capability of 6 vegetation indices (NDVI, CWMI, mND, PRI, MTCI, and MCARI2) using ordinary least squares analysis and compared them to a partial least squares model and two 62-band regression models (using ordinary least squares or a Bayesian shrinkage and variable selection method) (Aguate et al., 2017). Models were evaluated based on test data using leave-one-out cross validation methods and imaging was conducted on a weekly basis beginning at R1. Researchers determined that prediction accuracy increased with the later imaging dates resulting in cross-validation correlation values greater than 0.34. The best detecting VIs were mND and PRI. The VIs mND and NDVI were especially improved in average correlations based on data of the last two imaging time-points. The best overall model, the Bayesian model, had the highest estimated correlation of 0.47 (Aguate et al., 2017).

From the above-mentioned studies and others published hyperspectral imaging can be used to predict end-of-season grain yield but not with 100% reliability. Imaging later in the growth period results in more predictive models though the data and its analysis can be largely impacted by even

seemingly small details within the pre-processing methods. Trends in common wavebands exist but are not definitive, again largely impacted by experiment design and data. A fundamental drawback to the analysis methods and results described is that the models developed and described above are *specific* to those studies. Unfortunately for broader application, such as other locations and years, these models need to be re-calibrated with additional ground reference data. This drawback is widely acknowledged within the field of research (Hatfield et al., 2008b; Mulla, 2013). Research into remote sensing prediction of grain yield has not fully investigated the relationship of the maize hybrid's genetics with the analysis. The need for re-calibration with reference data and the observed specificity of models to single experiments may be due to the interplay of the hybrid's genetics with the remote sensing. Grain yield changes in maize hybrids developed over time have been well-documented due to genetic and agronomic improvements (Duvick, 2005; Sadras & Calderini, 2015; Tollenaar & Wu, 1999). Additional studies have detailed the greater yield reducing effect of low N conditions on older versus newer hybrids (Echarte et al., 2008). And finally, other era studies have recognized changes in maize harvest index, the ratio of grain per total biomass produced (Mueller et al., 2019). Such physiological changes may be part of the variation in predictability of grain yield through remote sensing. Additional research is needed to understand this relationship since the greatest utility of remote sensing exists when methods are applicable across genetically diverse hybrids in terms of genetics and eras.

1.12 Nitrogen Nutrition Index

A N measure which remote sensing has recently been used to predict in maize is the N Nutrition Index (NNI) originally defined by Lemaire and Gastal (1997). The researchers defined it as the ratio of the actual N plant content divided by the critical N content which is based on the above-ground plant dry weight (1997).

$$NNI = \frac{\%Na}{\%Nc}$$

And

$$\%Nc = 3.4 * W^{0.37}$$

Where

NNI = Nitrogen Nutrition Index

%Na = plant nitrogen concentration

%Nc = critical plant nitrogen

W = crop mass in t/ha

Thus obtaining this index requires measuring both N concentration and plant mass, which are very labor intensive measures (Sadras & Lemaire, 2014). If NNI = 1 at any specific aboveground biomass, then the plant is deemed to have sufficient N. An NNI > 1 indicates that the plant has been over-fertilized, the term described as "luxury consumption." And, NNI < 1 is the converse (Lemaire & Gastal, 1997). This measure conveys the plant's N status in terms of providing enough N fertilizer to obtain the maximum yield as well as providing insight for interpretation of agronomic experiments and the potential indirect effects of N (Gastal et al., 2015).

Cilia et al. (2014) used hyperspectral imaging of maize (of unknown genetic background) to predict NNI with the goal of developing a variable rate N fertilization map. The researchers achieved good agreement ($R^2 = 0.70$, $p < 0.001$) between the actual NNI values at approximately V10 and those predicted by the contemporary imaging. In this study 13 vegetation indices were considered for estimating the NNI input parameters of biomass and percent N. The VI with the best prediction for biomass was MTVI2 ($R^2 = 0.80$) (Cilia et al., 2014). The researchers determined that MCARI/MTVI2 estimated percent N best ($R^2 = 0.59$) selecting it because it had the highest coefficient of determination while not being significantly related to LAI. Cilia et al. (2014) surmised that this lack of correlation to LAI means the VI was not affected by canopy structure.

In another publication scientists evaluated 21 vegetation indices for predicting the components of NNI and 13 VIs for predicting NNI directly using data for 5 cultivars from 5 site years with imaging and sampling at V6, V9, and V12 (Zhao et al., 2018). Based on model performance for both calibration and validation data sets the best model for predicting NNI indirectly, i.e. based on prediction of the components, was based off the RVI II and MSAVI VIs (RMSEP = 0.14, REP = 9.5%, and RRMSE = 16.86%) (Zhao et al., 2018). For direct prediction of NNI the model based off NDVI at 710 and 512nm or the model based off RSI at 705 and 507nm were the most stable

and accurate models; all validation statistical parameters were lower than for the indirect model described above (Zhao et al., 2018). The authors propose that the direct method models are more stable since the indirect method requires estimation of two VIs thus increasing error with the indirect methodology (2018).

1.13 Nitrogen Parameters Studied

As mentioned previously recent research suggests that NNI is useful for communicating a plant's N status and providing insight into agronomic experiments (Gastal et al., 2015). A recent review proposes using NNI at silking as a measure of the plant's reproductive photosynthetic potential so critical to final grain yields in order to facilitate fertilization decisions (Fernandez et al., 2020). However, for studying and improving a crop's NUE it is important to study the associated processes such as uptake, translocation, assimilation, and remobilization of N (Moll et al., 1982; Salvagiotti et al., 2009). Study into these processes has been facilitated by research into the major components of NUE which have been defined as N Recovery Efficiency (NRE) and N Internal Efficiency (NIE) (Ciampitti & Vyn, 2011; Moll et al., 1982; Salvagiotti et al., 2009). Conceptually NUE is impacted by the plant's ability to absorb available N in the soil (NRE) and the plant's ability to produce grain per unit N in the plant (NIE), and thus NUE = NRE x NIE. Mathematical definitions are shown below. Another important component to a plant's use of N is the N Conversion Efficiency (NCE) which is a measure of how efficient a plant is at producing biomass for each available unit of N in the plant (Keru Chen & Tony J Vyn, 2017; Sadras & Calderini, 2015). This component is a measure of a plant's ability to translocate and assimilate the absorbed N and is an in-season reflection of a plant's biomass production efficiency relative to N.

1. Nitrogen Internal Efficiency (NIE)
   $NIE = Y/N_{plant}$
   where Y = grain yield at 0% moisture
   N_{plant} = total plant nitrogen (N) content
2. Nitrogen Recovery Efficiency (NRE)
   $NRE = ((N_{plant} - N_L)/ (F_H - F_L)) * 100$
   where N_L = mean total plant nitrogen (N) content of low (0N) treatment
   F_H = amount of applied N fertilizer in high N treatment
   F_L = amount of applied N fertilizer in low N treatment
3. Nitrogen Use Efficiency (NUE)
   $NUE = (Y_H - Y_L) / (N_H - N_L)$
   where Y_H = grain yield at 0% moisture for high N fertilization treatment

Y_L = grain yield at 0% moisture for low N fertilization treatment
N_H = amount of N in high nitrogen treatment
N_L = amount of N in low nitrogen treatment

4. Nitrogen Conversion Efficiency (NCE)

$NCE = BM_{tot} / N_{plant}$

where BM_{tot} = whole plant biomass weight
N_{plant} = total plant N content

Extensive work has been done to utilize these parameters to understand the physiological changes that have occurred in maize breeding over time providing insight into how genotypes have changed in their use of N through breeding (Ciampitti & Vyn, 2012, 2013; DeBruin et al., 2017; Haegele et al., 2013). Unfortunately, these NUE parameters are quite labor intensive to study because they are based on N content and biomass information. Phenotyping for NUE traits in large plant breeding programs is a bottleneck to further advancement in this area.

A broad search of the current literature resulted in no discussions or research investigating the ability of remote sensing, specifically hyperspectral sensing, to predict or estimate these NUE parameters in maize. As detailed above, hyperspectral remote sensing has been used extensively in maize to predict end of season grain yields, plant biomass, N and chlorophyll content, and N status based on the N nutrition index with success. Given (a) the need for agricultural research on N use and improvement of NUE in maize, (b) the huge need for improvements and efficiencies in phenotyping research, and (c) limited studies in predicting N parameters using remote sensing, I propose studying hyperspectral remote sensing to predict maize N content and the following N parameters: N concentration, NIE, and NCE.

1.14 Objective I

(A) conduct investigations into N Internal Efficiency (NIE) of approximately 300 corn hybrids in two field-based locations grown under a single low N rate identifying the hybrids significantly different from each other in NIE or grain yield and categorizing hybrids into the highest and lowest performing entries in each maturity group for either grain yield or NIE value

(B) identify potential correlations between available physiological measurements and NIE seeking out hybrids which are significantly different

(C) conduct an exploratory investigation into differences visible through aerial or remotely sensed imagery based on GeoVantage jpg and geotiff data inspecting for visual differences apparent in plant health, analyzing VI for correlations between VI and crop physiological characteristics as well as differences between maize hybrids, study temporal differences between images, and expand the remote sensing inquiries by obtaining high resolution data from Digital Globe during the study period

1.15 Objective II

(A) establish the field-based N parameters of 9 hybrids grown in 3 site years under 3 N rates, processing the hyperspectral imagery to generate 20 vegetation indices for each location and imaging date in order to evaluate the relationship between VI and N content (TNC at V12, R1 or R6), N concentration at R6, or NUE parameters of N concentration, NCE, and NIE, examining correlations in order to identify the strongest relationships

(B) develop predictive models for estimating N parameters from the VI using statistical mixed effects models analyzing estimated values relative to ground reference values and comparing field-based to model-based hybrid rankings

(C) evaluate the impact of downsampling images from high to low resolution on VI values and the corresponding hybrid rankings

1.16 Objective III

(A) process mid-season hyperspectral imagery from Objective II using a classification method to identify and mask out soil pixels to obtain hyperspectral reflectance values and determine the hyperspectral regions and bands most strongly correlated to the end-season N parameters of plant N concentration and NUE parameters of NCE and NIE

(B) extract features from images by generating cross-validated partial least squares regression (PLSR) models to estimate N parameters (plant N concentration, NCE and NIE) comparing results to ground reference values of unseen test data

(C) determine if the PLSR models allow for hybrid differentiation and predict the ground reference outcomes for each hybrid

1.17 References

Aguate, F. M., Trachsel, S., Pérez, L. G., Burgueño, J., Crossa, J., Balzarini, M., Gouache, D., Bogard, M., & Campos, G. d. l. (2017). Use of Hyperspectral Image Data Outperforms Vegetation Indices in Prediction of Maize Yield. *Crop Science*, *57*(5), 2517. https://doi.org/10.2135/cropsci2017.01.0007

Al-Abbas, A., Barr, R., Hall, J., Crane, F., & Baumgardner, M. (1974). Spectra of normal and nutrient-deficient maize leaves. *Agronomy Journal*, *66*(1), 16-20.

Alchanatis, V., Schmilovitch, Z., & Meron, M. (2005). In-Field Assessment of Single Leaf Nitrogen Status by Spectral Reflectance Measurements [journal article]. *Precision Agriculture*, *6*(1), 25-39. https://doi.org/10.1007/s11119-005-0682-7

Andrade, F. H., Vega, C., Uhart, S., Cirilo, A., Cantarero, M., & Valentinuz, O. (1999). Kernel number determination in maize. *Crop Science*, *39*(2), 453-459.

Araus, J. L., & Cairns, J. E. (2014). Field high-throughput phenotyping: the new crop breeding frontier. *Trends in Plant Science*, *19*(1), 52-61. https://doi.org/https://doi.org/10.1016/j.tplants.2013.09.008

Atzberger, C., Guérif, M., Baret, F., & Werner, W. (2010). Comparative analysis of three chemometric techniques for the spectroradiometric assessment of canopy chlorophyll content in winter wheat. *Computers and Electronics in Agriculture*, *73*(2), 165-173. https://doi.org/10.1016/j.compag.2010.05.006

Banziger, M., Edmeades, G., Beck, D., & Bellón, M. (2000). Breeding for drought and nitrogen stress tolerance in maize: From theory to practice.

Baret, F., Houles, V., & Guerif, M. (2007). Quantification of plant stress using remote sensing observations and crop models: the case of nitrogen management. *J Exp Bot*, *58*(4), 869-880. https://doi.org/10.1093/jxb/erl231

Bausch, W. C., & Diker, K. (2001). Innovative remote sensing techniques to increase nitrogen use efficiency of corn. *Communications in Soil Science and Plant Analysis*, *32*(7-8), 1371-1390.

Bender, R. R., Haegele, J. W., Ruffo, M. L., & Below, F. E. (2013). Nutrient Uptake, Partitioning, and Remobilization in Modern, Transgenic Insect-Protected Maize Hybrids. *Agronomy Journal*, *105*(1), 161. https://doi.org/10.2134/agronj2012.0352

Bioucas-Dias, J. M., Plaza, A., Camps-Valls, G., Scheunders, P., Nasrabadi, N., & Chanussot, J. (2013). Hyperspectral Remote Sensing Data Analysis and Future Challenges. *IEEE Geoscience and Remote Sensing Magazine*, *1*(2), 6-36. https://doi.org/10.1109/mgrs.2013.2244672

Blackburn, G. A., & Ferwerda, J. G. (2008). Retrieval of chlorophyll concentration from leaf reflectance spectra using wavelet analysis. *Remote Sensing of Environment*, *112*(4), 1614-1632.

Blackmer, T., & Schepers, J. (1995). Use of a chlorophyll meter to monitor nitrogen status and schedule fertigation for corn. *Journal of Production Agriculture*, *8*(1), 56-60.

Blackmer, T. M., Schepers, J. S., & Varvel, G. E. (1994). Light reflectance compared with other nitrogen stress measurements in corn leaves. *Agronomy Journal*, *86*(6), 934-938.

Blackmer, T. M., Schepers, J. S., Varvel, G. E., & Meyer, G. E. (1996). Analysis of aerial photography for nitrogen stress within corn fields. *Agronomy Journal*, *88*(5), 729-733.

Blackmer, T. M., Schepers, J. S., Varvel, G. E., & Walter-Shea, E. A. (1996). Nitrogen deficiency detection using reflected shortwave radiation from irrigated corn canopies. *Agronomy Journal*, *88*(1), 1-5.

Bullock, D., Bollero, G., & Anderson, D. (1995). Evaluation of the Minolta SPAD-520 Chlorophyll Meter for On-Farm N Management of Corn in Illinois. Illinois Fertilizer Conference Proceedings, January (pp. 23-25).

Bullock, D. G., & Anderson, D. S. (1998). Evaluation of the Minolta SPAD-502 chlorophyll meter for nitrogen management in corn. *Journal of Plant Nutrition*, *21*(4), 741-755. https://doi.org/10.1080/01904169809365439

C. Bausch, W., & R. Duke, H. (1996). Remote Sensing of Plant Nitrogen Status in Corn. *Transactions of the ASAE*, *39*(5), 1869. https://doi.org/https://doi.org/10.13031/2013.27665

Campbell, J. B., & Wynne, R. H. (2011). *Introduction to remote sensing*. Guilford Press.

Campbell, P., Middleton, E., McMurtrey, J., & Chappelle, E. (2007). Assessment of vegetation stress using reflectance or fluorescence measurements. *Journal of Environmental Quality*, *36*(3), 832-845.

Carlson, T. N., & Ripley, D. A. (1997). On the relation between NDVI, fractional vegetation cover, and leaf area index. *Remote Sensing of Environment*, *62*(3), 241-252.

Cassman, K. G., Dobermann, A., & Walters, D. T. (2002). Agroecosystems, nitrogen-use efficiency, and nitrogen management. *AMBIO: A Journal of the Human Environment*, *31*(2), 132-140.

Chen, K., & Vyn, T. J. (2017). Post-silking Factor Consequences for N Efficiency Changes Over 38 Years of Commercial Maize Hybrids. *Frontiers in Plant Science*, *8*, 1737.

Chen, P., Haboudane, D., Tremblay, N., Wang, J., Vigneault, P., & Li, B. (2010). New spectral indicator assessing the efficiency of crop nitrogen treatment in corn and wheat. *Remote Sensing of Environment*, *114*(9), 1987-1997. https://doi.org/10.1016/j.rse.2010.04.006

Ciampitti, I. A., Murrell, S. T., Camberato, J. J., Tuinstra, M., Xia, Y., Friedemann, P., & Vyn, T. J. (2013). Physiological Dynamics of Maize Nitrogen Uptake and Partitioning in Response to Plant Density and Nitrogen Stress Factors: II. Reproductive Phase. *Crop Science*, *53*(6), 2588. https://doi.org/10.2135/cropsci2013.01.0041

Ciampitti, I. A., & Vyn, T. J. (2011). A comprehensive study of plant density consequences on nitrogen uptake dynamics of maize plants from vegetative to reproductive stages. *Field Crops Research*, *121*(1), 2-18. https://doi.org/10.1016/j.fcr.2010.10.009

Ciampitti, I. A., & Vyn, T. J. (2012). Physiological perspectives of changes over time in maize yield dependency on nitrogen uptake and associated nitrogen efficiencies: A review. *Field Crops Research*, *133*, 48-67. https://doi.org/10.1016/j.fcr.2012.03.008

Ciampitti, I. A., & Vyn, T. J. (2013). Grain Nitrogen Source Changes over Time in Maize: A Review. *Crop Science*, *53*(2), 366. https://doi.org/10.2135/cropsci2012.07.0439

Cilia, C., Panigada, C., Rossini, M., Meroni, M., Busetto, L., Amaducci, S., Boschetti, M., Picchi, V., & Colombo, R. (2014). Nitrogen Status Assessment for Variable Rate Fertilization in Maize through Hyperspectral Imagery. *Remote Sensing*, *6*(7), 6549-6565. https://doi.org/10.3390/rs6076549

Clay, D., Kim, K.-I., Chang, J., Clay, S., & Dalsted, K. (2006). Characterizing water and nitrogen stress in corn using remote sensing. *Agronomy Journal*, *98*(3), 579-587.

Cobb, J. N., DeClerck, G., Greenberg, A., Clark, R., & McCouch, S. (2013). Next-generation phenotyping: requirements and strategies for enhancing our understanding of genotype–phenotype relationships and its relevance to crop improvement [journal article]. *Theoretical and Applied Genetics*, *126*(4), 867-887. https://doi.org/10.1007/s00122-013-2066-0

Curran, P. J. (1989). Remote sensing of foliar chemistry. *Remote Sensing of Environment*, *30*(3), 271-278. https://doi.org/https://doi.org/10.1016/0034-4257(89)90069-2

Daughtry, C., Walthall, C., Kim, M., De Colstoun, E. B., & McMurtrey III, J. (2000). Estimating corn leaf chlorophyll concentration from leaf and canopy reflectance. *Remote Sensing of Environment*, *74*(2), 229-239.

DeBruin, J., Messina, C. D., Munaro, E., Thompson, K., Conlon-Beckner, C., Fallis, L., Sevenich, D. M., Gupta, R., Dhugga, K. S., & Lübberstedt, T. (2013). N distribution in maize plant as a marker for grain yield and limits on its remobilization after flowering. *Plant Breeding*, n/a-n/a. https://doi.org/10.1111/pbr.12051

DeBruin, J. L., Schussler, J. R., Mo, H., & Cooper, M. (2017). Grain Yield and Nitrogen Accumulation in Maize Hybrids Released during 1934 to 2013 in the US Midwest. *Crop Science*, *0*(0), 0. https://doi.org/10.2135/cropsci2016.08.0704

Doering, O., Galloway, J., Theis, T., Aneja, V., Boyer, E., Cassman, K., Cowling, E., Dickerson, R., Herz, W., & Hey, D. (2011). Reactive Nitrogen in the United States: an analysis of inputs, flows, consequences, and management options. *United States Environmental Protection Agency*.

Donald, C. M. (1968). The breeding of crop ideotypes. *Euphytica*, *17*(3), 385-403. https://doi.org/10.1007/bf00056241

Duvick, D. N. (2005). The contribution of breeding to yield advances in maize (Zea mays L.). *Advances in Agronomy*, *86*, 83-145.

Echarte, L., Rothstein, S., & Tollenaar, M. (2008). The response of leaf photosynthesis and dry matter accumulation to nitrogen supply in an older and a newer maize hybrid. *Crop Science*, *48*(2), 656-665.

Elsayed, S., & Darwish, W. (2017). Hyperspectral remote sensing to assess the water status, biomass, and yield of maize cultivars under salinity and water stress. *Bragantia*, *76*, 62-72. http://www.scielo.br/scielo.php?script=sci_arttext&pid=S0006-87052017000100062&nrm=iso

Fernandez, J. A., DeBruin, J., Messina, C. D., & Ciampitti, I. A. (2020). Late-season nitrogen fertilization on maize yield: A meta-analysis. *Field Crops Research*, *247*, 107586.

Gastal, F., Lemaire, G., Durand, J.-L., & Louarn, G. (2015). Quantifying crop responses to nitrogen and avenues to improve nitrogen-use efficiency. In *Crop Physiology (Second Edition)* (pp. 161-206). Elsevier.

Gausman, H. W. (1977). Reflectance of leaf components. *Remote Sensing of Environment*, *6*(1), 1-9. https://doi.org/https://doi.org/10.1016/0034-4257(77)90015-3

Gausman, H. W., & Allen, W. A. (1973). Optical Parameters of Leaves of 30 Plant Species. *Plant Physiology*, *52*(1), 57-62. https://doi.org/10.1104/pp.52.1.57

Gautam, R., & Panigrahi, S. (2007). Leaf nitrogen determination of corn plant using aerial images and artificial neural networks. *Canadian Biosystems Engineering*, *49*, 7.

Goel, P. K., Prasher, S. O., Landry, J. A., Patel, R. M., Bonnell, R. B., Viau, A. A., & Miller, J. R. (2003). Potential of airborne hyperspectral remote sensing to detect nitrogen deficiency and weed infestation in corn. *Computers and Electronics in Agriculture*, *38*(2), 99-124. https://doi.org/https://doi.org/10.1016/S0168-1699(02)00138-2

Goel, P. K., Prasher, S. O., Landry, J. A., Patel, R. M., Viau, A. A., & Miller, J. R. (2003). Estimation of crop biophysical parameters through airborne and field hyperspectral remote sensing. *Transactions of the ASAE*, *46*(4), 1235-1246.

Greenwood, D., Neeteson, J., & Draycott, A. (1986). Quantitative relationships for the dependence of growth rate of arable crops on their nitrogen content, dry weight and aerial environment. In *Fundamental, Ecological and Agricultural Aspects of Nitrogen Metabolism in Higher Plants* (pp. 367-387). Springer.

Haboudane, D., Tremblay, N., Miller, J. R., & Vigneault, P. (2008). Remote Estimation of Crop Chlorophyll Content Using Spectral Indices Derived From Hyperspectral Data. *IEEE Transactions on Geoscience and Remote Sensing*, *46*(2), 423-437. https://doi.org/10.1109/tgrs.2007.904836

Haegele, J. W., Cook, K. A., Nichols, D. M., & Below, F. E. (2013). Changes in Nitrogen Use Traits Associated with Genetic Improvement for Grain Yield of Maize Hybrids Released in Different Decades. *Crop Science*, *53*(4), 1256. https://doi.org/10.2135/cropsci2012.07.0429

Hatfield, J. L., Gitelson, A. A., Schepers, J. S., & Walthall, C. L. (2008). Application of Spectral Remote Sensing for Agronomic Decisions. *Agronomy Journal*, *100*(Supplement_3), S-117. https://doi.org/10.2134/agronj2006.0370c

Huanxue, Z., Qiangzi, L., & Miao, Z. (2014). The Effects of Spatial Resolution on the Maize acreage estimation by Remote Sensing. IOP Conference Series: Earth and Environmental Science (EES),

Hunt Jr, E. R., Doraiswamy, P. C., McMurtrey, J. E., Daughtry, C. S., Perry, E. M., & Akhmedov, B. (2013). A visible band index for remote sensing leaf chlorophyll content at the canopy scale. *International Journal of Applied Earth Observation and Geoinformation*, *21*, 103-112.

IFA Statistics. (2016). http://www.fertilizer.org/statistics

Inoue, Y., Guerif, M., Baret, F., Skidmore, A., Gitelson, A., Schlerf, M., Darvishzadeh, R., & Olioso, A. (2016). Simple and robust methods for remote sensing of canopy chlorophyll content: a comparative analysis of hyperspectral data for different types of vegetation. *Plant Cell Environ*, *39*(12), 2609-2623. https://doi.org/10.1111/pce.12815

Jiang, Z., Chen, Y., Li, J., & Dou, W. (2005). The impact of spatial resolution on NDVI over heterogeneous surface. *RN*, *2*(2), 2.

Jin, X., Zarco-Tejada, P., Schmidhalter, U., Reynolds, M. P., Hawkesford, M. J., Varshney, R. K., Yang, T., Nie, C., Li, Z., & Ming, B. (2020). High-throughput estimation of crop traits: A review of ground and aerial phenotyping platforms. *IEEE Geoscience and Remote Sensing Magazine*, 1-33.

Karimi, Y., Prasher, S., Madani, A., & Kim, S. (2008). Application of support vector machine technology for the estimation of crop biophysical parameters using aerial hyperspectral observations. *Canadian Biosystems Engineering*, *50*(7), 13-20.

Kempeneers, P., De Backer, S., Debruyn, W., Coppin, P., & Scheunders, P. (2005). Generic wavelet-based hyperspectral classification applied to vegetation stress detection. *IEEE Transactions on Geoscience and Remote Sensing*, *43*(3), 610-614.

Lawanson, A. O., Akindele, B. B., Fasalojo, P. B., & Akpe, B. L. (1972). Time-course of anthocyanin formation during deficiencies of nitrogen, phosphorus and potassium in seedlings of zea mays Linn. var. E.S. 1. *Zeitschrift für Pflanzenphysiologie*, *66*(3), 251-253. https://doi.org/https://doi.org/10.1016/S0044-328X(72)80079-5

Lemaire, G., & Gastal, F. (1997). N uptake and distribution in plant canopies. In *Diagnosis of the nitrogen status in crops* (pp. 3-43). Springer.

Li, F., Miao, Y., Feng, G., Yuan, F., Yue, S., Gao, X., Liu, Y., Liu, B., Ustin, S. L., & Chen, X. (2014). Improving estimation of summer maize nitrogen status with red edge-based spectral vegetation indices. *Field Crops Research*, *157*, 111-123. https://doi.org/10.1016/j.fcr.2013.12.018

Lillesand, T., Kiefer, R. W., & Chipman, J. (2014). *Remote sensing and image interpretation*. John Wiley & Sons.

Liu, M., Yu, T., Gu, X., Sun, Z., Yang, J., Zhang, Z., Mi, X., Cao, W., & Li, J. (2020). The Impact of Spatial Resolution on the Classification of Vegetation Types in Highly Fragmented Planting Areas Based on Unmanned Aerial Vehicle Hyperspectral Images. *Remote Sensing*, *12*(1), 146.

Mahajan, G. R., Sahoo, R. N., Pandey, R. N., Gupta, V. K., & Kumar, D. (2014). Using hyperspectral remote sensing techniques to monitor nitrogen, phosphorus, sulphur and potassium in wheat (Triticum aestivum L.) [journal article]. *Precision Agriculture*, *15*(5), 499-522. https://doi.org/10.1007/s11119-014-9348-7

Markwell, J., Osterman, J. C., & Mitchell, J. L. (1995). Calibration of the Minolta SPAD-502 leaf chlorophyll meter. *Photosynthesis Research*, *46*(3), 467-472.

Masoni, A., Ercoli, L., & Mariotti, M. (1996). Spectral Properties of Leaves Deficient in Iron, Sulfur, Magnesium, and Manganese. *Agronomy Journal*, *88*(6), 937-943. https://doi.org/10.2134/agronj1996.00021962003600060015x

Moll, R. H., Kamprath, E. J., & Jackson, W. A. (1982). Analysis and Interpretation of Factors Which Contribute to Efficiency of Nitrogen Utilization. *Agronomy Journal*, *74*, 562-564. https://doi.org/10.2134/agronj1982.00021962007400030037x

Moose, S., Below, F. (2009). Biotechnology approaches to improving maize nitrogen use efficiency. In A. L. Kriz & B. A. Larkins (Eds.), *Molecular genetic approaches to maize improvement* (pp.65-77). Springer Berlin Heidelberg. https://doi.org/10.1007/978-3-540-68922-5_6

Mueller, S. M., Messina, C. D., & Vyn, T. J. (2019). Simultaneous gains in grain yield and nitrogen efficiency over 70 years of maize genetic improvement. *Sci Rep*, *9*(1), 1-8.

Mulla, D. J. (2013). Twenty five years of remote sensing in precision agriculture: Key advances and remaining knowledge gaps. *Biosystems Engineering*, *114*(4), 358-371. https://doi.org/10.1016/j.biosystemseng.2012.08.009

Muñoz-Huerta, R. F., Guevara-Gonzalez, R. G., Contreras-Medina, L. M., Torres-Pacheco, I., Prado-Olivarez, J., & Ocampo-Velazquez, R. V. (2013). A review of methods for sensing the nitrogen status in plants: advantages, disadvantages and recent advances. *Sensors*, *13*(8), 10823-10843. https://doi.org/10.3390/s130810823

Osborne, S. L., Schepers, J. S., Francis, D. D., & Schlemmer, M. R. (2002a). Detection of Phosphorus and Nitrogen Deficiencies in Corn Using Spectral Radiance Measurements. *Agronomy Journal*, *94*(6), 1215-1221. https://doi.org/10.2134/agronj2002.1215

Osborne, S. L., Schepers, J. S., Francis, D. D., & Schlemmer, M. R. (2002b). Use of spectral radiance to estimate in-season biomass and grain yield in nitrogen- and water- stressed corn. *Crop Science*, *42*(1), 165-171.

Pinter, P. J. J., Hatfield, J. L., Schepers, J., Daughtry, C., Barnes, E., Moran, M. S., & Upchurch, D. R. (2003). Remote Sensing for Crop Management. *Photogrammetric Engineering & Remote sensing*, *69*(6), 647-664.

Pons, T., Lambers, H., & Chapin III, F. (2008). Plant physiological ecology.

Quemada, M., Gabriel, J., & Zarco-Tejada, P. (2014). Airborne Hyperspectral Images and Ground-Level Optical Sensors As Assessment Tools for Maize Nitrogen Fertilization. *Remote Sensing*, *6*(4), 2940-2962. https://doi.org/10.3390/rs6042940

Ribaudo, M., Hansen, L., Livingston, M., Mosheim, R., Williamson, J., & Delgado, J. (2011). Nitrogen in agricultural systems: Implications for conservation policy.

Ribaudo, M., Livingston, M., & Williamson, J. (2012). *Nitrogen Management on US Corn Acres, 2001-2010* (Economic Brief, Issue.

Rodrigues Junior, F., Ortiz-Monasterio, I., Zarco-Tejada, P. J., Ammar, K., & Gérard, B. (2014). Using precision agriculture and remote sensing techniques to improve genotype selection in a breeding program.

Sadras, V. O., & Calderini, D. F. (2015). *Crop physiology: applications for genetic improvement and agronomy* (V. O. Sadras & D. F. Calderini, Eds. 2nd ed.). Academic Press.

Sadras, V. O., & Lemaire, G. (2014). Quantifying crop nitrogen status for comparisons of agronomic practices and genotypes. *Field Crops Research*, *164*, 54-64. https://doi.org/10.1016/j.fcr.2014.05.006

Sahoo, R. N., Ray, S. S., & Manjunath, K. R. (2015). Hyperspectral remote sensing of agriculture [Article]. *Current Science (00113891)*, *108*(5), 848-859. http://search.ebscohost.com/login.aspx?direct=true&db=aph&AN=101659167&site=ehost-live

Salvagiotti, F., Castellarín, J. M., Miralles, D. J., & Pedrol, H. M. (2009). Sulfur fertilization improves nitrogen use efficiency in wheat by increasing nitrogen uptake. *Field Crops Research*, *113*(2), 170-177. https://doi.org/https://doi.org/10.1016/j.fcr.2009.05.003

Sawyer, J. E., Lundvall, J., Hawkins, J. S., & Barker, D. W. (2011). Sensing nitrogen stress in corn.

Schepers, J. S., Francis, D. D., Vigil, M., & Below, F. E. (1992). Comparison of corn leaf nitrogen concentration and chlorophyll meter readings. *Communications in Soil Science and Plant Analysis*, *23*(17-20), 2173-2187. https://doi.org/10.1080/00103629209368733

Schlemmer, M., Gitelson, A., Schepers, J., Ferguson, R., Peng, Y., Shanahan, J., & Rundquist, D. (2013). Remote estimation of nitrogen and chlorophyll contents in maize at leaf and canopy levels. *International Journal of Applied Earth Observation and Geoinformation*, *25*, 47-54. https://doi.org/https://doi.org/10.1016/j.jag.2013.04.003

Schlemmer, M. R., Francis, D. D., Shanahan, J., & Schepers, J. S. (2005). Remotely measuring chlorophyll content in corn leaves with differing nitrogen levels and relative water content. *Agronomy Journal*, *97*(1), 106-112.

Sims, D. A., & Gamon, J. A. (2002). Relationships between leaf pigment content and spectral reflectance across a wide range of species, leaf structures and developmental stages. *Remote Sensing of Environment*, *81*(2), 337-354.

Thenkabail, P. S., Gumma, M. K., Teluguntla, P., & Mohammed, I. A. (2014). Hyperspectral remote sensing of vegetation and agricultural crops. *Photogrammetric Engineering & Remote Sensing (PE&RS)*, *80*(8), 697-723.

Thenkabail, P. S., Lyon, J. G., & Huete, A. (2012). *Hyperspectral remote sensing of vegetation* (P. S. Thenkabail, J. G. Lyon, & A. Huete, Eds.) [Book]. CRC Press.

Thenkabail, P. S., Smith, R. B., & De Pauw, E. (2000). Hyperspectral vegetation indices and their relationships with agricultural crop characteristics. *Remote Sensing of Environment*, *71*(2), 158-182.

Thorp, K., French, A., & Rango, A. (2013). Effect of image spatial and spectral characteristics on mapping semi-arid rangeland vegetation using multiple endmember spectral mixture analysis (MESMA). *Remote Sensing of Environment*, *132*, 120-130.

Tollenaar, M., & Wu, J. (1999). Yield Improvement in Temperate Maize is Attributable to Greater Stress Tolerance. *Crop Science*, *39*(6), 1597. https://doi.org/10.2135/cropsci1999.3961597x

Uhart, S. A., & Andrade, F. H. (1995a). Nitrogen Defeciency in Maize: I. Effects on Crop Growth, Development, Dry Matter Partitioning, and Kernel Set. *Crop Science*, *35*(5), 1376-1383. https://doi.org/10.2135/cropsci1995.0011183X003500050020x

Uhart, S. A., & Andrade, F. H. (1995b). Nitrogen Deficiency in Maize: II. Carbon-Nitrogen Interaction Effects on Kernel Number and Grain Yield. *Crop Science*, *35*(5), 1384-1389. https://doi.org/10.2135/cropsci1995.0011183X003500050021x

Unkovich, M., Herridge, D., Peoples, M., Cadisch, G., Boddey, B., Giller, K., Alves, B., & Chalk, P. (2008). *Measuring plant-associated nitrogen fixation in agricultural systems*. Australian Centre for International Agricultural Research (ACIAR).

Uno, Y., Prasher, S. O., Lacroix, R., Goel, P. K., Karimi, Y., Viau, A., & Patel, R. M. (2005). Artificial neural networks to predict corn yield from Compact Airborne Spectrographic Imager data. *Computers and Electronics in Agriculture*, *47*(2), 149-161. https://doi.org/10.1016/j.compag.2004.11.014

Viña, A., Gitelson, A. A., Nguy-Robertson, A. L., & Peng, Y. (2011). Comparison of different vegetation indices for the remote assessment of green leaf area index of crops. *Remote Sensing of Environment*, *115*(12), 3468-3478.

Walburg, G., Bauer, M. E., Daughtry, C., & Housley, T. (1982). Effects of nitrogen nutrition on the growth, yield, and reflectance characteristics of corn canopies. *Agronomy Journal*, *74*(4), 677-683.

Walters, D. (2003). Diagnosis of nitrogen deficiency in maize and the influence of hybrid and plant density. North central extension-industry soil fertility conference,

White, J. W., Andrade-Sanchez, P., Gore, M. A., Bronson, K. F., Coffelt, T. A., Conley, M. M., Feldmann, K. A., French, A. N., Heun, J. T., Hunsaker, D. J., Jenks, M. A., Kimball, B. A., Roth, R. L., Strand, R. J., Thorp, K. R., Wall, G. W., & Wang, G. (2012). Field-based phenomics for plant genetics research. *Field Crops Research*, *133*, 101-112. https://doi.org/10.1016/j.fcr.2012.04.003

Yendrek, C. R., Tomaz, T., Montes, C. M., Cao, Y., Morse, A. M., Brown, P. J., McIntyre, L. M., Leakey, A. D., & Ainsworth, E. A. (2017). High-Throughput Phenotyping of Maize Leaf Physiological and Biochemical Traits Using Hyperspectral Reflectance. *Plant Physiol*, *173*(1), 614-626. https://doi.org/10.1104/pp.16.01447

Yoder, B. J., & Pettigrew-Crosby, R. E. (1995). Predicting nitrogen and chlorophyll content and concentrations from reflectance spectra (400–2500 nm) at leaf and canopy scales. *Remote Sensing of Environment*, *53*(3), 199-211.

Zhao, B., Duan, A., Ata-Ul-Karim, S. T., Liu, Z., Chen, Z., Gong, Z., Zhang, J., Xiao, J., Liu, Z., Qin, A., & Ning, D. (2018). Exploring new spectral bands and vegetation indices for estimating nitrogen nutrition index of summer maize. *European Journal of Agronomy*, *93*, 113-125. https://doi.org/10.1016/j.eja.2017.12.006

Zhao, D., Raja Reddy, K., Kakani, V. G., Read, J. J., & Carter, G. A. (2003). Corn (Zea mays L.) growth, leaf pigment concentration, photosynthesis and leaf hyperspectral reflectance properties as affected by nitrogen supply. *Plant and Soil*, *257*(1), 205-218. https://doi.org/10.1023/a:1026233732507

Zhou, K., Cheng, T., Zhu, Y., Cao, W., Ustin, S. L., Zheng, H., Yao, X., & Tian, Y. (2018). Assessing the Impact of Spatial Resolution on the Estimation of Leaf Nitrogen Concentration Over the Full Season of Paddy Rice Using Near-Surface Imaging Spectroscopy Data. *Frontiers in Plant Science*, *9*, 964-964. https://doi.org/10.3389/fpls.2018.00964

CHAPTER 2. PHYSIOLOGICAL- AND IMAGERY-BASED SECONDARY TRAITS FOR NITROGEN INTERNAL EFFICIENCY COMPARISONS IN TEST-CROSS MAIZE HYBRIDS

2.1 Abstract

Development of maize hybrids capable of using N more efficiently can lead to environmental benefits as well as helping farmers increase yields in nutrient-deficit production and realize higher profits by reducing fertilization costs. However, because breeding for N-improved hybrids is labor intensive and expensive, improvements in current methods are needed. Research was conducted to investigate in-season parameters that may help identify more N efficient genotypes at maturity in terms of grain yields or yield per unit of accumulated plant N (Nitrogen Internal Efficiency, NIE). A total of 285 hybrids in both early and late maturity groups from Dow AgroSciences (DAS; where 242 hybrids were derived from test crosses to a single tester) and USDA germplasm (33 hybrids), plus 10 replicated checks, were grown under low N conditions (67 kg N ha^{-1}) at two Indiana locations in 2015. Secondary traits such as plant height, stalk diameter, and LAI were collected at R1 while LAI, leaf SPAD and green leaf counts were collected at R2/R3. Additionally, two vegetation indices (NDVI and SR) from imaging at R1 and R3/R4 were studied for their relationships to final grain yield, total plant N and hybrid NIE differences. Top performing hybrids for grain (DAS026 and DAS166) and NIE (DAS039 and DAS087) were identified as significantly different from the bottom hybrids in both traits. No secondary traits were found to be strongly correlated to NIE, while leaf SPAD (at R2/R3) measurements were strongly correlated ($r > 0.60$) to both yields and plant N. However, mixed models based on the SPAD measurements did not provide hybrid rankings similar to those based on yield, indicating challenges with using SPAD from the ear-leaf as a surrogate measure. Vegetation indices from imaging were unsuccessful for prediction of plant N or grain yield at maturity using linear regression models ($R^2 < 0.35$). Imaging-based mixed models were also unable to detect significant differences between hybrids or maturity groups ($P > 0.05$). Unfortunately, the efforts to identify secondary in-season traits predictive of NIE, whether via physiological measurements or through imagery, when these hybrids were grown at a single low N rate were unsuccessful and further research is encouraged.

2.2 Introduction

Nitrogen (N) is an essential nutrient in agriculture necessary for plant growth and adequate yields (Ribaudo et al., 2011). With the advent of the Haber-Bosch process in the early 1900s which produced cheap N fertilizer, agricultural yields increased (Erisman et al., 2008; Follett et al., 2010). However, excess fertilization can result in significant human health and environmental effects (Doering et al., 2011; Ribaudo et al., 2011). Studies of worldwide trends have identified improvements in agronomic and environmental trends of N use in some countries but not in others (Lassaletta et al., 2014). Agronomic advances such as better N management, reduced N inputs, and increased use of legumes in crop rotation have increased N use efficiency (Lassaletta et al., 2014). Thus a goal for agricultural researchers has been to study and improve the efficiency at which a plant uses N – thus produce more grain yield per unit of fertilizer provided (N Use Efficiency, NUE) (Moll et al., 1982). How a plant uses N for production of yield is a complex process. This process is affected by a plant's ability to uptake N during the growing season, use it for vegetative growth and eventually remobilize and uptake additional N for the successful production of viable seeds (Moll et al., 1982; Salvagiotti et al., 2009). In investigating these dynamics, researchers have found it useful to break NUE down into its components of N Internal Efficiency (NIE) and N Recovery Efficiency (NRE) (Ciampitti & Vyn, 2011; Moll et al., 1982; Salvagiotti et al., 2009). As defined by scientists, NIE is the amount of grain yield produced per unit of N in the plant and thus measures efficiency in conversion of N while NRE is the amount of N in the plant per unit N fertilizer provided to the plant, a measure of the plant's uptake efficiency (Ciampitti & Vyn, 2011; Moll et al., 1982; Salvagiotti et al., 2009).

Recent U.S. trends have shown increasing NUE in maize growing areas, though in some major maize producing states, NUE levels increased for 1970 to 1999, but then began decreasing after 2000 (Lu et al., 2019). The increases are largely due to yield increases from improved genetics, more irrigation, greater stress tolerance and improved management (Castleberry et al., 1984; Duvick, 1997; Tollenaar & Wu, 1999; Ying et al., 2000). Studies have investigated differences between older and newer hybrids and have found that newer hybrids are more N efficient (NUE) (Ciampitti & Vyn, 2012; Haegele et al., 2013; Mueller et al., 2019). This improvement is largely driven by an increase in NIE from older to newer hybrids (Ciampitti & Vyn, 2012). However, these improvements have been due to indirect breeding efforts focused on yield improvements and

not specific N-breeding efforts (Ciampitti & Vyn, 2012; Moose & Below, 2009). It has been well documented that genotype impacts NUE (Ciampitti & Vyn, 2011; D'Andrea et al., 2009) yet researchers have suggested that it may not be possible to improve yield with the current genetics since at high N fertilization levels yields flatten and NUE decreases (Lu et al., 2019). However, methods have been developed for breeding genotypes for low N environments such as those published by CIMMYT (Banziger et al., 2000). Additionally, global N research has identified genotypes capable of tolerating low N conditions (Garnett et al., 2015; Gondwe, 2014) suggesting there is real potential for improving N efficiencies within the current genetics.

Ciampitti and Vyn (2011) opined that breeding for N improvement is likely to be difficult since plants with the highest yields are often not the most N-efficient. However, NIE varies a great deal depending on the environment or management practices and seems to be closely linked to kernel number and kernel weight development (Ciampitti & Vyn, 2011), thus breeding improvements in NIE may be easier to target than NUE. Also, due to the impact of grain yield on NIE, this variable seems to balance the economic productivity critical for growers and potential environmental benefits at the ecological level.

However, breeding for N is expensive since the methods necessary for N determination of tissue samples, such as the gold-standard method of Dumas combustion, require intensive efforts in both the field and laboratory often multiple times throughout the growing season (Muñoz-Huerta et al., 2013; Unkovich et al., 2008; Zhao et al., 2003). Additionally, phenotyping is essential even with the advent of molecular breeding strategies (Araus & Cairns, 2014). High throughput efforts are being investigated by various seed companies, governmental organizations and plant research institutions through several avenues, including remote imaging (Araus & Cairns, 2014). Vegetation indices, which are calculations of reflectance or digital brightness values from remote imaging, have been studied for prediction of physiological measures such as biomass or LAI (Campbell & Wynne, 2011; Mulla, 2013).

Because of the need to identify genotypes with improved NUE under midwestern environments and to assist in genetic selection through improved phenotyping methods in maize, two intensive field-based studies were conducted primarily to investigate NIE in approximately 300 maize hybrids grown under low N conditions. NIE was chosen as the focused N parameter because

previous research by Ciampitti and Vyn (2011) indicated it may be an easier target than NUE, especially due to its close link to kernel number and kernel weight. Also, this metric integrates both economics (grain yield produced) and environment (N availability and plant uptake of N). The main objectives addressed in this study were to: (1) assess and identify hybrids significantly different from each other in NIE or grain yield when grown under low N conditions; (2) evaluate physiological measures for strong correlations to NIE as potential surrogate measurements of NIE; and (3) conduct an exploratory investigation of remote aerial imagery examining relationships between vegetation indices and crop physiological characteristics as well as differences among maize hybrids.

2.3 Methodology

Field studies involving 285 hybrids were conducted at two Purdue agricultural centers in Indiana in 2015. In West Lafayette, IN, seeds provided by DAS were planted on May 9, 2015, at the Agricultural Center for Research and Education (ACRE) in silty clay loam soil with a Raub-Brenton complex. Farther north in Wanatah, IN, the field experiment was located on a loamy soil (Sebawa Loam) at the Pinney Purdue Agricultural Center (PPAC). The planting date at PPAC was May 19, 2015. In both cases, field areas used had soybean planted in 2014 so that the fields represented the common maize-soybean rotation that dominates agriculture in the Eastern Cornbelt.

2.3.1 Soil Fertility

Soil from the top 20 cm was analyzed for fertility measurements after sampling (one composite sample per field rep) on May 18, 2015, at ACRE and June 5, 2015, at PPAC. Soils in both fields had similar pH levels (Table 2.1). Phosphorus (P) and potassium (K) levels were above or near the critical soil test levels (15 ppm for P; ~ 115 -119 ppm for K). N soil levels (NO_3^- or NH_4 +) were not measured. The secondary nutrients measured, magnesium and calcium, were well above adequate levels for crop production (≥50 ppm and ≥200ppm, respectively). The range of the soil cation exchange capacity (CEC) is typical for the soil types used.

Table 2.1. Soil fertility analysis results

Location	pH	Organic Matter (%)	Phosphorus (ppm)	Potassium (ppm)	Magnesium (ppm)	Calcium (ppm)	CEC
ACRE	6.3	3.5	13	130	492	1932	16.1
PPAC	6.1	4.4	22	105	530	1959	17.7

2.3.2 Weather

Weather data was collected at each agricultural center and is reported below in the results section.

2.3.3 Experimental Design

A modified augmented design was employed to evaluate the 285 hybrids at each location. Multiple replicates (6 or more) of 10 Checks were planted. Remaining entries from two different seed sources (DAS and USDA) were planted in triplicate 4-row plots (7.6m x 3.0m). All entries had been crossed with a common female tester (2FACC). Entries were grouped by two maturity groups, early and late. See Table 2.2 for the exact number of hybrids by maturity group.

Table 2.2. Number of hybrids for each maturity group and seed source

Maturity Group	Source	Number of Hybrids	Number of Replicates per Hybrid
Early	Check	6	6+
	Dow AgroSciences	139	3
	USDA	12	3
Late	Check	4	6+
	Dow AgroSciences	103	3
	USDA	21	3

Maize borders were planted around and between each replicate block. Urea ammonium nitrate (UAN) was applied pre-plant at a rate of 67 kg N ha^{-1}. A single N rate was chosen to limit the sampling efforts needed in this extremely large experiment with nearly 300 hybrids. The low N rate was selected to induce yet manage N stress as recommended by Banziger et al. (2000). Seeding density with the 4-row precision planter was approximately 89,000 plants ha^{-1}.

2.3.4 Sampling Methodology

Biomass sampling and all in-season physiological measurements obtained were conducted on 10 representative plants selected from rows 2 or 3 of each 4-row plot. At the R1 stage, plant height, stalk diameter (widest portion of 1st node), percent silking, and ear-leaf SPAD (chlorophyll meter SPAD-502Plus from Konica Minolta, Inc., Tokyo, Japan) measurements were obtained. Between R2 and R3 another ear-leaf SPAD measurement and two total retained green leaf counts were collected. At R5 leaf area index measurements were collected with a LAI-2200C Plant Canopy Analyzer (LI-COR Biosciences, NE, USA). Finally, at R6 biomass sampling was conducted for determining fresh and dried stover and ear weights as well as kernel number and weights. Nitrogen content and concentration of the stover, kernels and ears were measured. After further drying, a plot combine was employed to determine yield and moisture content from the center 2 rows. All combine grain yield data was adjusted to a consistent 15.5% moisture content.

2.3.5 Remote Sensing Data Sources

No imagery from Digital Globe Worldview-3 was available for the required period at ACRE [40 29 4.1393 N, 86 59 44.0343 W] or PPAC [41 26 37.2255 N, 86 56 28.4595 W]). Consequently, all procedures were conducted using the 4 aerial georeferenced geotiff images from GeoVantage (Peabody, MA). GeoVantage also provided jpg images of RGB and NDVI images they processed and generated. Images at ACRE were acquired on July 21, 2015 and August 22, 2015. The PPAC images were acquired on July 31, 2015, and August 24, 2015. At the first image acquisition date, the maize plants were developmentally at R1 and at R3/4 during the second imaging date at each location.

Geotiff images consisted of 4 bands in the near-infrared (NIR), red (R), green (G), and blue (B) wavelengths. According to personal communication with GeoVantage personnel, sensors were calibrated for pixel alignment prior to the mission and the cameras' gain and shutter time were adjusted over the target for each flight separately. Each camera was calibrated independently for 60 out of 255 counts to achieve good exposure without saturation.

Data were not corrected for sun angle or atmosphere. No reference panels or ground control points were used. Data provided were digital numbers, not reflectance data. GeoVantage reported that

data were corrected for backscatter, shadows, and flight motion. Proprietary auto-vignetting was used to create each mosaicked image. After that, brightness was adjusted separately by GeoVantage for each band with NIR, R, and G normalized to 1500 counts and B normalized to 1100 counts. Histograms of R1 images at each location are shown below (Figure 2.1 and Figure 2.2). The x-axis shows brightness of each pixel (0 = minimum, black; 255 = maximum, white) and the y-axis are pixel counts. Note how the RGB histograms start at 0 and are quite similar across the same image, evidence of the separate band adjustment described above.

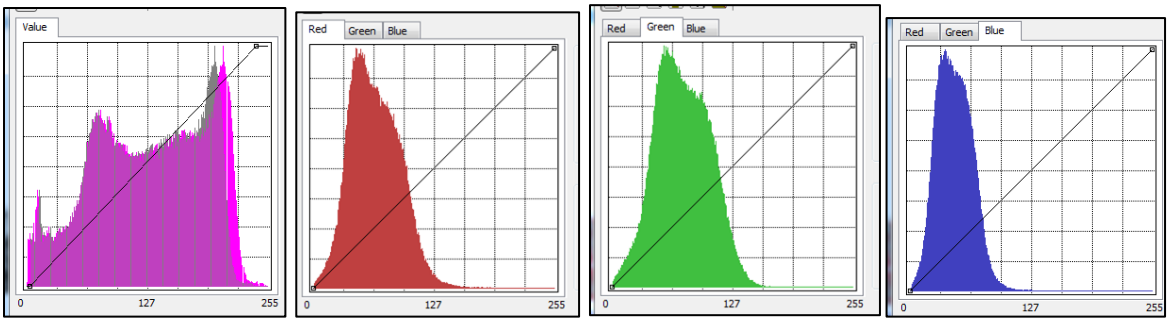

Figure 2.1. Histograms for R1 geotiff image at ACRE (NIR, R, G and B bands)

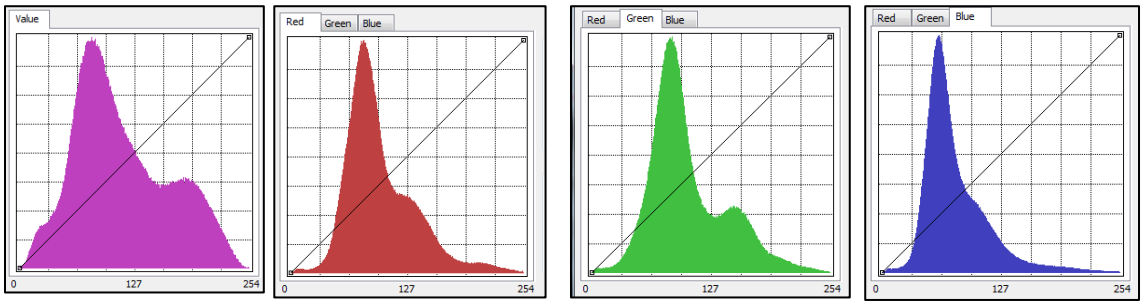

Figure 2.2. Histograms for R1 geotiff image at PPAC (NIR, R, G and B bands)

2.3.6 Remote Sensing Processing Procedures

Processing of geotiff remote sensing imagery was conducted using ArcMap (Environmental Systems Research Institute, Inc., Redlands, CA).

Georeferencing Images

Figure 2.3. 8/22/16 geotiff RGB image from ACRE with control points circled in black

Upon close inspection of the geotiff images, it was noted that the images at ACRE were slightly distorted from each other thus georeferencing was performed to co-register the images. Six control points, some circled in black, were selected on the images (Figure 2.3). Because there were no pre-determined ground control points during imaging nor any physical structures in the images themselves, these hand-selected control points were difficult to align. At high zoom levels it became evident that the shadows in the images were distorting the field edges being used to perform the georeferencing and thus it was difficult to determine precisely where the field edges lay. During planting two passes were misaligned on the western and eastern ends of the field (Figure 2.3 and Figure 2.6). This planting error at ACRE surprisingly benefited the subsequent differentiation of the edges for the control points.

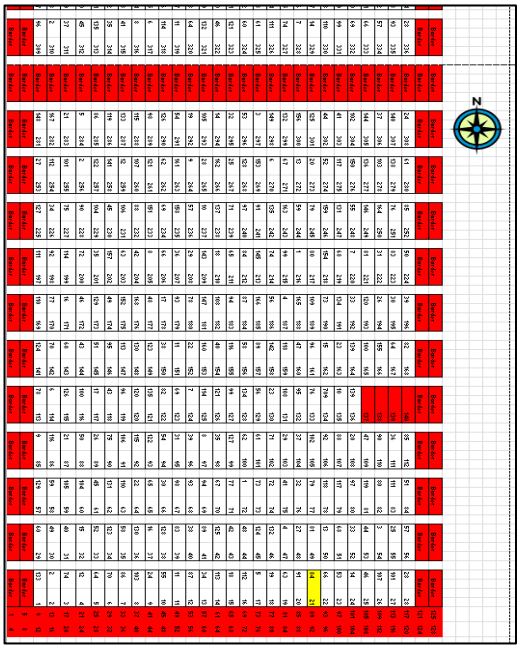

Figure 2.4. Portion of plot map for ACRE experiment as drawn in Microsoft Excel

Drawing Polygons

Polygons were drawn around each plot in the image to match the Microsoft Excel plot map shown in Figure 2.4. Plots were 3.0 m wide and 7.6 m long with a 0.8 m aisle between plots. The misaligned passes described above were drawn so the polygons incorporated this planting error. Figure 2.5 shows the eastern pass highlighted in blue and shifted

southward. The southern portion of the field at ACRE with the polygons drawn is shown in Figure 2.6.

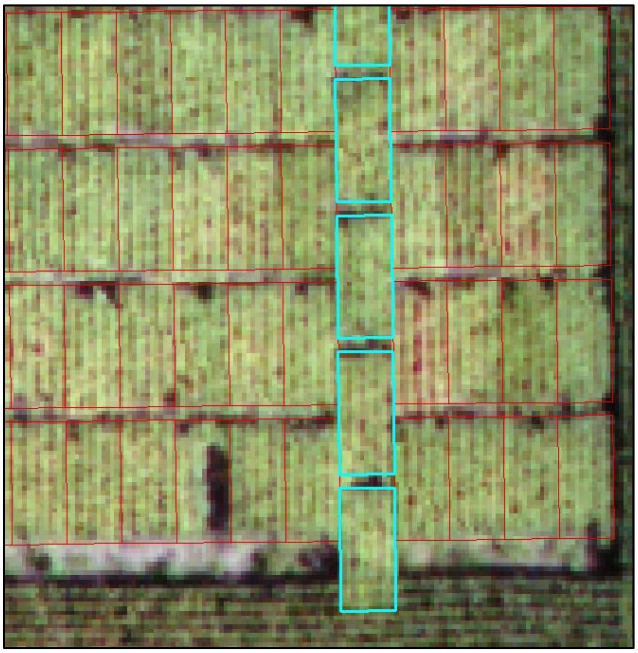

Figure 2.5. Eastern pass at ACRE mis-planted and shifted southward of other plots (highlighted in turquoise)

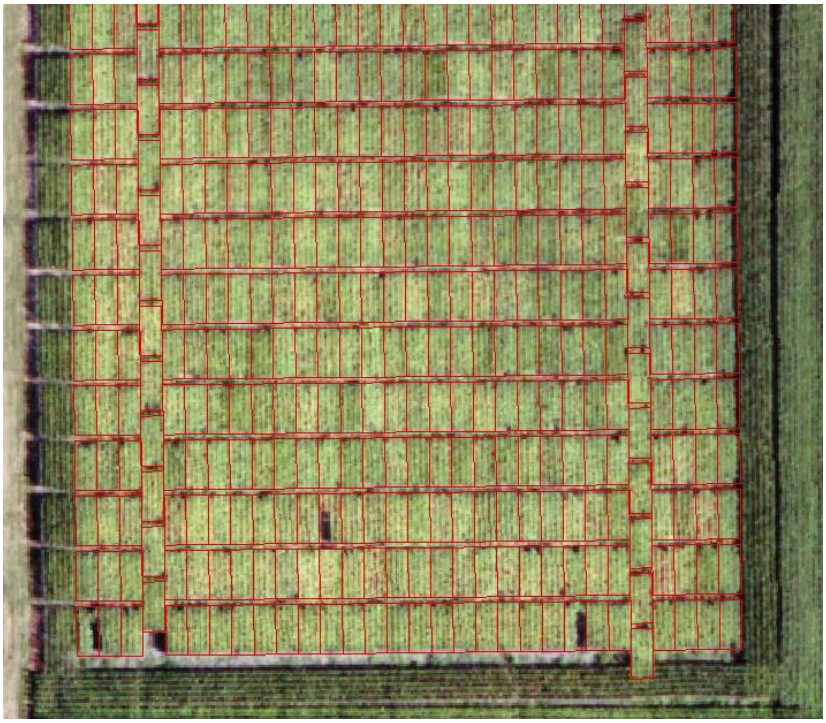

Figure 2.6. Polygons drawn in ACRE field; RGB geotiff image

2.3.7 Calculations – Phenotyping Data

As defined in the literature, NIE was calculated with the following equation:

NIE = Y/Total N

Where:

Y = Grain yield (kg ha^{-1} at 15.5% moisture) obtained from 10-plant biomass collection area

Total N = Plant nitrogen for stover and kernels from 10-plant biomass collection area (kg N ha^{-1})

Also, shelling grain harvest index (Grain HI) was defined as:

Grain HI = Y_0/BM

Where:

Y_0 = Grain yield (0% moisture) obtained from 10-plant biomass collection area (kg ha^{-1})

BM = Dry weight of stover and cobs from 10-plant biomass collection area (kg ha^{-1}) plus grain yield (0% moisture) obtained from 10-plant biomass collection area (kg ha^{-1})

2.3.8 Calculations – Remote Sensing Vegetation Indices

After labeling the polygons by plot number, the vegetation indices were calculated by bringing in the bands separately and using the raster calculator in the Map Algebra section of the Spatial Analyst Tools of ArcMap to calculate the following indices, each as a separate raster:

- NDVI = (NIR-R)/(NIR+R)
- Simple Ratio = R/NIR

2.3.9 Statistical Analysis

Restricted maximum likelihood (REML) mixed effects methods were used to analyze for significant effects ($\alpha = 0.05$) with either combine grain yield (adjusted to 15.5% moisture) or NIE as the response. Entries and maturity groups were considered fixed effects. For the imaging data mixed models, separated out by location (ACRE or PPAC) were used to analyze for significant effects ($\alpha = 0.05$) with NDVI or SR as the response. Entries and maturity groups were considered fixed effects while rep, pass[rep], range[rep], and rep*maturity group were the random effects. When effects were significant, a least square means Tukey HSD comparison ($\alpha = 0.05$) was run to determine significant differences within the means. Both SAS and JMP Pro (SAS Institute, Inc.) were used in the data analysis.

Linear regression models were analyzed for prediction of grain yield or plant N (not including cob N levels; termed Total Plant N) from the vegetation indices. Correlation matrices based on the pairwise method were generated for vegetation index responses versus grain yield or total plant N.

2.4 Results and Discussion

2.4.1 Weather

The weather in 2015 was much wetter than normal in spring and early summer, but August and September were much drier than normal. Maximum temperature and daily precipitation levels are shown for both locations in Figure 2.7 and Figure 2.8.

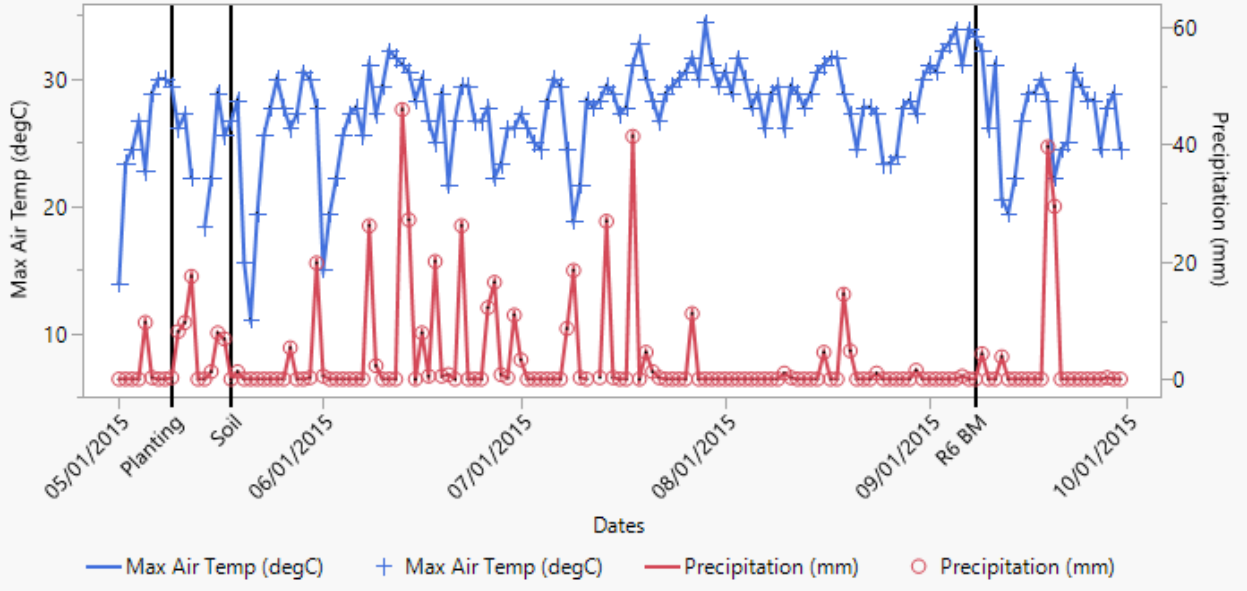

Figure 2.7. Daily weather conditions (maximum air temperature and precipitation) at ACRE. Planting = planting date. Soil = soil fertility collection date. R6 BM = Biomass collection date at R6 stage.

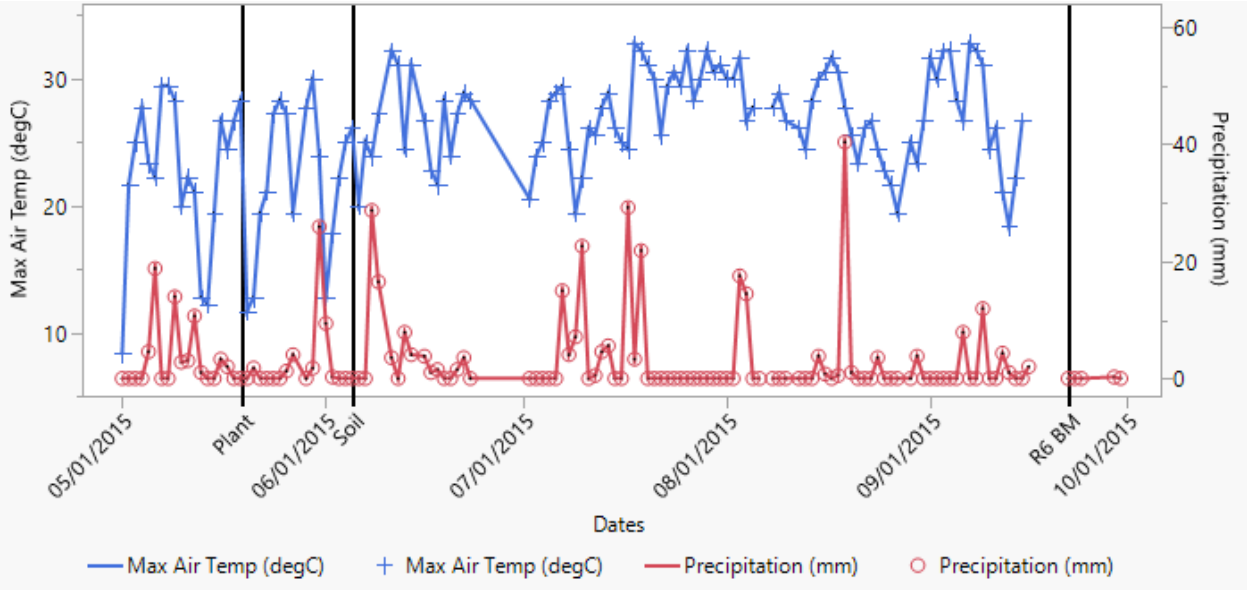

Figure 2.8. Daily weather conditions (maximum air temperature and precipitation) at PPAC. Plant = planting date. Soil = soil fertility collection date. R6 BM = Biomass collection date at R6 stage.

2.4.2 Planting Density

Final stand counts at V3-V4 averaged 84,000 plants ha^{-1} (34,000 plants per acre) with all seed sources (Checks, DAS, and USDA) and both locations very similar to each other.

2.4.3 General Performance-Combine Grain Yields

Overall mean combine maize grain yields at 15.5% moisture at ACRE were 8124 kg ha^{-1}. Yields by source differed with averages of 9038 kg ha^{-1} for Check hybrids, 8152 kg ha^{-1} (close to the overall experiment mean) for DAS hybrids and 7119 kg ha^{-1} for USDA hybrids. Overall yields at PPAC were higher than at ACRE with mean yields of 9637 kg ha^{-1}. Similar to ACRE, the yields for the Check hybrids at PPAC were higher (10,370 kg ha^{-1}). DAS hybrids yields were similar to the overall mean (9675 kg ha^{-1}) and USDA hybrids averaged 8476 kg ha^{-1}. See Appendix A (late maturity) and Appendix B (early maturity) for the mean yields for the top and bottom performing hybrids by maturity group across both locations.

A visual comparison of the mean combine yields by hybrid, maturity group, and location is shown below in Figure 2.9. Across locations, mean grain yields for early hybrids were lower than for the late maturity group hybrids. This is expected due to the shorter grain filling period of early maturing hybrids. The distribution of mean grain yields was approximately normal at both

locations and by maturity group, although the PPAC early group had more hybrids with yields higher than the mean and the PPAC late group's distribution tended to skew to the lower yields. Across maturity groups the trend previously described of yield differences by source continued (Checks > DAS > USDA).

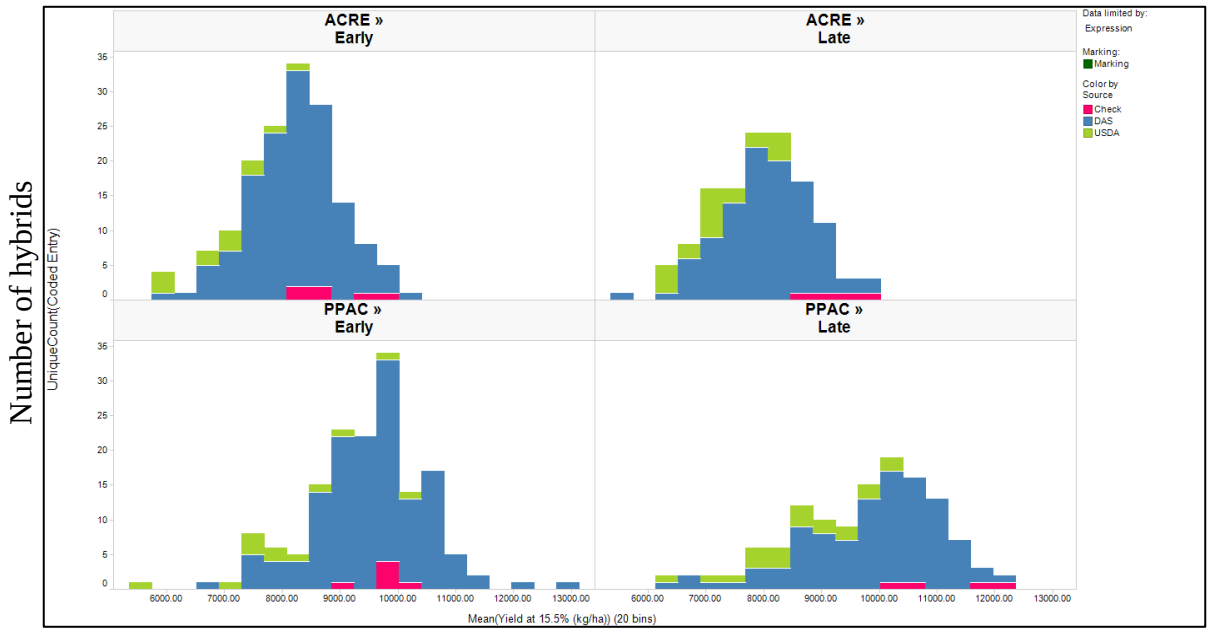

Figure 2.9. Grain yield averages at 15.5% moisture by location (ACRE or PPAC) and maturity group (early or late)

Heat maps of the combine grain yields for each plot on representative plot maps for each location are shown below in Figure 2.10 and Figure 2.11. Note that the color scales for each location represent different yield ranges but high yields are represented in red and low yields are represented in blue. With these maps it is clear to see that plot location within the field affected plant yields. At ACRE the yields in the top left corner (northwest corner) were lower than yields in the eastern quadrant (Figure 2.10). Due to the excessive rains during the summer there was ponding in the northwestern edges of the border near the experiment. Though no ponding was visible in the area of the experimental hybrids, yields apparently were detrimentally affected by the excessive moisture in that region. At PPAC there was no area of concentrated lower yields but there was one spot in the top right northeast quadrant of the field where yields trended higher than in other areas of the field (Figure 2.11).

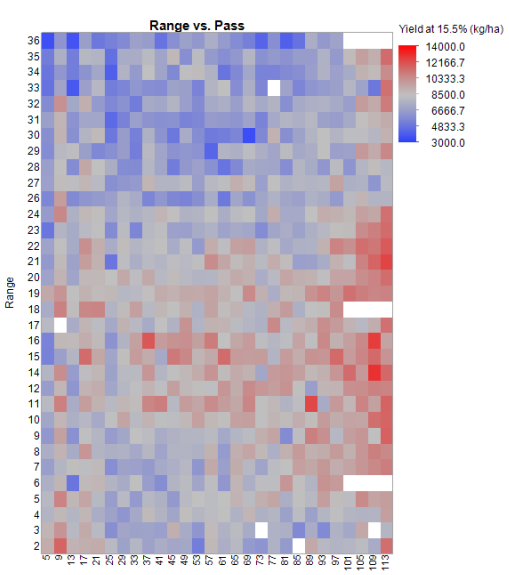

Figure 2.10. Heat map of grain yields (kg ha^{-1}) at ACRE for each plot organized by plot map

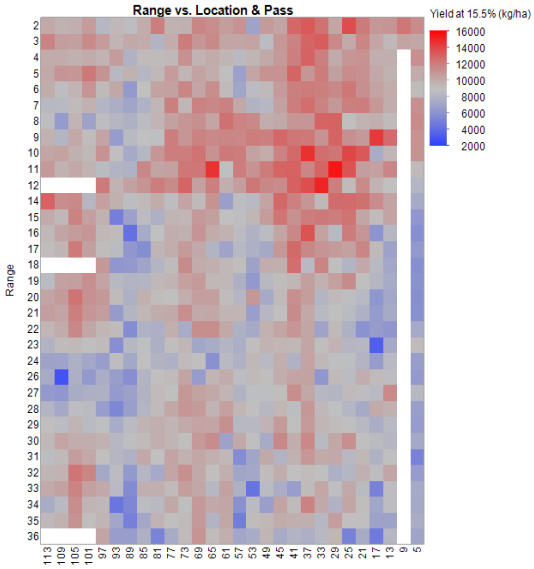

Figure 2.11. Heat map of grain yields (kg ha^{-1}) at PPAC for each plot organized by plot map

The patterns observed in yield differences were also reflected earlier in the season when RGB and NDVI jpg images were taken in late-August, at R3/R4 (Figure 2.12 and Figure 2.13). NDVI jpg images, which reflect plant stress as red and low stress as green, showed stressed plants in the northern quadrant at ACRE and decreased stress in the lower eastern quadrant (Figure 2.12). At PPAC lower stress levels were evident in the top right quadrant and higher stress in the southern quadrant (Figure 2.13).

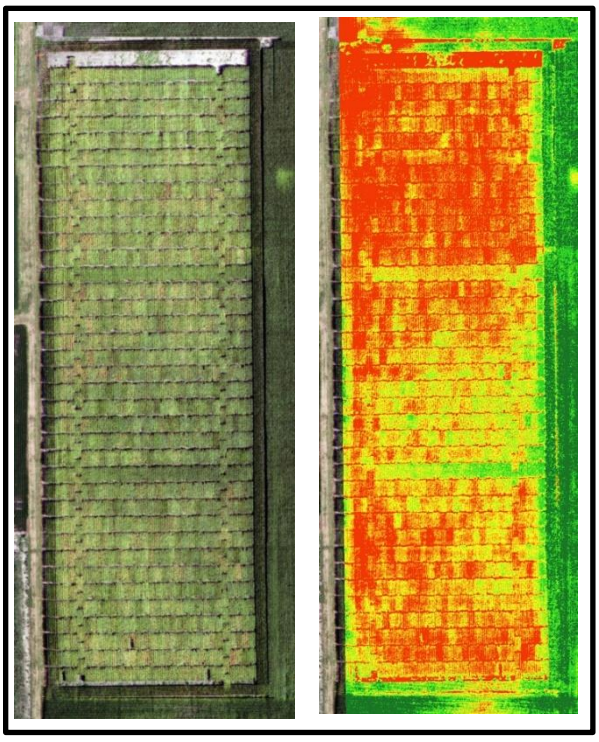

Figure 2.12. RGB (left) and NDVI (right) jpg images from ACRE on 8/22/15 (at R3/R4)

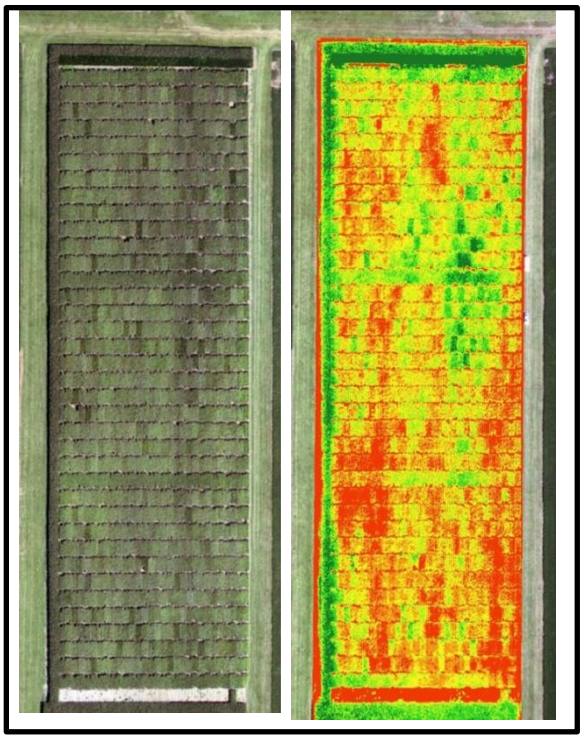

Figure 2.13. RGB (left) and NDVI (right) jpg images from PPAC on 8/24/15 (at R3/R4)

Mean grain harvest index values (Grain HI) were higher at ACRE than at PPAC for both maturity groups especially when comparing within sources (Table 2.3 and Table 2.4). Since yields were lower at ACRE, the increased Grain HI is due to lower overall biomass values. This difference is evident in the mean height and stalk diameter values also shown in Table 2.3 and Table 2.4. The ACRE plants (by source) had smaller stalks and shorter heights than the PPAC plants in each maturity group. The Grain HI differed by source across locations and maturity groups with a similar pattern of Check HI > DAS HI > USDA HI. Grain HI was at least 5% lower in the USDA hybrids versus the Check hybrids at both locations. The HI differential of 10 to 12%, depending on maturity group, was similar to that found by Mueller et al. (2019) in an era study evaluating hybrids from the 1940s to 2015. This was a much larger range than the 5% change in the era study by Haegele et al. (2013).

Table 2.3. Plant trait means for the early maturity group. Averages of plant height (height; cm), plant stalk diameter (stalk; mm), two SPAD readings (SPAD #1 and #2), leaf area index (LAI), kernel weight at 0% moisture (KW; mg kernel^{-1}), and estimated number of kernels per plant (Est. K P^{-1}), grain yield at 15.5% moisture (Yield; kg ha^{-1}), grain harvest index (Grain HI).

Sampling Stage		**R1**			**R2/R3**	**R5**	**R6**			
Location	**Source**	**Height (cm)**	**Stalk (mm)**	**SPAD #1**	**SPAD #2**	**LAI**	**KW (mg kernel^{-1})**	**Est. K P^{-1}**	**Yield (kg ha^{-1})**	**Grain HI**
ACRE	Check	222	22.3	45.7	40.3	2.6	218	385	8851	50.2
ACRE	DAS	213	21.0	44.9	38.3	2.4	222	359	8233	49.1
ACRE	USDA	212	20.9	42.9	36.2	2.8	235	297	6931	43.3
PPAC	Check	258	25.3	45.6	40.7	2.8	236	376	9888	45.4
PPAC	DAS	250	24.3	44.7	40.2	2.8	237	361	9539	44.7
PPAC	USDA	253	24.4	34.9	39.8	3.0	241	319	8199	39.8

Five additional physiological measurement means are shown for each maturity group in Table 2.3 and Table 2.4. They include leaf chlorophyll concentration (SPAD #1 and #2), leaf area index (LAI), kernel weight (KW) and the estimated number of kernels per plant (Est. K/P). In terms of the grain components, the mean number of kernels per plant were always highest for the Checks, the DAS hybrids were second in number, and the USDA hybrids lowest regardless of maturity group at each location (K/P = Checks > DAS > USDA). The number of kernels in this experiment were lower than those found by Haegele et al. (2013) at a similar N rate. Instead, these counts were more like Haegele's at 0N. The pattern for kernel weights was different across sources depending on the maturity group. For the early hybrids, USDA hybrid kernels were heaviest, the DAS kernels were lighter, and the Check kernels were lightest of all (KW_{early} = USDA > DAS > Checks). For the late maturity group at ACRE the Check kernels were heaviest (ACRE KW_{late} = Checks > USDA = DAS) while at PPAC the DAS kernels were heaviest (PPAC KW_{late} = DAS > Checks > USDA). The kernel weights in this study match weights for hybrids from the 1980s-2000s grown side-by-side at 67 kg N ha^{-1} fertilizer (Haegele et al., 2013). Yet, these weights are lower than those obtained by Ciampitti et al. (2013).

Leaf area index (LAI) mean values for the early maturity group ranked differently by source at each location, but the USDA hybrids always had higher mean LAI. In the late maturity group the Checks had the largest LAI with the USDA hybrids second and the DAS hybrids third. Source order for the SPAD readings was more consistent within location and maturity group. The Checks always produced the highest mean SPAD readings, the DAS hybrids had slightly lower chlorophyll

concentrations, and the USDA hybrids possessed the lowest mean chlorophyll concentrations levels (SPAD = Checks > DAS > USDA).

Table 2.4. Plant trait means for the late maturity group. Averages of plant height (height; cm), plant stalk diameter (stalk; mm), two SPAD readings (SPAD #1 and #2), leaf area index (LAI), kernel weight at 0% moisture (KW; mg kernel^{-1}), and estimated number of kernels per plant (Est. K P^{-1}), grain yield at 15.5% moisture (Yield; kg ha^{-1}), grain harvest index (Grain HI)

Sampling Stage		**R1**			**R2/R3**	**R5**	**R6**			
Location	**Source**	**Height (cm)**	**Stalk (mm)**	**SPAD #1**	**SPAD #2**	**LAI**	**KW (mg kernel^{-1})**	**Est. K P^{-1}**	**Yield (kg ha^{-1})**	**Grain HI**
ACRE	Check	215	22.4	43.6	38.1	3.2	228	380	9302	51.2
ACRE	DAS	214	21.1	43.2	37.0	2.8	219	359	8041	48.9
ACRE	USDA	215	21.6	42.2	35.7	3.1	219	309	7226	44.0
PPAC	Check	255	25.7	46.3	44.0	4.0	245	391	10989	45.8
PPAC	DAS	261	24.2	46.2	42.3	3.5	248	369	9861	44.1
PPAC	USDA	257	24.7	44.2	40.3	3.6	244	327	8631	38.8

2.4.4 General Performance-N Components

Nitrogen concentration and content levels of all plant parts (stover, kernels, and cobs) was measured at maturity and these mean values are presented in Table 2.5 by location and maturity groups.

Early hybrids

Among the 157 early hybrids, most hybrid sources had similar N concentration levels in the stover (0.46 - 0.49%) except for the USDA hybrids at PPAC which had increased concentration levels (0.55%). The mean concentration levels of N in the kernels were always highest for the USDA hybrids, DAS hybrids were lower, and Check hybrids lowest of the three for both locations ($\%N_{kernels}$ = USDA > DAS > Checks). The mean N concentration levels in the cobs were similar within sources at both locations with means ranging from 0.50% to 0.54% for the early maturity group ($\%N_{cobs}$ = USDA ≈ DAS ≈ Checks).

The aboveground N content, or the total quantity of N per unit area, is a function of biomass yield as well as the N concentrations of different plant components. N content was always numerically higher in the stover for the hybrids at PPAC (means greater than 40 kg N ha^{-1}) than at ACRE

(means ranging from 27.2 to 32.0 kg N ha^{-1}) but was relatively similar across sources at the same location. Higher N contents in the stover at PPAC is not surprising given the much lower HI at this location. Mean kernel N content of the early hybrids was also higher at PPAC (means ranging from 68.7 to 71.9 kg N ha^{-1}) than at ACRE (57.1 - 65.3 kg N ha^{-1}) because of the higher grain yields at PPAC. There were relatively similar N content levels across sources at the same location. Statistical differences were not analyzed. However, N levels in the cobs were similar *across* locations within sources; USDA hybrids had higher amounts of N in the cobs than the DAS hybrids, and the Checks had the lowest levels of N (N_{cob} = USDA > DAS > Checks). For Nitrogen Internal Efficiency (NIE) index values, the Checks had the highest mean values while the DAS hybrids had higher mean values than the USDA hybrids (NIE = Checks > DAS > USDA).

Late hybrids

For the 128 late hybrids there was a greater contrast in mean N concentration between locations than within sources; mean N concentration levels in the stover at PPAC ranged from 0.54% to 0.56% for the three different hybrid sources while at ACRE they ranged from 0.44% to 0.46%. N concentration levels in the kernels were also higher at PPAC than at ACRE, but there were greater differences across the hybrid sources. Mean kernel N concentration levels were highest for the USDA hybrids, DAS hybrids were second, and the Checks were third ($\%N_{kernels}$ = USDA > DAS > Checks). Cob N concentration levels were relatively similar within both locations for the late hybrids (0.50 - 0.51%) except for the DAS hybrids at PPAC which had mean N concentration levels in the cob of 0.57% and the USDA hybrids had a mean of 0.54%. The high N concentration levels suggest that N translocation to the grain was not limiting yield, but either kernel weight or kernel number. A regression of N concentration to grain yield, across maturity groups, showed no linear relationship between these two factors (R^2 = 0.01) supporting the premise. A regression of kernel N content to yield (across maturity groups) showed a strong linear relationship between the two (R^2 = 0.58; Yield = 4180 + 75.6[Kernel N content]). Furthermore, a regression of kernel number to yield (across maturities) also revealed a moderately strong linear relationship (R^2 = 0.39; Yield = 4472 + 12.6[Kernels/plant]).

Mean NIE index values for the late hybrids showed similar groupings across sources as for the early hybrids (NIE = Checks > DAS > USDA). Interestingly, the highest mean NIE value was for

the Check hybrids at ACRE with 99.6 kg grain per kg N. For the late hybrids, the DAS and USDA sources ranged in mean NIE values from 66.9 to 91.6 kg per kg N.

Table 2.5. Mean nitrogen levels (concentration and content) for various plant components (stover, kernels, and cobs) and mean nitrogen internal efficiency (NIE; kg grain per kg N) values.

Location	Maturity Group	Seed Source	%N in stover	%N in kernels	%N in cobs	Stover N content (kgN ha^{-1})	Kernel N content (kgN ha^{-1})	Cob N content (kgN ha^{-1})	NIE[SK]
ACRE	Early	Check	0.48	0.86	0.54	32.0	65.3	4.6	92.7
ACRE	Early	DAS	0.48	0.91	0.52	29.8	64.5	5.3	89.3
ACRE	Early	USDA	0.46	0.98	0.53	29.8	57.1	5.8	80.1
ACRE	Late	Check	0.44	0.83	0.50	29.3	66.5	5.1	99.6
ACRE	Late	DAS	0.46	0.90	0.51	27.2	60.9	5.7	91.6
ACRE	Late	USDA	0.46	0.94	0.51	29.1	56.5	6.1	82.6
PPAC	Early	Check	0.49	0.90	0.53	40.4	71.7	4.9	83.9
PPAC	Early	DAS	0.49	0.94	0.54	40.1	71.9	5.6	81.0
PPAC	Early	USDA	0.55	1.03	0.50	47.9	68.7	5.8	67.9
PPAC	Late	Check	0.54	0.87	0.51	49.5	76.3	5.6	82.9
PPAC	Late	DAS	0.55	0.94	0.57	48.6	76.1	6.7	77.1
PPAC	Late	USDA	0.56	1.01	0.54	52.7	71.3	6.6	66.9

2.4.5 Assessment and Identification of N-tolerant Hybrids

Grain Analysis

To analyze the maize grain response a mixed model was built using REML methods consisting of entries and maturity groups (MG) as the fixed effects; and replicate(loc), pass, range, location, MG x Location, rep(loc) x MG, and entry(MG) x Location as the random effects. The model had an adjusted R^2 of 0.80 and a coefficient of variance (CV) of 10.2%. Statistical analysis of the grain as the response indicated that there were significant differences (P-value < 0.0001) between the entries but no statistically significant differences between maturity groups. Spatial components (range, pass, rep) accounted for 52% of the variability in the model (Table 2.6). Location accounted for 21% of the variability while genotype x environment interactions only accounted for 5%.

Table 2.6. Mixed model variance component estimates for models at both locations. Spatial components are defined as replicate(location), pass, and range.

	% of Total Variance			
REML Variance Component Estimates	**Grain Yield Model**	**NIE Model**	**SPAD #1 Model**	**SPAD #2 Model**
Spatial Components	52	8	42	46
Location	21	54	0	0
G x E	5	8	12	11
Residual	22	31	46	43

A least square means Tukey HSD comparison ($\alpha = 0.05$) was used to evaluate potential differences between entries. Figure 2.14 is a plot of the least square mean values from the models separated out by seed source, across maturity groups. Variability within entries was large resulting in a large amount of overlap between entries and only the top 6 entries (DAS166, 2C799, DAS026, DAS130, 2J794, and 2G685) were found to be significantly different from the bottom 8 entries (B87, DAS076, Mo1W, DAS096, T8, Pa880, 4226 and R4). Least square mean yield values for all entries in the top and bottom 10 for each maturity group are shown in Appendices A and B. The yield response (Figure 2.14) at this low N was comparable to that found by Ciampitti et al. (2013) and Haegele et al. (2013). The yield differential (range of minimum to maximum) by maturity group across all hybrids in this experiment was 4753 kg ha^{-1} for the early hybrids or 3940 kg ha^{-1} for the late hybrids. This was a wider response than that observed by Haegele et al. (2013) in their era analysis of 21 maize hybrids with a 2700 kg ha^{-1} yield range at similar N levels. In our experiment the mean yields for the USDA hybrids in Figure 2.14 were lower than for the DAS and Check hybrids. Though no genetic information was provided for the DAS and Check hybrids, the USDA hybrids were generated from publicly available inbred lines thus could be categorized as having "older" genetics. In this study the older USDA hybrids had lower yields than the newer (DAS and Check) hybrids, confirming previous maize era studies in which the older hybrids yielded less than the newer hybrids (Ciampitti & Vyn, 2012; Haegele et al., 2013).

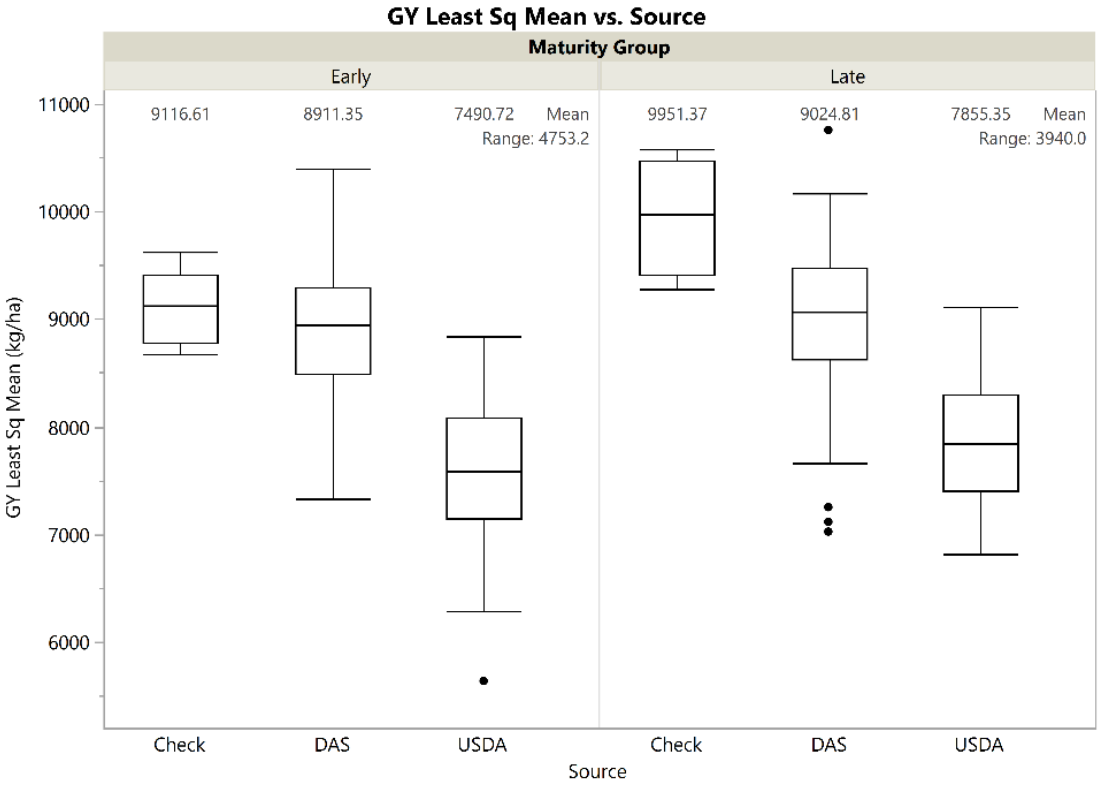

Figure 2.14. Outlier box plots of least square mean grain yield values by seed source and maturity group across both locations in 2015. Box is bracketing the interquartile range with the midline as the median sample value. Whiskers extend out to the farthest data point within (1.5*interquartile range) from the 1st or 3rd quartile. Dots past the whiskers are outliers. Mean value, by seed source, and range, by maturity group, are captioned at top.

NIE Analysis

A mixed model was built to analyze the NIE response from both locations using REML methods consisting of entries and maturity groups (MG) as the fixed effects and replicate(loc), pass, range, location, MG x Location, rep(loc) x MG, and entry(MG) x Location as the random effects. After transformation of the data, the model had an adjusted R^2 of 0.71 and a CV of 14.2%. Statistical analysis of NIE indicated that there were significant differences (P-value <0.0001) between the entries but no statistically significant differences between maturity groups. Grouped variance component estimates are shown in Table 2.6. The model had a residual of 31%. Spatial components only accounted for 8% of the variability in the model while location accounted for 54%. The large amount of variance accounted for by location in the NIE model was striking when compared to the amount of variance for the yield model (54% vs. 21%). This indicates that location is quite important for NIE. It suggests that to fully characterize a hybrid's general NIE value (i.e. what a genotype would do across multiple environments of soil, location, weather)

researchers need to have several environments in the study. Thus, for NIE multiple locations are essential for characterizing genotypes.

A least square means Tukey HSD comparison ($\alpha = 0.05$) was employed to test differences between entries. Figure 2.15 shows the box plots of the least square mean values from the models separated by seed source and maturity group. Across maturity group mean value for the Check hybrids was 90 kg per kg N, 85 kg per kg N for the DAS hybrids, and 75 kg per kg N for the USDA genotypes. These values are higher than the 56 kg grain/kg N cited in the literature under general agronomic management conditions (Ciampitti & Vyn, 2012; Mueller & Vyn, 2016). However, higher NIE values are expected at low N fertilization (Ladha et al., 2005; Uribelarrea et al., 2007). Based on the assumptions that the Check and DAS hybrids are from newer genetics than the USDA hybrids, these results confirm Ciampitti and Vyn (2012) who found that NIE for new era hybrids was higher than for old era hybrids. The range in NIE for the early and late maturity groups (34 and 37 kg/kg N, respectively) was a similar range to that found by Ciampitti and Vyn (2011), 36 kg/kg N, at similar density but higher N. However, our results were in contrast to those by Haegele et al. (2013) who detected no NIE change in their evaluation of era hybrids.

NIE least square mean values for all entries are shown in Appendices C and D; entries not connected by the same letter or symbol are significantly different. High variability resulted in a large amount of overlap between entries and few significant differences even when the top 10 and bottom 10 hybrid entries were separated within early (Table 2.7) and late (Table 2.8) maturity groups. The fields used in these studies had not been depleted of N (via low N fertilizer rates) in prior years and had been planted with soybeans the previous year (following the normal maize/soybean rotation). Variance in this study may have been minimized by the use of dedicated fields for low N studies, use of non-leguminous crops during the previous season as well as removal of the prior year's stover immediately after harvest (Banziger et al., 2000). Variability in NIE for this experiment, as measured by the coefficient of variance (CV) by hybrid, was driven mainly by a larger mean CV for yield (20%) than for Total N (18%). Those hybrids with the largest CV in NIE had a 4% greater mean CV for yield. As previously mentioned the grain component of kernel numbers in this experiment were lower than similar N studies by Haegele et al. (2013). The experimental design, which did not block by maturity group, may have had a

detrimental impact on pollination and the subsequent number of kernels thus blocking by maturity group may have resulted in a decrease in NIE variability.

Comparison of the top and bottom NIE hybrids (Table 2.7 and Table 2.8) with the top and bottom hybrids for grain yield (Appendix A and Appendix B) reveal that two early hybrids, DAS039 and DAS026, were in the top 10 hybrids for both NIE and yield. Three late hybrids, DAS136, DAS130, and DAS131, were in the top 10 hybrids for both NIE and yield as well. There were more hybrids in common for NIE and yield in the bottom ranked hybrids: 5707, 4226, MBPM, PA875, and R4 for the early hybrids and B87, VA14, T8, Mo1W, DAS076, Pa880, and DAS096 amongst the late hybrids. The fact that only 5 out of nearly 300 hybrids were high ranking in both NIE and yield suggests that the comment by Ciampitti and Vyn (2011) about the difficulty in breeding for NUE due to the lack of direct association between high NUE and yields may be true. Conversely, it may indicate that high NIE hybrids are not present in the high yielding group because they were not selected for high NIE. However, the broad ranges in NIE and yield shown in this experiment, as well as the discovery of 5 top performing hybrids for both traits, demonstrates that there is genetic variability with potential for NIE improvement in maize breeding.

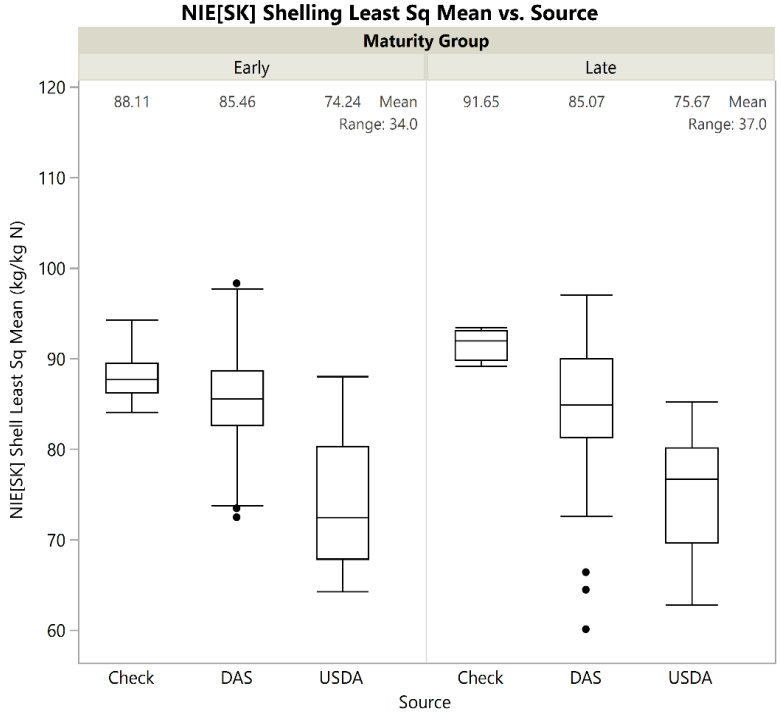

Figure 2.15. Outlier box plots of least square mean NIE values by seed source and maturity group across both locations in 2015. Box is bracketing the interquartile range with the midline as the median sample value. Whiskers extend out to the farthest data point within (1.5*interquartile range) from the 1st or 3rd quartile. Dots past the whiskers are outliers. Mean value, by seed source, and range, by maturity group, are captioned at top.

Table 2.7. Top and bottom 10 entries from the early maturity group based on NIE least square means (NIE LSqM) (kg grain per kg N) across both locations in 2015. SPAD rankings provided. Those highlighted in red have large differences in rankings between NIE and SPAD rankings.

NIE Ranking	Entry	NIE LSqM	SPAD #1 Ranking	SPAD # 2 Ranking
1	[Early]DAS039	98.3	129	147
2	[Early]DAS174	97.7	11	34
3	[Early]2V489	94.3	116	99
4	[Early]DAS026	93.9	55	48
5	[Early]DAS062	93.7	68	75
6	[Early]DAS227	93.1	64	56
7	[Early]DAS041	92.5	103	116
8	[Early]DAS040	92.2	39	23
9	[Early]DAS060	91.9	22	25
10	[Early]DAS191	91.8	67	55
148	[Early]H95	74.3	65	41
149	[Early]DAS164	73.8	87	28
150	[Early]DAS063	72.8	143	144
151	[Early]DAS180	72.5	107	83
152	[Early]5707	70.8	48	115
153	[Early]78371A	70.7	145	143
154	[Early]4226	68.3	157	154
155	[Early]MBPM	67.9	123	117
156	[Early]Pa875	66.6	77	142
157	[Early]R4	64.3	156	153

Table 2.8. Top and bottom 10 entries from the late maturity group based on NIE least square means (NIE LSqM; kg grain per kg N) across both locations in 2015. SPAD rankings provided. Those highlighted in red have the largest differences in ranking between NIE and SPAD rankings.

NIE Ranking	Entry	NIE LSqM	SPAD #1 Ranking	SPAD #2 Ranking
1	[Late]DAS087	97.1	51	22
2	[Late]DAS136	96.5	109	125
3	[Late]DAS120	96.4	116	119
4	[Late]DAS130	96.4	49	30
5	[Late]DAS090	95.6	71	46
6	[Late]DAS080	95.5	124	114
7	[Late]DAS129	94.8	40	68
8	[Late]DAS138	93.9	4	1
9	[Late]DAS132	93.9	29	50
10	[Late]DAS131	93.6	21	8
119	[Late]B87	72.4	125	126
120	[Late]Va14	70.3	47	57
121	[Late]T8	69.2	73	91
122	[Late]Mo1W	67.4	126	121
123	[Late]WF9	67.2	55	26
124	[Late]DAS076	66.4	127	115
125	[Late]Va85	65.1	91	79
126	[Late]DAS169	64.5	56	104
127	[Late]Pa880	62.9	120	86
128	[Late]DAS096	60.1	128	128

2.4.6 Evaluation of Potential Surrogate Measurements for NIE

In-field measurements were studied as potential surrogates of NIE and plant N. Certain physiological traits, such as SPAD, LAI, etc., are easily measured in the field especially when compared to the labor-intensive effort required to determine NIE and plant N, which necessitate both field and lab work. A correlation matrix was calculated based on the pairwise method. The Pearson product-moment correlations for each pair of measured responses (multiple in-season physiological measurements, grain yield, NIE index, and plant N) are shown in Table 2.9.

Grain yield was strongly and positively related to SPAD measurements at both sampling times (Table 2.9). A moderate positive linear relationship was noted between yield and mean green leaf counts (GL #1 Mean and GL #2 Mean) and plant heights. Mean stalk diameter and LAI only showed a weak positive linear relationship to yield with correlation values less than 0.45.

For NIE, only plant height and stalk diameter showed weak negative linear relationships with significant correlation values of -0.40 and -0.35, respectively. All other physiological measurements showed little evidence of a linear relationship with NIE (<|0.30|). Investigating the relationships of the NIE components (grain and total plant N content) showed a stronger positive correlation to N content than yield for all three surrogate measures of height, stalk, and LAI. It is important to acknowledge that a correlation with grain yield was not calculated due to multicollinearity.

The basis for analyzing the correlation between in-season physiological measures and NIE is due to the resource intensive aspect of this index, specifically the plant N component. Consequently, a pairwise correlation was calculated between the physiological measurements and total plant nitrogen (Total N) to determine if any linear relationships exist between those variables. Strong positive linear relationships between Total N and both SPAD readings and grain yield were observed (r = 0.68, 0.75 and 0.76). SPAD meters are active sensors developed as a surrogate measurement of leaf chlorophyll (Markwell et al., 1995; Minolta, 2009) thus the results of a strong relationship to Total N at R6 is logical since chlorophyll contains a substantial amount of N. Moderate linear relationships between the two green leaf counts, plant height, stalk diameter and Total N were also observed. Interestingly, only a weak positive linear relationship was found between LAI and Total N, similar to the relationship between LAI and grain yield.

Figure 2.16 contains the scatter plots of Total N and the various physiological measures with correlations greater than 0.50. For the leaf SPAD measurements there seemed an almost curvilinear relationship to Total N. As suggested by the Pearson correlations the green leaf plots reveal a less linear pattern, while the stalk and heights plots reveal that the relationship to Total N is weaker at higher values of stalk diameter or total heights.

SPAD meters measure absorbance at the red and NIR (650 nm and 940 nm) regions of the electromagnetic spectrum (Markwell et al., 1995). Since R1 and R2/R3 SPAD measurements are strongly related to Total N in these study we suggest additional investigations into other NIR:R vegetation indices. These indices, such as MSAVI, OSAVI and others, may be associated to NIE.

Table 2.9. Pearson product-moment correlation table of SPAD measurements (readings taken approximately 2 weeks apart), LAI, two mean green leaf count (GL), mean plant height, and mean stalk diameter relative to grain yield (kg ha $^{-1}$), NIE (kg grain per kg N), and plant (stover plus kernel) nitrogen levels (kg N ha $^{-1}$).

Phenotype	Yield	NIE	Total N (no cob)
SPAD #1	0.64***	-0.02	0.68***
SPAD #2	0.71***	-0.08*	0.75***
LAI	0.36***	-0.26***	0.36***
Yield		Nc	0.76***
GL # 1 Mean	0.50***	-0.01	0.55***
GL # 2 Mean	0.53***	-0.03	0.56***
Heights Mean	0.48***	-0.40***	0.61***
Stalk Diameter Mean	0.43***	-0.35***	0.60***

* Significant at P≤0.01
***Significant at P≤0.0001
Nc = Not calculated due to multicollinearity between responses.

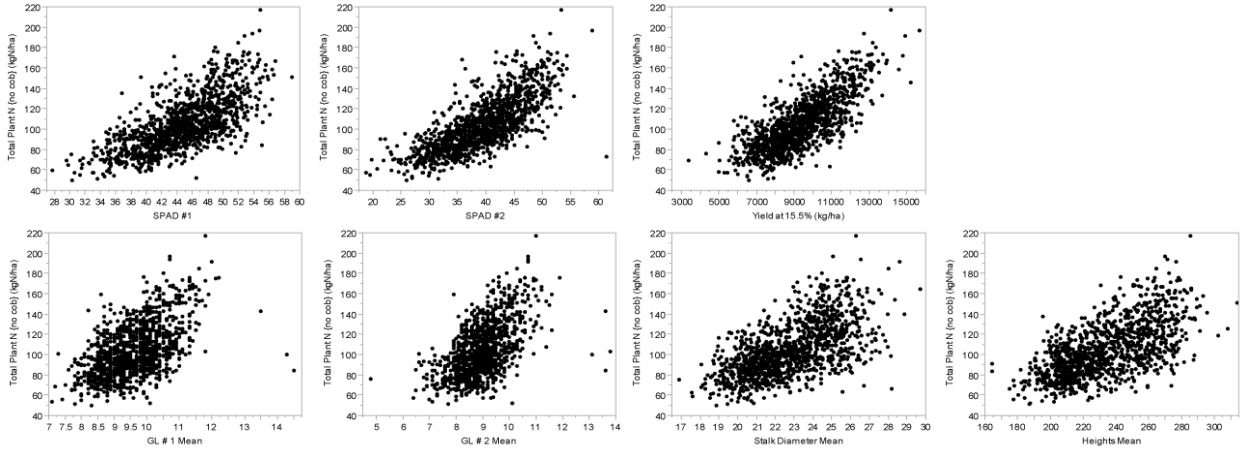

Figure 2.16. Plot of physiological measurements or yield by plant (stover and kernel) nitrogen (Total Plant N) (kg N ha^{-1})

A linear regression of Total N with leaf SPAD #2 is shown in Figure 2.17 (note Total N had to be natural log transformed). This model had an R^2 of 0.58 and RMSE of 0.16. The equation for this model is the following:

$$LnTotN_{nocob} = 3.4916489 + 0.028674*SPAD\ \#2$$

Because both leaf SPAD readings had a strong linear correlation to yield, mixed models were built analyzing differences between entries for each of the SPAD readings. Random and fixed effects

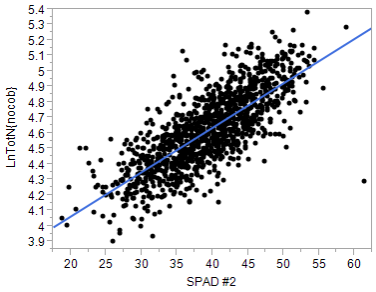

Figure 2.17. Plot of Total Nitrogen by SPAD #2

were the same as the previous models. The adjusted R^2 value for SPAD #1 model was 0.60 with an RSME = 3.47. The adjusted R^2 value for SPAD #2 model was 0.64 with an RMSE = 4.21. Regarding the fixed effects for both models, maturity groups were not significantly different from each other but entries were ($P<0.0001$). The variance component estimates in Table 2.6 confirm that neither location nor the genotype x environment interaction accounted for much of the variance, but t the spatial components (rep, pass, and range) were most impactful in these two SPAD models.

A least square means Tukey HSD analysis determined that for leaf SPAD reading #1 only the top SPAD entry, [Late]PHM49, was significantly different from the bottom SPAD entry, [Late]DAS096 (Table 2.10). None of the entries in the early maturity group were significantly different from each other in the SPAD #1 analysis. Examination of the grain yield rankings reveals that PHM49 had a mean yield of 8513 kg ha^{-1} and was ranked 91 amongst all 128 late maturity entries. DAS096 had nearly the lowest yield ranking (126/128) for all late maturity group entries with a yield of 7024 kg ha^{-1}. Thus the pattern observed between leaf SPAD #1 and grain yield for DAS096 in which for both responses DAS096 had poor rankings was not confirmed for PHM49.

Table 2.10. Comparison of the rankings for SPAD #1 and combine grain yield based on REML mixed models

	SPAD #1		**Grain Yield**	
Entries	**LSqMeans**	**Ranking**	**LSqMeans**	**Ranking**
PHM49	53.0	1	8513	91
DAS096	37.4	128	7024	126

Additional significant differences were found amongst entries for SPAD reading #2 and are shown in Table 2.11 along with their SPAD rankings side by side the yield rankings. At the top of the list are DAS138, DAS153, DAS095 and DAS078. Of those, only DAS078 also had a high yield ranking. The lowest leaf SPAD #2 entry was DAS096, which was also the worst for SPAD #1 as well as having the poorest grain yield among late DAS entries.

The rankings from both SPAD models for the top and bottom 10 NIE entries are shown in Table 2.7 and Table 2.8. Many of the leaf SPAD rankings were similar to each other. However, there

was less similarity in entry position ranking between the NIE and SPAD rankings. Among the early entries DAS039, 2V489, DAS041, 5707, Pa875, H95, and DAS164 had the largest differences in rankings and those are marked in red font. Among the late entries DAS136, DAS120, DAS080, Va14, and WF9 had the largest differences in rankings between the NIE and SPAD rankings; those are also marked in red font.

Table 2.11. Tukey HSD least square mean letters, values and rankings of second SPAD reading only for entries significantly different from each other. Entries not shown were not significantly different (Least square means difference letters = ABC)

Entries	Difference Letters	Least Square Mean	SPAD #2 Rankings	Grain Yield Rankings (128)
[Late]DAS138	A	46.80	1	35
[Late]DAS153	A	46.06	2	42
[Late]DAS095	AB	45.34	4	90
[Late]DAS078	AB	44.76	5	5
[Late]DAS197	AB	44.74	6	61
[Late]DAS103	AB	44.32	7	80
[Late]DAS131	AB	44.22	8	7
[Late]DAS141	AB	43.97	9	24
[Late]DAS122	AB	43.90	10	83
[Late]DAS107	AB	43.89	11	21
[Late]DAS230	AB	43.66	12	107
[Late]DAS111	AB	43.53	13	27
[Late]DAS094	AB	43.43	14	85
[Late]DAS113	AB	43.38	15	46
[Late]DAS086	AB	43.33	16	47
[Late]DAS154	AB	43.27	17	26
[Late]DAS209	AB	43.24	18	19
[Late]DAS140	AB	43.07	21	48
[Late]2C799	AB	41.88	32	2
[Late]B55	BC	30.09	127	119
[Late]DAS096	C	27.82	128	126

2.4.7 Selection of Top and Bottom Hybrids for NIE

The distributions of the top and bottom 10 NIE hybrids (20 per maturity group) can be seen in Figure 2.18. Of those 20 hybrids selected from each maturity group, there was only one Check hybrid (2V489). It had a high NIE value and belonged within the early maturity group. The DAS hybrids had both high and low NIE values within each maturity group though there were more DAS hybrids in the top rankings than in the lower rankings (19 vs. 6). In contrast, the 14 USDA hybrids had only low NIE values. Entries with high NIE values often did not have high grain yields nor high leaf SPAD values. Additional investigations into these entries of interest are recommended at multiple N rates in multiple environments.

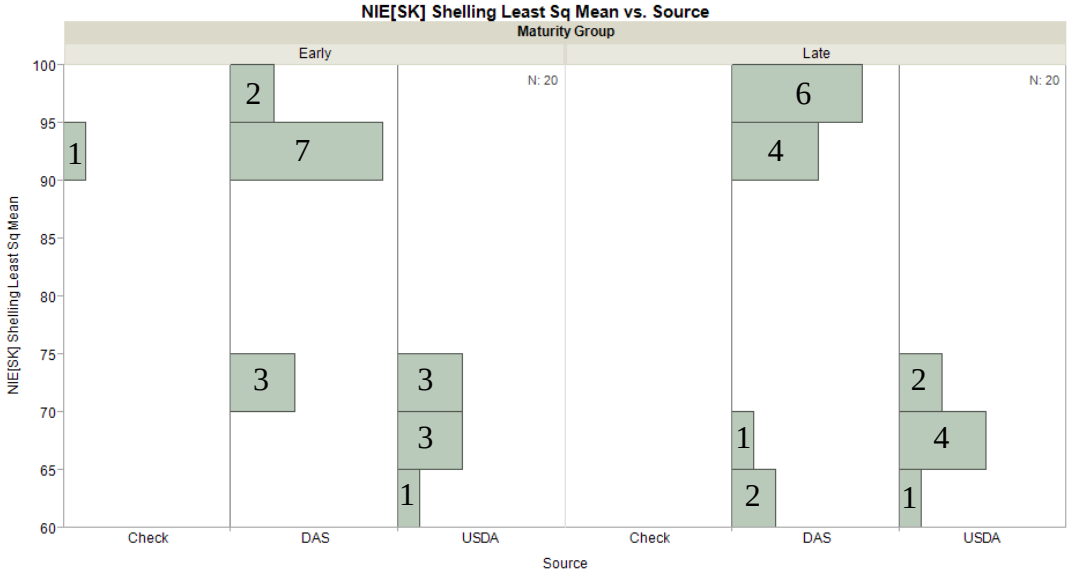

Figure 2.18. Histogram of hybrids in the top and bottom 20 rankings for NIE (kg grain per kg N) by maturity group and hybrid source as determined by REML model for both locations in 2015. Numbers within each bar indicate the hybrid count.

Lines with higher NIE values (Table 2.12) tended to have higher mean grain yields, higher mean grain HI, and greater numbers of estimated kernels per plant in comparison to the overall mean values of all 285 hybrids evaluated in 2015 at both locations (Table 2.13). The early maturity lines with higher NIE values (Table 2.12) tended to be shorter but have bigger-diameter stalks than the overall means (Table 2.13) while the late maturity lines were taller but with stalk diameters comparable to the late maturity overall means. Regarding kernel weights, the early maturity lines with higher NIE values tended to have lower kernel weights while the late maturity lines had higher

kernel weights than the overall means within the same maturity group. The other physiological measurements presented for the top NIE hybrids (LAI and SPAD) were very similar to the overall means.

Table 2.12. Means of top NIE hybrids only (19 DAS hybrids and 1 Check) from each maturity group. Averages of combine grain yield at 15.5% moisture (Yield), grain harvest index (Grain HI), plant height (height), plant stalk diameter (stalk), leaf area index (LAI), two SPAD readings (SPAD #1 and #2), kernel weight at 0% moisture (KW), and estimated number of kernels per plant (Est. K P^{-1}).

Maturity Group	R1			R2/R3	R5	R6			
	Height (cm)	Stalk (mm)	SPAD #1	SPAD #2	LAI	KW (mg kernel^{-1})	Est. K P^{-1}	Yield (kg ha^{-1})	Grain HI
Early	231	23.2	44.3	39.8	2.5	222	409	9681	50.0
Late	245	22.5	44.4	39.9	3.0	236	396	9399	50.0

Table 2.13. Means of all DAS, USDA, and check hybrids from each maturity group. Averages of combine grain yield at 15.5% moisture, grain harvest index (Grain HI), plant height (height), plant stalk diameter (stalk), leaf area index (LAI), two SPAD readings (SPAD #1 and #2), kernel weight at 0% moisture (KW), and estimated number of kernels per plant (Est. K P^{-1}).

Maturity Group	R1			R2/R3	R5	R6			
	Height (cm)	Stalk (mm)	SPAD #1	SPAD #2	LAI	KW (mg kernel^{-1})	Est. K P^{-1}	Yield (kg ha^{-1})	Grain HI
Early	233	22.7	44.8	39.3	2.6	230	358	8837	46.7
Late	236	22.9	44.5	39.5	3.1	233	359	8909	45.9

2.4.8 Exploration of Remote Imagery for Phenotyping

ACRE Vegetation Index Results

The R1 NDVI geotiff image at ACRE taken on 7/21/2015 is shown on the left of Figure 2.21. The corresponding R3/4 NDVI geotiff image (8/22/2015) from ACRE is shown on the right (Green = 1 and Red = -1). Visual inspection of the images reveals that NDVI values decreased suggesting that during the month of the early grain-fill period, the plants became stressed. Figure 2.20 shows the Simple Ratio raster images for ACRE at R1 and R3/4, respectively. In these images white is the maximum value with the range of 0-68 at R1 and 0-115 at R3/4. Overall, white values increased at R3/4 indicating that the overall NIR signal must have decreased and suggesting that stress levels had increased. The final season grain yields at ACRE are shown in Figure 2.22 with the highest yields shown in red. Note that the higher yield areas in Figure 2.22 (circled in purple) match the greener, less red, NDVI areas in the R3/4 NDVI image (Figure 2.21).

PPAC Vegetation Index Results

Figure 2.23 shows the NDVI images for PPAC. The only large differences in NDVI are in a small pocket of greener pixels near the top right section. In the R1 image this area is greener than the surrounding yellow and red plots. At R3/4, this same area is yellower than the surrounding reddish plots. This area matches the higher yield area in Figure 2.25 (circled in blue). A darker area is visible in a similar portion of the R3/4 image of the SR index but not in the R1 image (Figure 2.24).

2.4.9 Linear Regression

The ability of the mean of each vegetation index (by time point) to predict Total Plant N was assessed with linear regression by location. All models provided poor linear fit values with R^2 values less than 0.30 (Table 2.14). Linear regression was used to relate each vegetation index (VI) to grain yield. Again, all models provided a poor linear fit as seen in the table below (Table 2.15). The model with the best fit ($R^2 = 0.32$) is shown in Figure 2.19.

Table 2.14. R^2 values for linear regression models of VI for predicting Total Plant N

Total N	Mean NDVI at R1	Mean SR at R1	Mean NDVI at R3/4	Mean SR at R3/4
ACRE	0.15	0.14	0.11	0.11
PPAC	0.15	0.10	0.28	0.28

Table 2.15. R^2 values for linear regression models of mean VI for predicting Grain Yield

Grain Yield	Mean NDVI at R1	Mean SR at R1	Mean NDVI at R3/4	Mean SR at R3/4
ACRE	0.32	0.30	0.24	0.21
PPAC	0.10	0.07	0.28	0.28

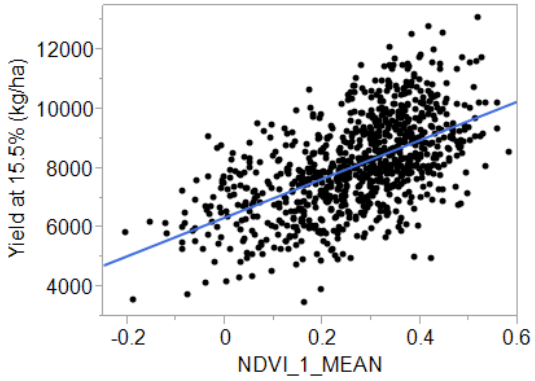

Figure 2.19. Linear fit of Yield by R1 NDVI at ACRE (R^2 =0.32)

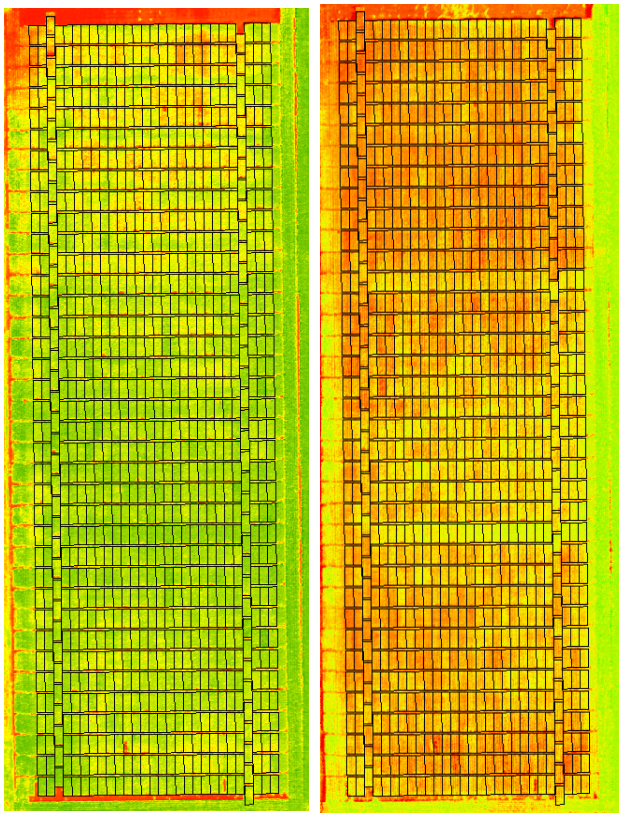

Figure 2.20. Image on left is NDVI at R1 (7/21/2015) at ACRE (green = 1, red = -1). On right is NDVI at R3/4 at ACRE (8/22/2015)

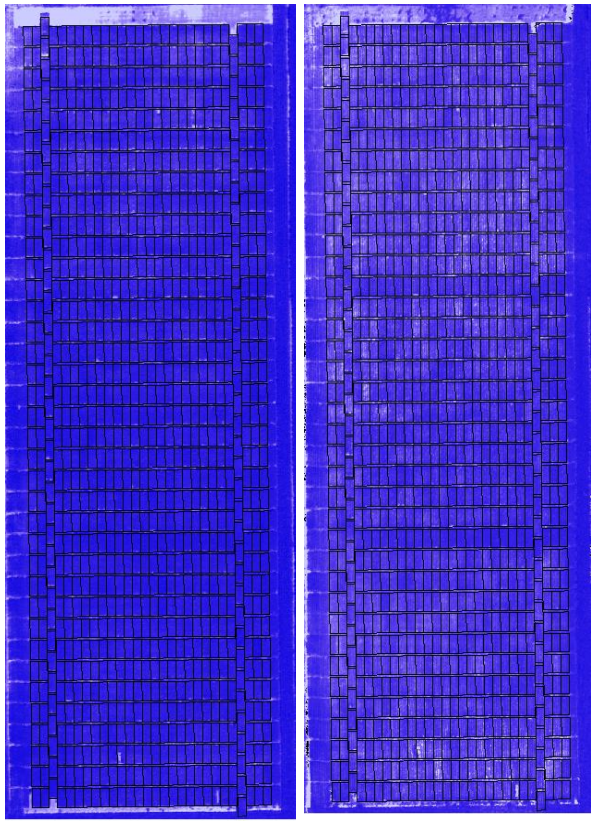

Figure 2.21. SR at R1 at ACRE (7/21/2015) (white = maximum value) on left. SR at R3/4 at ACRE on right plot (8/22/2015)

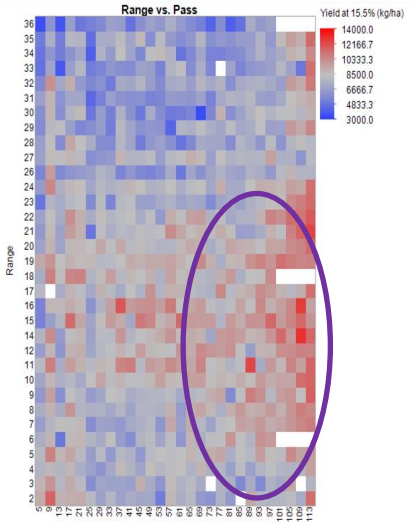

Figure 2.22. Heat map of grain yields (kg ha^{-1}) at ACRE organized by plot map

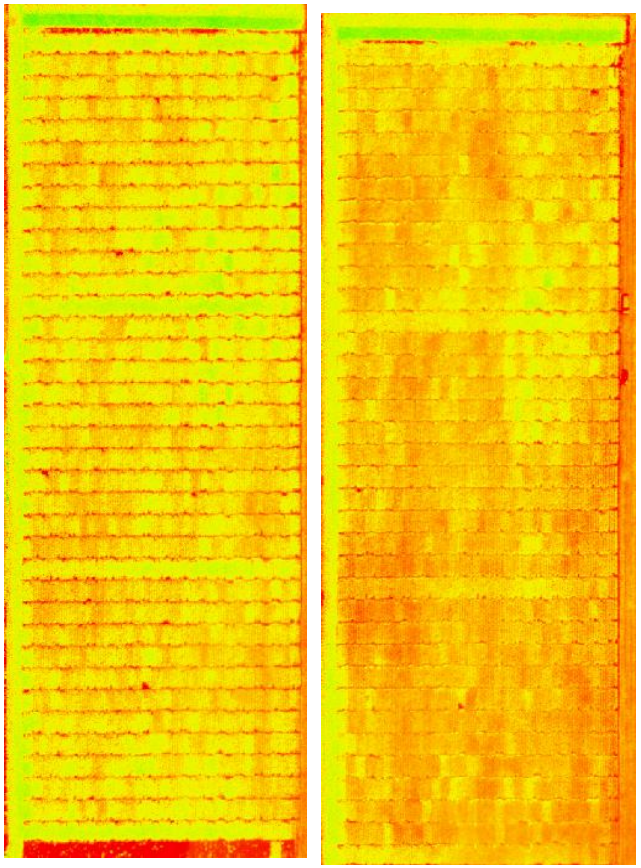

Figure 2.23. NDVI at R1 (7/31/2015) at PPAC on left. NDVI at R3/4 (8/24/2015) at PPAC on right

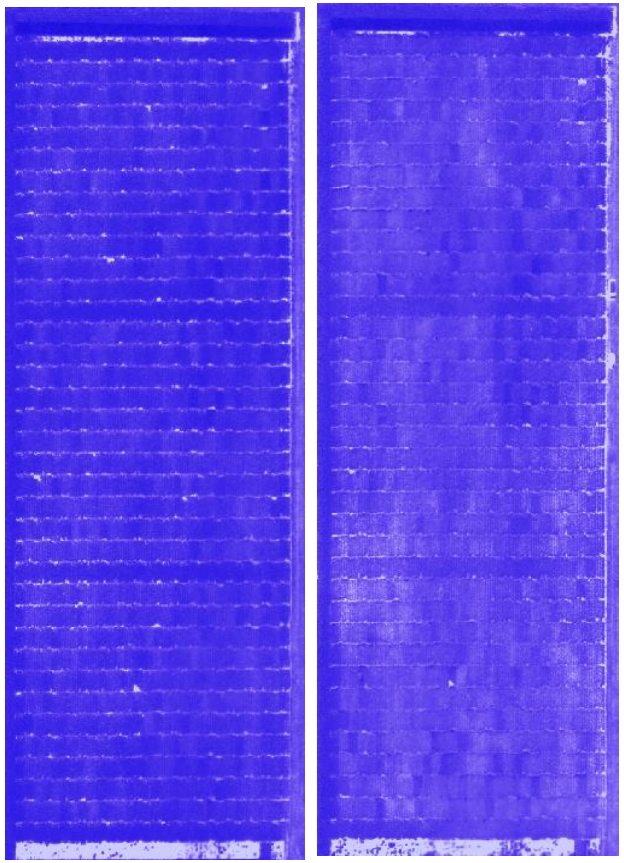

Figure 2.24. SR at R1 (7/31/2015) at PPAC on left. SR at R3/4 (8/24/2015) at PPAC on right.

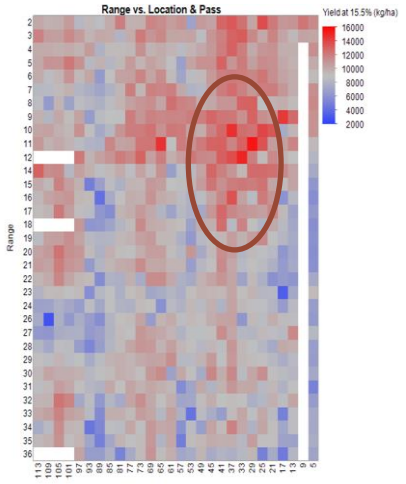

Figure 2.25. Heat map of grain yields (kg ha^{-1}) at PPAC for each plot organized by plot map

Linear Correlations

Correlation matrices were calculated based on the pairwise method. The scatterplot matrices for Total Plant N and the vegetation indices are shown in Figure 2.26 with the Pearson product-moment correlations for the responses as indicated. All were significant at $P \leq 0.0001$. The scatterplot matrices for grain yield and the vegetation indices are shown in Figure 2.27 with the Pearson product-moment correlations for the responses as indicated. All were significant at $P \leq 0.0001$. All responses showed weak to moderate linear relationships, dependent on location and time point. As expected, NDVI always had a positive relationship with plant N or yield while SR had a negative relationship with plant N or yield.

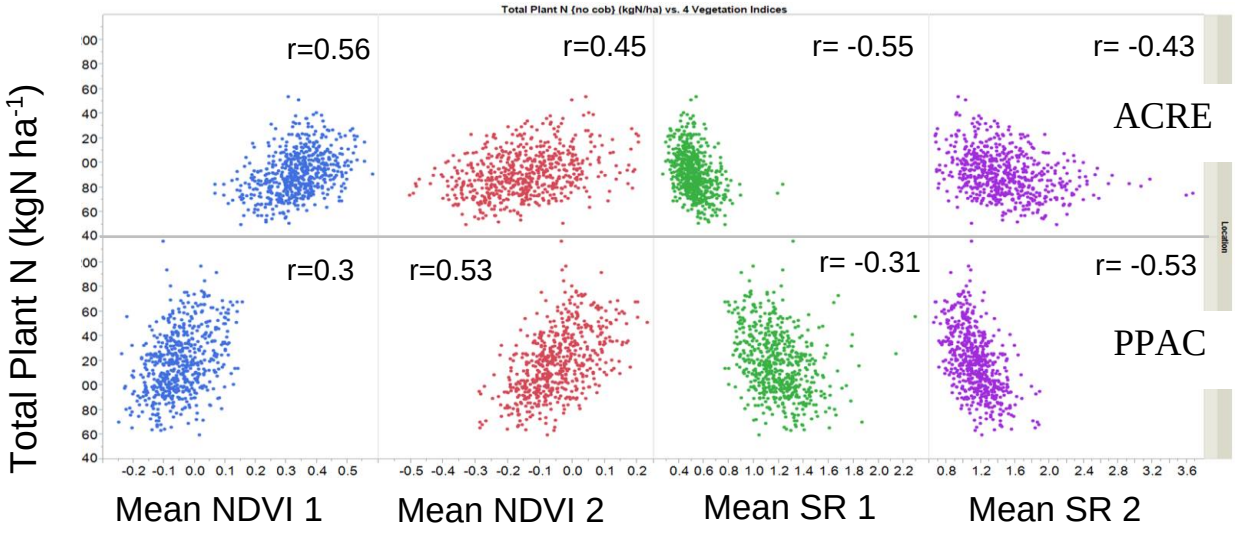

Figure 2.26. Scatter plot matrix for Total Plant N and Vegetation Indices by time point and location. Correlations shown. All significant at P≤0.0001. Time point 1 = R1 and Time point 2 = R3/4.

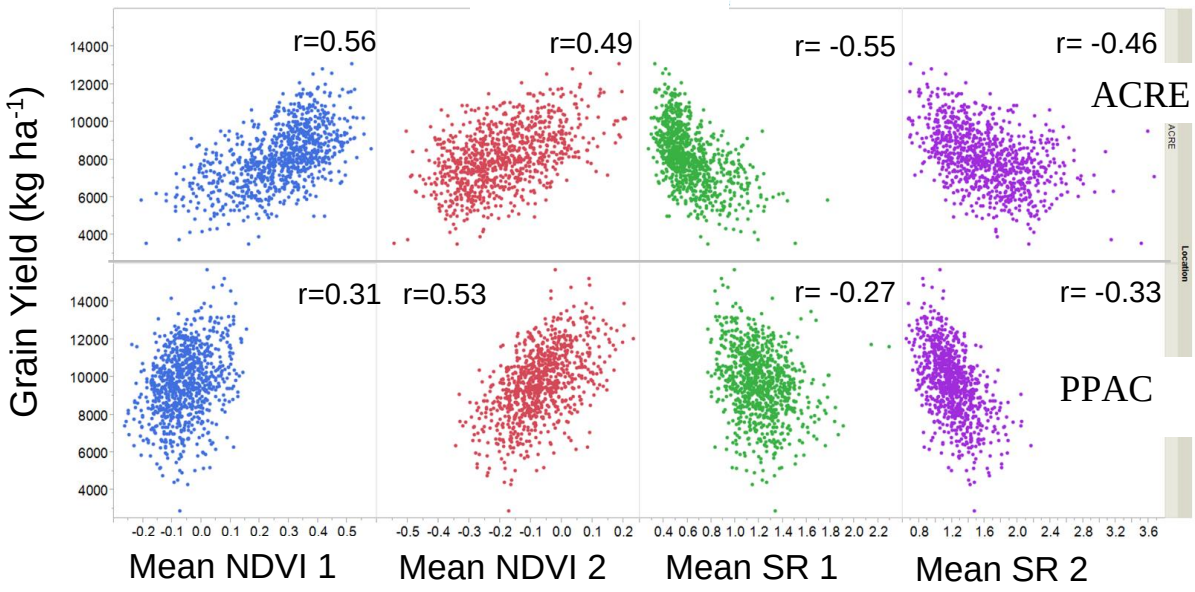

Figure 2.27. Scatterplot matrix for Grain Yield (kg ha^{-1}) and Vegetation Indices separated out by location. Correlations shown. All significant at P≤0.0001. Time point 1 = R1 and Time point 2 = R3/4.

Temporal Evaluation

Because bands were normalized separately across dates, a true temporal analysis could not be performed on the data. Instead, a comparison of the mean distributions at each time point was performed. Figure 2.27 shows the distributions of the VIs at the different timeframes by location. Mean values of R1 NDVI at ACRE were approximately 0.4. This was lower than completely healthy plants, but reflects the experiment design since only one low N rate was applied with the goal of placing the plants under low-N stress. At ACRE by R3/4 the NDVI values had dropped substantially to approximately -0.2 indicating high stress conditions. This result is reasonable as the plants are filling kernels and thus remobilizing both N and carbohydrates to the kernels. Mean values of R1 NDVI at PPAC were nearly zero and remained near zero at R3/4. At ACRE SR values increased from R1 to R3/4, while there was no change in mean SR values at PPAC from R1 to R3/4.

Location Evaluation

Once again, it is acknowledged that, due to the separate normalization of the geotiff images, a statistical analysis of the VI across locations could not be performed. Mean distributions were evaluated for numerical differences and general trends. NDVI values were higher during R1 at

ACRE compared to PPAC (Figure 2.27). And, SR values were highest during R3/4 at ACRE. The higher NDVI values at ACRE during R1 and the consistently low NDVI values at PPAC suggest that overall yields at ACRE would be higher than at PPAC. However, overall grain yields at PPAC were higher than at ACRE (9637 vs 8124 kg ha $^{-1}$, respectively). Also, during harvest the plants at PPAC were visibly larger and healthier-looking. In summary, visual differences were always location specific. The lack of VI response at PPAC was unexpected especially since there were higher overall grain yields at PPAC. Non-standardized pre-processing techniques in addition to a lack of ground control points and reference panels prevented a true quantitative multi-temporal and multi-location analysis.

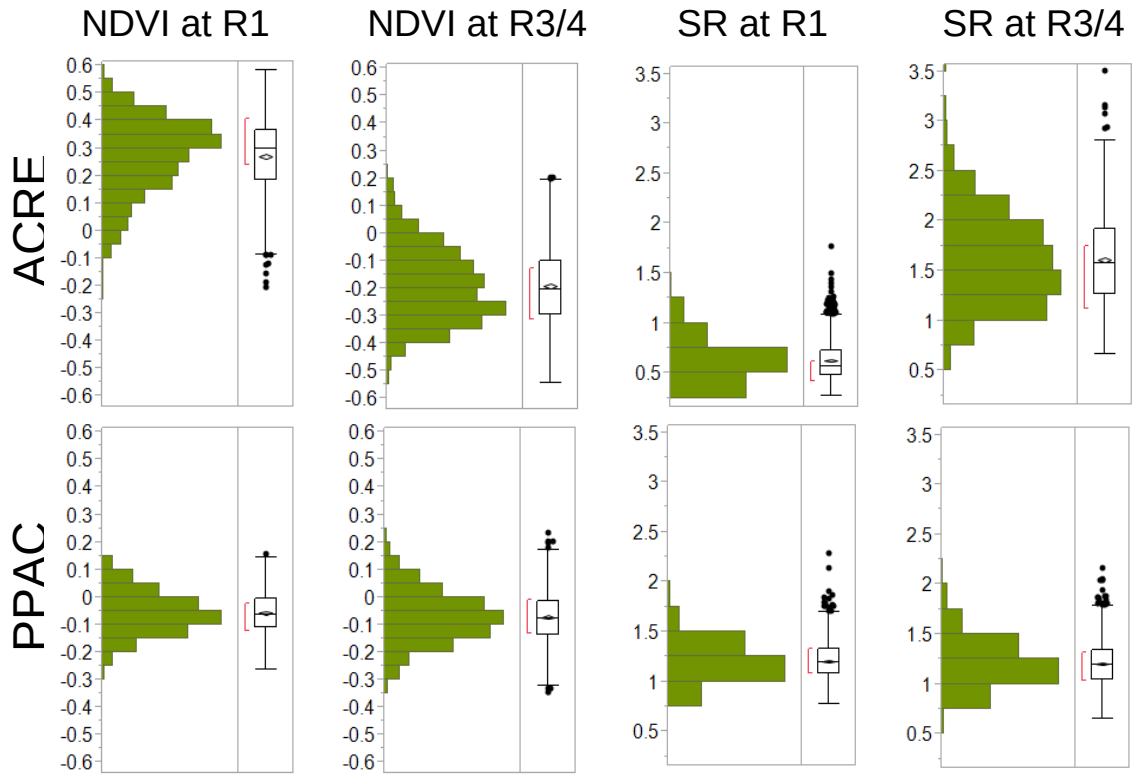

Figure 2.28. Histograms of NDVI and SR distributions at time points R1 and R3/4 for ACRE and PPAC

2.4.10 Hybrid Evaluation

The final goal of this project was to evaluate for statistical differences between the different hybrids based on the replicated VI values and determine if the hybrids that were identified as statistically different from each other using the VIs were the same as those identified through the

grain yield and NIE analyses. Two VIs (each at a single time point) were analyzed initially: mean NDVI at R1 and mean SR at R3/4.

For mean NDVI at R1 a mixed model was built using REML methods consisting of hybrids and maturity groups as the fixed effects; and replicate, pass(rep), range(rep), rep x MG as the random effects with each model by location (data not shown). The ACRE model had an adjusted R^2 of 0.80 and a RMSE of 0.07. Statistical analysis of the mean NDVI at R1 indicated that there were no significant differences (P-value > 0.05) among the hybrids nor between maturity groups. The PPAC model had an adjusted R^2 of 0.60 and RMSE of 0.05. Statistical analysis of the mean NDVI at R1 indicated that there were no significant differences (P-value > 0.05) between the hybrids nor between maturity groups.

For mean SR at R3/4 a mixed model was built using REML methods consisting of hybrids and maturity groups as the fixed effects; and replicate, pass(rep), range(rep), rep x MG as the random effects with each model by location (data not shown). The ACRE model had an adjusted R^2 of 0.67 and a RMSE of 0.28. Statistical analysis of the mean SR at R3/4 indicated that there were no significant differences (P-value > 0.05) among the hybrids nor between maturity groups. The PPAC model had an adjusted R^2 of 0.65 and a RMSE of 0.15. Statistical analysis of the mean SR at R3/4 indicated that there were no significant differences (P-value > 0.05) between the hybrids nor between maturity groups. Since no significant differences were found between hybrids for NDVI at R1 or SR at R3/4, no additional statistical models were analyzed.

From this investigation 5 hybrids were identified as high in yield and NIE. These results prove that there is genetic potential in maize for use in breeding for N efficiency. We suggest further research into these 5 hybrids under multiple N treatments to fully characterize their physiological characteristics and their response to N stress over the growing season in addition to determining the N uptake efficiency (NRE) of the targeted hybrids. Due to the scope of this research, hybrid comparisons were limited to a single low N rate. This resulted in the inability to control for background soil N by normalizing with the 0N treatment. Ideally, N efficient hybrids yield well under both high and low N conditions thus it is necessary to study these hybrids under those situations. Hopefully future breeding efforts with these hybrids can generate N efficient hybrids for commercial use.

2.5 Conclusions

This intensive analysis provided the ability to study nearly 300 diverse hybrids (but crossed with a common tester) in their response to N stress under two Eastern Cornbelt production environments. The top and bottom entries for both grain yield and NIE in both early and late maturity groups were identified. However, due to high levels of variance, several of these entries were not significantly different from each other. Nevertheless, five hybrids (DAS039, DAS026, DAS136, DAS130, and DAS131) were identified as top performers in both yield and NIE. This rare finding shows that genetic potential exists to further improve NIE through traditional maize breeding.

The investigation of secondary-trait measurements through correlation analysis revealed that ear-leaf SPAD measurements at the R2/R3 stages were strongly related to both yield and Total N at R6, but not to final NIE. Thus, no surrogate in-season measurements for NIE were identified. Unfortunately, use of ear-leaf SPAD as an alternate assessment for yield or Total N resulted in imprecise hybrid rankings.

In the exploratory investigation of aerial imagery, both of the vegetation indices evaluated in this project, NDVI and SR, suggested trends in end-of-season grain yields and total plant N levels. However, no strong statistically significant relationships or hybrid differences were found between either VI versus grain yield or total N-levels. Due to repeated band normalization (across time points and locations), a lack of calibration, ground control points, and reference panels only *qualitative* conclusions could be drawn from the remote sensing images.

Acknowledgements

We gratefully appreciate the funding and collaboration of heritage Dow AgroSciences LLC, now Corteva Agriscience, as well as the very helpful assistance of Bob Hall and Pablo Valverde. We acknowledge all efforts and contributions of multiple parties from Purdue University, both graduate and undergraduate students and technicians, especially Weifeng Xiong. Additional thanks go to GeoVantage personnel, Alan Peck and Andy Mullen.

2.6 References

Araus, J. L., & Cairns, J. E. (2014). Field high-throughput phenotyping: the new crop breeding frontier. *Trends Plant Sci*, *19*(1), 52-61. https://doi.org/10.1016/j.tplants.2013.09.008

Banziger, M., Edmeades, G., Beck, D., & Bellón, M. (2000). Breeding for drought and nitrogen stress tolerance in maize: From theory to practice.

Campbell, J. B., & Wynne, R. H. (2011). *Introduction to remote sensing*. Guilford Press.

Castleberry, R., Crum, C., & Krull, C. (1984). Genetic yield improvement of US maize cultivars under varying fertility and climatic environments 1. *Crop Science*, *24*(1), 33-36.

Ciampitti, I. A., Murrell, S. T., Camberato, J. J., Tuinstra, M., Xia, Y., Friedemann, P., & Vyn, T. J. (2013). Physiological dynamics of maize nitrogen uptake and partitioning in response to plant density and nitrogen stress hactors: II. Reproductive phase. *Crop Science*, *53*(6), 2588. https://doi.org/10.2135/cropsci2013.01.0041

Ciampitti, I. A., & Vyn, T. J. (2011). A comprehensive study of plant density consequences on nitrogen uptake dynamics of maize plants from vegetative to reproductive stages. *Field Crops Research*, *121*(1), 2-18. https://doi.org/10.1016/j.fcr.2010.10.009

Ciampitti, I. A., & Vyn, T. J. (2012). Physiological perspectives of changes over time in maize yield dependency on nitrogen uptake and associated nitrogen efficiencies: A review. *Field Crops Research*, *133*, 48-67. https://doi.org/10.1016/j.fcr.2012.03.008

D'Andrea, K. E., Otegui, M. E., Cirilo, A. G., & Eyhérabide, G. H. (2009). Ecophysiological traits in maize hybrids and their parental inbred lines: Phenotyping of responses to contrasting nitrogen supply levels. *Field Crops Research*, *114*(1), 147-158. https://doi.org/10.1016/j.fcr.2009.07.016

Doering, O., Galloway, J., Theis, T., Aneja, V., Boyer, E., Cassman, K., Cowling, E., Dickerson, R., Herz, W., & Hey, D. (2011). Reactive Nitrogen in the United States: an analysis of inputs, flows, consequences, and management options. *United States Environmental Protection Agency*.

Duvick, D. N. (1997). What is yield. *Developing drought and low N-tolerant maize. CIMMYT, El Batan, Mexico*, 332-335.

Erisman, J. W., Sutton, M. A., Galloway, J., Klimont, Z., & Winiwarter, W. (2008). How a century of ammonia synthesis changed the world. *Nature Geoscience*, *1*(10), 636-639.

Follett, J. R., Follett, R. F., & Herz, W. C. (2010). Environmental and human impacts of reactive nitrogen. *Advances in Nitrogen Management for Water Quality*, 1-37.

Garnett, T., Plett, D., Conn, V., Conn, S., Rabie, H., Rafalski, J. A., Dhugga, K., Tester, M. A., & Kaiser, B. N. (2015). Variation for N uptake system in maize: genotypic response to N supply. *Frontiers in Plant Science*, *6*, 936.

Gondwe, B. M. (2014). *Evaluation of maize (zea mays l) genotypes for nitrogen use efficiency* M. Sc. thesis, University of Zambia, Zambia].

Haegele, J. W., Cook, K. A., Nichols, D. M., & Below, F. E. (2013). Changes in nitrogen use traits associated with genetic improvement for grain yield of maize hybrids released in different decades. *Crop Science*, *53*(4), 1256. https://doi.org/10.2135/cropsci2012.07.0429

Ladha, J. K., Pathak, H., Krupnik, T. J., Six, J., & van Kessel, C. (2005). Efficiency of fertilizer nitrogen in cereal production: retrospects and prospects. *Advances in Agronomy*, *87*, 85-156.

Lassaletta, L., Billen, G., Grizzetti, B., Anglade, J., & Garnier, J. (2014). 50 year trends in nitrogen use efficiency of world cropping systems: the relationship between yield and nitrogen input to cropland. *Environmental Research Letters*, *9*(10), 105011. https://doi.org/10.1088/1748-9326/9/10/105011

Lu, C., Zhang, J., Cao, P., & Hatfield, J. L. (2019). Are we getting better in using nitrogen?: Variations in nitrogen use efficiency of two cereal crops across the United States. *Earth's Future*, *7*(8), 939-952.

Markwell, J., Osterman, J. C., & Mitchell, J. L. (1995). Calibration of the Minolta SPAD-502 leaf chlorophyll meter. *Photosynthesis research*, *46*(3), 467-472. https://doi.org/https://doi.org/10.1007/BF00032301

Minolta, K. (2009). Chlorophyll Meter SPAD 502 instructions.

Moll, R. H., Kamprath, E. J., & Jackson, W. A. (1982). Analysis and Interpretation of Factors Which Contribute to Efficiency of Nitrogen Utilization. *Agronomy Journal*, *74*, 562-564. https://doi.org/10.2134/agronj1982.00021962007400030037x

Moose, S., & Below, F. E. (2009). Biotechnology Approaches to improving maize nitrogen use efficiency. In A. L. Kriz & B. A. Larkins (Eds.), *Molecular Genetic Approaches to Maize Improvement* (pp. 65-77). Springer Berlin Heidelberg. https://doi.org/10.1007/978-3-540-68922-5_6

Mueller, S. M., Messina, C. D., & Vyn, T. J. (2019). Simultaneous gains in grain yield and nitrogen efficiency over 70 years of maize genetic improvement. *Sci Rep*, *9*(1), 1-8.

Mueller, S. M., & Vyn, T. J. (2016). Maize plant resilience to N stress and post-silking N capacity changes over time: A Review. *Front Plant Sci*, *7*, 53. https://doi.org/10.3389/fpls.2016.00053

Mulla, D. J. (2013). Twenty five years of remote sensing in precision agriculture: Key advances and remaining knowledge gaps. *Biosystems Engineering*, *114*(4), 358-371. https://doi.org/10.1016/j.biosystemseng.2012.08.009

Muñoz-Huerta, R. F., Guevara-Gonzalez, R. G., Contreras-Medina, L. M., Torres-Pacheco, I., Prado-Olivarez, J., & Ocampo-Velazquez, R. V. (2013). A review of methods for sensing the nitrogen status in plants: advantages, disadvantages and recent advances. *Sensors*, *13*(8), 10823-10843. https://doi.org/10.3390/s130810823

Ribaudo, M., Hansen, L., Livingston, M., Mosheim, R., Williamson, J., & Delgado, J. (2011). Nitrogen in agricultural systems: Implications for conservation policy.

Salvagiotti, F., Castellarín, J. M., Miralles, D. J., & Pedrol, H. M. (2009). Sulfur fertilization improves nitrogen use efficiency in wheat by increasing nitrogen uptake. *Field Crops Research*, *113*(2), 170-177. https://doi.org/10.1016/j.fcr.2009.05.003

Tollenaar, M., & Wu, J. (1999). Yield improvement in temperate maize is attributable to greater Stress Tolerance. *Crop Science*, *39*(6), 1597. https://doi.org/10.2135/cropsci1999.3961597x

Unkovich, M., Herridge, D., Peoples, M., Cadisch, G., Boddey, B., Giller, K., Alves, B., & Chalk, P. (2008). *Measuring plant-associated nitrogen fixation in agricultural systems*. Australian Centre for International Agricultural Research (ACIAR).

Uribelarrea, M., Moose, S. P., & Below, F. E. (2007). Divergent selection for grain protein affects nitrogen use in maize hybrids. *Field Crops Research*, *100*(1), 82-90.

Ying, J., Lee, E., & Tollenaar, M. (2000). Response of maize leaf photosynthesis to low temperature during the grain-filling period. *Field Crops Research*, *68*(2), 87-96.

Zhao, D., Raja Reddy, K., Kakani, V. G., Read, J. J., & Carter, G. A. (2003). Corn (Zea mays L.) growth, leaf pigment concentration, photosynthesis and leaf hyperspectral reflectance properties as affected by nitrogen supply. *Plant and Soil*, *257*(1), 205-218. https://doi.org/10.1023/a:1026233732507

2.7 Appendix

Appendix A. Top and Bottom 10 entries in late maturity group by combine grain yield least square mean (LSqM) values (α = 0.05) (kg ha $^{-1}$) for both locations in 2015

Ranking	Entry	Least Square Means Differences Letters														LSqM
1	[Late]DAS166	A	B													10752.8
2	[Late]2C799	A														10568.6
3	[Late]DAS130	A	B	C	D	E	F		H							10167.4
4	[Late]2J794	A	B	C												10165.0
5	[Late]DAS078	A	B	C	D	E	F	G	H							10107.7
6	[Late]DAS152	A	B	C	D	E	F	G	H	I	J	K				10018.6
7	[Late]DAS131	A	B	C	D	E	F	G	H	I						9948.1
8	[Late]DAS136	A	B	C	D	E	F	G	H	I	J	K				9899.6
9	[Late]DAS108	A	B	C	D	E	F	G	H	I	J	K				9882.4
10	[Late]DAS099	A	B	C	D	E	F	G	H	I	J	K				9877.9
119	[Late]B55				D	E	F	G	H	I	J	K	L	M	N	7550.5
120	[Late]WF9			C	D	E	F	G	H	I	J	K	L	M	N	7534.7
121	[Late]Va14						F	G		I	J	K	L	M	N	7270.2
122	[Late]DAS175						F	G		I	J	K	L	M	N	7251.0
123	[Late]B87							G		I	J	K	L	M	N	7208.7
124	[Late]DAS076									I	J	K	L	M	N	7109.6
125	[Late]Mo1W							G		I	J	K	L	M	N	7093.9
126	[Late]DAS096										J	K	L	M	N	7024.0
127	[Late]T8											K	L	M	N	6997.7
128	[Late]Pa880												L	M	N	6812.8

Appendix B. Top and Bottom 10 entries in early maturity group by combine grain yield least square mean (LSqM) values (α = 0.05) (kg ha $^{-1}$) at both locations in 2015

Ranking	Entry	Least Square Means Differences Letters														LSqM
1	[Early]DAS026	A	B	C	D		F									10390.1
2	[Early]DAS039	A	B	C	D	E	F	G		I	J					10299.8
3	[Early]DAS002	A	B	C	D	E	F	G		I	J	K				10106.0
4	[Early]DAS016	A	B	C	D	E	F	G	H	I	J	K				10003.0
5	[Early]DAS007	A	B	C	D	E	F	G	H	I	J	K	L			9918.9
6	[Early]DAS055	A	B	C	D	E	F	G	H	I	J	K	L			9761.0
7	[Early]DAS045	A	B	C	D	E	F	G	H	I	J	K	L			9750.7
8	[Early]DAS006	A	B	C	D	E	F	G	H	I	J	K	L			9740.9
9	[Early]DAS066	A	B	C	D	E	F	G	H	I	J	K	L			9723.8
10	[Early]DAS041	A	B	C	D	E	F	G	H	I	J	K	L			9715.9
148	[Early]78371A	A	B	C	D	E	F	G	H	I	J	K	L	M	N	7695.6
149	[Early]DAS234		B	C	D	E	F	G	H	I	J	K	L	M	N	7687.6
150	[Early]DAS204		B	C	D	E	F	G	H	I	J	K	L	M	N	7644.0
151	[Early]PHT77			C	D	E	F	G	H	I	J	K	L	M	N	7482.7
152	[Early]MBPM					E		G	H	I	J	K	L	M	N	7367.9
153	[Early]DAS173					E		G	H	I	J	K	L	M	N	7329.8
154	[Early]5707					E		G	H	I	J	K	L	M	N	7228.0
155	[Early]Pa875								H				L	M	N	7125.7
156	[Early]4226													M	N	6295.9
157	[Early]R4														N	5636.9

Appendix C. Entries in early [E] maturity group ranked by NIE least square mean values (α = 0.05) (LSqM) (kg grain per kg N) across both locations in 2015.

Rank	Entry																																				LSqM
1	[E]DAS039	A			D			G	H	I	J		L		N	O																					98.3
2	[E]DAS174	A	B		D			G	H	I	J		L		N	O																					97.7
3	[E]2V489	A	B		D			G	H	I	J		L		N	O	P	Q																			94.3
4	[E]DAS026	A	B	C	D			G	H	I	J		L		N	O	P	Q	R	S	T	U		W		Y	Z										93.9
5	[E]DAS062	A	B	C	D			G	H	I	J		L		N	O	P	Q	R	S	T	U		W		Y	Z										93.7
6	[E]DAS227	A	B	C	D			G	H	I	J		L		N	O	P	Q	R	S	T	U		W		Y	Z										93.1
7	[E]DAS041	A	B	C	D	E	F	G	H	I	J	K	L		N	O	P	Q	R	S	T	U	V	W	X	Y	Z	[	\	]	^	_		a				92.5
8	[E]DAS040	A	B	C	D	E		G	H	I	J		L		N	O	P	Q	R	S	T	U	V	W	X	Y	Z	[	\	]								92.2
9	[E]DAS060	A	B	C	D	E	F	G	H	I	J		L		N	O	P	Q	R	S	T	U	V	W	X	Y	Z	[	\	]	^							91.9
10	[E]DAS191	A	B	C	D	E	F	G	H	I	J		L		N	O	P	Q	R	S	T	U	V	W	X	Y	Z	[	\	]	^							91.8
11	[E]DAS221	A	B	C	D	E	F	G	H	I	J		L		N	O	P	Q	R	S	T	U	V	W	X	Y	Z	[	\	]	^							91.8
12	[E]DAS031	A	B	C	D	E	F	G	H	I	J		L		N	O	P	Q	R	S	T	U	V	W	X	Y	Z	[	\	]	^							91.8
13	[E]DAS002	A	B	C	D	E	F	G	H	I	J		L		N	O	P	Q	R	S	T	U	V	W	X	Y	Z	[	\	]	^							91.5
14	[E]DAS055	A	B	C	D	E	F	G	H	I	J		L		N	O	P	Q	R	S	T	U	V	W	X	Y	Z	[	\	]	^							91.4
15	[E]DAS057	A	B	C	D	E	F	G	H	I	J		L		N	O	P	Q	R	S	T	U	V	W	X	Y	Z	[	\	]	^							91.4
16	[E]DAS170	A	B	C	D	E	F	G	H	I	J		L		N	O	P	Q	R	S	T	U	V	W	X	Y	Z	[	\	]	^							91.4
17	[E]DAS013	A	B	C	D	E	F	G	H	I	J	K	L		N	O	P	Q	R	S	T	U	V	W	X	Y	Z	[	\	]	^	_		a				91.2
18	[E]DAS067	A	B	C	D	E	F	G	H	I	J	K	L		N	O	P	Q	R	S	T	U	V	W	X	Y	Z	[	\	]	^	_		a				91.1
19	[E]DAS009	A	B	C	D	E	F	G	H	I	J	K	L		N	O	P	Q	R	S	T	U	V	W	X	Y	Z	[	\	]	^	_		a				91.0
20	[E]DAS034	A	B	C	D	E	F	G	H	I	J	K	L		N	O	P	Q	R	S	T	U	V	W	X	Y	Z	[	\	]	^	_		a				90.9
21	[E]DAS056	A	B	C	D	E	F	G	H	I	J	K	L		N	O	P	Q	R	S	T	U	V	W	X	Y	Z	[	\	]	^	_		a				90.8
22	[E]DAS151	A	B	C	D	E	F	G	H	I	J	K	L		N	O	P	Q	R	S	T	U	V	W	X	Y	Z	[	\	]	^	_		a				90.6
23	[E]DAS038	A	B	C	D	E	F	G	H	I	J	K	L		N	O	P	Q	R	S	T	U	V	W	X	Y	Z	[	\	]	^	_		a				90.1
24	[E]DAS052	A	B	C	D	E	F	G	H	I	J	K	L		N	O	P	Q	R	S	T	U	V	W	X	Y	Z	[	\	]	^	_		a				89.8
25	[E]DAS068	A	B	C	D	E	F	G	H	I	J	K	L		N	O	P	Q	R	S	T	U	V	W	X	Y	Z	[	\	]	^	_		a				89.7
26	[E]DAS161	A	B	C	D	E	F	G	H	I	J	K	L		N	O	P	Q	R	S	T	U	V	W	X	Y	Z	[	\	]	^	_		a				89.7
27	[E]DAS025	A	B	C	D	E	F	G	H	I	J	K	L		N	O	P	Q	R	S	T	U	V	W	X	Y	Z	[	\	]	^	_		a				89.5
28	[E]DAS016	A	B	C	D	E	F	G	H	I	J	K	L		N	O	P	Q	R	S	T	U	V	W	X	Y	Z	[	\	]	^	_		a				89.5
29	[E]DAS042	A	B	C	D	E	F	G	H	I	J	K	L	M	N	O	P	Q	R	S	T	U	V	W	X	Y	Z	[	\	]	^	_	`	a	b	c	d	89.3
30	[E]DAS158	A	B	C	D	E	F	G	H	I	J	K	L	M	N	O	P	Q	R	S	T	U	V	W	X	Y	Z	[	\	]	^	_	`	a	b	c	d	89.0
31	[E]DAS014	A	B	C	D	E	F	G	H	I	J	K	L	M	N	O	P	Q	R	S	T	U	V	W	X	Y	Z	[	\	]	^	_	`	a	b	c	d	88.9
32	[E]DAS181	A	B	C	D	E	F	G	H	I	J	K	L	M	N	O	P	Q	R	S	T	U	V	W	X	Y	Z	[	\	]	^	_	`	a	b	c	d	88.9
33	[E]DAS072	A	B	C	D	E	F	G	H	I	J	K	L	M	N	O	P	Q	R	S	T	U	V	W	X	Y	Z	[	\	]	^	_	`	a	b	c	d	88.8
34	[E]DAS058	A	B	C	D	E	F	G	H	I	J	K	L	M	N	O	P	Q	R	S	T	U	V	W	X	Y	Z	[	\	]	^	_	`	a	b	c	d	88.8
35	[E]DAS070	A	B	C	D	E	F	G	H	I	J	K	L	M	N	O	P	Q	R	S	T	U	V	W	X	Y	Z	[	\	]	^	_	`	a	b	c	d	88.7
36	[E]DAS006	A	B	C	D	E	F	G	H	I	J	K	L	M	N	O	P	Q	R	S	T	U	V	W	X	Y	Z	[	\	]	^	_	`	a	b	c	d	88.7
37	[E]DAS061	A	B	C	D	E	F	G	H	I	J	K	L	M	N	O	P	Q	R	S	T	U	V	W	X	Y	Z	[	\	]	^	_	`	a	b	c	d	88.6
38	[E]DAS228	A	B	C	D	E	F	G	H	I	J	K	L	M	N	O	P	Q	R	S	T	U	V	W	X	Y	Z	[	\	]	^	_	`	a	b	c	d	88.6
39	[E]DAS147	A	B	C	D	E	F	G	H	I	J	K	L	M	N	O	P	Q	R	S	T	U	V	W	X	Y	Z	[	\	]	^	_	`	a	b	c	d	88.5
40	[E]DAS035	A	B	C	D	E	F	G	H	I	J	K	L	M	N	O	P	Q	R	S	T	U	V	W	X	Y	Z	[	\	]	^	_	`	a	b	c	d	88.3
41	[E]DAS008	A	B	C	D	E	F	G	H	I	J	K	L	M	N	O	P	Q	R	S	T	U	V	W	X	Y	Z	[	\	]	^	_	`	a	b	c	d	88.3
42	[E]DAS183	A	B	C	D	E	F	G	H	I	J	K	L	M	N	O	P	Q	R	S	T	U	V	W	X	Y	Z	[	\	]	^	_	`	a	b	c	d	88.3
43	[E]DAS200	A	B	C	D	E	F	G	H	I	J	K	L	M	N	O	P	Q	R	S	T	U	V	W	X	Y	Z	[	\	]	^	_	`	a	b	c	d	88.3

44	[E]DAS064	A	B	C	D	E	F	G	H	I	J	K	L	M	N	O	P	Q	R	S	T	U	V	W	X	Y	Z	[	\	]	^	_	`	a	b	c	d	88.3
45	[E]DAS163	A	B	C	D	E	F	G	H	I	J	K	L	M	N	O	P	Q	R	S	T	U	V	W	X	Y	Z	[	\	]	^	_	`	a	b	c	d	88.1
46	[E]DAS047	A	B	C	D	E	F	G	H	I	J	K	L	M	N	O	P	Q	R	S	T	U	V	W	X	Y	Z	[	\	]	^	_	`	a	b	c	d	88.1
47	[E]DAS219	A	B	C	D	E	F	G	H	I	J	K	L	M	N	O	P	Q	R	S	T	U	V	W	X	Y	Z	[	\	]	^	_	`	a	b	c	d	88.1
48	[E]PHK76	A	B	C	D	E	F	G	H	I	J	K	L	M	N	O	P	Q	R	S	T	U	V	W	X	Y	Z	[	\	]	^	_	`	a	b	c	d	88.0
49	[E]2T498	A	B	C	D	E	F	G	H	I	J	K	L		N	O	P	Q	R	S	T	U	V	W	X	Y	Z	[	\	]	^	_		a				88.0
50	[E]DAS194	A	B	C	D	E	F	G	H	I	J	K	L	M	N	O	P	Q	R	S	T	U	V	W	X	Y	Z	[	\	]	^	_	`	a	b	c	d	87.9
51	[E]2T619	A	B	C	D	E	F	G	H	I	J		L		N	O	P	Q	R	S	T	U	V	W	X	Y	Z	[	\	]	^							87.8
52	[E]DAS162	A	B	C	D	E	F	G	H	I	J	K	L	M	N	O	P	Q	R	S	T	U	V	W	X	Y	Z	[	\	]	^	_	`	a	b	c	d	87.8
53	[E]DAS185	A	B	C	D	E	F	G	H	I	J	K	L	M	N	O	P	Q	R	S	T	U	V	W	X	Y	Z	[	\	]	^	_	`	a	b	c	d	87.8
54	[E]DAS053	A	B	C	D	E	F	G	H	I	J	K	L	M	N	O	P	Q	R	S	T	U	V	W	X	Y	Z	[	\	]	^	_	`	a	b	c	d	87.7
55	[E]2D599	A	B	C	D	E	F	G	H	I	J	K	L		N	O	P	Q	R	S	T	U	V	W	X	Y	Z	[	\	]	^	_		a				87.5
56	[E]DAS203	A	B	C	D	E	F	G	H	I	J	K	L	M	N	O	P	Q	R	S	T	U	V	W	X	Y	Z	[	\	]	^	_	`	a	b	c	d	87.4
57	[E]DAS001	A	B	C	D	E	F	G	H	I	J	K	L	M	N	O	P	Q	R	S	T	U	V	W	X	Y	Z	[	\	]	^	_	`	a	b	c	d	87.3
58	[E]DAS187	A	B	C	D	E	F	G	H	I	J	K	L	M	N	O	P	Q	R	S	T	U	V	W	X	Y	Z	[	\	]	^	_	`	a	b	c	d	87.3
59	[E]DAS222	A	B	C	D	E	F	G	H	I	J	K	L	M	N	O	P	Q	R	S	T	U	V	W	X	Y	Z	[	\	]	^	_	`	a	b	c	d	87.3
60	[E]DAS215	A	B	C	D	E	F	G	H	I	J	K	L	M	N	O	P	Q	R	S	T	U	V	W	X	Y	Z	[	\	]	^	_	`	a	b	c	d	87.2
61	[E]DAS049	A	B	C	D	E	F	G	H	I	J	K	L	M	N	O	P	Q	R	S	T	U	V	W	X	Y	Z	[	\	]	^	_	`	a	b	c	d	87.2
62	[E]DAS029	A	B	C	D	E	F	G	H	I	J	K	L	M	N	O	P	Q	R	S	T	U	V	W	X	Y	Z	[	\	]	^	_	`	a	b	c	d	87.0
63	[E]2Y669a	A	B	C	D	E	F	G	H	I	J	K	L	M	N	O	P	Q	R	S	T	U	V	W	X	Y	Z	[	\	]	^	_	`	a	b	c	d	86.9
64	[E]DAS069	A	B	C	D	E	F	G	H	I	J	K	L	M	N	O	P	Q	R	S	T	U	V	W	X	Y	Z	[	\	]	^	_	`	a	b	c	d	86.9
65	[E]DAS208	A	B	C	D	E	F	G	H	I	J	K	L	M	N	O	P	Q	R	S	T	U	V	W	X	Y	Z	[	\	]	^	_	`	a	b	c	d	86.8
66	[E]DAS024	A	B	C	D	E	F	G	H	I	J	K	L	M	N	O	P	Q	R	S	T	U	V	W	X	Y	Z	[	\	]	^	_	`	a	b	c	d	86.7
67	[E]DAS195	A	B	C	D	E	F	G	H	I	J	K	L	M	N	O	P	Q	R	S	T	U	V	W	X	Y	Z	[	\	]	^	_	`	a	b	c	d	86.7
68	[E]DAS223	A	B	C	D	E	F	G	H	I	J	K	L	M	N	O	P	Q	R	S	T	U	V	W	X	Y	Z	[	\	]	^	_	`	a	b	c	d	86.7
69	[E]DAS044	A	B	C	D	E	F	G	H	I	J	K	L	M	N	O	P	Q	R	S	T	U	V	W	X	Y	Z	[	\	]	^	_	`	a	b	c	d	86.5
70	[E]DAS211	A	B	C	D	E	F	G	H	I	J	K	L	M	N	O	P	Q	R	S	T	U	V	W	X	Y	Z	[	\	]	^	_	`	a	b	c	d	86.4
71	[E]DAS032	A	B	C	D	E	F	G	H	I	J	K	L	M	N	O	P	Q	R	S	T	U	V	W	X	Y	Z	[	\	]	^	_	`	a	b	c	d	86.2
72	[E]DAS050	A	B	C	D	E	F	G	H	I	J	K	L	M	N	O	P	Q	R	S	T	U	V	W	X	Y	Z	[	\	]	^	_	`	a	b	c	d	86.2
73	[E]DAS184	A	B	C	D	E	F	G	H	I	J	K	L	M	N	O	P	Q	R	S	T	U	V	W	X	Y	Z	[	\	]	^	_	`	a	b	c	d	86.1
74	[E]DAS236	A	B	C	D	E	F	G	H	I	J	K	L	M	N	O	P	Q	R	S	T	U	V	W	X	Y	Z	[	\	]	^	_	`	a	b	c	d	85.7
75	[E]DAS021	A	B	C	D	E	F	G	H	I	J	K	L	M	N	O	P	Q	R	S	T	U	V	W	X	Y	Z	[	\	]	^	_	`	a	b	c	d	85.7
76	[E]DAS157	A	B	C	D	E	F	G	H	I	J	K	L	M	N	O	P	Q	R	S	T	U	V	W	X	Y	Z	[	\	]	^	_	`	a	b	c	d	85.6
77	[E]DAS011	A	B	C	D	E	F	G	H	I	J	K	L	M	N	O	P	Q	R	S	T	U	V	W	X	Y	Z	[	\	]	^	_	`	a	b	c	d	85.4
78	[E]DAS205	A	B	C	D	E	F	G	H	I	J	K	L	M	N	O	P	Q	R	S	T	U	V	W	X	Y	Z	[	\	]	^	_	`	a	b	c	d	85.4
79	[E]DAS214	A	B	C	D	E	F	G	H	I	J	K	L	M	N	O	P	Q	R	S	T	U	V	W	X	Y	Z	[	\	]	^	_	`	a	b	c	d	85.1
80	[E]DAS028	A	B	C	D	E	F	G	H	I	J	K	L	M	N	O	P	Q	R	S	T	U	V	W	X	Y	Z	[	\	]	^	_	`	a	b	c	d	85.0
81	[E]DAS010	A	B	C	D	E	F	G	H	I	J	K	L	M	N	O	P	Q	R	S	T	U	V	W	X	Y	Z	[	\	]	^	_	`	a	b	c	d	85.0
82	[E]DAS065	A	B	C	D	E	F	G	H	I	J	K	L	M	N	O	P	Q	R	S	T	U	V	W	X	Y	Z	[	\	]	^	_	`	a	b	c	d	84.8
83	[E]DAS226	A	B	C	D	E	F	G	H	I	J	K	L	M	N	O	P	Q	R	S	T	U	V	W	X	Y	Z	[	\	]	^	_	`	a	b	c	d	84.7
84	[E]DAS149	A	B	C	D	E	F	G	H	I	J	K	L	M	N	O	P	Q	R	S	T	U	V	W	X	Y	Z	[	\	]	^	_	`	a	b	c	d	84.6
85	[E]DAS066	A	B	C	D	E	F	G	H	I	J	K	L	M	N	O	P	Q	R	S	T	U	V	W	X	Y	Z	[	\	]	^	_	`	a	b	c	d	84.4
86	[E]DAS022	A	B	C	D	E	F	G	H	I	J	K	L	M	N	O	P	Q	R	S	T	U	V	W	X	Y	Z	[	\	]	^	_	`	a	b	c	d	84.4
87	[E]MBST	A	B	C	D	E	F	G	H	I	J	K	L	M	N	O	P	Q	R	S	T	U	V	W	X	Y	Z	[	\	]	^	_	`	a	b	c	d	84.4
88	[E]DAS030	A	B	C	D	E	F	G	H	I	J	K	L	M	N	O	P	Q	R	S	T	U	V	W	X	Y	Z	[	\	]	^	_	`	a	b	c	d	84.3
89	[E]DAS005	A	B	C	D	E	F	G	H	I	J	K	L	M	N	O	P	Q	R	S	T	U	V	W	X	Y	Z	[	\	]	^	_	`	a	b	c	d	84.3
90	[E]DAS192	A	B	C	D	E	F	G	H	I	J	K	L	M	N	O	P	Q	R	S	T	U	V	W	X	Y	Z	[	\	]	^	_	`	a	b	c	d	84.2
91	[E]DAS186	A	B	C	D	E	F	G	H	I	J	K	L	M	N	O	P	Q	R	S	T	U	V	W	X	Y	Z	[	\	]	^	_	`	a	b	c	d	84.2

92	[E]DAS046	A	B	C	D	E	F	G	H	I	J	K	L	M	N	O	P	Q	R	S	T	U	V	W	X	Y	Z	[	\	]	^	_	`	a	b	c	d	84.1
93	[E]2A627c	A	B	C	D	E	F	G	H	I	J	K	L	M	N	O	P	Q	R	S	T	U	V	W	X	Y	Z	[	\	]	^	_	`	a	b	c	d	84.1
94	[E]DAS240	A	B	C	D	E	F	G	H	I	J	K	L	M	N	O	P	Q	R	S	T	U	V	W	X	Y	Z	[	\	]	^	_	`	a	b	c	d	84.0
95	[E]DAS233	A	B	C	D	E	F	G	H	I	J	K	L	M	N	O	P	Q	R	S	T	U	V	W	X	Y	Z	[	\	]	^	_	`	a	b	c	d	84.0
96	[E]DAS045	A	B	C	D	E	F	G	H	I	J	K	L	M	N	O	P	Q	R	S	T	U	V	W	X	Y	Z	[	\	]	^	_	`	a	b	c	d	83.9
97	[E]DAS003	A	B	C	D	E	F	G	H	I	J	K	L	M	N	O	P	Q	R	S	T	U	V	W	X	Y	Z	[	\	]	^	_	`	a	b	c	d	83.9
98	[E]DAS206	A	B	C	D	E	F	G	H	I	J	K	L	M	N	O	P	Q	R	S	T	U	V	W	X	Y	Z	[	\	]	^	_	`	a	b	c	d	83.9
99	[E]DAS043	A	B	C	D	E	F	G	H	I	J	K	L	M	N	O	P	Q	R	S	T	U	V	W	X	Y	Z	[	\	]	^	_	`	a	b	c	d	83.9
100	[E]DAS165	A	B	C	D	E	F	G	H	I	J	K	L	M	N	O	P	Q	R	S	T	U	V	W	X	Y	Z	[	\	]	^	_	`	a	b	c	d	83.9
101	[E]DAS216	A	B	C	D	E	F	G	H	I	J	K	L	M	N	O	P	Q	R	S	T	U	V	W	X	Y	Z	[	\	]	^	_	`	a	b	c	d	83.9
102	[E]DAS189	A	B	C	D	E	F	G	H	I	J	K	L	M	N	O	P	Q	R	S	T	U	V	W	X	Y	Z	[	\	]	^	_	`	a	b	c	d	83.9
103	[E]DAS018	A	B	C	D	E	F	G	H	I	J	K	L	M	N	O	P	Q	R	S	T	U	V	W	X	Y	Z	[	\	]	^	_	`	a	b	c	d	83.8
104	[E]DAS007	A	B	C	D	E	F	G	H	I	J	K	L	M	N	O	P	Q	R	S	T	U	V	W	X	Y	Z	[	\	]	^	_	`	a	b	c	d	83.6
105	[E]DAS190	A	B	C	D	E	F	G	H	I	J	K	L	M	N	O	P	Q	R	S	T	U	V	W	X	Y	Z	[	\	]	^	_	`	a	b	c	d	83.3
106	[E]DAS004	A	B	C	D	E	F	G	H	I	J	K	L	M	N	O	P	Q	R	S	T	U	V	W	X	Y	Z	[	\	]	^	_	`	a	b	c	d	83.2
107	[E]DAS145	A	B	C	D	E	F	G	H	I	J	K	L	M	N	O	P	Q	R	S	T	U	V	W	X	Y	Z	[	\	]	^	_	`	a	b	c	d	83.1
108	[E]DAS196	A	B	C	D	E	F	G	H	I	J	K	L	M	N	O	P	Q	R	S	T	U	V	W	X	Y	Z	[	\	]	^	_	`	a	b	c	d	82.9
109	[E]DAS207	A	B	C	D	E	F	G	H	I	J	K	L	M	N	O	P	Q	R	S	T	U	V	W	X	Y	Z	[	\	]	^	_	`	a	b	c	d	82.9
110	[E]DAS017	A	B	C	D	E	F	G	H	I	J	K	L	M	N	O	P	Q	R	S	T	U	V	W	X	Y	Z	[	\	]	^	_	`	a	b	c	d	82.8
111	[E]DAS202	A	B	C	D	E	F	G	H	I	J	K	L	M	N	O	P	Q	R	S	T	U	V	W	X	Y	Z	[	\	]	^	_	`	a	b	c	d	82.7
112	[E]DAS027	A	B	C	D	E	F	G	H	I	J	K	L	M	N	O	P	Q	R	S	T	U	V	W	X	Y	Z	[	\	]	^	_	`	a	b	c	d	82.7
113	[E]DAS150	A	B	C	D	E	F	G	H	I	J	K	L	M	N	O	P	Q	R	S	T	U	V	W	X	Y	Z	[	\	]	^	_	`	a	b	c	d	82.7
114	[E]DAS023	A	B	C	D	E	F	G	H	I	J	K	L	M	N	O	P	Q	R	S	T	U	V	W	X	Y	Z	[	\	]	^	_	`	a	b	c	d	82.6
115	[E]DAS033	A	B	C	D	E	F	G	H	I	J	K	L	M	N	O	P	Q	R	S	T	U	V	W	X	Y	Z	[	\	]	^	_	`	a	b	c	d	82.6
116	[E]DAS146	A	B	C	D	E	F	G	H	I	J	K	L	M	N	O	P	Q	R	S	T	U	V	W	X	Y	Z	[	\	]	^	_	`	a	b	c	d	82.5
117	[E]DAS059	A	B	C	D	E	F	G	H	I	J	K	L	M	N	O	P	Q	R	S	T	U	V	W	X	Y	Z	[	\	]	^	_	`	a	b	c	d	82.2
118	[E]DAS182	A	B	C	D	E	F	G	H	I	J	K	L	M	N	O	P	Q	R	S	T	U	V	W	X	Y	Z	[	\	]	^	_	`	a	b	c	d	82.2
119	[E]DAS193	A	B	C	D	E	F	G	H	I	J	K	L	M	N	O	P	Q	R	S	T	U	V	W	X	Y	Z	[	\	]	^	_	`	a	b	c	d	81.8

120	[E]DAS231	A	B	C	D	E	F	G	H	I	J	K	L	M	N	O	P	Q	R	S	T	U	V	W	X	Y	Z	[	\	]	^	_	`	a	b	c	d	81.6
121	[E]DAS020	A	B	C	D	E	F	G	H	I	J	K	L	M	N	O	P	Q	R	S	T	U	V	W	X	Y	Z	[	\	]	^	_	`	a	b	c	d	81.6
122	[E]DAS051	A	B	C	D	E	F	G	H	I	J	K	L	M	N	O	P	Q	R	S	T	U	V	W	X	Y	Z	[	\	]	^	_	`	a	b	c	d	81.4
123	[E]DAS173	A	B	C	D	E	F	G	H	I	J	K	L	M	N	O	P	Q	R	S	T	U	V	W	X	Y	Z	[	\	]	^	_	`	a	b	c	d	81.2
124	[E]LH59	A	B	C	D	E	F	G	H	I	J	K	L	M	N	O	P	Q	R	S	T	U	V	W	X	Y	Z	[	\	]	^	_	`	a	b	c	d	81.0
125	[E]DAS204	A	B	C	D	E	F	G	H	I	J	K	L	M	N	O	P	Q	R	S	T	U	V	W	X	Y	Z	[	\	]	^	_	`	a	b	c	d	80.8
126	[E]DAS179	A	B	C	D	E	F	G	H	I	J	K	L	M	N	O	P	Q	R	S	T	U	V	W	X	Y	Z	[	\	]	^	_	`	a	b	c	d	80.7
127	[E]DAS238	A	B	C	D	E	F	G	H	I	J	K	L	M	N	O	P	Q	R	S	T	U	V	W	X	Y	Z	[	\	]	^	_	`	a	b	c	d	80.5
128	[E]DAS054	A	B	C	D	E	F	G	H	I	J	K	L	M	N	O	P	Q	R	S	T	U	V	W	X	Y	Z	[	\	]	^	_	`	a	b	c	d	80.3
129	[E]DAS172	A	B	C	D	E	F	G	H	I	J	K	L	M	N	O	P	Q	R	S	T	U	V	W	X	Y	Z	[	\	]	^	_	`	a	b	c	d	79.6
130	[E]DAS015	A	B	C	D	E	F	G	H	I	J	K	L	M	N	O	P	Q	R	S	T	U	V	W	X	Y	Z	[	\	]	^	_	`	a	b	c	d	79.6
131	[E]DAS234	A	B	C	D	E	F	G	H	I	J	K	L	M	N	O	P	Q	R	S	T	U	V	W	X	Y	Z	[	\	]	^	_	`	a	b	c	d	79.5
132	[E]DAS188	A	B	C	D	E	F	G	H	I	J	K	L	M	N	O	P	Q	R	S	T	U	V	W	X	Y	Z	[	\	]	^	_	`	a	b	c	d	79.4
133	[E]DAS048	A	B	C	D	E	F	G	H	I	J	K	L	M	N	O	P	Q	R	S	T	U	V	W	X	Y	Z	[	\	]	^	_	`	a	b	c	d	79.4
134	[E]DAS012	A	B	C	D	E	F	G	H	I	J	K	L	M	N	O	P	Q	R	S	T	U	V	W	X	Y	Z	[	\	]	^	_	`	a	b	c	d	79.1
135	[E]DAS148	A	B	C	D	E	F	G	H	I	J	K	L	M	N	O	P	Q	R	S	T	U	V	W	X	Y	Z	[	\	]	^	_	`	a	b	c	d	78.8
136	[E]DAS171	A	B	C	D	E	F	G	H	I	J	K	L	M	N	O	P	Q	R	S	T	U	V	W	X	Y	Z	[	\	]	^	_	`	a	b	c	d	78.7
137	[E]B97	A	B	C	D	E	F	G	H	I	J	K	L	M	N	O	P	Q	R	S	T	U	V	W	X	Y	Z	[	\	]	^	_	`	a	b	c	d	78.7
138	[E]DAS071	A	B	C	D	E	F	G	H	I	J	K	L	M	N	O	P	Q	R	S	T	U	V	W	X	Y	Z	[	\	]	^	_	`	a	b	c	d	78.7
139	[E]DAS155	A	B	C	D	E	F	G	H	I	J	K	L	M	N	O	P	Q	R	S	T	U	V	W	X	Y	Z	[	\	]	^	_	`	a	b	c	d	78.5
140	[E]DAS037	A	B	C	D	E	F	G	H	I	J	K	L	M	N	O	P	Q	R	S	T	U	V	W	X	Y	Z	[	\	]	^	_	`	a	b	c	d	78.5
141	[E]DAS019	A	B	C	D	E	F	G	H	I	J	K	L	M	N	O	P	Q	R	S	T	U	V	W	X	Y	Z	[	\	]	^	_	`	a	b	c	d	78.5
142	[E]DAS237	A	B	C	D	E	F	G	H	I	J	K	L	M	N	O	P	Q	R	S	T	U	V	W	X	Y	Z	[	\	]	^	_	`	a	b	c	d	78.4
143	[E]DAS036	A	B	C	D	E	F	G	H	I	J	K	L	M	N	O	P	Q	R	S	T	U	V	W	X	Y	Z	[	\	]	^	_	`	a	b	c	d	78.0

144	[E]DAS178	A	B	C	D	E	F	G	H	I	J	K	L	M	N	O	P	Q	R	S	T	U	V	W	X	Y	Z	[	\	]	^	_	`	a	b	c	d	77.0
145	[E]DAS144	A	B	C	D	E	F	G	H	I	J	K	L	M	N	O	P	Q	R	S	T	U	V	W	X	Y	Z	[	\	]	^	_	`	a	b	c	d	76.6
146	[E]DAS220	A	B	C	D	E	F	G	H	I	J	K	L	M	N	O	P	Q	R	S	T	U	V	W	X	Y	Z	[	\	]	^	_	`	a	b	c	d	76.6
147	[E]PHT77		B	C		E	F					K		M			P	Q	R	S	T	U	V	W	X	Y	Z	[	\	]	^	_	`	a	b	c	d	75.9
148	[E]H95			C		E	F					K		M					R	S	T	U	V	W	X	Y	Z	[	\	]	^	_	`	a	b	c	d	74.3
149	[E]DAS164			C		E	F					K		M					R	S	T	U	V	W	X	Y	Z	[	\	]	^	_	`	a	b	c	d	73.8
150	[E]DAS063			C		E	F					K		M					R	S	T	U	V	W	X	Y	Z	[	\	]	^	_	`	a	b	c	d	72.8
151	[E]DAS180			C		E	F					K		M					R	S	T	U	V	W	X	Y	Z	[	\	]	^	_	`	a	b	c	d	72.5
152	[E]5707			C		E	F					K		M					R	S	T	U	V	W	X	Y	Z	[	\	]	^	_	`	a	b	c	d	70.8
153	[E]78371A			C		E	F					K		M					R	S	T	U	V	W	X	Y	Z	[	\	]	^	_	`	a	b	c	d	70.7
154	[E]4226					E	F					K		M									V		X			[	\	]	^	_	`	a	b	c	d	68.3
155	[E]MBPM						F					K		M																	^	_	`	a	b	c	d	67.9
156	[E]Pa875											K		M																		_	`	a	b	c	d	66.6
157	[E]R4													M																			`		b	c	d	64.3

Appendix D. Entries in late maturity group ranked by NIE least square mean values (α = 0.05) across both locations in 2015 (kg grain per kg N)

Rank	Level																																				LSqM
1	[Late]DAS087	A	B	C		E	F					K		M																								97.1
2	[Late]DAS136	A	B	C	D	E	F					K		M					R																			96.5
3	[Late]DAS120	A	B	C	D	E	F					K		M					R																			96.4
4	[Late]DAS130	A	B	C	D	E	F					K		M					R																			96.4
5	[Late]DAS090	A	B	C	D	E	F	G				K		M					R	S			V															95.6
6	[Late]DAS080	A	B	C	D	E	F	G	H			K		M					R	S	T		V		X													95.5
7	[Late]DAS129	A	B	C	D	E	F	G	H	I		K		M					R	S	T	U	V		X			[									94.8
8	[Late]DAS138	A	B	C	D	E	F	G	H	I	J	K		M					R	S	T	U	V	W	X			[	\								93.9
9	[Late]DAS132	A	B	C	D	E	F	G	H			K		M					R	S	T		V		X													93.9
10	[Late]DAS131	A	B	C	D	E	F	G	H	I		K		M					R	S	T	U	V		X			[									93.6
11	[Late]2J794	A	B	C	D	E	F					K		M					R																			93.4
12	[Late]DAS100	A	B	C	D	E	F	G	H	I	J	K		M					R	S	T	U	V	W	X			[	\								93.0
13	[Late]DAS079	A	B	C	D	E	F	G	H	I	J	K		M					R	S	T	U	V	W	X			[	\								93.0
14	[Late]DAS128	A	B	C	D	E	F	G	H	I	J	K		M					R	S	T	U	V	W	X			[	\								92.8
15	[Late]DAS091	A	B	C	D	E	F	G	H	I	J	K		M					R	S	T	U	V	W	X			[	\								92.7
16	[Late]DAS152	A	B	C	D	E	F	G	H	I	J	K	L	M	N	O	P		R	S	T	U	V	W	X	Y	Z	[	\	]	^	_	`	a	b	c	d	92.5
17	[Late]2C799	A	B	C	D	E	F	G	H			K		M					R	S	T		V		X													92.4
18	[Late]DAS119	A	B	C	D	E	F	G	H	I	J	K		M					R	S	T	U	V	W	X			[	\								92.3
19	[Late]DAS083	A	B	C	D	E	F	G	H	I	J	K	L	M					R	S	T	U	V	W	X	Y		[	\	]	^	_	`					91.7
20	[Late]2G685	A	B	C	D	E	F	G	H			K		M					R	S	T		V		X													91.6
21	[Late]DAS115	A	B	C	D	E	F	G	H	I	J	K	L	M					R	S	T	U	V	W	X	Y		[	\	]	^	_	`					91.6
22	[Late]DAS075	A	B	C	D	E	F	G	H	I	J	K	L	M					R	S	T	U	V	W	X	Y		[	\	]	^	_	`					91.5
23	[Late]DAS099	A	B	C	D	E	F	G	H	I	J	K	L	M	N				R	S	T	U	V	W	X	Y	Z	[	\	]	^	_	`	a	b			90.9
24	[Late]DAS098	A	B	C	D	E	F	G	H	I	J	K	L	M	N				R	S	T	U	V	W	X	Y	Z	[	\	]	^	_	`	a	b			90.9
25	[Late]DAS113	A	B	C	D	E	F	G	H	I	J	K	L	M	N				R	S	T	U	V	W	X	Y	Z	[	\	]	^	_	`	a	b			90.7
26	[Late]DAS097	A	B	C	D	E	F	G	H	I	J	K	L	M	N				R	S	T	U	V	W	X	Y	Z	[	\	]	^	_	`	a	b			90.4
27	[Late]DAS241	A	B	C	D	E	F	G	H	I	J	K	L	M	N				R	S	T	U	V	W	X	Y	Z	[	\	]	^	_	`	a	b			90.4
28	[Late]DAS210	A	B	C	D	E	F	G	H	I	J	K	L	M	N				R	S	T	U	V	W	X	Y	Z	[	\	]	^	_	`	a	b			90.1
29	[Late]DAS139	A	B	C	D	E	F	G	H	I	J	K	L	M	N	O			R	S	T	U	V	W	X	Y	Z	[	\	]	^	_	`	a	b	c		90.0
30	[Late]DAS074	A	B	C	D	E	F	G	H	I	J	K	L	M	N	O			R	S	T	U	V	W	X	Y	Z	[	\	]	^	_	`	a	b	c		89.4
31	[Late]2V709	A	B	C	D	E	F	G	H	I	J	K		M					R	S	T	U	V	W	X			[	\									89.3
32	[Late]DAS078	A	B	C	D	E	F	G	H	I	J	K	L	M	N	O			R	S	T	U	V	W	X	Y	Z	[	\	]	^	_	`	a	b	c		89.3
33	[Late]DAS105	A	B	C	D	E	F	G	H	I	J	K	L	M	N	O			R	S	T	U	V	W	X	Y	Z	[	\	]	^	_	`	a	b	c		89.1
34	[Late]DAS134	A	B	C	D	E	F	G	H	I	J	K	L	M	N	O			R	S	T	U	V	W	X	Y	Z	[	\	]	^	_	`	a	b	c		89.0
35	[Late]DAS141	A	B	C	D	E	F	G	H	I	J	K	L	M	N	O	P		R	S	T	U	V	W	X	Y	Z	[	\	]	^	_	`	a	b	c	d	88.2
36	[Late]DAS114	A	B	C	D	E	F	G	H	I	J	K	L	M	N	O	P		R	S	T	U	V	W	X	Y	Z	[	\	]	^	_	`	a	b	c	d	88.2
37	[Late]DAS209	A	B	C	D	E	F	G	H	I	J	K	L	M	N	O	P		R	S	T	U	V	W	X	Y	Z	[	\	]	^	_	`	a	b	c	d	88.0
38	[Late]DAS235	A	B	C	D	E	F	G	H	I	J	K	L	M	N	O	P	Q	R	S	T	U	V	W	X	Y	Z	[	\	]	^	_	`	a	b	c	d	88.0
39	[Late]DAS225	A	B	C	D	E	F	G	H	I	J	K	L	M	N	O	P		R	S	T	U	V	W	X	Y	Z	[	\	]	^	_	`	a	b	c	d	87.9
40	[Late]DAS217	A	B	C	D	E	F	G	H	I	J	K	L	M	N	O	P		R	S	T	U	V	W	X	Y	Z	[	\	]	^	_	`	a	b	c	d	87.7
41	[Late]DAS093	A	B	C	D	E	F	G	H	I	J	K	L	M	N	O	P		R	S	T	U	V	W	X	Y	Z	[	\	]	^	_	`	a	b	c	d	87.7
42	[Late]DAS166	A	B	C	D	E	F	G	H	I	J	K	L	M	N	O	P		R	S	T	U	V	W	X	Y	Z	[	\	]	^	_	`	a	b	c	d	87.7
43	[Late]DAS239	A	B	C	D	E	F	G	H	I	J	K	L	M	N	O	P		R	S	T	U	V	W	X	Y	Z	[	\	]	^	_	`	a	b	c	d	87.6
44	[Late]DAS122	A	B	C	D	E	F	G	H	I	J	K	L	M	N	O	P		R	S	T	U	V	W	X	Y	Z	[	\	]	^	_	`	a	b	c	d	87.6
45	[Late]DAS135	A	B	C	D	E	F	G	H	I	J	K	L	M	N	O	P		R	S	T	U	V	W	X	Y	Z	[	\	]	^	_	`	a	b	c	d	87.1
46	[Late]DAS198	A	B	C	D	E	F	G	H	I	J	K	L	M	N	O	P	Q	R	S	T	U	V	W	X	Y	Z	[	\	]	^	_	`	a	b	c	d	86.8
47	[Late]DAS082	A	B	C	D	E	F	G	H	I	J	K	L	M	N	O	P		R	S	T	U	V	W	X	Y	Z	[	\	]	^	_	`	a	b	c	d	86.5
48	[Late]DAS126	A	B	C	D	E	F	G	H	I	J	K	L	M	N	O	P	Q	R	S	T	U	V	W	X	Y	Z	[	\	]	^	_	`	a	b	c	d	86.0
49	[Late]DAS092	A	B	C	D	E	F	G	H	I	J	K	L	M	N	O	P	Q	R	S	T	U	V	W	X	Y	Z	[	\	]	^	_	`	a	b	c	d	85.8

50	[Late]DAS153	A	B	C	D	E	F	G	H	I	J	K	L	M	N	O	P	Q	R	S	T	U	V	W	X	Y	Z	[	\	]	^	_	`	a	b	c	d	85.8
51	[Late]DAS201	A	B	C	D	E	F	G	H	I	J	K	L	M	N	O	P	Q	R	S	T	U	V	W	X	Y	Z	[	\	]	^	_	`	a	b	c	d	85.5
52	[Late]DAS117	A	B	C	D	E	F	G	H	I	J	K	L	M	N	O	P	Q	R	S	T	U	V	W	X	Y	Z	[	\	]	^	_	`	a	b	c	d	85.4
53	[Late]PHG35	A	B	C	D	E	F	G	H	I	J	K	L	M	N	O	P	Q	R	S	T	U	V	W	X	Y	Z	[	\	]	^	_	`	a	b	c	d	85.3
54	[Late]DAS089	A	B	C	D	E	F	G	H	I	J	K	L	M	N	O	P	Q	R	S	T	U	V	W	X	Y	Z	[	\	]	^	_	`	a	b	c	d	85.2
55	[Late]DAS085	A	B	C	D	E	F	G	H	I	J	K	L	M	N	O	P	Q	R	S	T	U	V	W	X	Y	Z	[	\	]	^	_	`	a	b	c	d	85.1
56	[Late]DAS224	A	B	C	D	E	F	G	H	I	J	K	L	M	N	O	P	Q	R	S	T	U	V	W	X	Y	Z	[	\	]	^	_	`	a	b	c	d	85.0
57	[Late]DAS121	A	B	C	D	E	F	G	H	I	J	K	L	M	N	O	P	Q	R	S	T	U	V	W	X	Y	Z	[	\	]	^	_	`	a	b	c	d	85.0
58	[Late]DAS104	A	B	C	D	E	F	G	H	I	J	K	L	M	N	O	P	Q	R	S	T	U	V	W	X	Y	Z	[	\	]	^	_	`	a	b	c	d	84.8
59	[Late]DAS084	A	B	C	D	E	F	G	H	I	J	K	L	M	N	O	P	Q	R	S	T	U	V	W	X	Y	Z	[	\	]	^	_	`	a	b	c	d	84.7
60	[Late]B106	A	B	C	D	E	F	G	H	I	J	K	L	M	N	O	P	Q	R	S	T	U	V	W	X	Y	Z	[	\	]	^	_	`	a	b	c	d	84.7
61	[Late]NC232	A	B	C	D	E	F	G	H	I	J	K	L	M	N	O	P	Q	R	S	T	U	V	W	X	Y	Z	[	\	]	^	_	`	a	b	c	d	84.5
62	[Late]DAS137	A	B	C	D	E	F	G	H	I	J	K	L	M	N	O	P	Q	R	S	T	U	V	W	X	Y	Z	[	\	]	^	_	`	a	b	c	d	84.1
63	[Late]DAS109	A	B	C	D	E	F	G	H	I	J	K	L	M	N	O	P	Q	R	S	T	U	V	W	X	Y	Z	[	\	]	^	_	`	a	b	c	d	83.9
64	[Late]DAS110	A	B	C	D	E	F	G	H	I	J	K	L	M	N	O	P	Q	R	S	T	U	V	W	X	Y	Z	[	\	]	^	_	`	a	b	c	d	83.8
65	[Late]DAS218	A	B	C	D	E	F	G	H	I	J	K	L	M	N	O	P	Q	R	S	T	U	V	W	X	Y	Z	[	\	]	^	_	`	a	b	c	d	83.7
66	[Late]DAS108	A	B	C	D	E	F	G	H	I	J	K	L	M	N	O	P	Q	R	S	T	U	V	W	X	Y	Z	[	\	]	^	_	`	a	b	c	d	83.6
67	[Late]DAS095	A	B	C	D	E	F	G	H	I	J	K	L	M	N	O	P	Q	R	S	T	U	V	W	X	Y	Z	[	\	]	^	_	`	a	b	c	d	83.6
68	[Late]DAS116	A	B	C	D	E	F	G	H	I	J	K	L	M	N	O	P	Q	R	S	T	U	V	W	X	Y	Z	[	\	]	^	_	`	a	b	c	d	83.5
69	[Late]DAS140	A	B	C	D	E	F	G	H	I	J	K	L	M	N	O	P	Q	R	S	T	U	V	W	X	Y	Z	[	\	]	^	_	`	a	b	c	d	83.4
70	[Late]DAS103	A	B	C	D	E	F	G	H	I	J	K	L	M	N	O	P	Q	R	S	T	U	V	W	X	Y	Z	[	\	]	^	_	`	a	b	c	d	83.3
71	[Late]DAS242	A	B	C	D	E	F	G	H	I	J	K	L	M	N	O	P	Q	R	S	T	U	V	W	X	Y	Z	[	\	]	^	_	`	a	b	c	d	83.0
72	[Late]DAS106	A	B	C	D	E	F	G	H	I	J	K	L	M	N	O	P	Q	R	S	T	U	V	W	X	Y	Z	[	\	]	^	_	`	a	b	c	d	82.9
73	[Late]DAS127	A	B	C	D	E	F	G	H	I	J	K	L	M	N	O	P	Q	R	S	T	U	V	W	X	Y	Z	[	\	]	^	_	`	a	b	c	d	82.8
74	[Late]DAS177	A	B	C	D	E	F	G	H	I	J	K	L	M	N	O	P	Q	R	S	T	U	V	W	X	Y	Z	[	\	]	^	_	`	a	b	c	d	82.8
75	[Late]DAS124	A	B	C	D	E	F	G	H	I	J	K	L	M	N	O	P	Q	R	S	T	U	V	W	X	Y	Z	[	\	]	^	_	`	a	b	c	d	82.6
76	[Late]DAS229	A	B	C	D	E	F	G	H	I	J	K	L	M	N	O	P	Q	R	S	T	U	V	W	X	Y	Z	[	\	]	^	_	`	a	b	c	d	82.3
77	[Late]DAS107	A	B	C	D	E	F	G	H	I	J	K	L	M	N	O	P	Q	R	S	T	U	V	W	X	Y	Z	[	\	]	^	_	`	a	b	c	d	82.3
78	[Late]DAS094	A	B	C	D	E	F	G	H	I	J	K	L	M	N	O	P	Q	R	S	T	U	V	W	X	Y	Z	[	\	]	^	_	`	a	b	c	d	82.2
79	[Late]DAS081	A	B	C	D	E	F	G	H	I	J	K	L	M	N	O	P	Q	R	S	T	U	V	W	X	Y	Z	[	\	]	^	_	`	a	b	c	d	82.0
80	[Late]DAS123	A	B	C	D	E	F	G	H	I	J	K	L	M	N	O	P	Q	R	S	T	U	V	W	X	Y	Z	[	\	]	^	_	`	a	b	c	d	82.0
81	[Late]PHR47	A	B	C	D	E	F	G	H	I	J	K	L	M	N	O	P	Q	R	S	T	U	V	W	X	Y	Z	[	\	]	^	_	`	a	b	c	d	82.0
82	[Late]DAS142	A	B	C	D	E	F	G	H	I	J	K	L	M	N	O	P	Q	R	S	T	U	V	W	X	Y	Z	[	\	]	^	_	`	a	b	c	d	81.9
83	[Late]DAS088	A	B	C	D	E	F	G	H	I	J	K	L	M	N	O	P	Q	R	S	T	U	V	W	X	Y	Z	[	\	]	^	_	`	a	b	c	d	81.7
84	[Late]DAS111	A	B	C	D	E	F	G	H	I	J	K	L	M	N	O	P	Q	R	S	T	U	V	W	X	Y	Z	[	\	]	^	_	`	a	b	c	d	81.6
85	[Late]DAS102	A	B	C	D	E	F	G	H	I	J	K	L	M	N	O	P	Q	R	S	T	U	V	W	X	Y	Z	[	\	]	^	_	`	a	b	c	d	81.5
86	[Late]DAS197	A	B	C	D	E	F	G	H	I	J	K	L	M	N	O	P	Q	R	S	T	U	V	W	X	Y	Z	[	\	]	^	_	`	a	b	c	d	81.3
87	[Late]B100	A	B	C	D	E	F	G	H	I	J	K	L	M	N	O	P	Q	R	S	T	U	V	W	X	Y	Z	[	\	]	^	_	`	a	b	c	d	81.1
88	[Late]DAS073	A	B	C	D	E	F	G	H	I	J	K	L	M	N	O	P	Q	R	S	T	U	V	W	X	Y	Z	[	\	]	^	_	`	a	b	c	d	81.1
89	[Late]DAS077	A	B	C	D	E	F	G	H	I	J	K	L	M	N	O	P	Q	R	S	T	U	V	W	X	Y	Z	[	\	]	^	_	`	a	b	c	d	80.9
90	[Late]DAS232	A	B	C	D	E	F	G	H	I	J	K	L	M	N	O	P	Q	R	S	T	U	V	W	X	Y	Z	[	\	]	^	_	`	a	b	c	d	80.6
91	[Late]DAS160	A	B	C	D	E	F	G	H	I	J	K	L	M	N	O	P	Q	R	S	T	U	V	W	X	Y	Z	[	\	]	^	_	`	a	b	c	d	80.6
92	[Late]DAS156	A	B	C	D	E	F	G	H	I	J	K	L	M	N	O	P	Q	R	S	T	U	V	W	X	Y	Z	[	\	]	^	_	`	a	b	c	d	80.4
93	[Late]DAS159	A	B	C	D	E	F	G	H	I	J	K	L	M	N	O	P	Q	R	S	T	U	V	W	X	Y	Z	[	\	]	^	_	`	a	b	c	d	80.4
94	[Late]DAS230	A	B	C	D	E	F	G	H	I	J	K	L	M	N	O	P	Q	R	S	T	U	V	W	X	Y	Z	[	\	]	^	_	`	a	b	c	d	80.3
95	[Late]DAS143	A	B	C	D	E	F	G	H	I	J	K	L	M	N	O	P	Q	R	S	T	U	V	W	X	Y	Z	[	\	]	^	_	`	a	b	c	d	79.9
96	[Late]DAS086	A	B	C	D	E	F	G	H	I	J	K	L	M	N	O	P	Q	R	S	T	U	V	W	X	Y	Z	[	\	]	^	_	`	a	b	c	d	79.7
97	[Late]DAS118	A	B	C	D	E	F	G	H	I	J	K	L	M	N	O	P	Q	R	S	T	U	V	W	X	Y	Z	[	\	]	^	_	`	a	b	c	d	79.7
98	[Late]DAS168	A	B	C	D	E	F	G	H	I	J	K	L	M	N	O	P	Q	R	S	T	U	V	W	X	Y	Z	[	\	]	^	_	`	a	b	c	d	79.6
99	[Late]MDF-13D	A	B	C	D	E	F	G	H	I	J	K	L	M	N	O	P	Q	R	S	T	U	V	W	X	Y	Z	[	\	]	^	_	`	a	b	c	d	79.3
100	[Late]DAS112	A	B	C	D	E	F	G	H	I	J	K	L	M	N	O	P	Q	R	S	T	U	V	W	X	Y	Z	[	\	]	^	_	`	a	b	c	d	79.3
101	[Late]PHV63	A	B	C	D	E	F	G	H	I	J	K	L	M	N	O	P	Q	R	S	T	U	V	W	X	Y	Z	[	\	]	^	_	`	a	b	c	d	79.3
102	[Late]DAS212	A	B	C	D	E	F	G	H	I	J	K	L	M	N	O	P	Q	R	S	T	U	V	W	X	Y	Z	[	\	]	^	_	`	a	b	c	d	79.3
103	[Late]DAS133	A	B	C	D	E	F	G	H	I	J	K	L	M	N	O	P	Q	R	S	T	U	V	W	X	Y	Z	[	\	]	^	_	`	a	b	c	d	79.2

104	[Late]DAS125	A	B	C	D	E	F	G	H	I	J	K	L	M	N	O	P	Q	R	S	T	U	V	W	X	Y	Z	[	\	]	^	_	`	a	b	c	d	79.1
105	[Late]CR1Ht	A	B	C	D	E	F	G	H	I	J	K	L	M	N	O	P	Q	R	S	T	U	V	W	X	Y	Z	[	\	]	^	_	`	a	b	c	d	78.8
106	[Late]DAS199	A	B	C	D	E	F	G	H	I	J	K	L	M	N	O	P	Q	R	S	T	U	V	W	X	Y	Z	[	\	]	^	_	`	a	b	c	d	78.0
107	[Late]VA99	A	B	C	D	E	F	G	H	I	J	K	L	M	N	O	P	Q	R	S	T	U	V	W	X	Y	Z	[	\	]	^	_	`	a	b	c	d	78.0
108	[Late]DAS101	A	B	C	D	E	F	G	H	I	J	K	L	M	N	O	P	Q	R	S	T	U	V	W	X	Y	Z	[	\	]	^	_	`	a	b	c	d	77.8
109	[Late]DAS175	A	B	C	D	E	F	G	H	I	J	K	L	M	N	O	P	Q	R	S	T	U	V	W	X	Y	Z	[	\	]	^	_	`	a	b	c	d	77.5
110	[Late]PHM49	A	B	C	D	E	F	G	H	I	J	K	L	M	N	O	P	Q	R	S	T	U	V	W	X	Y	Z	[	\	]	^	_	`	a	b	c	d	77.1
111	[Late]DAS154	A	B	C	D	E	F	G	H	I	J	K	L	M	N	O	P	Q	R	S	T	U	V	W	X	Y	Z	[	\	]	^	_	`	a	b	c	d	77.0
112	[Late]NC364	A	B	C	D	E	F	G	H	I	J	K	L	M	N	O	P	Q	R	S	T	U	V	W	X	Y	Z	[	\	]	^	_	`	a	b	c	d	76.8
113	[Late]B55	A	B	C	D	E	F	G	H	I	J	K	L	M	N	O	P	Q	R	S	T	U	V	W	X	Y	Z	[	\	]	^	_	`	a	b	c	d	76.7
114	[Late]PHW65	A	B	C	D	E	F	G	H	I	J	K	L	M	N	O	P	Q	R	S	T	U	V	W	X	Y	Z	[	\	]	^	_	`	a	b	c	d	76.4
115	[Late]DAS213	A	B	C	D	E	F	G	H	I	J	K	L	M	N	O	P	Q	R	S	T	U	V	W	X	Y	Z	[	\	]	^	_	`	a	b	c	d	75.8
116	[Late]PHR32				D			G	H	I	J		L		N	O	P	Q	R	S	T	U	V	W	X	Y	Z	[	\	]	^	_	`	a	b	c	d	74.6
117	[Late]DAS167	A	B	C	D	E	F	G	H	I	J	K	L	M	N	O	P	Q	R	S	T	U	V	W	X	Y	Z	[	\	]	^	_	`	a	b	c	d	74.5
118	[Late]DAS176							G	H	I	J		L		N	O	P	Q		S	T	U	V	W	X	Y	Z	[	\	]	^	_	`	a	b	c	d	72.7
119	[Late]B87								H	I	J		L		N	O	P	Q			T	U		W	X	Y	Z	[	\	]	^	_	`	a	b	c	d	72.4
120	[Late]Va14									I	J		L		N	O	P	Q				U		W		Y	Z	[	\	]	^	_	`	a	b	c	d	70.3
121	[Late]T8										J		L		N	O	P	Q						W		Y	Z		\	]	^	_	`	a	b	c	d	69.2
122	[Late]Mo1W												L		N	O	P	Q								Y	Z			]	^	_	`	a	b	c	d	67.4
123	[Late]WF9												L		N	O	P	Q								Y	Z			]	^	_	`	a	b	c	d	67.2
124	[Late]DAS076														N	O	P	Q									Z							a	b	c	d	66.4
125	[Late]Va85															O	P	Q																		c	d	65.1
126	[Late]DAS169															O	P	Q																		c	d	64.5
127	[Late]Pa880																P	Q																			d	62.9
128	[Late]DAS096																	Q																				60.1

CHAPTER 3. HYPERSPECTRAL INDICES FOR NITROGEN USE EFFICIENCY PREDICTION IN MAIZE HYBRIDS

3.1 Abstract

Nitrogen (N), as an essential nutrient for plant growth, is used by farmers to increase grain yield production in maize. Enhancing the N efficiency of maize hybrids is a common goal of many researchers. Unfortunately, studying and breeding for maize hybrids which utilize N most efficiently is a laborious process due to the costly need for repeated field and laboratory measurements. Hyperspectral remote sensing has recently been investigated for measuring and predicting biomass, N content, and grain yield in maize. We hypothesized that vegetation indices obtained through hyperspectral remote sensing could predict N parameters of Nitrogen Conversion Efficiency (NCE) and Nitrogen Internal Efficiency (NIE), both of which are measures of the plant's ability to produce biomass or grain yield for each unit of N taken up, respectively. Analysis of 20 hyperspectral indices from imaging at V16/18 and R1/R2 by manned aircraft and UAVs over three site-years using mixed models showed that two indices, HBSI1 and HBS2, were predictive of NCE, and two indices, HBCI8 and HBCI9 were predictive of NIE for actual data collected from five to as many as nine hybrids and multiple N rates at maturity. Statistical differentiation of hybrids in their NCE or NIE performance was possible based on the models with the greatest accuracy obtained for NIE. The indices most predictive of NCE were NIR:Red indices developed for studying structural plant components. Those predictive of NIE were indices based on the green or green:blue portions of the spectrum initially established for studying biochemical plant components. Confirmation of these indices for the predictability of the N parameters with other hybrids, locations and remote sensing platforms could lead to the application of these indices facilitating N efficiency research with a potential for significant advancements in the N efficiency of maize hybrids.

3.2 Introduction

Nitrogen (N) is an essential nutrient for plants and is commonly found in various fertilizer forms to support agricultural production (Ribaudo et al., 2011). Unfortunately, the actual N available to maize plants is often much less than the fertilizer amounts applied, since mineral N availability is

affected by a multitude of factors such as precipitation, temperature, microbial effects, soil type, rate of application, placement, timing, fertilizer source, etc. (Ribaudo et al., 2011). Ciampitti and Vyn (2012) found a 44% N recovery efficiency (NRE, plant N uptake per unit of applied N fertilizer) at moderate N rates for maize hybrids commercialized after 1990. However, more recently Mueller et al. (2019) found NRE to be approximately 50-55% at high N levels for hybrids commercialized after 2000, suggesting that much of the applied N is still lost. N recovery efficiencies tend to improve at low N rates, but applying lower than agronomic optimum N rates also result in yield declines for growers. Such excessive losses are an economic as well as environmental cost, negatively affecting air and water quality as well as human health (Doering et al., 2011; Ribaudo et al., 2011). Therefore, a large opportunity exists to decrease N use and loss by increasing maize's efficiency in using this important nutrient.

Though breeding for yield in maize has improved plant N uptake efficiency indirectly (K. Chen & T. J. Vyn, 2017; Ciampitti & Vyn, 2012; DeBruin et al., 2017; Moose et al., 2009), greater focused research into plant N efficiency has been encouraged by experts (Doering et al., 2011). Crop physiology research has advanced in the understanding of in-season N dynamics and plant component partitioning, and has developed various N uptake and utilization parameters to describe N use efficiency (Moll et al., 1982; Shrawat et al., 2018). A plant's N use consists of a multitude of processes such as N uptake, translocation, assimilation, and remobilization. Nitrogen use efficiency (NUE) is a measure of the productivity and agronomic efficiency of plant response to N. For grain producing crops, NUE compares the amount of grain produced by the crop relative to the amount of fertilizer provided to the crop (Moll et al., 1982; Salvagiotti et al., 2009). The major components of NUE, two additional N parameters, are Nitrogen Internal Efficiency (NIE) and Nitrogen Recovery Efficiency (NRE) (Ciampitti & Vyn, 2011; Moll et al., 1982). NIE measures the end consequences of season-long N translocation and utilization based on the amount of grain produced by the plant per unit of plant N at maturity. NRE, a measure of N uptake, is the amount of total plant N per unit of applied N fertilizer. Another important component to a plant's use of N is the Nitrogen Conversion Efficiency (NCE) parameter which is a measure of how much biomass a plant produces per unit N in the plant (K. Chen & T. J. Vyn, 2017; Gastal et al., 2015).

These N parameters are potentially useful in studying N dynamics. They are based on field sampling and laboratory based methods such as Dumas combustion for N tissue determination.

Though well established, these methods require destructive tissue sampling which is time consuming and costly (Muñoz-Huerta et al., 2013; Unkovich et al., 2008; Zhao et al., 2003). While there have been extensive advancements in the field of genotyping during the last 20 years, the current bottleneck to breeding and genetic advancement is in phenotyping (Araus & Cairns, 2014; Cobb et al., 2013; Jin et al., 2020). Efforts to hasten NUE research through more high throughput phenotyping have come to the forefront in recent years due to technological advancements in remote sensing through the use of hand-held or proximal sensing and platforms (Jin et al., 2020; Nguyen & Kant, 2018; Shrawat et al., 2018). Remote sensing is also advantageous as it is non-destructive. Additionally, it is expected that once methods are standardized, remote sensing can decrease the labor costs inherent in today's hands-on phenotyping methods (Araus & Cairns, 2014; Cobb et al., 2013; Rodrigues Junior et al., 2014; White et al., 2012).

Hyperspectral sensors commonly collect image data in nearly continuous narrow bandwidths (ranging from 1 nm to 70 nm) over the spectral range of 300 nm to 2500 nm. Datasets from these sensors contain hundreds of bands, many of which are correlated. The benefit to hyperspectral data is greater spectral resolution, which provides differentiation between materials with absorbance or reflectance characteristics in very narrow wavelength intervals (Lillesand et al., 2014).

Image-based vegetation indices (VI) are calculated typically as ratios of reflectance or digital brightness values using multi- or hyperspectral bands. They are used to predict specific physiological measures (Campbell & Wynne, 2011) or to assess canopy attributes such as Leaf Area Index (LAI) or biomass (Mulla, 2013). A range of VIs have been well studied in maize for prediction of biomass (Goel, Prasher, Landry, Patel, Viau, et al., 2003; Osborne et al., 2002c; Thenkabail et al., 2014; Thenkabail et al., 2000), grain yield (Blackmer, Schepers, Varvel, & Walter-Shea, 1996; Elsayed & Darwish, 2017; Osborne et al., 2002c; Thenkabail et al., 2014) and N or chlorophyll levels (Campbell et al., 2007; Goel, Prasher, Landry, Patel, Viau, et al., 2003; Osborne et al., 2002a; Schlemmer et al., 2005; Thenkabail et al., 2012; Zhao et al., 2003). However, direct prediction of the previously described N use efficiency parameters with hyperspectral VI have not been studied in maize.

The objectives of this study were to: (1) evaluate and identify the statistically best VI for predicting the N use efficiency parameters of NCE and NIE; (2) compare the hybrid rankings based on field-level N parameters to VI hybrid rankings, thereby identifying those VIs most similar to the ground reference; and (3) determine the impact of downsampling the images from high to low spatial resolution on VIs and the subsequent effect on hybrid rankings.

3.3 Materials and Methods

3.3.1 Experimental Design and Site Description

A two-year experiment was conducted during the summers of 2014 and 2017. For 2014 two fields in Woodland, California (CA), (Gorman, 38.751, -121.789; Rominger, 38.727, -121.832) were planted as part of a corn/wheat rotation. Prior to planting and trial establishment, all cover crop and previous crop residue (wheat straw) was removed from the field to further reduce soil organic matter levels and N availability. Soils at Gorman consisted of Yolo silt loam, and those at Rominger field were Brentwood silty clay loam. The 2017 experiment was located at the Agronomy Center for Research and Education (ACRE, 40.483, -86.994) near West Lafayette, Indiana (IN), on land that had previously been planted with soybeans, and consisted of Drummer soils, Milford silty clay loam, and Raub-Brenton complex.

The experimental design with a split-plot design (randomized complete block) consisted of 4 replicates and was blocked by N treatment as the main plot. Experiment details are provided in Table 3.1. N treatments were separated with border plots. Hybrids and densities were completely randomized within N treatments. In 2014 nine commercial Mycogen® hybrids (DAS01 through DAS09), with an intentionally high amount of genetic diversity, were planted in the north-south direction at 2 different densities (65,000 and 95,000 plants per hectare). These hybrids had relative maturity ratings from 99 to 116 days. Plots were 6 rows wide (4.6 m) with 76 cm row spacing and 12 m long (including a 76 cm alley between replicates). At both Woodland, CA, locations, all plots were irrigated with drip tape to ensure plants experienced no water stress. Before planting overhead sprinklers were used to prewet the area. In 2017 five commercial Mycogen® hybrids (DAS02 through DAS05 and DAS09), a subset of those from 2014, were planted at two planting densities (69,100 and 99,600 plants per hectare). The subset of hybrids had relative maturity

ratings from 110 to 116 days. Plots were four rows wide (3 m) with 76 cm row spacing and 15 m long, not including a 76 cm alley between replicates. The IN experiment was wholly rainfed.

For the 2014 experiment N fertilizer, urea ammonium nitrate (UAN, 32-0-0), was applied through the irrigation system at a depth of 30 cm. Three N treatment rates were used: 0 kg N ha^{-1}, 56 kg N ha^{-1} applied at V4, and 224 kg N ha^{-1}. The high N treatment was applied in the following manner: 24.7 kg N ha^{-1} applied at pre-plant, 50.4 kg N ha^{-1} applied at V4 and 151.3 kg N ha^{-1} at V8. In CA, phosphorus (P), potassium (K) and micronutrients were applied at pre-plant using 0-15-15-S-Zn at a rate of 40 kg ha^{-1} of P or K for the low or medium N treatments. The high N treatment had a pre-plant application of 8-16-8-S-Zn at a rate of 25 kg ha^{-1} of N or P and 48 kg K ha^{-1}. In the IN experiment N fertilizer (28% UAN) was coulter-band injected between corn rows at physiological growth stage V5. Total N amounts for each N treatment in IN were the same as for the CA plantings. No micronutrients were applied in IN.

The field experiments experienced no visible water stress, and weeds and insects were controlled to avoid additional stress to the plants. Historical and monthly weather data for this experiment are outlined in Table 3.3. Thirty year averages were obtained from Woodland (USC00049781), CA, and West Lafayette, IN, stations available from the online data portal of Midwestern Regional Climate Center's cliMATE system (https://mrcc.illinois.edu/CLIMATE/). Monthly averages for ACRE were obtained from the Purdue automated ACRE station, West Lafayette, IN, from the Indiana State Climate Office (https://www.iclimate.org/).

Table 3.1. Experiment design with sampling and imaging dates. Note: w = wide; l = long; Trt = treatment; Appl = application; BM = Biomass; pre = pre-plant; RS = remote sensing.

Year	Location	Planting Date	Harvest Date	Final Plant Density (plants ha^{-1})	Plot size (w x l)	N Trt (kg N ha^{-1}) [Appl Time]	BM Sampling Stages & Dates	Hybrids	RS Dates
2014	Woodland, CA (Gorman)	5/14	9/17	65,000 95,000	4.6m x 12m (6 rows)	0 56 [V4] 224 [pre, V4 & V8]	V12 (6/25) V18 (7/14) R2 (7/22) R6 (9/17)	DAS01 DAS02 DAS03 DAS04	V18 (7/11) R1 (7/24)
	Woodland, CA (Rominger)	5/27	10/2				V12 (7/7) R1 (7/25) R6 (10/2)	DAS05 DAS06 DAS07 DAS08 DAS09	V18 (7/11) R2 (7/24)
2017	West Lafayette, IN (ACRE)	5/17	10/17	69,100 99,600	3m x 15m (4 rows)	0 56 [V5] 224 [V5]	V12 (7/12) R1 (7/24) R6 (10/5)	DAS02 DAS03 DAS04 DAS05 DAS09	V5 (6/16) V8 (6/27) V16/17 (7/18) R1 (7/25) R3/R4 (8/20) R5 (9/8) R5/R6 (9/22)

Soil testing for N was performed with pre-plant probing of the top 30 cm via two increments of 0-15 cm and 15-30 cm in CA. In IN soil cores were collected at both V3 and V12 from two depth increments of 0-30 cm and 30-60 cm. CA soil testing was conducted by Dellavalle Laboratory, Inc. (Fresno, CA) using Soil, Plant, and Water Reference Methods for the Western Region (Miller et al., 2013). Chemical testing of IN soils was conducted by A&L Great Lakes Laboratories, Inc. (Fort Wayne, IN) using the Mehlich 3 extraction procedure (NCERA-13 et al., 2015) and colorimetry EPA method 350.1 (EPA, 1993b) for nitrate determination and colorimetery EPA method 353.2 (EPA, 1993a) for ammonia soil determination.

Table 3.2. Soil N testing results. Note: G = Gorman; R = Rominger; LN = Low N treatment plots; HN = High N treatment plots; na = not available.

N levels (mg kg^{-1})										
Sampling Time	**Pre-plant**				**V3**		**V12**			
Sampling Depth (cm)	**G NO_3^- N LN**	**G NO_3^- N HN**	**R NO_3^- N LN**	**R NO_3^- N HN**	**ACRE NO_3^- N LN**	**ACRE NH_4^+ N LN**	**ACRE NO_3^- N LN**	**ACRE NO_3^- N HN**	**ACRE NH_4^+ N LN**	**ACRE NH_4^+ N HN**
0-15	19	24	9	10	14	4	2	3	6	6
15-30	29	25	9	12						
30-60	na	na	na	na	11	3	2	4	4	4

Early season nitrate-N levels (Table 3.2) were in the normal range at both Gorman and Rominger based on the Dellavalle agronomist soil interpretation (Dellavalle Laboratory Inc., 2014). IN nitrate-N soil levels were low at both samplings times.

Standard soil fertility samples were collected at pre-plant (CA) or at V3 (IN), prior to UAN application (IN). Soil analysis results are shown in Table 3.4 and are discuss here relative to local benchmarks (Dellavalle Laboratory Inc., 2014; Vitosh et al., 1995). Soil pH was similar across both CA fields while the soil at ACRE was more acidic, but still within the desired ranges. The CA soils had lower organic matter than the IN soils. Phosphorus (P) levels at Gorman ranged from a high value in the top 15 cm to a more normal range deeper in the soil At Rominger P was consistently in the low range while potassium (K) was at normal levels in both CA soils. Average magnesium (Mg) and calcium (Ca) levels were also higher at Gorman than Rominger, but still within normal range. Mean soil cation exchange capacity (CEC) levels at Gorman were slightly

lower than at Rominger. P and K levels at ACRE in IN were above critical levels for maize. The secondary nutrients of Mg and Ca in IN, and CEC levels were also at or above adequate levels.

Table 3.3. Monthly weather averages

Year	Location	Month	Average monthly total Precipitation (mm)	Average Air Temperature (deg C)	30-year average monthly total precipitation (mm)	30-year average temperature (deg C)
2014	Woodland	May	0	21.3	16.8	20.2
		June	0	23.3	5.6	23.5
		July	0	24.9	0	25.4
		August	0.8	23.6	1.3	24.8
		September	10.4	22.8	2.8	23.4
		October	22.6	19.6	21.3	18.8
2017	ACRE	May	156.0	15.8	120.4	16.7
		June	156.5	22.3	125.5	21.8
		July	179.8	23.5	112.8	22.9
		August	123.9	20.7	94.5	21.9
		September	50.5	19.2	78.0	18.4
		October	67.9	14.2	78.5	12.0

Table 3.4. Soil status characteristics

Year	Location	Soil Depth (cm)	pH	Organic Matter (%)	K (mg kg^{-1})	P (mg kg^{-1})	Mg (meq l^{-1})	Ca (meq l^{-1})	CEC (meq $100g^{-1}$)
2014	Gorman	0-15	7.6	1.60	225	43	3.0	2.8	22.5
		15-30	7.8	1.47	237	13	3.9	3.6	23.2
	Rominger	0-15	7.6	2.70	225	7	1.6	1.6	25.8
		15-30	7.6	2.26	169	4	1.7	1.9	26.9
2017	ACRE	0-20	6.4	3.1	151	20	610 ppm	2221 ppm	18.7

3.3.2 Plant Measurements and Physiological N Parameters Measured

Above ground plant sampling and harvest were both carried out on the center 2 rows (rows 3 and 4 in 2014 and rows 2 and 3 in 2017) on the biomass sampling dates in Table 3.1. In 2014 the center rows were divided into six 1 m long segments (sampling area of 1.22-1.53 m^2 of 10-15 plants depending on planting density) for the in-season hand sampling, and one 3 m segment for the R6 sampling zone (sampling area of 4.64 m^2 with 30 plants in the low density or 42 plants in the high planting density). All 2014 plots were completely hand harvested. For in-season hand sampling in 2017, the center rows were divided into three 10-plant segments (sampling areas of 1.45 m^2 for the low planting density or 1.01 m^2 for the high density), each at least 1 m from the

others. The 2017 R6 yields were obtained by combine harvesting the center 2 rows after the hand sampling areas had been removed (sampling areas of 18.87 or 20.20 m^2). After partitioning plants into leaves, stalk/tassel, and ears (if present), plant parts were dried to a constant weight and ground to 1 mm. N concentration (%) of samples (stover or grain) was determined through Dumas combustion at the Dow AgroSciences Analytical Laboratory for the 2014 samples (Indianapolis, IN) and A&L Great Lakes Laboratories, Inc. for the 2017 experiment. All grain yield is reported at 15.5 % moisture.

The N parameters were calculated with the following equations using field sampling and laboratory N analysis data obtained as described above.

Nitrogen Conversion Efficiency (NCE) kg $kg^{-1}N$

$NCE = BM_{tot} / N_{plant}$

where BM_{tot} = whole plant aboveground biomass weight

N_{plant} = total plant nitrogen (N) content

Nitrogen Internal Efficiency (NIE) kg $kg^{-1}N$

$NIE = Y/N_{plant}$

where Y = grain yield at 0% moisture

N_{plant} = total plant N content

3.3.3 Remote Sensing Data

All remote sensing data acquired over the 2014 fields in CA was conducted by SpecTIR LLC, based in Reno, Nevada, from a manned aircraft flown at 405 m at Gorman and 410 m at Rominger on the dates shown in Table 3.1. The hyperspectral camera was a ProSpecTir-VS pushbroom system with a spectral range of 390 to 2450 nm at 5 nm (360 bands) and a 320-pixel swath. Spatial resolution was 0.5 m for this data set; thus, each swath was approximately 160 m wide. All data was collected with the sun at ≥40° elevation angle. Data for this study was gathered in a single strip, so no overlap was needed between flight lines. Additional QA/QC processing routines were conducted by SpecTIR. ATCOR® (Atmospheric and Topographic Correction) software was used to convert the radiance data to reflectance values, and spectral polishing was achieved using a proprietary program based on the Savitsky-Golay algorithm. Geocorrection was based on a 12 channel GPS system with real-time differential corrections provided to the inertial navigation

system (INS). A 10 m resolution digital elevation model was used to orthorectify the images. Data was provided in the UTM Zone 10 – WGS – 84 map projection and datum.

At ACRE hyperspectral data was acquired at desired physiologically relevant timepoints (Table 3.1) by a Nano-Hyperspec® VNIR pushbroom scanner (Headwall Photonics, Inc., MA, USA) mounted on a DJI Spreading Wings S1000 octocopter (Guangdong, China) flown approximately 60 m above the ground at 8 m s^{-1} velocity, resulting in a 24 m field-of-view (640 pixels per scan line). Each image had 272 bands, 4 cm spatial resolution and 2.2 nm spectral resolution. An Applanix APX-15 V3 GNSS/INS unit provided navigation information. Hyperspectral data was orthorectified using the Headwall Photonics SpectralView software and processed to reflectance using FLAASH in the ENVI software (Harris Geospatial Solutions, Inc., CO, USA). Individual flights were mosaicked with ENVI 5.5 software. Data from images at similar phenotypic time points across all 3 locations were grouped. Specifically, imaging data from V18 in CA was grouped with imaging data from V16/17 in IN. Similarly, R1/R2 data from CA was pooled with imaging data from IN at R1.

3.3.4 Feature Extraction with Hyperspectral Indices (HSI)

Because the 2014 CA images had lower spatial resolution (50 cm), the 2017 IN images were downsampled spatially by averaging the spectral values of all the pixels in each 50 x 50 cm spatial area. This enabled comparison of images and data of similar spatial resolution for similar phenotypic time points. Indices shown in Table 3.5 were calculated. The 20 hyperspectral vegetation indices (HSI) were chosen based on literature references documenting the study of these for predicting plant biomass, chlorophyll or N concentration, grain yield, or plant stress. Imaging data was binned to 5 nm for all HSI calculations to minimize noise. However, bands at 855 and 910 nm for HBSI1 and HBSI2, respectively, were binned to 20 nm as recommended by Thenkabail et al. (2014). Soil pixels were removed through thresholding techniques for each imaging date and location. For each plot of maize in the imaging data, subplots of the inner 2 rows were extracted, avoiding the areas within 1 m of the alleys and in-season sampling areas. This resulted in subplots 152 cm wide and approximately 6.5 m long. Finally, the remaining pixels within these subplots were averaged to obtain the final HSI data. The high spatial resolution imaging data from IN was treated similarly for generation of the HSI.

Table 3.5. Summary of hyperspectral indices (HSI) evaluated

Category	Spectral Index	Equation	Reference
Biomass	NDVI	(R800-R670)/(R800+R670)	(Rouse et al., 1974)
	MSAVI	0.5 *(2*R800 + 1 - (sqrt((2 * R800 +1)^2 - 8 * (R800 - R670)))	(Qi et al., 1994)
	RTVI	(100 * (R750 - R730) - (10 * (R750 - R550)) * sqrt(R700/R670))	(P.-f. Chen et al., 2010)
Grain Yield/ Structural	PSRI	(R678-R500)/R750	(Merzlyak et al., 1999)
	HBSI1	(R855-R682)/(R855+R682)	(Thenkabail et al., 2014) and (Thenkabail et al., 2012)
	HBSI2	(R910-R682)/(R910+R682)	
	HBSI3	(R550-R682)/(R550+R682)	
Chlorophyll or N Concentration	HBCI8	(R550-R515)/(R550+R515)	(Thenkabail et al., 2014) and (Thenkabail et al., 2012)
	HBCI9	(R550-R490)/(R550+R490)	
	HBCI10	(R720-R550)/(R720+R550)	
	MCARI	((R700-R670)-0.2*(R700-R550))*(R700/R670)	(Daughtry et al., 2000)
	DCNI	(R720-R700)/(R700-R670)/(R720-R670+0.03)	(P. Chen et al., 2010)
	RVI II	R810/R560	(Xue et al., 2004)
	TCARI	3*((R700-R670)-0.2*(R700-R550)*(R700/R670))	(Kim et al., 1994) & (Kim, 1994)
	OSAVI	((1+0.16)*(R800-R670))/(R800+R670+0.16)	(Rondeaux et al., 1996)
	TCARI/OSAVI	TCARI/OSAVI	(Haboudane et al., 2002)
Plant Stress	HREI15	(R855-R720)/(R855+R720)	(Thenkabail et al., 2014) and (Thenkabail et al., 2012)
	HREI16	(R910-R705)/(R910+R705)	(Thenkabail et al., 2014) and (Thenkabail et al., 2012)
	NDRE	(R790-R720)/(R790+R720)	(Barnes et al., 2000)
	CI_{RE}	(R750-R800)/(R695-R740) -1	(Gitelson et al., 2003)

3.3.5 Statistical Analysis

Statistical analysis was based on JMP 14.3.0 and SAS Enterprise Guide 7.1 (SAS Institute Inc., Cary, NC, USA). Mixed models (PROC MIXED) with the Restricted Maximum Likelihood Method (REML) were used in the analysis. Model assumptions of constant variance and normality were evaluated visually (Montgomery et al., 2012). When necessary, values were transformed to satisfy model assumptions and parametric bootstrap procedures were used to estimate confidence limits (1000 bootstrap samples).

Treatment Effects

Mixed models were developed to examine the effects of the N treatment, plant density, hybrids and their two-way interactions on the physiological parameters of total biomass at R6 (TDM), N

concentration at R6 (%, pN), total nitrogen content (TNC), or grain yield at R6 (GY), with a significance level of $\alpha = 0.10$. Each model had hybrid, N treatment, plant density, and their 2-way interactions as fixed effects. Random effects included environmental effects such as location, block[location], location * hybrid, location * plant density, and location * N treatment. Random effects were removed when they accounted for less than 1% of the total variance within the data. Analyses for the physiological parameters (TDM at R6, pN, TNC at V12, R1 and R6, and GY) were conducted for the data "globally" across all three site-years, accounting for location effects through the random effect in the mixed model. Means comparisons for statistically significant fixed effects in the mixed models were analyzed for statistical separation based on a Tukey-Kramer HSD means comparison at $\alpha = 0.10$.

Hybrid Rankings

Comparison of the hybrid's relative response in the N parameters (Y = pN, TNC, NCE or NIE) to the environment and treatment effects was established through mixed models with hybrid, N treatment, plant density, and 2-way interactions as fixed effects. Hybrid rankings were ascertained by globally grouping all three locations, as well as for the ACRE location-only, to allow for comparison in the spatial resolution analysis described below. For the global analysis of all locations, environment was the random effect (block[location], location, location * hybrid, location * N treatment). For the ACRE-only analysis, environment random effects were pass and block only. Rankings for the N parameters were defined when the fixed effect of hybrid was significant at $\alpha = 0.10$ in the model, and there was hybrid separation based on a Tukey Kramer HSD means comparison ($\alpha = 0.10$).

3.3.6 Relationship of HSI to N Parameters

HSI Selection

Relationships between the 20 HSI and each of the N parameters were explored by location based on the Pearson correlation coefficients (r) and the Spearman (non-linear) rank correlation coefficients (ρ). Correlation coefficients for each of the three locations were examined for sign and magnitude. HSI were selected for further statistical analysis when all three locations were either

approximately positively or negatively correlated and at least one location had a Pearson correlation coefficient approximately ≥ |0.30| (magnitude) (step A in Figure 3.1).

Mixed models for predicting the N parameters (dependent variable, Y) across all three site-years consisted of the HSI at a defined time point (V16/18 or R1/R2) along with hybrid and hybrid * HSI as the fixed effects. Random effects included location only to avoid overfitting the model. Treatment effects such as plant density and N were not included due to confounding effects in the model.

To enable comparison across the different indices, HSI data was standardized to mean = 0 and standard deviation = 1, defined as z-scores. A decision tree with six criteria (see Figure 3.1) was used to select the best HSIs for predicting the N parameters:

A) survey correlation statistics based on directionality and magnitude as described previously;

B) examine residual diagnostics, selecting HSI models where statistical assumptions are satisfied;

C) select models where hybrid is a significant effect at $\alpha = 0.10$;

D) compare statistical values of each model with preference for models with smaller Akaike's Information Criterion (AIC), % residual < 75%, and larger coefficient estimate for the standardized (z-score) HSI effect;

E) compare hybrid rankings (Tukey-Kramer's HSD level letters) of the HSI model to the ground reference rankings for similarity;

F) visually inspect charts of the difference in the hybrid least square mean values of the HSI and ground reference models as well as plots of the predicted by measured values at the per-plot level; preference is given to the models with smallest variance.

The impact of reduced spatial resolution for the ACRE hyperspectral data was evaluated using a matched pairs t-test ($\alpha = 0.05$) in JMP based on those indices identified as most predictive of the N parameters from the previous section. Downsampling effects on hybrid rankings were established by examination of Pearson correlation coefficients as well as building mixed models similar to those used for predicting the N parameters from the HSI in the global analysis described

previously (Y = N parameter; Fixed effects: HSI, hybrid, and hybrid * HSI; Random effects: Pass and Block). Models were run with the high or low resolution standardized HSI data. Rankings were based on the hybrid least square means estimates and Tukey-Kramer means comparison (α = 0.10) obtained from the mixed models. The ground reference hybrid rankings and those obtained for the high and low resolution models were compared.

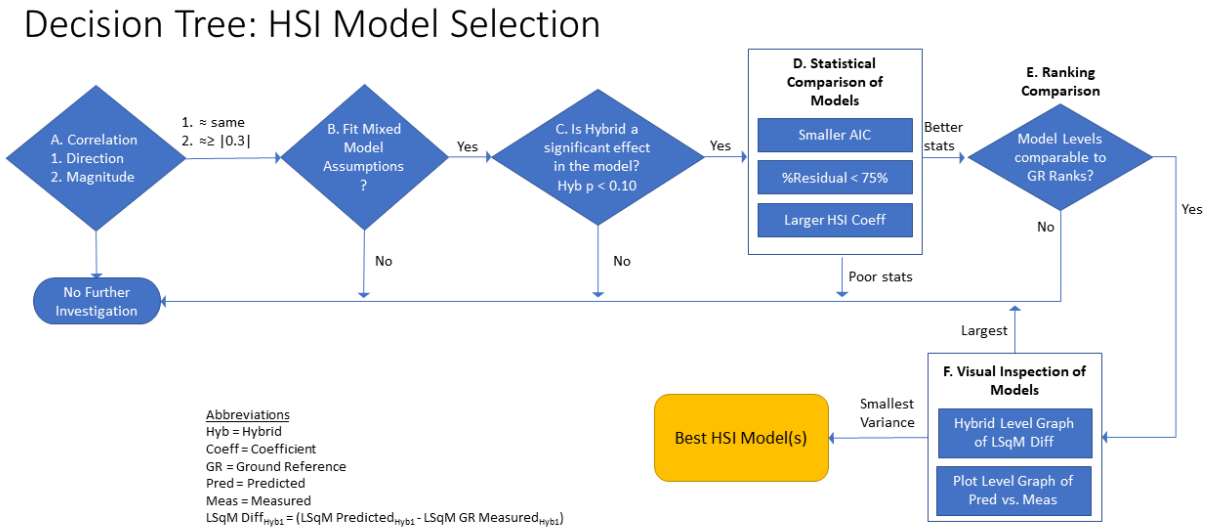

Figure 3.1. Decision tree used for selecting best HSI models

3.4 Results and Discussion

3.4.1 Treatment Effect on Physiological Parameters

Effect on biomass at R6

The individual main effects of hybrid, N treatment, and plant density were significant in the mixed model for α = 0.10, yet none of the interactions were significant for the stover + grain biomass at R6 (total dry matter = TDM) (Table 3.6). Hybrids had a significant effect on plant biomass at R6 (Table 3.7). Hybrids with the highest biomass, averaged across N rates and densities, were DAS05 and DAS08 which were significantly greater than DAS09 (t(12) = 3.53 and t(12) = 3.55, respectively). N treatment, also significant, resulted in greater plant biomass with higher fertilizer rates as expected (Boomsma et al., 2009; Chen et al., 2015; Plénet & Lemaire, 2000). However,

the interaction between these two fixed effects, hybrid * N, was not significant. Higher planting densities resulted in significantly higher biomass levels in our experiment, differing from previous work in which different hybrids planted at densities similar to the ones used in this experiment led to similar or only incremental biomass differences (K. Chen & T. J. Vyn, 2017; Ciampitti & Vyn, 2011). Neither the interactions between planting density and hybrid nor between planting density and N, were significant. In the mixed model for TDM as the response variable, the residual was 43.0%, indicating that approximately 60% of the variability in the data was accounted for by the model. Location effects, which included the blocking effects, accounted for the largest portion of explained variability. This was not surprising considering the large difference in environment between our locations in CA and IN. Another 10.0% of the variability in the data was due to each of the interactions between location and the main effects of N or hybrid. The interaction between plant density and location was so small that it was removed from the model.

Effect on total N concentration

For the whole plant N concentration at R6, the main effects of hybrid, N, and plant density were significant (Table 3.6). Location accounted for nearly 60% of the variability in the data, and the interaction between N and location was almost 23% (leaving an unexplained variability of about 17%). There was clear hybrid separation into three levels with DAS06 having significantly higher %N than DAS03, DAS04, and DAS07 (Table 3.7). However, several hybrids (DAS01, DAS02, DAS05, and DAS08) were indistinguishable from the top or bottom hybrids. The statistical significance of hybrids based on %N further motivated the study of HSIs for predicting this N parameter in our study. Noticeable whole plant %N hybrid differences have been observed in previous research on N and genotypes (K. Chen & T. J. Vyn, 2017; Chevalier & Schrader, 1977).

Plants grown under high N treatment had, as expected, significantly higher %N than the low N treatment (Table 3.7). Further, those plants at high density had significantly lower %N than the low density plots (Table 3.7). The difference in %N observed in this study was more pronounced than in previous research, although the overall impact of higher %N at lower densities is well established (K. Chen & T. J. Vyn, 2017; Gastal et al., 2015). Interactions were evident in this experiment for %N, specifically N or plant density crossed with hybrid were significant, while N * plant density was not (Table 3.6). This contrasts with some previous N research in which these

2-way interactions were not significant (Chen et al., 2015). This difference could be attributed to dissimilar genotypes between the two studies, as well as a larger number of hybrids in our study, which were specifically chosen to span a broad range of genetic diversity.

Effect on total N content

Total N content (TNC) was measured at V12, R1 and R6, and models were built for each of these measurements. The models for TNC had good fit with residuals ranging from 18% to less than 30% (Table 3.6). Location alone accounted for more than 60% of the variability in the data across all three models, indicating the substantial effect that environment had on the availability and uptake of N (Chenu, 2015; Connor et al., 2011; Schepers & Raun, 2008). This is not unexpected as it is well documented that mineral N availability is strongly affected by precipitation, temperature, microbial flora, and soil type (Ribaudo et al., 2011). For TNC at V12, only N and plant density had significant effects on the model (Table 3.6). By R1, neither hybrid nor N alone were significant main effects for TNC, though plant density continued as a significant fixed effect. Interestingly, there was some hybrid separation at R1 (Table 3.7). DAS03 had significantly higher R1 TNC than DAS07. At R6 all three main fixed effects, hybrid, N, and plant density were significant. However, there was no significant hybrid separation in the conservative Tukey Kramer analysis. Hence, TNC was not identified as a N-parameter warranting further investigation with HSIs. Across the growing season TNC at high N was always greater than at low N. The greater TNC with high plant density treatments than for the low plant density treatments from V12 to R6 was similar to prior reports (Chen et al., 2015; Ciampitti & Vyn, 2011). There were no significant interactions at V12 for TNC (Table 3.6). At R1, both hybrid interactions were significant in the model (hybrid * N and hybrid * plant density), yet the interactions were no longer significant by R6.

Effect on grain yield

The mixed model evaluating the treatment effects on grain yield at all 3 locations explained about 70% of the variability in the data (Table 3.6). Location and blocking effects accounted for approximately 37% of the variability, while the interactions with location accounted for another 35%. Hybrid was a significant fixed effect for yield, but neither the main effect of N nor plant

density were significant (Table 3.6). Grain yield mean estimates for the main fixed effects are in Table 3.7, along with the Tukey-Kramer HSD means comparisons. Hybrids for these experiments were specifically selected to have a high amount of genetic diversity, and DAS03 and DAS08 had significantly higher grain yields than DAS09 and DAS07. Hybrid differences in response to N are well documented (Bundy & Carter, 1988; Jeschke & DeBruin, 2016). As expected, yields increased with higher N treatment rates (Table 3.7)

Interactions between hybrid and N were not significant (Table 3.6), indicating that all hybrids in these experiments at high N levels had consistently higher yields than at low N. However, the interactions of plant density, with hybrid or N, were significant (Table 3.6). The effect of hybrid * plant density indicates that for some hybrids, yields at high planting density were higher than for hybrids at low planting density, yet for other hybrids this was reversed. An example in our study was DAS08 which at high plant density had numerically higher yields than at low plant density ($\overline{m}$ = 14.74 Mg ha^{-1}, SE = 1.15 vs. $\overline{m}$ = 13.96 Mg ha^{-1}, SE = 1.15). However, DAS05 at high plant density had *lower yields* than at low plant density ($\overline{m}$ = 12.34 Mg ha^{-1}, SE = 1.08 vs. $\overline{m}$ = 13.23 Mg ha^{-1}, SE = 1.08). Thus, the combination of hybrid and planting density affects grain yields. This confirms previous work which has shown yield differences with various hybrids and plant densities due to G x E interactions, which occurs particularly between older and newer hybrids (Assefa et al., 2016; Chen et al., 2017; Tollenaar, 1989, 1992).

The interaction between plant density and N on grain yields was also evident in this study. A deeper look into these interactions with the Tukey-Kramer HSD means comparison indicates that for the high N treatment, there was a significant difference in yield between the high and low planting densities, ($\overline{m}$ = 14.62 Mg ha^{-1}, SE = 1.14 vs. $\overline{m}$ = 13.82 Mg ha^{-1}, SE = 1.14). However, for the low and medium N there was no significant difference between the planting densities, t(436) = -1.12 and t(436) = -0.9, respectively. Finally, there was clear differentiation between the high density, high N treatment and either of the low N treatments (Tukey HSD p = 0.018 for high density and p = 0.035 for low density).

Table 3.6. Mixed model analysis of treatment effects & interactions on physiological characteristics across 3 site-years ($\alpha = 0.10$)

Var	Summary of Fit Model Statistics		Random Effects REML Var Comp Est (% of Total)		Type 3 Tests of Fixed Effects				
					Effect	DF	Den DF	F Value	Pr > F
TDM	N Obs	427	Loc	37.4	H	8	12	2.82	0.052
					N	2	4	5.67	0.068
	AIC	1892.2	N*Loc	10.4	PD	1	363	36.66	<.0001
					H*N	16	363	0.89	ns
	Res(%)	43.0	H*Loc	9.2	H*PD	8	363	0.18	ns
					N*PD	2	363	1.28	ns
N Conc (%)	N Obs	363	Loc	58.1	H	8	12	4.05	0.015
					N	2	4	8.32	0.038
	AIC	-394.4	N*Loc	22.9	PD	1	299	43.88	<.0001
					H*N	16	299	1.55	0.080
	Res(%)	17.2	H*Loc	1.9	H*PD	8	299	1.85	0.069
					N*PD	2	299	1.13	ns
TNC V12	N Obs	364	Loc	69.6	H	8	12	1.94	ns
					N	2	3	25.55	0.013
	AIC	-37.7			PD	1	301	9.72	0.002
			N*Loc	2.2	H*N	16	301	1.14	ns
	Res(%)	28.2			H*PD	8	301	1.5	ns
					N*PD	2	301	0.06	ns
TNC R1	N Obs	252	Loc	66.2	H	8	12	2.18	ns
					N	2	4	3.81	ns
	AIC	2138	N*Loc	10.8	PD	1	190	8.85	0.003
					H*N	16	190	1.76	0.040
	Res(%)	20.3	H*Loc	2.7	H*PD	8	190	2.75	0.007
					N*PD	2	190	0.35	ns
TNC R6	N Obs	363	Loc	60.3	H	8	12	2.47	0.077
					N	2	4	8.73	0.035
	AIC	3132.1	N*Loc	18.3	PD	1	299	4.06	0.045
					H*N	16	299	1.14	ns
	Res(%)	18.4	H*Loc	3	H*PD	8	299	1.03	ns
					N*PD	2	299	0.56	ns
GY	N Obs	501	Loc	37.2	H	8	12	5.28	0.005
					N	2	4	3.78	ns
	AIC	1747.9	N*Loc	25.4	PD	1	436	2.08	ns
					H*N	16	436	1.26	ns
	Res(%)	27.2	H*Loc	10.3	H*PD	8	436	2.37	0.016
					N*PD	2	436	7.29	0.001

TDM = Total Dry Matter (Mg ha^{-1}) (stover + grain); N Conc = Total Plant Percent Nitrogen Concentration (%); TNC = Total Nitrogen Content (kg N ha^{-1}); GY = Grain Yield at 15.5% moisture content; N Obs = number of observations; AIC = Akaike's Information Criterion; Loc = Location and Blocking effects; N = Nitrogen Treatment; H = Hybrid; PD = Plant Density; DF = Degrees of Freedom for numerator; Den DF = Degrees of Freedom for denominator; ns = Not Significant at $\alpha = 0.10$. For random effects % of total variability reported. For fixed effects, p-value reported.

Table 3.7. Least square mean estimates for main fixed effects. Standard errors (SE) reported for all except N Concentration and TNC V12 where 95% upper and lower confidence limits (CL) are shown due to transformation of the response variable. Levels with different letters are significantly different by Tukey-Kramer HSD ($\alpha = 0.10$) within a treatment class(trt class) and physiological variable; ns = not significant.

Trt Class	Main Fixed Effects	TDM R6 Estimate (Mg ha^{-1})			R6 N Concentration Estimate (%)				TNC V12 Estimate (kg N ha^{-1})				TNC R1 Estimate (kg N ha^{-1})			TNC R6 Estimate (kg N ha^{-1})			GY Estimate (Mg ha^{-1})		
		Means		SE	Means		LCL	UCL	Means		LCL	UCL	Means		SE	Means		SE	Means		SE
H	DAS01	22.53	AB	1.53	0.97	ABC	0.94	1.00	130	ns	127	133	170	AB	31	212	ns	28	13.82	AB	1.13
	DAS02	22.71	AB	1.44	0.96	ABC	0.93	0.98	138	ns	136	140	173	AB	30	211	ns	27	12.76	ABC	1.07
	DAS03	23.47	AB	1.44	0.92	BC	0.90	0.94	133	ns	131	135	195	A	30	209	ns	27	14.32	A	1.07
	DAS04	22.24	AB	1.44	0.91	BC	0.89	0.94	134	ns	132	137	167	AB	30	199	ns	27	13.33	AB	1.07
	DAS05	24.08	A	1.44	0.93	ABC	0.91	0.95	137	ns	135	140	174	AB	30	218	ns	27	12.79	ABC	1.07
	DAS06	22.25	AB	1.53	1.01	A	0.98	1.03	139	ns	136	142	179	AB	30	214	ns	28	12.19	ABC	1.13
	DAS07	21.37	AB	1.53	0.89	C	0.86	0.92	118	ns	116	121	148	B	31	185	ns	28	10.48	C	1.13
	DAS08	24.54	A	1.53	0.94	ABC	0.90	0.97	126	ns	124	129	184	AB	31	223	ns	28	14.35	A	1.13
	DAS09	20.68	B	1.44	0.97	AB	0.95	0.99	130	ns	128	132	170	AB	30	194	ns	27	11.59	BC	1.07
N	High_N	24.25	A	1.41	1.04	A	1.03	1.05	157	A	155	158	199	ns	31	251	A	29	14.22	ns	1.14
	Low_N	21.03	B	1.41	0.86	B	0.84	0.88	110	B	109	112	155	ns	31	169	B	29	11.36	ns	1.14
	Med_N	22.67	AB	1.41	0.92	AB	0.90	0.94	132	A	130	134	166	ns	31	202	AB	29	12.96	ns	1.14
PD	High	23.33	A	1.30	0.92	B	0.91	0.93	136	A	135	137	179	A	29	210	A	27	12.93	ns	0.97
	Low	21.97	B	1.30	0.96	A	0.95	0.98	127	B	126	128	168	B	29	205	B	27	12.76	ns	0.97

3.4.2 Treatment and Time Effect on N Parameters

Effect on NCE: Ground Reference Model

Over the three site-years, the mean NCE increased over the growing season from 51.3 kg kgN^{-1} at V12 to 107.3 kg kgN^{-1} at R6. This was similar to previous studies documenting maize biomass increases, even under N stress (Sadras & Calderini, 2015). The increase in standard deviation of NCE at R1 was driven by an increase in the standard deviation for both plant dry matter (PDM) and TNC, the two NCE components. Over the growing season, the variance of the distribution of NCE increased and became skewed to the right by season end (R6) (Figure 3.2). This was driven by an increase in the standard deviation in TNC from R1 to R6, which also became skewed to the right. The increase in TNC from R1 to R6 shows differences in post-silking N uptake for the different hybrids.

Histograms of NCE values by plant stage and N treatment (data not shown) indicated mean NCE values early in the season to be similar at the differing N treatments (At V12: 56.8 kg kgN^{-1} for low N, 48.3 kg kgN^{-1} for medium N, and 46.5 kg kgN^{-1} for high N), with approximately only a 10 kg kgN^{-1} range in means. By R6, the range between treatments had increased to roughly 26 kg kgN^{-1}, and the sample distributions had also changed. The mean R6 NCE values for the low N treatment increased to 122.0 kg kgN^{-1} but with a wider range (80.0 kg kgN^{-1}) while the high N treatment had a relatively normal distribution at R6, with a mean of 95.6 kg kgN^{-1} and a smaller range (31.2 kg kgN^{-1}). The lower NCE values under high N conditions for both time points are consistent with prior research, which shows NCE increasing more for low N than high N over the season (K. Chen & T. J. Vyn, 2017; Plénet & Lemaire, 2000).

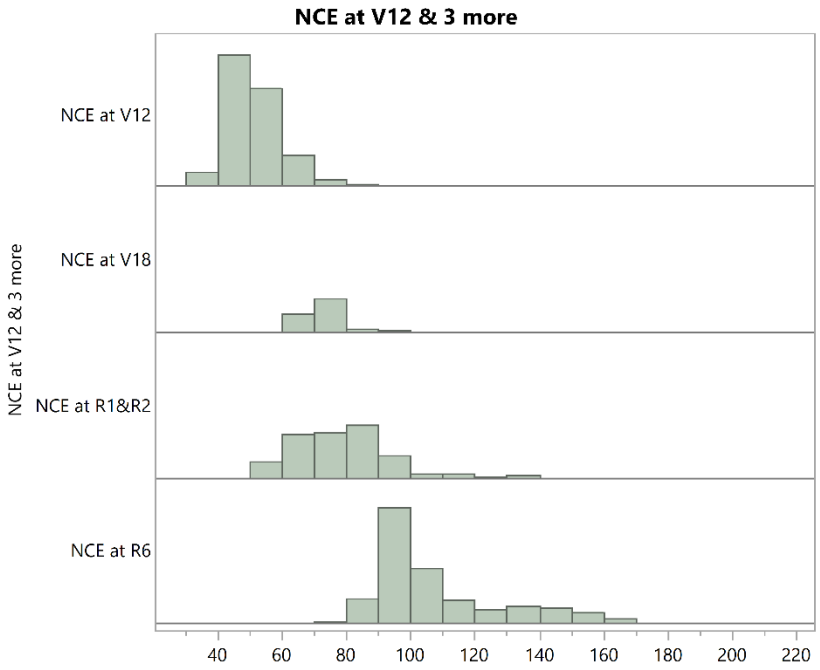

Figure 3.2. Distribution of NCE values (kg kgN^{-1}) across all three site-years by plant developmental stage of V12, V18, R1/R2 and R6.

Statistical analysis of the ground reference based mixed model for NCE indicated that location alone accounted for the majority of the variability in the model while the interaction of N * location explained 25% (Table 3.8). The global mixed model for NCE at R6 across the 3 locations and treatments indicated that all main effects and interactions, except for N * plant density, were significant to the model. Thus, hybrid, N treatment and plant density all had significant impacts on NCE.

Hybrid Rankings by NCE at R6

Hybrid least square mean NCE values with 95% confidence limits, along with Tukey-Kramer means difference letters, are shown in Table 3.9 based on the global or ACRE-only data. Hybrids DAS04 and DAS07 had the highest NCE values. They were significantly larger than DAS06 and DAS09, the two lowest ranking hybrids by NCE. The ACRE model provided slightly different hybrid rankings. As in the global model, DAS03 ranked significantly better than DAS09. However, while DAS04 was one of the top-ranked hybrids in the global model, at ACRE it was not significantly different from the poorly ranked DAS09. This difference between the models highlights the importance of testing hybrids across multiple environments to provide a broader

perspective of a hybrid in a grower's field and to have greater statistical confidence of a hybrid's performance.

Effect on NIE: Ground Reference Model

For NIE, the overall mean of all three site-years across all N treatments was 50.2 kg kgN^{-1} (at R6). N translocation and utilization efficiency decreased as N fertilizer increased, with the distribution of the hybrid NIE values skewing towards the higher values at low N rates and a less skewed distribution at the high N rates (Figure 3.3). Thus, the low N treatment hybrids had the highest mean NIE values (55.0 kg kgN^{-1}). The NIE means were 51.0 kg kgN^{-1} and 45.8 kg kgN^{-1}h for medium and high N treatments, respectively, decreasing in value with higher N treatment, as expected (Ciampitti & Vyn, 2011; Haegele et al., 2013).

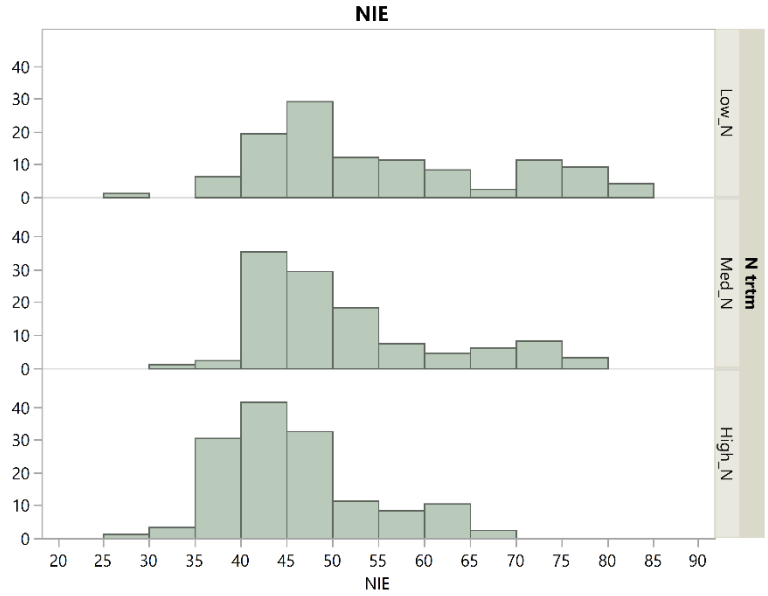

Figure 3.3. Distribution of NIE (kg kgN^{-1}) values across three site-years by nitrogen treatment (N trtm).

The global mixed model for NIE (3 locations) had less than 10% unexplained variability (Table 3.8). The random effects of location and the corresponding interactions accounted for more than 90% of the variability in the data. Hybrid was a significant fixed effect with clear separation between some of the hybrids. This result of hybrid effect on NIE agrees with other results showing the genotype impact on NIE (D'Andrea et al., 2009). N treatment and the interaction between hybrid * plant density were also significant. The remaining fixed effects in the model were not significant.

Hybrid Rankings by R6 NIE

In the Tukey-Kramer HSD least square means difference analysis of the global model there were only three levels across the nine hybrids (Table 3.9). Highest in NIE was DAS03. The lowest tiered hybrids, significantly different from the top tier, were DAS05 and DAS07. DAS03 also had significantly higher NIE than DAS06 and DAS09. At ACRE-only, DAS03 was also significantly higher in NIE than DAS09. However, the distinction between DAS03 and DAS02 at ACRE was not apparent in the global model.

Table 3.8. Mixed model analysis of treatment effects and interactions on N parameters across 3 site-years (For %N see Table 6)

Var	Summary of Fit Model Statistics		Random Effects REML Var Comp Est (% of Total)		Type 3 Tests of Fixed Effects				
					Effect	DF	Den DF	F Value	Pr > F
NCE	N Obs	363	Loc	58.3	H	8	311	13.58	<.0001
					N	2	4	8.06	0.040
	AIC	-6400.2			PD	1	311	44.65	<.0001
			N*Loc	24.9	H*N	16	311	1.63	0.060
	Res(%)	16.8			H*PD	8	311	2.34	0.019
					N*PD	2	311	0.82	ns
NIE	N Obs	363	Loc	84	H	8	12	6.76	0.002
					N	2	4	7.99	0.040
	AIC	1947.2	N*Loc	4.7	PD	1	299	0.32	ns
					H*N	16	299	1.4	ns
	Res(%)	8.8	H*Loc	2.5	H*PD	8	299	5.47	<.0001
					N*PD	2	299	1.53	ns

Var = Y-variable of the mixed model; NCE = Nitrogen Conversion Efficiency at R6 (kg kgN^{-1}); NIE = Nitrogen Internal Efficiency (kg kgN^{-1}); N Obs = number of observations; AIC = Akaike's Information Criterion; Res = Residual; Var Comp Est = Variance Component Estimates; Loc = Location and Blocking effects; N = Nitrogen Treatment; H = Hybrid; PD = Plant Density; DF = Degrees of Freedom for numerator; Den DF = Degrees of Freedom for denominator; ns = Not Significant at $\alpha = 0.10$. For random effects % of total variability reported. For fixed effects, p-value reported.

Table 3.9. NCE and NIE least square mean values from ground reference global models across two$^{\theta}$ or three site years or at ACRE-only. 95% confidence limits (CL) reported for each hybrid. Tukey-Kramer means differences reported ($\alpha = 0.10$); means with the same letter are not significantly different. (Not-est = not estimable)

		NCE kg kgN^{-1}				NIE kg kgN^{-1}			
Analysis	**Hybrid**	**Means**		**LCL**	**UCL**	**Means**		**LCL**	**UCL**
Global	DAS01$^{\theta}$	102.7	ABC	100.0	105.5	56.8	AB	44.3	69.3
	DAS02	104.4	BCD	102.5	106.6	53.0	ABC	40.6	65.4
	DAS03	106.7	DE	104.6	108.9	57.8	A	45.4	70.2
	DAS04	109.5	EF	107.0	112.3	56.5	AB	44.1	68.9
	DAS05	105.9	CDE	103.9	108.3	49.0	C	36.6	61.4
	DAS06$^{\theta}$	98.8	A	96.4	101.2	49.7	BC	37.2	62.2
	DAS07$^{\theta}$	111.1	F	108.0	114.6	47.9	C	35.4	60.4
	DAS08$^{\theta}$	106.6	CDEF	103.5	109.9	55.5	AB	43.0	68.0
	DAS09	102.2	AB	100.2	104.2	51.1	BC	38.7	63.4
ACRE only	DAS02	122.7	AB	120.7	124.7	67.2	B	65.3	69.1
	DAS03	128.7	A	126.5	131.1	71.4	A	69.8	73.0
	DAS04	123.4	AB	121.3	125.5	68.8	AB	66.7	71.0
	DAS05	Not-est				Not-est			
	DAS09	120.2	B	118.2	122.2	66.6	B	65.0	68.3

3.4.3 Evaluating the Relationship Between N Parameters and HSI

Exploratory investigations into the relationship between the N parameters (%N, NCE and NIE) and the HSI began through visualizations of the data with scatterplots and correlation analysis. Initial observations noted that for many HSI there was very little overlap in the distribution of the data when grouping the data across years. For several HSI there were also large differences in the scale or magnitude of the data distribution, even when overlapping. For example, R1/2 TCARI data in 2014 ranged from -88.2 to 8.5 while the 2017 data ranged from 0.05 to 0.13, a 1000-fold difference. The mean reflectance values at the TCARI bands of 550 nm and 700 nm were similar across years but not at 670 nm. At this band, the reflectance values in 2014 had a broader range and extremely low reflectance, much smaller than in 2017. Because these differences appeared to separate out by year instead of location, we hypothesize that the scaling differences are likely due to relative differences in the spectral responses of the two imaging systems used rather than a location-only difference. However, other potential causes for these spectral differences could be due to year or agricultural locality. Such differences in the data sometimes led to observation of Simpson's paradox when exploring those HSI as a group in which trends reverse or disappear depending on the groupings. To avoid this, all data was evaluated for correlations by location.

3.4.4 Correlation Between N parameter (%N, NCE, NIE) and HSI

Pearson correlation coefficients between the 3 N parameters at R6 and the HSI at V16/18 and R1/2 for each location were evaluated (Figure 3.4). Initial observations showed very few of the 20 HSIs were strongly correlated ($r > 0.6$) with the N parameters at all three locations. Similarity in relationships (i.e. directionality) and magnitude of correlation were more evident between Gorman and Rominger, the two CA locations, than with ACRE, the IN location, likely due to spatial resolution similarities. However, several HSI (15 for %N, 16 for NCE, and 14 for NIE) were selected for further investigation based on the criteria of consistent directionality and magnitude of correlation (step A in Figure 3.1). Spearman's rank correlations (data not shown) and the Pearson correlation coefficients had the same signs. As hypothesized, the HSI that were more strongly correlated to %N were also those most strongly correlated to NCE and NIE. Since a lack of N can cause plant stress, it was surprising that none of the plant stress HSIs (HREI15, HREI16, NDRE, and CI_{RE}), were highly correlated with %N at any of the three locations. This result was in contrast to previous studies which showed CI_{re} and other red edge HSIs reliably predicting N content in plants with low N levels (Schlemmer et al., 2013; Thenkabail et al., 2012). DCNI, an HSI developed for N detection by P. Chen et al. (2010), was also not strongly linearly related to %N. However, our findings supported work by Zhao et al. (2018) who found poor predictability for plant N with this index. Previous findings of MCARI, TCARI, and TCARI/OSAVI that were strongly predictive or correlated to chlorophyll (Haboudane et al., 2008; Hunt Jr et al., 2013) were not supported by our results, which had inconsistent or small correlations with %N dependent upon location.

Figure 3.4. Pearson correlation coefficients(r) by V16/18 or R1/2 HSI for N concentration at R6 (pN), NCE at R6, and NIE at R6 for each location. Blue = ACRE (IN), Red = Gorman (CA), and Yellow = Rominger (CA). Dotted lines at |0.3| are for reference only.

Correlation coefficients were often larger for %N and NCE, relative to NIE, especially at ACRE. Since NCE is the amount of dry matter per unit of N in the plant, an analysis of variance was conducted to evaluate if there was less dry matter in 2014 than in 2017 to account for the stronger correlations observed in 2017. This would suggest that the HSI are simply sensing biomass differences in the fields. Welch's Anova for the model with year as the independent variable indicated significant differences ($\alpha = 0.05$) between years at V12 and R6 for plant dry matter (PDM) and at R6 for TDM. However, at both plant stages the biomass in 2014 was greater than in 2017. Since the biomass differences had patterns opposite from the HSI correlation, this suggests that the indices were not just sensing biomass differences between the years. An analysis of the statistical difference in plant N (TNC) by year indicated that at all time points (V12, R1/R2, and R6) TNC in 2014 was statistically greater than in 2017 suggesting N detection was driving the stronger NCE correlations with the indices (Welch's Anova and ANOVA, $\alpha = 0.05$). There were no obvious changes in the magnitude of the correlations between HSIs and NCE at V16 or R1. Conversely, for NIE the correlations changed depending on the HSI and imaging timepoint suggesting some indices may be more sensitive to NIE changes and thus more predictive.

3.4.5 N Parameter Estimation by HSI

Predicting %N with hyperspectral indices

Of the 15 plant stage-HSI models selected based on the value of the correlation coefficient between %N at R6 and HSI, only five fit the mixed model statistical assumptions [normality and constant variance] (step B in Figure 3.1): HBCI8 at V16, and HBCI8, HBCI9, HBSI2, and HRE16 at R1 (Table 3.10). For two (HBCI8 and HBCI9) of the 5 models hybrid was not a significant effect so these models were not considered further (step C).

The model statistics (step D) indicated that V16 HBCI8 had a very low AIC value but a very large residual (Table 3.10). The statistics for the remaining two models were relatively similar thus the next consideration (step E) was the hybrid rankings.

The hybrid rankings based on ground reference %N resulted in 3 levels which are shown in Table 3.10. Of the two HSIs identified as predictive of %N, HBSI2 and HREI16 at R1, both resulted in two tiers. In HBSI2 there was only clear differentiation between DAS09 and DAS04. The HBSI2

model was unable to delineate between DAS06 or DAS07. Similarly, while HREI16 distinguished between DAS06 and DAS03 and DAS04 as in the reference model, it, too, did not differentiate between DAS06 and DAS07. Thus, the hybrid rankings for %N by either HSI were not consistent with the reference data.

Visual inspection of the plots (step F) illustrated the statistical findings. Figure 3.6 shows that R1 HBSI2 underestimated the hybrid means, while HREI16 overestimated them. Overall, R1 HBSI2 had the smallest predicted means difference for all hybrids except for DAS07. Interestingly, DAS07 was one of the least accurately estimated hybrids by both models. The cause of the poor estimates of DAS07 is unknown. Inspection of the parentage of these hybrids reveals that DAS07 was the only hybrid with a different female inbred, suggesting the potential interaction of genotype and HSI. Future investigations of this interaction are recommended.

The predicted vs. measured %N graph based on each of the selected HSI is shown in Figure 3.5. The individual by-plot estimates have slightly lower variance of the residuals for HREI16 than HBSI2, especially at the lower %N. The least square hybrid means shown in Figure 3.6 indicate HREI16 was the most accurate model of HSI for %N at the hybrid level. Figure 3.5 and Figure 3.6 show that the models are similar in predictions, but not similar enough for implementation. Based on these comparisons, HBSI2 and HREI16 at R1 were the best HSIs for predicting %N within those evaluated. However, neither was able to clearly separate out hybrids at R6 based on in-season imaging.

Table 3.10. Fit statistics and least square means estimations for ground reference and HSI models for N concentration (%N).

Hybrid	%N Ground Ref Means		%N Est from V16 HSI		%N Est from R1 HSI					
			hbci8		hbci8	hbci9	hbsi2		hrei16	
DAS01	0.97	ABC	0.97	A	1.00	1.00	0.93	AB	1.00	AB
DAS02	0.96	ABC	0.99	A	0.97	1.00	0.94	AB	0.97	AB
DAS03	0.92	BC	0.97	A	0.95	0.99	0.89	AB	0.92	B
DAS04	0.91	BC	0.99	A	1.00	0.99	0.88	B	0.91	B
DAS05	0.93	ABC	0.97	A	0.98	1.00	0.89	AB	0.93	B
DAS06	1.01	A	0.98	A	0.98	0.99	0.97	AB	1.03	A
DAS07	0.89	C	0.92	A	0.91	0.90	0.94	AB	0.94	AB
DAS08	0.94	ABC	0.93	A	0.97	0.96	0.88	AB	0.98	AB
DAS09	0.97	AB	0.94	A	0.95	0.96	0.96	A	1.01	A
AIC	-349.4		-134.2		-148.2	-178.5	-9.2		-39.2	
N	363		363		345	345	345		345	
%Res	17.2		98.1		45.6	71.3	33.9		64.3	
HYB P-VAL	0.015		0.077		ns	ns	0.016		0.001	
HSI P-VAL	NA		0.004		<.0001	<.0001	0.002		<.0001	
HSI Coeff	NA		-0.146		-0.159	-0.238	0.054		0.263	

Note: AIC = Akaike's Information Criterion, N = total number of observations, %Res = Percent of total variance for the residual; HYB P-VAL = p-value of fixed effect hybrid; HSI P-VAL = p-value of fixed effect HSI; HSI Coeff = coefficient of the solution for the HSI effect; ns = not significant at $\alpha = 0.10$. Levels connected by the same letter are not significantly different according to Tukey-Kramer HSD ($\alpha = 0.10$).

The primary HSI of interest for %N was HBSI2, described by Thenkabail et al. (2014) as a "hyperspectral biomass and structural index" uniquely positioned for evaluating biomass, plant height, and grain yield. This index is a normalized ratio of red:NIR similar to NDVI but centered at 682 and 910 nm instead of the traditional 670 and 800 nm (Rouse et al., 1974). The band zone of 682 nm, the far-red absorption maxima of chlorophyll, shows a decrease in reflection upon increasing leaf chlorophyll concentrations (Buschmann & Nagel, 1993). The band at 910 nm is the peak of NIR reflectance for vegetation used for studying moisture, biomass and protein as well as in moisture sensitive indices (Thenkabail et al., 2014).

The other HSI of interest for %N, HREI16, also contains spectral information from the 910 nm band, similar to HBSI2. The 705 nm band is in the red-edge region, the transition from red to near infrared occurring from 700 to 740 nm (Schlemmer et al., 2005; Thenkabail et al., 2014). This region is commonly found in indices predictive of N content under N stress conditions since the

movement of the inflection point is often identified as related to stress (Li et al., 2014; Schlemmer et al., 2013; Thenkabail et al., 2014). It is also associated to the plant chlorophyll/carotenoid ratio confirming the importance of mid-season plant pigments for end-season %N levels (Yang et al., 2010).

Interestingly, several indices such as MCARI, TCARI/OSAVI and CIre did not accurately predict %N in contrast with other N or chlorophyll research (Haboudane et al., 2008; Hunt Jr et al., 2013; Thenkabail et al., 2012). One reason for this difference may be that our imaging timepoints were earlier in the growing season (V16 and R1), yet the measurement we were attempting to predict was at season end (R6). Researchers have noted that it is problematic if the time interval between sampling and imaging dates are too large (Goel, Prasher, Landry, Patel, Viau, et al., 2003; Osborne et al., 2002c) especially as it is known that maize plant N levels change both over the season and within the various plant components being sensed (leaf, stem, grain, etc.) (Bender et al., 2013; DeBruin et al., 2013).

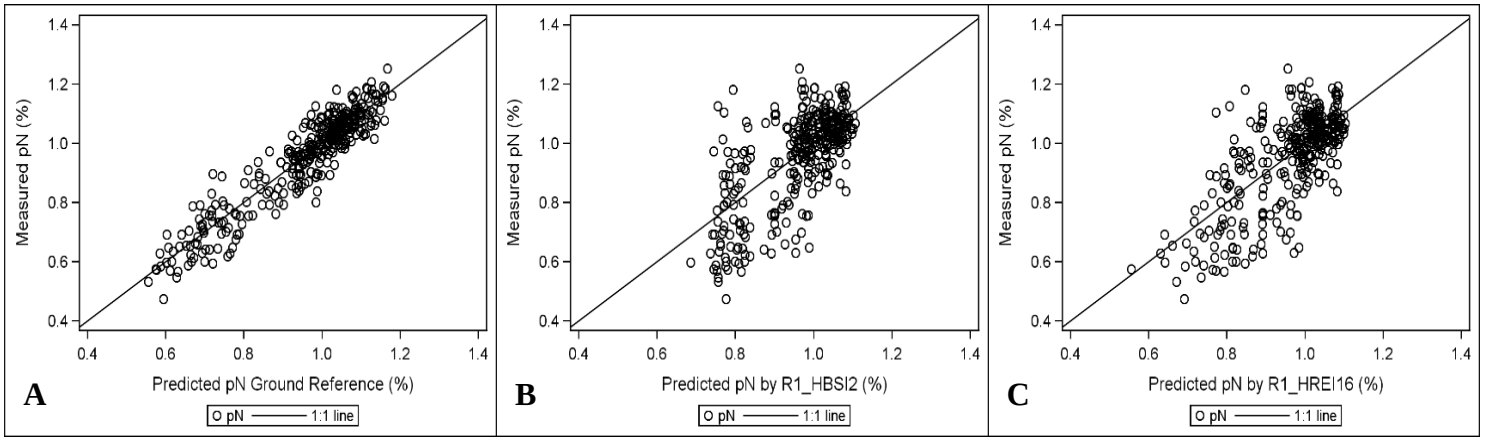

Figure 3.5. Predicted vs. Actual (measured) estimates of N concentration (%N or pN). A. Ground reference mixed model; B. R1 HBSI2; C. R1 HREI16 models.

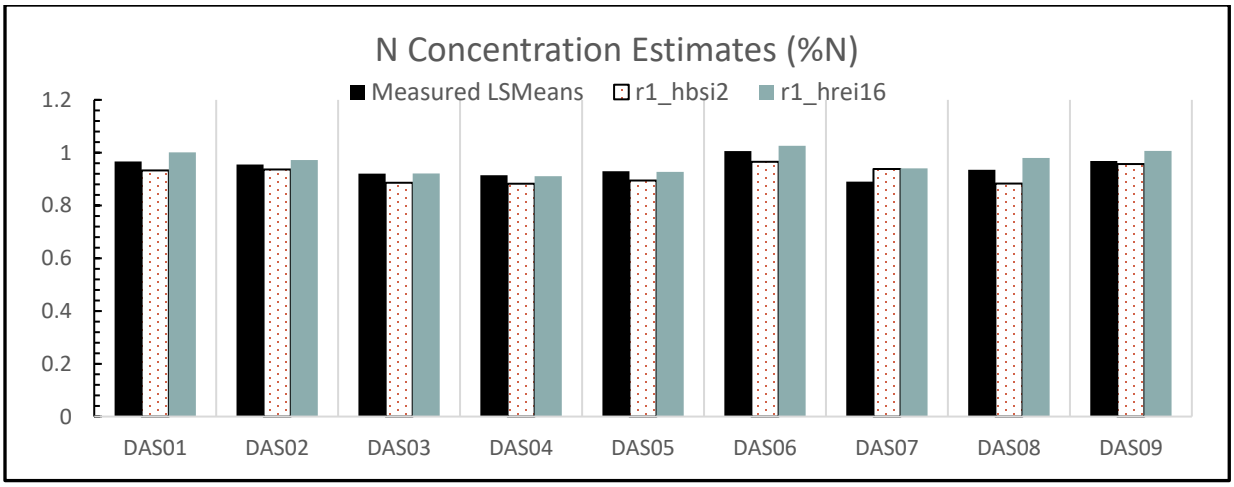

Figure 3.6. Least square means estimates of N concentration (%N) by hybrid for ground reference model, HBSI2 and HREI16 at R1 models

Predicting NCE with hyperspectral indices

Fifteen HSI-time point combinations were selected based on correlation values for evaluation of their ability to predict the ground reference NCE values. Of those only four, HBSI1, HBSI2, HBSI3 and HBCI9 at R1, had adequate fit to the model assumptions. Results are shown in Table 3.11. Constant variance was usually the assumption that was violated by the other models, removing them from consideration. The analysis following the decision tree of Figure 3.1, steps B through D, was followed as described in detail for %N.

HBSI1 and HBSI2, which had the best performance thus hybrid rankings were compared in step E (Figure 3.1). For the reference data hybrid rankings clearly show DAS07 = DAS04 > DAS09 = DAS06 (Table 3.11). The models for HBSI1 and HBSI2 only showed two level letters in the rankings. However, both models identified DAS04 > DAS09 = DAS06. Consequently, some of the differentiation from the HSI models matched the reference rankings though separation of DAS07 was missed by the HSI models. Additionally, all other hybrids were inseparable based on the HSI models.

Table 3.11. NCE (kg kg^{-1} N) least square means estimations and fit statistics.

Hybrid	NCE Ground Ref Means		NCE Estimates from R1 HSI							
			hbsi1		hbsi2		hbsi3		hbci9	
DAS01	102.7	ABC	106.6	AB	106.6	AB	102.1	ABC	100.0	
DAS02	104.4	BCD	107.2	AB	107.2	AB	102.6	AB	100.0	
DAS03	106.7	DE	111.1	AB	111.8	AB	103.7	AB	100.5	
DAS04	109.5	EF	114.0	B	113.2	B	107.2	ABC	101.5	
DAS05	105.9	CDE	111.1	AB	110.4	AB	103.7	AB	100.5	
DAS06	98.8	A	103.1	A	103.1	A	110.4	ABC	101.5	
DAS07	111.1	F	106.6	AB	106.0	AB	103.7	ABC	110.4	
DAS08	106.6	CDEF	112.5	AB	112.5	AB	115.5	C	104.3	
DAS09	102.2	AB	104.3	A	104.3	A	101.5	A	103.7	
AIC	-6400		-6074		-6076		-6121		-6248	
N	363		345		345		345		345	
%Res	16.8		31.8		33.3		100.0		73.3	
HYB P-VAL	<.0001		0.009		0.007		0.005		ns	
HSI P-VAL	NA		0.004		0.001		<.0001		<.0001	
HSI Coeff	NA		5.56E-06		5.17E-06		-2.00E-05		-2.00E-05	

Note: AIC = Akaike's Information Criterion, N = total number of observations, %Res = Percent of total variance for the residual; HYB P-VAL = p-value of fixed effect hybrid; HSI P-VAL = p-value of fixed effect HSI; HSI Coeff = coefficient of the solution for the HSI effect; ns = not significant at $\alpha = 0.10$. Levels connected by the same letter are not significantly different according to Tukey-Kramer HSD ($\alpha = 0.10$)

Inspection of the plots show comparable estimates between HSBI1 and HBSI2. Most of the predictions for HBSI1 and HBSI2 were greater than the measured means (Figure 3.8). DAS07 was an outlier again for both models by being the hybrid consistently underestimated. By plot, the scatter pattern was similar for both HSI with greater scatter in the upper measured NCE values (> 125 kg kgN^{-1}) (Figure 3.7). The overall by-hybrid estimates in Figure 3.8 were quite similar to the measured ground reference means. In summary, these 2 HSIs succeeded in providing ranking guidance for culling 2 of the lower performing hybrids (DAS06 and DAS09) for end-season NCE based on R1 imaging data.

HBSI2, already described, contains reflectance information from the 910 nm band while HBSI1 is centered at 855 nm. The lower wavelength is the center of the reflectance for crops in the NIR region and is strongly correlated to chlorophyll (Schepers et al., 1996; Thenkabail et al., 2002). These findings support previous investigations by Blackmer, Schepers, Varvel and Walter-Shea

(1996) who identified the band region around 800-900 nm as important in detecting N stress in corn.

In general, leaf pigments, including chlorophyll, are nearly transparent in the NIR (720-1300 nm) component in these two indices, resulting in low absorption and near maximum reflectance at the leaf level (Lambers et al., 2008; Sahoo et al., 2015). Research has shown that cellular structures and plant cavities, which vary upon changes in plant vigor, are responsible for variations of reflectance in the NIR region (Campbell & Wynne, 2011). Therefore, higher NIR reflectance indicates plant health and vitality (Campbell & Wynne, 2011) and lower reflectance occurs under low N conditions (Walburg et al., 1982; Zhao et al., 2003). NCE is a measure of biomass produced per unit of N in the plant, both of which are directly tied to plant health. Consequently, this newly identified link between these structural indices and NCE is reasonable and supports our hypothesis.

Under N stress and high density conditions, maize plants have lower final heights, producing less biomass (Boomsma et al., 2009). MSAVI is also a NIR:R ratio yet contains a self-adjusting soil brightness correction factor (Qi et al., 1994). It was originally developed for biomass detection in cotton (Qi et al., 1994) and later confirmed as predictive of maize biomass (Zhao et al., 2018). In other research Haboudane et al. (2008) found that MSAVI was consistently a good predictor of leaf chlorophyll content in maize and wheat. Due to the relationship of MSAVI to biomass and chlorophyll, we hypothesized a strong relationship to NCE. However, the data did not support this idea.

Interestingly, HBSI3, the other structural index proposed by Thenkabail et al. (2014), differed only by the fact that it is based on reflectance in the green region (550 nm) instead of the NIR portion of the spectrum. This band is known to be responsive to chlorophyll changes (Buschmann & Nagel, 1993; Thenkabail et al., 2002). Our results showed it to be less predictive of NCE than the other structural indices considered here.

Due to the ability of HBSI1 and HBSI2 to differentiate hybrids in NCE at R6 based on mid-season images, further investigation of this promising finding is recommended. Additional studies with other locations and hybrids for these specific HSI are needed to fully assess their applicability across environments and genotypes. Both HSI that were good predictors of NCE in this study were based on reflectance of NIR:R. Several NIR:R indices such as NDVI, MSAVI, and OSAVI

were also investigated in this research yet no relationship was found. However, in order to find more predictive HSIs many other NIR:R indices should be investigated, such as $PSSR_a$ or $PSSR_b$ (Blackburn, 1998) or NLI (Goel & Qin, 1994).

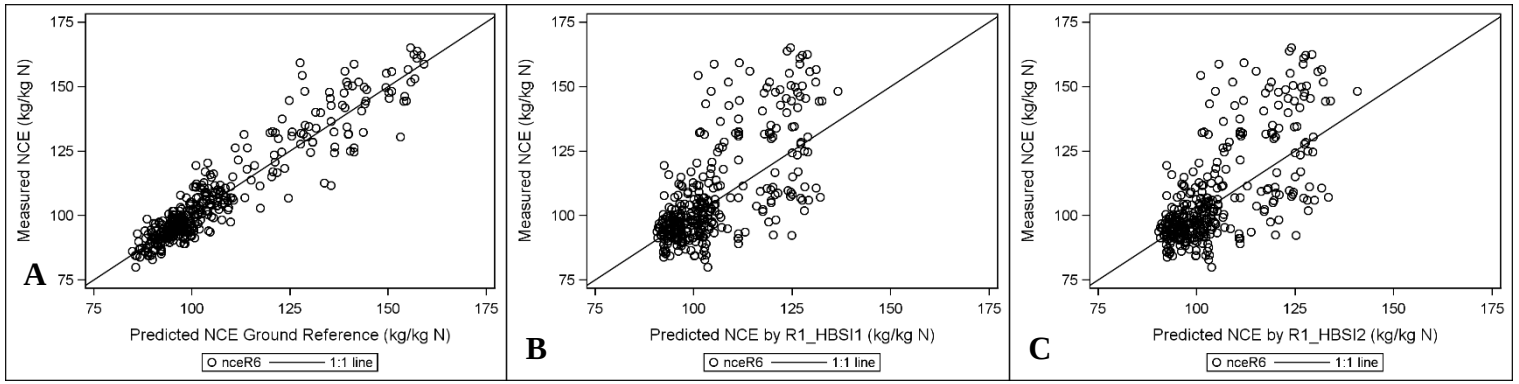

Figure 3.7. Predicted vs. actual (measured) estimates of NCE. A. Ground reference mixed model; B. R1 HBSI1 model; C. R1 HBSI2 model.

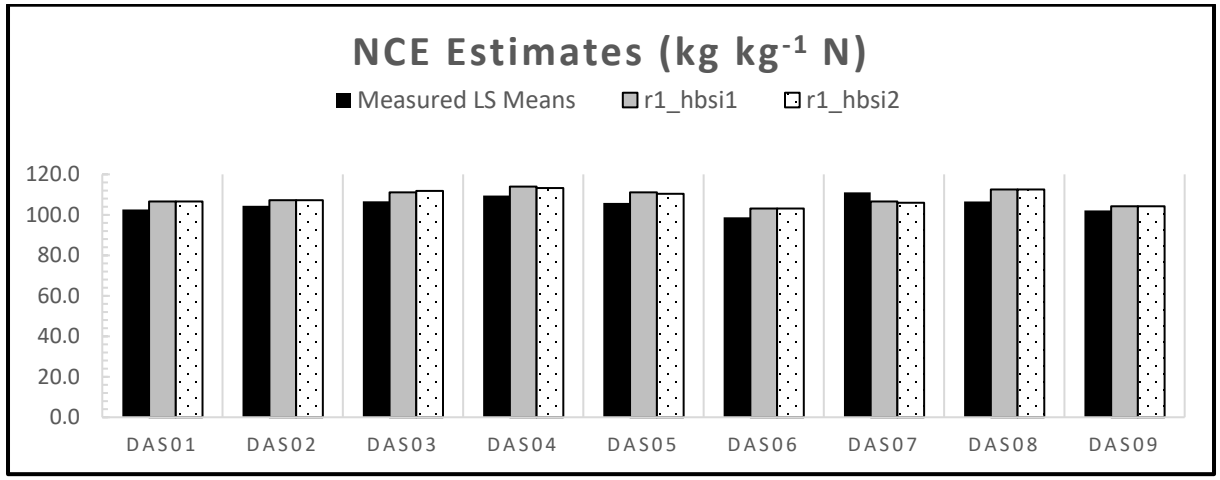

Figure 3.8. Least square means estimates of NCE by hybrid based on measured or HSI models.

Predicting NIE with hyperspectral indices

Fifteen HSI-time point combinations were selected as potential predictors of NIE. Six models, from both imaging time points, fitt the statistical assumptions (Table 3.12). Based on the decision tree in Figure 3.1, three HSI remained for consideration of the hybrid rankings at step E: HBCI8 at V16 and HBCI8 and HBCI9 at R1.

Hybrid rankings based on measured data resulted in 3 levels. DAS03 was significantly greater in NIE than DAS06, DAS09, DAS07, and DAS05. Additionally, DAS01, DAS04, and DAS08 also had significantly higher NIE means than DAS07 and DAS05. Hybrid differences in NIE were detected by many of the HSI models. For example, HBCI8 at V16 found significant differences between DAS03 > DAS09 ≥ DAS06 ≥ DAS05 = DAS07. However, it also detected differences between DAS01 ≥ DAS09 = DAS06, which were not identified by the field sampling. HBCI8 at R1 had 5 levels of separation with many differences matching the reference data such as: DAS03 > DAS09 ≥ DAS06 ≥ DAS07 ≥ DAS05. Similarly, DAS01 and DAS08 were found to be significantly different than DAS05 and DAS07. For this model, DAS02 was the only hybrid incorrectly assigned as being significantly different from several hybrids, while the ground reference NIE data showed no differences between DAS02 and any of the tested hybrids. HBCI9 at R1 correctly identified differences between DAS01 to DAS05 and DAS01 to DAS07 but it misclassified DAS09 as equivalent to DAS03 and different from DAS05.

Evaluation of the plots (step F) showed that the 3 HSI models often underestimated the hybrid mean values (Figure 3.10). The smallest differences between estimated and measured values were evident for HBCI8 at both imaging dates. The measured vs. predicted plots shown in Figure 3.9 showed a similar scatter around the 1:1 line for all three models. All had scatter only slightly more than that seen in the ground reference model. The three HSI models provided the ability to separate out the best hybrids in NIE (DAS01 and DAS03) from the bottom performing hybrids of DAS05 and DAS07 based on mid-season imaging data. This suggests that these HSI extracted from imaging during the growing season could be deployed in order to facilitate decision-based selection as part of an early stage breeding program.

The set of indices discussed here, HBCI8 and HBCI9, are classified as hyperspectral biochemical indices (HBCI) for studying pigments such as carotenoids and chlorophyll (Thenkabail et al.,

2014). Both HSI contain one band centered at 550 nm. At this band, as chlorophyll levels decrease, reflectance increases (Buschmann & Nagel, 1993). Accordingly, our results suggest that chlorophyll was a stronger factor on NIE prediction by HSI than other biophysical components of biomass or canopy structure.

The second band for HBCI8 is also focused on the green portion of the electromagnetic spectrum but at 515 nm. This waveband is quite sensitive to pigment changes (Bilger et al., 1989; Haegele et al., 2013) and thus known to show maximal changes in reflectance (Thenkabail et al., 2002). In contrast, the second band for HBCI9 is in the upper blue portion of the spectrum (490 nm). This section is sensitive to rates of senescence and carotenoid levels (Thenkabail et al., 2002).

NIE hybrid predictions were remarkably accurate based on HSI extracted from mid-season imaging. Further studies are recommended to validate this finding for other genotypes and environments. Additionally, the HSI identified as predictive of NIE (HBCI8 and HBCI9) were based on the green portion of the electromagnetic spectrum or the ratio of green:blue (G:B). No other G:G or G:B indices were investigated here. There is potential that similar indices may be more accurate predictors of NIE, thus we recommend further research into similar indices.

Table 3.12. NIE least square mean estimations (kg kg^{-1} N) and fit statistics for various HSI based models at V16 or R1 maize development stage.

Hybrid	NIE Ground Ref Means		NIE Estimates from V16 HSI						NIE Estimates from R1 HSI					
			hbci8		hbci9		hbsi3		hbci8		hbci9		rtvi	
DAS01	56.8	AB	56.5	A	54.9	A	51.7	AB	55.0	AB	55.8	A	49.9	ABCD
DAS02	53.0	ABC	50.5	BCD	47.9	C	50.1	Bᵠ	51.9	BC	50.1	CDE	47.6	CD
DAS03	57.8	A	55.4	A	53.3	A	54.3	A	55.7	A	54.5	AB	52.3	AB
DAS04	56.5	AB	53.3	ABC	51.8	AB	52.9	ABᵠ	53.3	ABC	53.0	AD	55.5	A
DAS05	49.0	C	48.3	D	45.9	C	46.3	Bᵠ	47.8	E	47.0	E	47.2	CD
DAS06	49.7	BC	48.8	CD	46.1	BC	42.2	Bᵠ	49.9	CDE	48.9	DE	42.3	D
DAS07	47.9	C	46.0	D	42.2	C	42.2	Bᵠ	47.6	DE	47.2	BCDE	40.7	D
DAS08	55.5	AB	54.1	AB	50.4	ABC	54.1	ABᵠ	53.9	AB	53.7	AC	48.7	BCD
DAS09	51.1	BC	52.1	BC	51.5	AB	49.3	Bᵠ	51.5	BCD	51.7	AD	49.1	BC
AIC	1947.2		2209.9		2191.2		2242.1		2076.1		2067.7		2141.1	
N	363		363		363		363		345		345		345	
%Res	8.8		28.3		100.0		99.7		15.8		32.7		100.0	
HYB P-VAL	0.0018		<.0001		<.0001		<.0001		<.0001		<.0001		<.0001	
HSI P-VAL	NA		<.0001		<.0001		<.0001		<.0001		<.0001		<.0001	
HSI Coeff	NA		2.64		8.20		8.35		1.76		4.28		-9.20	

Note: AIC = Akaike's Information Criterion, N = total number of observations, %Res = Percent of total variance for the residual; HYB P-VAL = p-value of fixed effect hybrid; HSI P-VAL = p-value of fixed effect HSI; HSI Coeff = coefficient of the solution for the HSI effect; ns = not significant at $\alpha = 0.10$. Levels connected by the same letter are not significantly different according to Tukey-Kramer HSD ($\alpha = 0.10$). φ = Lines display does not reflect all significant comparisons; additional pairs are significantly different: (DAS08,DAS06), (DAS04,DAS09), (DAS04,DAS05), (DAS04,DAS06), (DAS04,DAS07), (DAS02,DAS05).

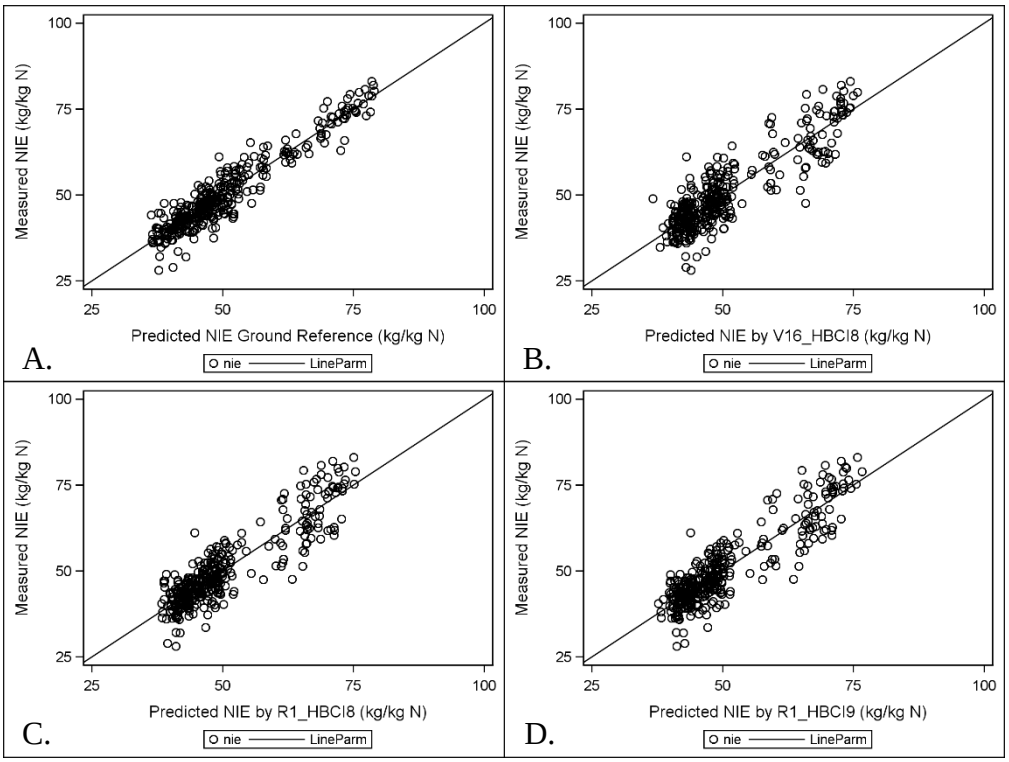

Figure 3.9. Predicted vs. actual (measured) estimates of NIE. A. Ground reference mixed model; B. V16 HBCI8 model; C. R1 HBCI8 model; D. R1 HBCI9 model

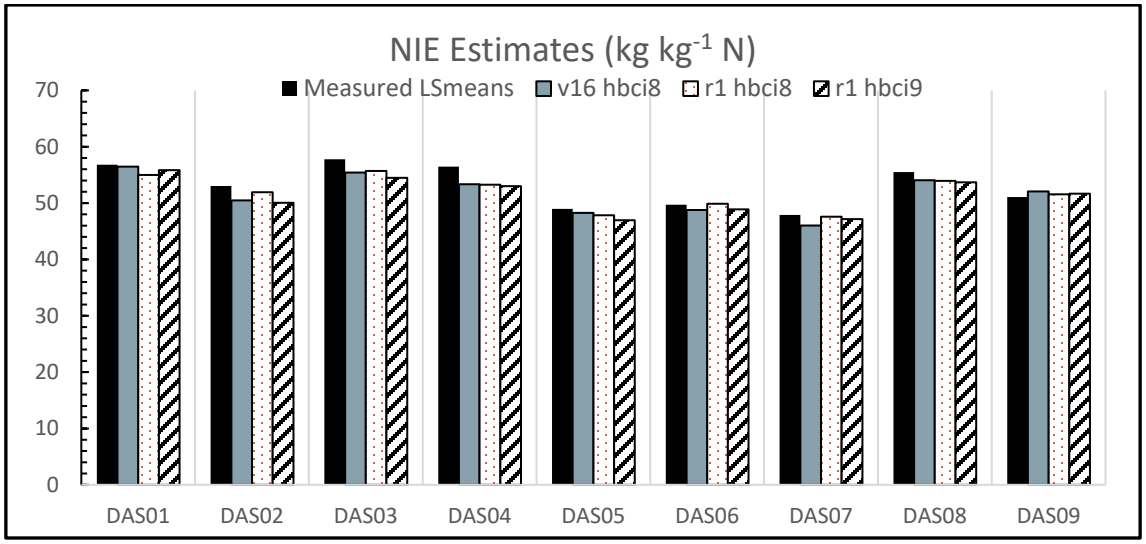

Figure 3.10. Least square means estimates of NIE by hybrid based on measured or HSI models.

3.4.6 Comparison of High to Low Spatial Resolution HSI

The image data obtained in 2017 at ACRE was of extremely high resolution (4 cm pixels). It was resampled to match the 2014 50 cm pixel data. The effect of this downsampling was examined here for the 5 HSI identified as predicting hybrid differences for NCE and NIE. Analysis for the resolution effect on %N was not conducted since the HSI did not detect hybrid differences in %N for the global dataset.

The analysis by each HSI (HBCI8, HBCI9, HBSI2, HBSI2 at R1 and HBCI8 at V16) showed that the low and high resolution data was highly positively correlated based on Pearson correlation coefficients ($r \geq 0.97$, n = 104). The matched pairs t-tests, both by plot and across plots, indicated HSI values were significantly different at the two resolutions. For all HSI the index values from the low resolution reflectance were greater than the high resolution index values. In this case, resampling of the high resolution images led to significantly increased index values in the images. We hypothesize the combining of values occurring with downsampling may be mitigating the shadowing and details captured with higher spatial resolution. An interesting pattern in the data was that as the average index values increased, the difference between the high and low resolution data also increased. This result confirms the theoretical analysis of the effect of spatial resolution on NDVI by Jiang et al. (2005) who found that NDVI-low resolution is greater than NDVI-high resolution. However in their analysis the largest difference was found at moderate and low vegetation levels (20-50%) and darker soils (Jiang et al., 2005). They found less difference in the two resolutions as vegetation proportion increased or with high red reflectance soils. In our research the HSI were calculated at V16/18 or R1/2 at which time the canopy had already closed thus little soil was visible. Additionally, at ACRE the visible soil had low levels of red reflectance.

Akbarian et al. (2020) and Zhou et al. (2018) found that as the image resolution of rice fields or sugarcane decreased the correlations between HSI and leaf N concentration levels also decreased. In our data for maize, the correlations between NCE or NIE at ACRE and our HSI of interest did not change consistently.

Impact of Resolution Difference on Rankings

Upon detection of the statistically significant effect of resampling and downgrading the 2017 image data, an analysis was conducted to determine the effect of resampling on hybrid rankings from the models themselves. For NCE all HSI, regardless of time-point or resolution, were unable to detect the hybrid differences evident in the measured data at ACRE (Table 3.13). The NCE model estimates were quite similar to the ground reference data, often correctly identifying the hybrid with the lowest and highest NCE numerical values. However, these differences were not statistically significant. Since the HSI were able to determine some statistical differences in hybrids for NCE when using all three site-years, this result suggests that the models based on imaging need larger quantities of data - more than what was available within our one location at ACRE.

Table 3.13. NCE hybrid rankings at ACRE for HSI of interest at low and high spatial resolution

		R1 HBSI1		R1 HBSI2	
Hybrid	**NCE GROUND REF**	**LOW**	**HIGH**	**LOW**	**HIGH**
DAS02	AB	A	A	A	A
DAS03	A	A	A	A	A
DAS04	AB	A	A	A	A
DAS05	not est	A	A	A	A
DAS09	B	A	A	A	A

Note: NCE Ground Ref = NCE measured data. Levels with different letters within resolution (low or high) and index are significantly different by Tukey-Kramer HSD ($\alpha = 0.10$); DF = 35 for each NCE analysis.

A similar analysis was conducted using the imaging data at ACRE for NIE prediction. We found slight statistical differences in hybrid rankings only for V16 HBCI8 (Table 3.14). The other 2 HSI did not show differences in hybrid rankings between the high and low resolution data. Overall, there was no consistent effect by the change in spatial resolution for NIE. Nonetheless, *none* of the image data (high or low resolution) was able to differentiate the hybrids as with the measured data, similar to the NCE findings. Consequently, the effect of resolution change on hybrids could not be fully evaluated.

The significant differences in the index values with no change in the correlations between HSI and N parameters, in addition to the inability to differentiate hybrids with either high or low resolution, are ambiguous results. The lack of corroboration with other research may be due to the fact that these images were taken after canopy closure and resolution tends to have a greater impact earlier in the season. Additional investigation into this research aspect is needed.

Table 3.14. NIE hybrid rankings at ACRE for HSI of interest at low and high spatial resolution

	NIE	V16 HBCI8		R1 HBCI8		R1 HBCI9	
Hybrid	GROUND REF	LOW	HIGH	LOW	HIGH	LOW	HIGH
DAS02	B	ABC	A	A	A	AB	AB
DAS03	A	A	A	A	A	A	A
DAS04	AB	AB	A	A	A	A	A
DAS05	not est	C	B	B	B	B	B
DAS09	B	BC	AB	AB	AB	AB	AB

Note: NIE Ground Ref = NIE measured data. Levels with different letters within resolution (low or high) and index are significantly different by Tukey-Kramer HSD ($\alpha = 0.10$); DF = 36 for each NIE analysis.

3.5 Conclusion

In this study we evaluated 20 HSI at two time-points (V16 and R1) across three site-years for detecting hybrid differences and predicting %N at R6, NCE at R6 and NIE. Our experiment encompassed strikingly different environments (California valley basin vs. Eastern Cornbelt) for five to nine common hybrids. The multiple N rates and plant densities resulted in a moderate range of NCE and NIE at maturity.

In these experiments, we found 2 HSI at R1, a structural index and a red-edge index ($HBSI2_{682,910}$ and $HREI16_{705,910}$), were well-suited for predicting plant N concentration at R6, but not for identification and separation of hybrid differences. For NCE, we identified two structural HSI at R1 ($HBSI1_{682,855}$ and $HBSI2_{682,910}$) as predictive of NCE and hybrid differences. Both HSI identified the hybrid with the highest NCE and the 2 hybrids with the lowest NCE. Finally, 2 biochemical HSIs ($HBCI8_{515,550}$ at V16 and R1 and $HBCI9_{490,550}$ at R1) were predictive of NIE, the amount of grain yield per unit plant N. These HSI also detected significant hybrid differences similar to those identified by the ground reference data. The top 2 NIE hybrids were differentiated from the lowest 3 hybrids. Overall, our findings indicated a greater ability to accurately predict

NIE than NCE and the predictability of %N was weakest. To our knowledge this is the first effort using vegetation indices from hyperspectral imaging in maize for predicting NCE and NIE.

In the global analysis across all three site-years the low resolution (50 cm) image data was adequate for detecting hybrid differences. However, our results from the resolution analysis indicated that index values changed, but the effect of resolution change on hybrid differentiation was not evident since hybrid differences were not apparent at either high (4 cm) or low (50 cm) pixel resolution. We hypothesized these ambiguous results were due to the smaller dataset.

The HSI newly identified as predictive of NCE and NIE correctly ranked the best hybrids early in the season (at V16 or R1), thus enabling opportunities for saving hand sampling and field data collection of hybrids with lower N efficiencies. We hope these HSI, after additional validation, can be applied directly for the foundational work needed in breeding for N efficiency in maize. Implementation of these HSI or other remote sensing methods into routine breeding efforts can only improve and hasten our understanding and development of N-efficient maize hybrids.

Acknowledgements

Funding acknowledgements go to Dow AgroSciences and Corteva Agriscience. Also, much appreciation for all field station support, especially that at Gorman and Rominger.

3.6 References

Akbarian, S., Xu, C., & Lim, S. (2020). Analysis on the Effect of Spatial and Spectral Resolution of Different Remote Sensing Data in Sugarcane Crop Yield Study. *ISPRS Annals of the Photogrammetry, Remote Sensing and Spatial Information Sciences*, *3*, 655-661.

Araus, J. L., & Cairns, J. E. (2014). Field high-throughput phenotyping: the new crop breeding frontier. *Trends Plant Sci*, *19*(1), 52-61. https://doi.org/10.1016/j.tplants.2013.09.008

Assefa, Y., Vara Prasad, P., Carter, P., Hinds, M., Bhalla, G., Schon, R., Jeschke, M., Paszkiewicz, S., & Ciampitti, I. A. (2016). Yield responses to planting density for US modern corn hybrids: A synthesis-analysis. *Crop Science*, *56*(5), 2802-2817.

Banziger, M., Edmeades, G., Beck, D., & Bellón, M. (2000). Breeding for drought and nitrogen stress tolerance in maize: From theory to practice.

Barnes, E., Clarke, T., Richards, S., Colaizzi, P., Haberland, J., Kostrzewski, M., Waller, P., Choi, C., Riley, E., & Thompson, T. (2000). Coincident detection of crop water stress, nitrogen status and canopy density using ground based multispectral data. Proceedings of the Fifth International Conference on Precision Agriculture, Bloomington, MN, USA,

Bender, R. R., Haegele, J. W., Ruffo, M. L., & Below, F. E. (2013). Nutrient Uptake, Partitioning, and Remobilization in Modern, Transgenic Insect-Protected Maize Hybrids. *Agronomy Journal*, *105*(1), 161. https://doi.org/10.2134/agronj2012.0352

Bilger, W., Björkman, O., & Thayer, S. S. (1989). Light-induced spectral absorbance changes in relation to photosynthesis and the epoxidation state of xanthophyll cycle components in cotton leaves. *Plant Physiology*, *91*(2), 542-551.

Blackburn, G. A. (1998). Quantifying Chlorophylls and Caroteniods at Leaf and Canopy Scales: An Evaluation of Some Hyperspectral Approaches. *Remote Sensing of Environment*, *66*(3), 273-285. https://doi.org/10.1016/S0034-4257(98)00059-5

Blackmer, T. M., Schepers, J. S., Varvel, G. E., & Walter-Shea, E. A. (1996). Nitrogen deficiency detection using reflected shortwave radiation from irrigated corn canopies. *Agronomy Journal*, *88*(1), 1-5.

Boomsma, C. R., Santini, J. B., Tollenaar, M., & Vyn, T. J. (2009). Maize Morphophysiological Responses to Intense Crowding and Low Nitrogen Availability: An Analysis and Review. *Agronomy Journal*, *101*(6), 1426. https://doi.org/10.2134/agronj2009.0082

Bundy, L., & Carter, P. (1988). Corn hybrid response to nitrogen fertilization in the northern corn belt. *Journal of Production Agriculture*, *1*(2), 99-104.

Buschmann, C., & Nagel, E. (1993). In vivo spectroscopy and internal optics of leaves as basis for remote sensing of vegetation. *International Journal of Remote Sensing*, *14*(4), 711-722. https://doi.org/10.1080/01431169308904370

Campbell, J. B., & Wynne, R. H. (2011). *Introduction to remote sensing*. Guilford Press.

Campbell, P., Middleton, E., McMurtrey, J., & Chappelle, E. (2007). Assessment of vegetation stress using reflectance or fluorescence measurements. *Journal of Environmental Quality, 36*(3), 832-845.

Chen, K., Camberato, J. J., & Vyn, T. J. (2017). Maize Grain Yield and Kernel Component Relationships to Morphophysiological Traits in Commercial Hybrids Separated by Four Decades. *Crop Science*, *57*(3), 1641-1657. https://doi.org/10.2135/cropsci2016.06.0540

Chen, K., Kumudini, S. V., Tollenaar, M., & Vyn, T. J. (2015). Plant biomass and nitrogen partitioning changes between silking and maturity in newer versus older maize hybrids. *Field Crops Research*, *183*, 315-328.

Chen, K., & Vyn, T. J. (2017). Post-silking Factor Consequences for N Efficiency Changes Over 38 Years of Commercial Maize Hybrids. *Front Plant Sci*, *8*, 1737. https://doi.org/10.3389/fpls.2017.01737

Chen, P.-f., Nicolas, T., Wang, J.-h., Philippe, V., Huang, W.-j., & Li, B.-g. (2010). New index for crop canopy fresh biomass estimation. *Spectroscopy and Spectral Analysis*, *30*(2), 512-517.

Chen, P., Haboudane, D., Tremblay, N., Wang, J., Vigneault, P., & Li, B. (2010). New spectral indicator assessing the efficiency of crop nitrogen treatment in corn and wheat. *Remote Sensing of Environment*, *114*(9), 1987-1997.

Chenu, K. (2015). Characterizing the crop environment–nature, significance and applications. In *Crop physiology* (pp. 321-348). Elsevier.

Chevalier, P., & Schrader, L. (1977). Genotypic Differences in Nitrate Absorption and Partitioning of N Among Plant Parts in Maize 1. *Crop Science*, *17*(6), 897-901.

Ciampitti, I. A., & Vyn, T. J. (2011). A comprehensive study of plant density consequences on nitrogen uptake dynamics of maize plants from vegetative to reproductive stages. *Field Crops Research*, *121*(1), 2-18. https://doi.org/10.1016/j.fcr.2010.10.009

Ciampitti, I. A., & Vyn, T. J. (2012). Physiological perspectives of changes over time in maize yield dependency on nitrogen uptake and associated nitrogen efficiencies: A review. *Field Crops Research*, *133*, 48-67. https://doi.org/10.1016/j.fcr.2012.03.008

Cobb, J. N., DeClerck, G., Greenberg, A., Clark, R., & McCouch, S. (2013). Next-generation phenotyping: requirements and strategies for enhancing our understanding of genotype–phenotype relationships and its relevance to crop improvement [journal article]. *Theoretical and Applied Genetics*, *126*(4), 867-887. https://doi.org/10.1007/s00122-013-2066-0

Connor, D. J., Loomis, R. S., & Cassman, K. G. (2011). *Crop ecology: productivity and management in agricultural systems*. Cambridge University Press.

D'Andrea, K. E., Otegui, M. E., Cirilo, A. G., & Eyhérabide, G. H. (2009). Ecophysiological traits in maize hybrids and their parental inbred lines: Phenotyping of responses to contrasting nitrogen supply levels. *Field Crops Research*, *114*(1), 147-158. https://doi.org/10.1016/j.fcr.2009.07.016

Daughtry, C., Walthall, C., Kim, M., De Colstoun, E. B., & McMurtrey III, J. (2000). Estimating corn leaf chlorophyll concentration from leaf and canopy reflectance. *Remote Sensing of Environment*, *74*(2), 229-239.

DeBruin, J., Messina, C. D., Munaro, E., Thompson, K., Conlon-Beckner, C., Fallis, L., Sevenich, D. M., Gupta, R., Dhugga, K. S., & Lübberstedt, T. (2013). N distribution in maize plant as a marker for grain yield and limits on its remobilization after flowering. *Plant Breeding*. https://doi.org/10.1111/pbr.12051

DeBruin, J. L., Schussler, J. R., Mo, H., & Cooper, M. (2017). Grain Yield and Nitrogen Accumulation in Maize Hybrids Released during 1934 to 2013 in the US Midwest. *Crop Science*, *57*(3), 1431-1446. https://doi.org/10.2135/cropsci2016.08.0704

Dellavalle Laboratory Inc. (2014). *Soil Interpretation Report*.

Doering, O., Galloway, J., Theis, T., Aneja, V., Boyer, E., Cassman, K., Cowling, E., Dickerson, R., Herz, W., & Hey, D. (2011). Reactive Nitrogen in the United States: an analysis of inputs, flows, consequences, and management options. *United States Environmental Protection Agency*.

Duvick, D., Smith, J., & Cooper, M. (2004). Long-term selection in a commercial hybrid maize breeding program. *Plant Breeding Reviews*, *24*(2), 109-152.

Duvick, D. N., & Cassman, K. G. (1999). Post–green revolution trends in yield potential of temperate maize in the North-Central United States. *Crop Science*, *39*(6), 1622-1630.

Elsayed, S., & Darwish, W. (2017). Hyperspectral remote sensing to assess the water status, biomass, and yield of maize cultivars under salinity and water stress. *Bragantia*, *76*, 62-72. http://www.scielo.br/scielo.php?script=sci_arttext&pid=S0006-87052017000100062&nrm=iso

EPA, U. (1993a). Method 353.2: Determination of Nitrate—Nitrite Nitrogen by Automated Colorimetry, Revision 2.0.

EPA, U. (1993b). Standard method 350.1: Nitrogen, ammonia (colorimetric, automated phenate).

Gastal, F., Lemaire, G., Durand, J.-L., & Louarn, G. (2015). Quantifying crop responses to nitrogen and avenues to improve nitrogen-use efficiency. In *Crop Physiology (Second Edition)* (pp. 161-206). Elsevier.

Gitelson, A. A., Gritz, Y., & Merzlyak, M. N. (2003). Relationships between leaf chlorophyll content and spectral reflectance and algorithms for non-destructive chlorophyll assessment in higher plant leaves. *Journal of Plant Physiology*, *160*(3), 271-282.

Goel, N. S., & Qin, W. (1994). Influences of canopy architecture on relationships between various vegetation indices and LAI and Fpar: A computer simulation. *Remote Sensing Reviews*, *10*(4), 309-347. https://doi.org/10.1080/02757259409532252

Goel, P. K., Prasher, S. O., Landry, J. A., Patel, R. M., Viau, A. A., & Miller, J. R. (2003). Estimation of crop biophysical parameters through airborne and field hyperspectral remote sensing. *Transactions of the ASAE*, *46*(4), 1235-1246.

Haboudane, D., Miller, J. R., Tremblay, N., Zarco-Tejada, P. J., & Dextraze, L. (2002). Integrated narrow-band vegetation indices for prediction of crop chlorophyll content for application to precision agriculture. *Remote Sensing of Environment*, *81*(2-3), 416-426.

Haboudane, D., Tremblay, N., Miller, J. R., & Vigneault, P. (2008). Remote Estimation of Crop Chlorophyll Content Using Spectral Indices Derived From Hyperspectral Data. *IEEE Transactions on Geoscience and Remote Sensing*, *46*(2), 423-437. https://doi.org/10.1109/tgrs.2007.904836

Haegele, J. W., Cook, K. A., Nichols, D. M., & Below, F. E. (2013). Changes in Nitrogen Use Traits Associated with Genetic Improvement for Grain Yield of Maize Hybrids Released in Different Decades. *Crop Science*, *53*(4), 1256. https://doi.org/10.2135/cropsci2012.07.0429

Hunt Jr, E. R., Doraiswamy, P. C., McMurtrey, J. E., Daughtry, C. S., Perry, E. M., & Akhmedov, B. (2013). A visible band index for remote sensing leaf chlorophyll content at the canopy scale. *International Journal of Applied Earth Observation and Geoinformation*, *21*, 103-112.

Jeschke, M., & DeBruin, J. (2016). Corn Hybrid Response to Nitrogen Fertilizer. *Crop Insights*, *26*(8), 1-7.

Jiang, Z., Chen, Y., Li, J., & Dou, W. (2005). The impact of spatial resolution on NDVI over heterogeneous surface. *RN*, *2*(2), 2.

Jin, X., Zarco-Tejada, P., Schmidhalter, U., Reynolds, M. P., Hawkesford, M. J., Varshney, R. K., Yang, T., Nie, C., Li, Z., & Ming, B. (2020). High-throughput estimation of crop traits: A review of ground and aerial phenotyping platforms. *IEEE Geoscience and Remote Sensing Magazine*, 1-33.

Kim, M. S. (1994). *The use of narrow spectral bands for improving remote sensing estimations of fractionally absorbed photosynthetically active radiation (fAPAR)* University of Maryland at College Park].

Kim, M. S., Daughtry, C., Chappelle, E., McMurtrey, J., & Walthall, C. (1994). The use of high spectral resolution bands for estimating absorbed photosynthetically active radiation (A par). *Proceedings of the 6th Symposium on Physical Measurements and Signatures in Remote Sensing*, 299-306.

Lambers, H., Chapin III, F. S., & Pons, T. L. (2008). *Plant physiological ecology*. Springer Science & Business Media.

Lemaire, G., & Gastal, F. (1997). N Uptake and Distribution in Plant Canopies. In G. Lemaire (Ed.), *Diagnosis of the Nitrogen Status in Crops* (pp. 3-43). Springer Berlin Heidelberg. https://doi.org/10.1007/978-3-642-60684-7_1

Lemaire, G., van Oosterom, E., Jeuffroy, M.-H., Gastal, F., & Massignam, A. (2008). Crop species present different qualitative types of response to N deficiency during their vegetative growth. *Field Crops Research*, *105*(3), 253-265.

Li, F., Miao, Y., Feng, G., Yuan, F., Yue, S., Gao, X., Liu, Y., Liu, B., Ustin, S. L., & Chen, X. (2014). Improving estimation of summer maize nitrogen status with red edge-based spectral vegetation indices. *Field Crops Research*, *157*, 111-123. https://doi.org/10.1016/j.fcr.2013.12.018

Lillesand, T., Kiefer, R. W., & Chipman, J. (2014). *Remote sensing and image interpretation*. John Wiley & Sons.

Luetchens, J. (2015). Evaluation of Genetic Gain for Dynamic Leaf Traits in Maize Using Field Spectroscopy.

Merzlyak, M. N., Gitelson, A. A., Chivkunova, O. B., & Rakitin, V. Y. J. P. p. (1999). Non-destructive optical detection of pigment changes during leaf senescence and fruit ripening. *106*(1), 135-141.

Miller, R. O., Gavlak, R., & Horneck, D. (2013). *Soil, Plant and Water Reference Methods for the Western Region* [Book].

Moll, R. H., Kamprath, E. J., & Jackson, W. A. (1982). Analysis and Interpretation of Factors Which Contribute to Efficiency of Nitrogen Utilization. *Agronomy Journal*, *74*, 562-564. https://doi.org/10.2134/agronj1982.00021962007400030037x

Montgomery, D. C., Peck, E. A., & Vining, G. G. (2012). *Introduction to linear regression analysis* (Fifth ed., Vol. 821). John Wiley & Sons.

Moose, S., Below, F. E. (2009). Biotechnology approaches to improving maize nitrogen use efficiency. In A. L. Kriz & B. A. Larkins (Eds.), *Molecular Genetic Approaches to Maize Improvement* (pp. 65-77). Springer Berlin Heidelberg. https://doi.org/10.1007/978-3-540-68922-5_6.

Mueller, S. M., Messina, C. D., & Vyn, T. J. (2019). Simultaneous gains in grain yield and nitrogen efficiency over 70 years of maize genetic improvement. *Sci Rep*, *9*(1), 1-8.

Mueller, S. M., & Vyn, T. J. (2018). Physiological constraints to realizing maize grain yield recovery with silking-stage nitrogen fertilizer applications. *Field Crops Research*, *228*, 102-109. https://doi.org/10.1016/j.fcr.2018.08.025

Mulla, D. J. (2013). Twenty five years of remote sensing in precision agriculture: Key advances and remaining knowledge gaps. *Biosystems Engineering*, *114*(4), 358-371. https://doi.org/10.1016/j.biosystemseng.2012.08.009

Muñoz-Huerta, R. F., Guevara-Gonzalez, R. G., Contreras-Medina, L. M., Torres-Pacheco, I., Prado-Olivarez, J., & Ocampo-Velazquez, R. V. (2013). A review of methods for sensing the nitrogen status in plants: advantages, disadvantages and recent advances. *Sensors*, *13*(8), 10823-10843. https://doi.org/10.3390/s130810823

NCERA-13, Eliason, R., Goos, R. J., & Hoskins, B. (2015). Recommended Chemical Soil Test Procedures for the North Central Region.

Nguyen, G. N., & Kant, S. (2018). Improving nitrogen use efficiency in plants: effective phenotyping in conjunction with agronomic and genetic approaches. *Functional Plant Biology*, *45*(6), 606. https://doi.org/10.1071/fp17266

Osborne, S. L., Schepers, J. S., Francis, D. D., & Schlemmer, M. R. (2002a). Detection of Phosphorus and Nitrogen Deficiencies in Corn Using Spectral Radiance Measurements. *Agronomy Journal*, *94*(6), 1215-1221.

Osborne, S. L., Schepers, J. S., Francis, D. D., & Schlemmer, M. R. (2002b). Use of spectral radiance to estimate in-season biomass and grain yield in nitrogen- and water- stressed corn. *Crop Science*, *42*(1), 165-171.

Plénet, D., & Lemaire, G. (2000). Relationships between dynamics of nitrogen uptake and dry matter accumulation in maize crops. Determination of critical N concentration. *Plant and Soil*, *216*(1-2), 65-82.

Qi, J., Chehbouni, A., Huete, A., Kerr, Y., & Sorooshian, S. (1994). A modified soil adjusted vegetation index. *48*(2), 119-126.

Ribaudo, M., Hansen, L., Livingston, M., Mosheim, R., Williamson, J., & Delgado, J. (2011). Nitrogen in agricultural systems: Implications for conservation policy.

Rodrigues Junior, F., Ortiz-Monasterio, I., Zarco-Tejada, P. J., Ammar, K., & Gérard, B. (2014). Using precision agriculture and remote sensing techniques to improve genotype selection in a breeding program.

Rondeaux, G., Steven, M., & Baret, F. (1996). Optimization of soil-adjusted vegetation indices. *Remote Sensing of Environment*, *55*(2), 95-107.

Rouse, J. W. J., Haas, R. H., Schell, J. A., Deering, D. W., & Harlan, J. C. (1974). Monitoring the vernal advancment and retrogradation (greenwave effect) of natural vegetation.

Sadras, V. O., & Calderini, D. F. (2015). *Crop physiology: applications for genetic improvement and agronomy* (V. O. Sadras & D. F. Calderini, Eds. 2nd ed.). Academic Press.

Sahoo, R. N., Ray, S. S., & Manjunath, K. R. (2015). Hyperspectral remote sensing of agriculture. *Current Science (00113891)*, *108*(5), 848-859. http://search.ebscohost.com/login.aspx?direct=true&db=aph&AN=101659167&site=ehost-live

Salvagiotti, F., Castellarín, J. M., Miralles, D. J., & Pedrol, H. M. (2009). Sulfur fertilization improves nitrogen use efficiency in wheat by increasing nitrogen uptake. *Field Crops Research*, *113*(2), 170-177. https://doi.org/10.1016/j.fcr.2009.05.003

Schepers, J. S., Blackmer, T., Wilhelm, W., & Resende, M. (1996). Transmittance and reflectance measurements of corn leaves from plants with different nitrogen and water supply. *Journal of Plant Physiology*, *148*(5), 523-529.

Schepers, J. S., & Raun, W. (2008). *Nitrogen in agricultural systems*. ASA-CSSA-SSSA.

Schlemmer, M., Gitelson, A., Schepers, J., Ferguson, R., Peng, Y., Shanahan, J., & Rundquist, D. (2013). Remote estimation of nitrogen and chlorophyll contents in maize at leaf and canopy levels. *International Journal of Applied Earth Observation and Geoinformation*, *25*, 47-54. https://doi.org/10.1016/j.jag.2013.04.003

Schlemmer, M. R., Francis, D. D., Shanahan, J., & Schepers, J. S. (2005). Remotely measuring chlorophyll content in corn leaves with differing nitrogen levels and relative water content. *Agronomy Journal*, *97*(1), 106-112.

Shrawat, A., Zayed, A., & Lightfoot, D. A. (2018). *Engineering Nitrogen Utilization in Crop Plants*. Cham : Springer International Publishing : Imprint: Springer.

Thenkabail, P. S., Gumma, M. K., Teluguntla, P., & Mohammed, I. A. (2014). Hyperspectral remote sensing of vegetation and agricultural crops. *Photogrammetric Engineering & Remote Sensing (PE&RS)*, *80*(8), 697-723.

Thenkabail, P. S., Lyon, J. G., & Huete, A. (2012). *Hyperspectral remote sensing of vegetation* (P. S. Thenkabail, J. G. Lyon, & A. Huete, Eds.) [Book]. CRC Press.

Thenkabail, P. S., Smith, R. B., & De Pauw, E. (2000). Hyperspectral vegetation indices and their relationships with agricultural crop characteristics. *Remote Sensing of Environment*, *71*(2), 158-182.

Thenkabail, P. S., Smith, R. B., & De Pauw, E. (2002). Evaluation of narrowband and broadband vegetation indices for determining optimal hyperspectral wavebands for agricultural crop characterization. *Photogrammetric Engineering and Remote Sensing*, *68*(6), 607-622.

Tollenaar, M. (1989). Genetic improvement in grain yield of commercial maize hybrids grown in Ontario from 1959 to 1988. *Crop Science*, *29*(6), 1365-1371.

Tollenaar, M. (1992). Is low plant density a stress in maize? *Maydica*, *37*(4), 305-311.

Unkovich, M., Herridge, D., Peoples, M., Cadisch, G., Boddey, B., Giller, K., Alves, B., & Chalk, P. (2008). *Measuring plant-associated nitrogen fixation in agricultural systems*. Australian Centre for International Agricultural Research (ACIAR).

Vitosh, M., Johnson, J., & Mengel, D. (1995). *Tri-state fertilizer recommendations for corn, soybeans, wheat and alfalfa*.

Walburg, G., Bauer, M. E., Daughtry, C., & Housley, T. (1982). Effects of nitrogen nutrition on the growth, yield, and reflectance characteristics of corn canopies. *Agronomy Journal*, *74*(4), 677-683.

White, J. W., Andrade-Sanchez, P., Gore, M. A., Bronson, K. F., Coffelt, T. A., Conley, M. M., Feldmann, K. A., French, A. N., Heun, J. T., Hunsaker, D. J., Jenks, M. A., Kimball, B. A., Roth, R. L., Strand, R. J., Thorp, K. R., Wall, G. W., & Wang, G. (2012). Field-based phenomics for plant genetics research. *Field Crops Research*, *133*, 101-112. https://doi.org/10.1016/j.fcr.2012.04.003

Xue, L., Cao, W., Luo, W., Dai, T., & Zhu, Y. J. A. J. (2004). Monitoring leaf nitrogen status in rice with canopy spectral reflectance. *96*(1), 135-142.

Yang, F., Li, J., Gan, X., Qian, Y., Wu, X., & Yang, Q. (2010). Assessing nutritional status of Festuca arundinacea by monitoring photosynthetic pigments from hyperspectral data. *Computers and Electronics in Agriculture*, *70*(1), 52-59. https://doi.org/10.1016/j.compag.2009.08.010

Zhao, B., Duan, A., Ata-Ul-Karim, S. T., Liu, Z., Chen, Z., Gong, Z., Zhang, J., Xiao, J., Liu, Z., Qin, A., & Ning, D. (2018). Exploring new spectral bands and vegetation indices for estimating nitrogen nutrition index of summer maize. *European Journal of Agronomy*, *93*, 113-125. https://doi.org/10.1016/j.eja.2017.12.006

Zhao, D., Raja Reddy, K., Kakani, V. G., Read, J. J., & Carter, G. A. (2003). Corn (Zea mays L.) growth, leaf pigment concentration, photosynthesis and leaf hyperspectral reflectance properties as affected by nitrogen supply. *Plant and Soil*, *257*(1), 205-218. https://doi.org/10.1023/a:1026233732507

Zhou, K., Cheng, T., Zhu, Y., Cao, W., Ustin, S. L., Zheng, H., Yao, X., & Tian, Y. (2018). Assessing the Impact of Spatial Resolution on the Estimation of Leaf Nitrogen Concentration Over the Full Season of Paddy Rice Using Near-Surface Imaging Spectroscopy Data. *Frontiers in Plant Science*, *9*, 964-964. https://doi.org/10.3389/fpls.2018.00964

CHAPTER 4. ESTIMATING NITROGEN USE EFFICIENCY IN MAIZE FROM PARTIAL LEAST SQUARES REGRESSION MODELS BASED ON CANOPY-LEVEL HYPERSPECTRAL IMAGING

4.1 Abstract

Nitrogen (N) is an essential nutrient in food production systems around the world, but overuse of N can lead to human health and environmental degradation. Therefore, genetic and management efforts to increase a plant's efficiency in using N abound. Two parameters related to N efficiency, N Conversion Efficiency (NCE) and N Internal Efficiency (NIE), measure the amount of total biomass (leaves, stem, grain) or grain, respectively, produced per unit of N in the plant. The ability to improve these efficiency measures through breeding in maize has the potential to positively impact N use in agriculture. Application of remote sensing to N efficiency research holds promise to complement or replace traditional labor-intensive whole-plant N assessments. We investigated in-season hyperspectral imaging for prediction of end-season N concentration (pN), NCE, and NIE, through the use of partial least squares regression (PLSR) models. Image data were collected at two growth stages (V16/V18 and R1/R2) from manned aircraft and unmanned aerial vehicles (UAV) for three site-years of up to 9 maize hybrids grown under 3 N treatments and 2 planting densities. PLSR models for unseen test data resulted in accurate predictions for pN at R6 (R^2 = 0.73, CV = 11%; R^2 = 0.68, CV = 10%) and NCE at R6 (R^2 = 0.71, CV = 10%; R^2 = 0.73, CV = 12%) for both imaging times. Neither timepoint resulted in accurate predictions for NIE as defined by $R^2 > 0.65$ and CV < 20%. Additionally, the PLSR models based on the R1 images accurately distinguished the highest and lowest ranked hybrids for pN and NCE. This methodology offers good prospects for practical application in early stage breeding programs focused on NCE by aiding in data-driven genotype selection. Further development of this approach is encouraged to investigate the effects of various genotypes and multiple environments on the accuracy of the PLSR model predictions.

4.2 Introduction

As world populations are expected to continue rising through 2050, increased agricultural production and efficiencies are needed (FAO, 2017). Nitrogen (N) fertilizer has been a leading

contributor to increased food production over the last 50 years of the 20th century (Smil, 2001), yet excessive application or use at inappropriate times can lead to severe water quality issues (Peterson et al., 2019) and other detrimental environmental or human health impacts (Doering et al., 2011). Agricultural sustainability is achieved at the juncture of high production from current agricultural lands, minimized N inputs for environmental stewardship, and adequate economic farmer profits (Cassman et al., 2002).

The amount of grain yield produced relative to the amount of applied N fertilizer, or Nitrogen Use Efficiency (NUE, grain yield produced per kilogram of applied N), is the endpoint of a complex process consisting of multiple physiological elements of N uptake, translocation, assimilation, and remobilization (Moll et al., 1982; Salvagiotti et al., 2009). In order to facilitate studying N use, multiple parameters have been defined which are based on field and laboratory measurements. The amount of yield produced per unit of N in the plant is defined as Nitrogen Internal Efficiency (NIE); this variable captures how efficiently plants utilize N for the final desired agricultural product of grain (Ciampitti & Vyn, 2011; Moll et al., 1982). Since maize biomass is closely related to final grain yields, as is N concentration (Plénet & Lemaire, 2000), another measure of N utilization is Nitrogen Conversion Efficiency (NCE) which quantifies the amount of biomass produced per unit of plant N (K. Chen & T. J. Vyn, 2017; Gastal et al., 2015).

Although NUE has increased in the United States since the 1980's (Cassman et al., 2002; Lassaletta et al., 2014), these improvements were driven by genetic yield gains and agronomic advances as opposed to N focused breeding efforts (Duvick, 2005). Worldwide NUE for cereals varies widely (Dobermann, 2005). Changes over time for NUE have also varied by country (Lassaletta et al., 2014). Some countries, such as Greece, have increasing NUE levels since the 1980's while others, such as China, have decreasing NUE levels (Lassaletta et al., 2014). In China, due to already high N input, recent increased N fertilization has only resulted in low yields gains (Lassaletta et al., 2014). Global agricultural sustainability goals inherently call for developing broadly applicable tools and methods to facilitate and improve N research methods. Reliable NUE data, though sorely needed, is difficult to obtain (Dobermann, 2005) as many of the methods for determining plant N status are expensive and time intensive, especially at field scale (Muñoz-Huerta et al., 2013).

Recent technological advancements in computing and imaging have enabled research into high throughput phenotyping for improvement of crop breeding techniques (Araus & Cairns, 2014; Jin et al., 2020). Remote sensing of plants through techniques such as photographic imaging, radar, or thermal sensors are useful since destruction of the sample is avoided (Lillesand et al., 2014). Optical properties of a plant, in terms of reflectance and transmittance, are affected by the internal components of the leaf (e.g. internal pigments, water content, and cellular structures), the physical structure (e.g. leaf and cuticle thickness), and canopy characteristics (e.g. stems, neighboring plants, and soil) (Campbell & Wynne, 2011; Curran, 1989; Gausman, 1977; Gausman & Allen, 1973; Hatfield et al., 2008a).

High spectral resolution imaging provides greater differentiation or discrimination through narrow wavelength intervals of the reflectance or absorbance characteristics of different materials (Lillesand et al., 2014). However, one drawback to hyperspectral imaging is that data of neighboring bands and pixels are highly correlated because neighboring spectra and pixels are characterizing similar materials (Bioucas-Dias et al., 2013). This multicollinearity results in the Hughes Phenomenon which states that as the number of multicollinear bands increases, the number of samples needed to train the model increases exponentially in order to have confidence in the model (Thenkabail et al., 2014). One technique developed to deal with multicollinearity and an insufficient number of samples of the response variable is partial least squares regression (PLSR) (Wold, 1966). This statistical technique uses all the information collected across the spectrum through transformation into linear factors which maximize the correlation in the data (Bajwa & Kulkarni, 2011). Also, in order to avoid overfitting, PLSR uses cross-validation to select the minimum number of latent factors, thus effectively reducing the dimensionality of the data (SAS Institute Inc., 2013; Sawatsky et al., 2015; Tobias, 1995). Another benefit to PLSR for analysis of reflectance data is that, unlike artificial neural networks, it is not a ‘black box’; variable importance projections, factor loadings, and regression coefficients help identify spectral regions of most importance to the model.

Strong correlations have been found between plant optical properties and N levels (Muñoz-Huerta et al., 2013). Under both field and growth chamber conditions, studies have shown that maize plants enduring N stress have higher reflectance in the green and red portions of the electromagnetic spectrum (Walburg et al., 1982; Zhao et al., 2003). Also, mid-season maize N

concentration levels can be predicted with reflectance-based regression models (Osborne et al., 2002a, 2002c).

PLSR has been successfully applied in predicting N and chlorophyll concentrations at the leaf level using spectroradiometers in field-based maize experiments. Fan et al. (2019) used PLSR models to predict leaf N concentrations of field grown maize ($R^2 = 0.77$) using hyperspectral data from a spectroradiometer. Yendrek et al. (2017) found that PLSR models were better than vegetation indices (VI) in predicting maize leaf traits such as N concentration of field and greenhouse plants grown under varying N conditions ($R^2 = 0.96$).

Extensive research has been conducted into proximal canopy level reflectance in which hyperspectral reflectance measurements are taken approximately 1 to 3 m above the canopy with spectroradiometers. Various analysis methods, coupled with dimension reduction techniques, have resulted in predictive models for N concentration or content levels in maize regression models (Osborne et al., 2002a) or VI (Li et al., 2014; Schlemmer et al., 2013; Wen et al., 2018). PLSR has been used extensively for N estimation in other crops such as creeping bentgrass (Kruse et al., 2006), rice (Zhou et al., 2018), and wheat (Hansen & Schjoerring, 2003). An investigation by Pimstein et al. (2007) showed both maize biomass and N concentration were better predicted ($R^2 = 0.69$ or 0.64, respectively) using PLSR models than VIs. More recently, N concentration in maize was accurately estimated with PLSR models based on the reflectance ($R^2 = 0.82$), or the first derivative of the reflectance ($R^2 = 0.64$), resulting in more accuracy than random forest models (Fan et al., 2019).

Aerial canopy level reflectance measurements (i.e. those assessed at heights greater than 3m common to drones and planes) have also been studied for predictions of N content or chlorophyll. Using stepwise multiple regression for selection of specific bands, Osborne et al. (2002c) was able to accurately predict plant biomass ($R^2 = 0.87$) and N concentration ($R^2 = 0.87$). Similarly, multiple regression or regression models combining reflectance and VI resulted in well predicted chlorophyll ($R^2 = 0.75$) and N levels ($R^2 = 0.83$) (Goel, Prasher, Landry, Patel, Viau, et al., 2003). Artificial neural networks (Gautam & Panigrahi, 2007) and support vector machines (Karimi et al., 2008) have also yielded models with N predictions highly correlated to the measured values ($r > 0.66$ and 0.82, respectively). A recent comparison of 4 supervised regression models for

predicting in-season N content (kg/ha) indicated Lasso ($R^2 = 0.83$) and PLSR ($R^2 = 0.83$) as the preferred models with root mean square error values at 15.3 and 15.4 kg ha^{-1}, respectively (Nigon et al., 2020).

Another factor for predictive modeling with remote sensing is the timing between imaging and field-based ground reference measurement. Most studies sample within a day or two of imaging. Osborne et al. (2002c) found reasonable models ($R^2 = 0.87$) for predicting V13-V16 biomass from imaging 2 days later. Yet when imaging occurred one to two months after the V6 or V14 imaging, model fit was poor ($R^2 < 0.60$). This is in contrast to Goel, Prasher, Landry, Patel, Viau, et al. (2003) and Quemada et al. (2014) who were able to predict biomass at R6 from imaging at tassel (VT) or R1. Analogously, many researchers have been able to predict grain yields (at R6) based on imaging captured at VT or R1 (Goel, Prasher, Landry, Patel, Viau, et al., 2003; Osborne et al., 2002c; Quemada et al., 2014; Shanahan et al., 2001; Uno et al., 2005). Prediction of end-season N levels based on mid-season imaging has been explored less. However, Osborne et al. (2002c) found good model fit for predicting N concentration ($R^2 \geq 0.80$) even with a gap of 1 to 2 months between imaging and the later sampling. Similarly, N content at R6 was well correlated with VIs based on R1 images, but not to those from V8 images (Quemada et al., 2014).

In addition to establishing the predictive ability of a model, true applicability for a method comes about when the model successfully differentiates between genotypes and provides equivalent conclusions as the more labor-intensive field measurements. In an effort to determine simple varietal discrimination, a partial least squares discriminant analysis (PLS-DA) for differentiation of 25 maize hybrids was conducted using canopy-level spectral data from a field spectrometer by Chivasa et al. (2019). Overall classification accuracies at flowering and senescence onset were ≥ 80% for pre-processed spectral data. However, it is important to note that these models only included wavebands significantly different in mean reflectance for the 5 maturity groups (Chivasa et al., 2019) as opposed to the more traditional method for PLSR of inclusion of all or most of the spectral information. An assessment of the predicted N concentration values obtained from a PLSR leaf spectra model was reported by Yendrek et al. (2017). The researchers found that the predictions from the PLSR models had similar significant factors as the measured data. A statistical means comparison test (ANOVA) established the significant impact of maize genotype on leaf N content at V7 to V10 yet no evident effect due to ozone treatment or the interaction

between ozone and genotype for both measured and predicted values (Yendrek et al., 2017). However, though mean N values (measured and modeled) with standard deviation for the genotypes are reported, no statistical test was provided to establish whether the genotype rankings differed based on the measured versus predicted values.

Plentiful research and evidence exist for predicting physiological parameters in maize using leaf-level hyperspectral reflectance data with PLSR models. However, studies are more limited for canopy-level reflectance data of maize and even rarer for use of such canopy-level data for prediction of N parameters such as N concentration or N content. The critical N efficiency parameters of NCE and NIE are missing from such studies. To our knowledge, no experiments have evaluated in-season canopy-level hyperspectral reflectance data of field-grown maize with PLSR models to accurately predict the important N parameters of end-season NCE or NIE, nor has such imaging data been used to successfully differentiate genotypes based on these N parameters.

In this study our objectives were the following: (1) Based on mid-season imaging at multiple timepoints determine which hyperspectral regions and bands are most strongly related to the end-season (R6) N parameters of N concentration, NCE, and NIE; (2) Generate cross-validated PLSR models based on mid-season canopy-level reflectance data and determine if they accurately predict the end-season N parameters of previously unseen test data; (3) Evaluate and determine if the selected PLSR models allow for hybrid discrimination and accurately predict the outcomes for each hybrid equivalent to ground reference data.

4.3 Materials and Methods

4.3.1 Experimental Design and Site Description

Full experimental details can be found in Chapter 3 but are briefly described here. Experiments were conducted in two locations in California in 2014 (Gorman, 38.751, -121.789; Rominger, 38.727, -121.832) and in one location in Indiana in 2017 (ACRE, 40.483, -86.994). Maize hybrids were planted in a split-plot design (randomized complete block) which consisted of 4 replicates, blocked by three N rates. Hybrid and planting density were completely randomized within N treatment. Nine Mycogen® hybrids with relative maturities ranging from 99 to 116 days (CRM)

were used in the California plantings and five hybrids, a subset of the original nine, were used in the Indiana plantings. All hybrids were planted at two densities. In California, plots were 6 rows wide (4.6 m) and 12 m long while the Indiana plots were 4 rows wide (3 m) and 15 m long. All three locations had equivalent (76 cm) row spacing and all rows were planted in the north-south direction. The California locations were irrigated while Indiana was rainfed. Total N treatments (224 kgN ha^{-1}, 56 kgN ha^{-1} and 0 kgN ha^{-1}) for all locations were the same though the maize in California was fertilized through the irrigation system using urea ammonium nitrate and the Indiana maize was fertilized with a coulter injection system.

4.3.2 Plant Measurements and Physiological N Parameters Measured

Plant sampling, including harvesting, occurred in the center two rows throughout the growing season at V12, R1/R2 and R6. All samples were partitioned into leaves, stalk with tassel, and ears (if developed) and then dried and ground to 1 mm. Percent of N concentration (pN) was obtained through Dumas combustion. Grain yields are reported at 15.5% moisture. N conversion efficiency (NCE) and N internal efficiency (NIE) were calculated as shown here based on field collected data and were defined as the N parameters investigated in this research, in addition to N concentration (pN).

Nitrogen Conversion Efficiency (NCE) kg kg^{-1}N

$NCE = BM_{tot} / N_{plant}$

where BM_{tot} = whole plant biomass weight

N_{plant} = total plant nitrogen (N) content

Nitrogen Internal Efficiency (NIE) kg kg^{-1}N

$NIE = Y/N_{plant}$

where Y =grain yield at 0% moisture

N_{plant} = total plant N content

4.3.3 Remote Sensing Data

Remote sensing platforms and sensors were fully described previously (Chapter 3), with highlights written here. California imaging data were collected using a manned aircraft flown approximately 405 m above maize at V18 and R1/R2 using a push-broom hyperspectral camera of a ProSpecTir-VS system (spectral range 390-2450 nm). The spectral resolution was 5 nm and spatial resolution was 50 cm. All radiance image data were converted to reflectance through a proprietary program based on ATCOR (SpecTIR LLC, Reno, NV, USA) and orthorectified. Imaging of the Indiana

field (at V5, V8, V16/17, R1, R3/R4, R5 and R5/R6) was achieved using a Spreading Wings S1000 octocopter (unmanned aerial vehicle) manufactured by DJI (Shenzhen, China) equipped with a Nano-Hyperspec® VNIR push-broom scanner (Headwall Photonics, Inc., MA, USA) flown at 60 m above the ground. Data cubes for Indiana had 272 bands at 2.2 nm spectral resolution (400-1000 nm) and spatial resolution of 4 cm. All data were orthorectified, converted to reflectance using the FLAASH algorithm and mosaicked. Images from the similar phenological time points were pooled for a global analysis (CA at V18 and IN at V16/V17; CA at R1/R2 and IN at R1).

4.3.4 Feature Extraction

The high resolution (4 cm pixel) images from 2017 were resampled to 50 cm pixels by averaging pixel values. Bands were binned to approximately 5 nm bandwidths. All bands below 410 nm or greater than 920 nm were removed due to excess noise resulting in a total of 89 bands for every image at each site. Soil pixels were identified through supervised classification based on support vector machines with a radial basis function kernel ($\gamma = 0.011$) in Envi 5.5 software (Harris Geospatial Solutions, Inc., CO, USA). Soil pixels were then removed and plot level spectral signatures obtained by averaging reflectance values.

4.3.5 Statistical Analysis

All statistics and data analysis were conducted in SAS Enterprise Guide (SAS Institute Inc., Cary, NC, USA) or JMP 15.1.0 (SAS Institute Inc., Cary, NC, USA). Correlations between N parameters (pN, NCE, and NIE) and plot reflectance values for each of the hyperspectral bands were assessed based on the Pearson product-moment correlation coefficient (r).

Prior to conducting the PLSR analysis, data were split into training (70%) and testing (30%) data using SAS PROC SURVEYSELECT based on the respective y-variable (%N, NCE, or NIE) and stratified by simple random selection so that each split had the same proportional distribution as the full data set in terms of location, N treatment and plant density.

Partial least squares analysis was conducted in SAS using PROC PLS with random sample ten-fold cross validation of the training set in order to choose the number of extracted factors in the model based on the smallest predicted residual sum of squares (PRESS) (Wold et al., 2001). For

the ‘Full Model’ all 89 hyperspectral bands were used as the predictors in the model in addition to a classification effect based on remote sensing platform (0 for California and 1 for Indiana imaging). Van der Boet’s randomization-based model comparison test was performed (with 1000 randomizations) on the training set to determine whether a model with fewer factors than the model with minimum PRESS was significantly different ($\alpha = 0.10$). The model with the smallest number of factors was selected and used for predicting y-values (pN, NCE and NIE) for both the training and test data set. Based on the *Variable Importance for Projection* (VIP) values of this full model (Wold, 1994), hyperspectral bands with values less than 0.8 were removed for the ‘Reduced Model’ (Umetrics, 1995). Cross-validation was conducted (as described above) for the reduced models to select the appropriate number of factors. Predictions of the y-values (pN, NCE and NIE) of both the training and test data sets were obtained.

Models were evaluated through visual inspection of the diagnostic residual plots. If necessary, the y-variables were transformed. After ensuring no severe violations of the model assumptions occurred, the models were evaluated through consideration of the percentage of variation accounted for in both the predictor and response variables (for the training data set), the predicted to measured plots of both the training and test data, and several model statistics for the training and test data sets as well (R^2; Standard Error of the Prediction, SEP; Root Mean Square Error, RMSE; and Coefficient of Variance, CV). Models were judged as acceptable when the R^2 values of the test data were greater than 65% and CV was less than 20%.

Hybrid differentiation was judged by the strength of the relationship between the measured and predicted values from the PLSR models. Pearson product-moment correlations (r) were determined and evaluated for magnitude and significance. In order to evaluate the ability of each PLSR model to differentiate hybrids accurately, the predicted values from the models were analyzed as the response in a mixed model (PROC MIXED) with a structure identical to the ground reference agronomic model from Chapter 3. Fixed effects were hybrid, N treatment, plant density, and all corresponding two-way interactions. Random effects included location, hybrid x location, N treatment x location, and block[loc]. If the model indicated that hybrids and N treatment were significant effects ($\alpha = 0.10$), thus matching the results from the agronomic model, then a Tukey Kramer’s means comparison was conducted and the resulting least square means differences and letter groupings were compared. Good hybrid discrimination was defined as the ability to

designate and remove 33% (3) of the weaker performing hybrids without any misidentification and elimination of the top 25% (2) performers. These selection criteria were developed with the strategy of filtering out poor performers to improve selection processes and breeding efficiencies with data-driven decisions.

4.4 Results and Discussion

Soil fertility and weather data for each location/year can be found in Chapter 3. Additionally, the statistical analysis and results for the ground reference mixed models based on agronomic effects such as N treatment, plant density, and hybrid for predicting %N, NCE, and NIE are also found in Chapter 3.

4.4.1 Response of Field-based Parameters (pN, NCE, NIE) Over Time and Location

Mean whole plant pN levels at R6, across N treatments and plant densities, were lower at ACRE than in either CA location (Figure 4.1). The variance of pN at ACRE and Rominger was quite large and nearly uniform while at Gorman pN had a more normal distribution. Inspection of the data revealed pN values increased with increasing fertilizer treatment at all locations, as expected (K. Chen & T. J. Vyn, 2017; Ciampitti & Vyn, 2011), although the difference between the low N and high N treatments at Gorman was less than the other two locations (Figure 4.2). ACRE had consistently lower mean pN values regardless of N treatment level, while Gorman levels were usually the highest (Figure 4.2). The one exception to this trend was under high N treatment in which the Gorman and Rominger pN means were nearly equivalent suggesting maximum N rates were attained at both sites under high N treatment.

NCE values at V12 were consistently lower than at R6 (Figure 4.1) as consistent with previous observations (Sadras & Calderini, 2015). Although mean NCE levels from V12 to R6 increased at all locations, the mean change at ACRE was the largest.

NIE mean values, across N treatments and plant densities (Figure 4.1) were numerically similar between Gorman and Rominger, yet much lower than at ACRE. However, all three locations demonstrated a similar and expected pattern of decreasing NIE with increasing N fertilizer (Ciampitti & Vyn, 2011; Haegele et al., 2013) (Figure 4.2).

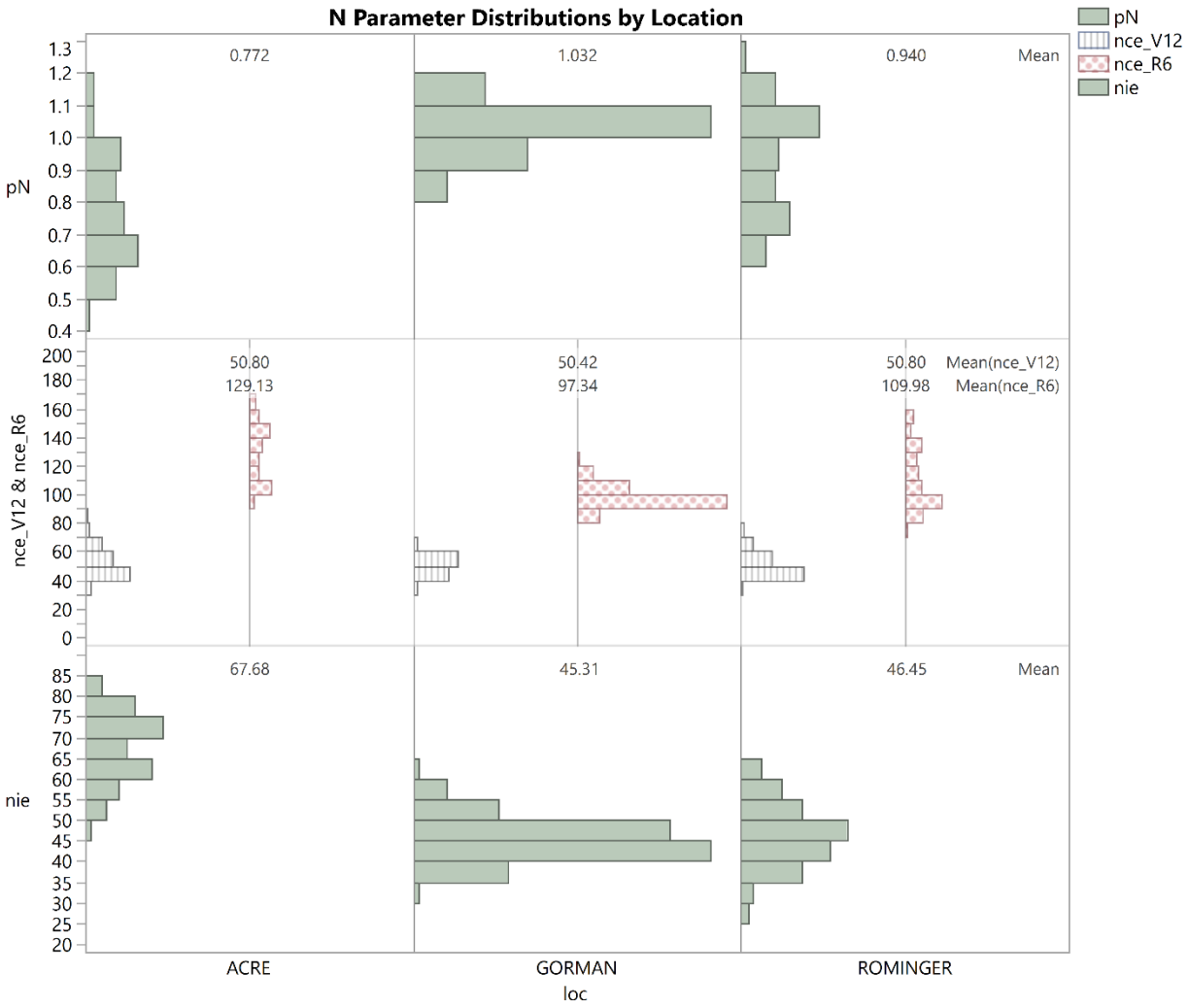

Figure 4.1. Population distributions of N concentration (pN, %) at R6, NCE (at V12 and R6) (kg $kg^{-1}N$) and NIE ($kgkg^{-1}N$) at R6 from each of the three locations (loc)

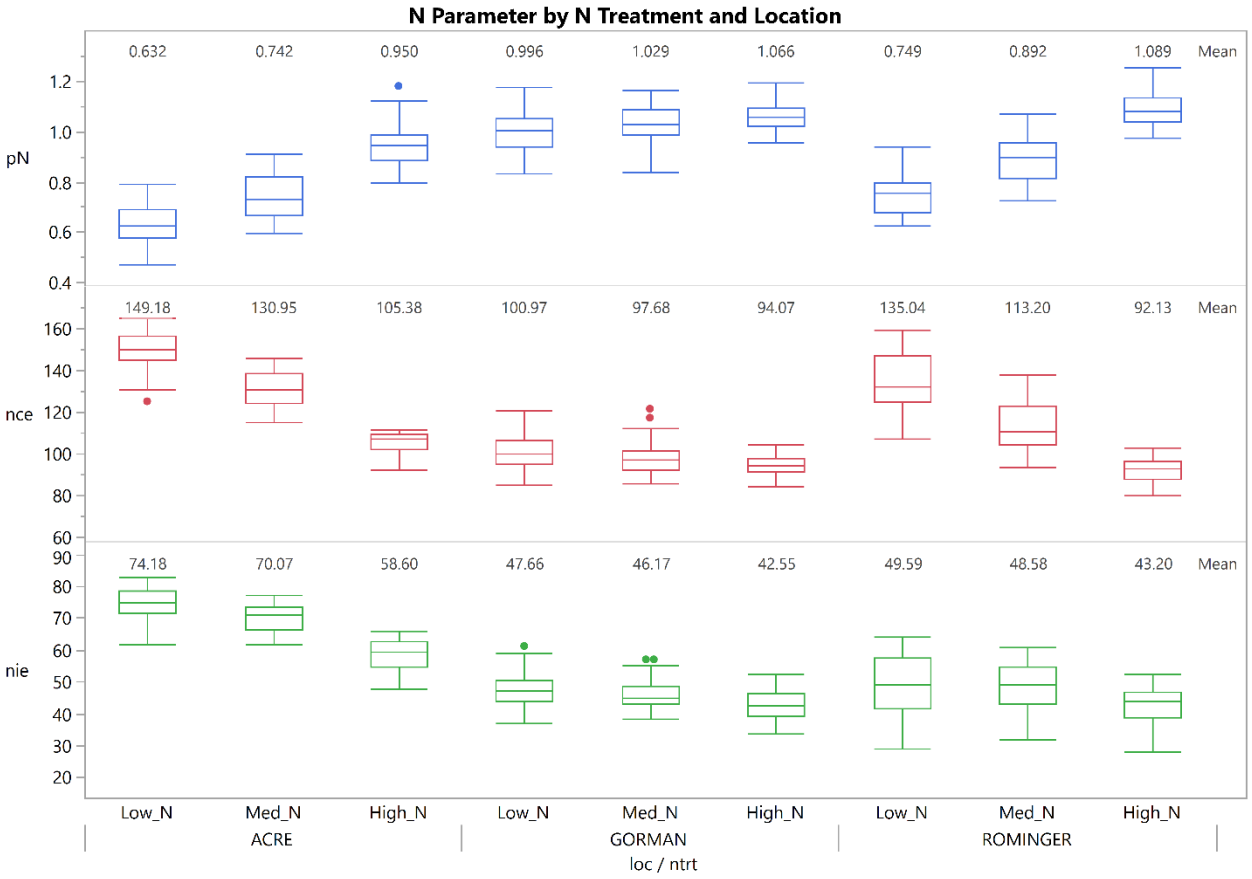

Figure 4.2. Outlier box plots of N concentration (pN, %), NCE (kg kg^{-1}N), and NIE (kg kg^{-1}N) by location (loc) and N treatment (ntrt). The horizontal line within the box is the median sample value and the ends of the box represent the 1st and 3rd quartiles. The whiskers represent the minimum and maximum values, within the distance as calculated by Quartile – 1.5*Interquartile Range. Individual dots are potential outliers.

4.4.2 Spectral Response Over Time, Location or N Treatment

The spectral response of the maize plantings at each location was examined. In the broad sense the reflectance data were inspected for similarity to known reflectance patterns of vegetation at each location. This provided an indication of the quality of the experiment and the acceptability of collecting and analyzing the reflectance data from all three locations. The average spectral responses for the high planting density treatments at all three locations at low and high N treatments are shown in Figure 4.3. The reflectance data for low plant density was similar to data shown in Figure 4.3 and thus not shown. A slight difference between the IN (ACRE) and CA (Gorman and Rominger) spectral responses was evident (e.g. a difference in slope and red-edge (RE) band region as well as a smoother spectral response in CA than IN). However, this difference in reflectance response was slight enough to permit evaluations across sites.

Additionally, the impact of N treatment on the spectral response was examined. A change in the reflectance for the different treatment effects would suggest that the remote imaging is sensing the treatment effects on the plants. The difference in spectral response between the high and low N treatment in Figure 4.3 (at either V16 or R1) was present but not large, likely due to the early season acquisition of the images. In general, N stress increases over the growing season as maize plant uptake capacity exceeds soil net N mineralization (Banziger et al., 2000). Pre-plant or V3 soil tests showed moderate nitrate-N levels at Rominger and ACRE (9, 14 mg kg^{-1}, respectively) with high nitrate-N at Gorman (24 mg kg^{-1}) in the top 30 cm of the low N plots indicating availability of mineralized soil N early in the growing season. In the NIR region the high N treatment had slightly greater reflectance levels at both ACRE and Rominger than the low N treatment, as expected for healthier vegetation not undergoing N stress (Walburg et al., 1982; Zhao et al., 2003). However, the opposite NIR response was evident at Gorman at both V16 and R1 (low N plants with higher NIR reflectance than high N plants). Early season (V12) differences between high and low N treatments in average total N content at Gorman decreased substantially by R1 (from 51 to 2 kgN ha^{-1}) then increased by R6 (29 kgN ha^{-1}). Hence, the spectral response at Gorman also corresponded to in-field plant sampling. In summary, the measured spectral responses paralleled the observed and expected field-based results.

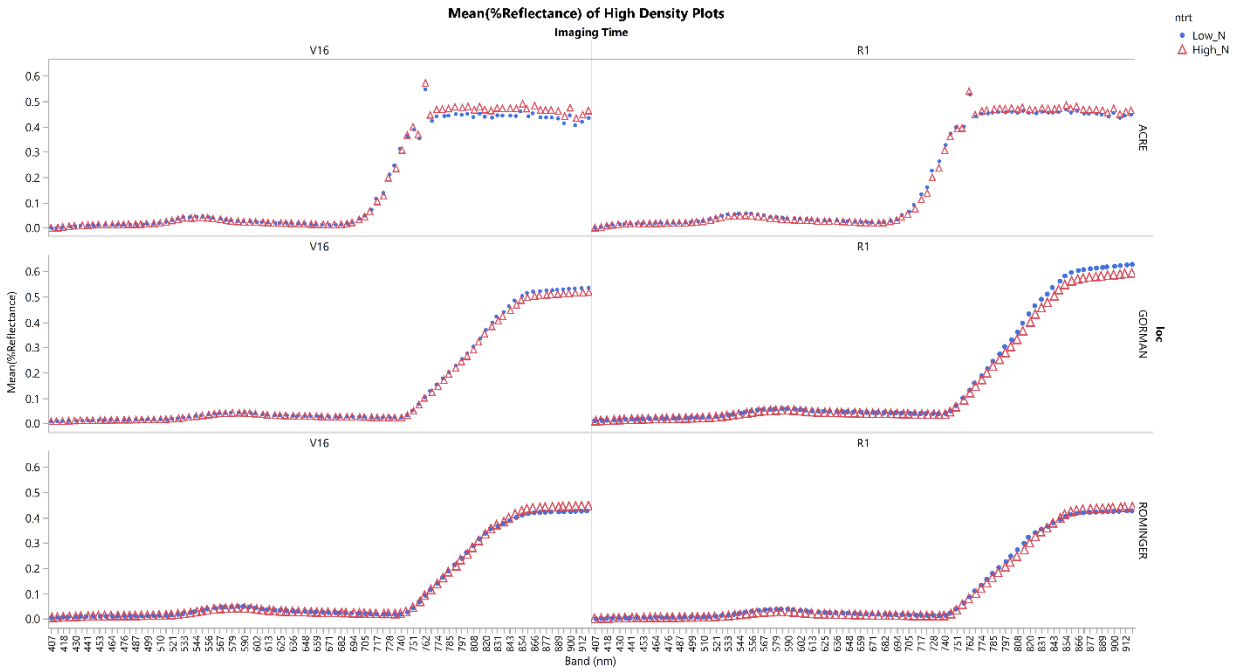

Figure 4.3. Average spectral signatures (% reflectance) at wavebands from 412 – 917 nm by location (ACRE, Gorman, Rominger) for high (red triangle) and low N (blue dot) treatment from imaging at V16/V18 or R1/R2 at high planting densities across all hybrids

4.4.3 Relationship Between N Parameters and Hyperspectral Bands

An analysis of the correlations between the N parameters (pN, NCE, and NIE) and the measured reflectance was conducted to study for the presence of a linear relationship and potential changes in reflectance over time (from V16 to R1) due to experimental conditions. In maize the relationship between reflectance and in-season pN hass been well studied at both leaf and canopy levels. However, to our knowledge, it is unknown whether there is a relationship between in-season canopy reflectance and end-season N parameters of NCE and NIE. We hypothesize a linear relationship between current plant reflectance and future N parameters exists for maize and is similar to those reported in the literature between reflectance and the individual N parameter components (grain yield, plant N, and biomass).

The correlations between plot reflectance at each band and the corresponding measured N parameter are shown in Figure 4.4, Figure 4.5, and Figure 4.6. Correlation patterns for pN (Figure 4.4) were largely the inverse of the NCE (Figure 4.5) and NIE (Figure 4.6) correlations. Thus, in instances where pN was highly positively correlated with the spectral data under high N (e.g. <440 nm and between 580 and 682 nm at V16), reflectance in these regions were strongly negatively

correlated to NCE and NIE at V16. These inverse relationships were also evident under low N. These results seem reasonable since plant N (as content or weight per area) is in the denominator of both NCE and NIE.

Correlations between reflectance and pN were high across much of the observed spectral range at both V16 and R1 (Figure 4.4), with positive correlations observed in the blue and red range and negative correlations in the low NIR (715 – 800 nm). The importance of the red and NIR regions in N detection was ascertained earlier by Blackmer, Schepers, Varvel and Walter-Shea (1996). For pN at V16, the largest N treatment difference occurred in the upper NIR region of 855 – 912 nm. Later in the season at R1, N treatments resulted in changes in the correlations across multiple regions of the spectrum. Correlations remained strongly positive for the lower N treatments in the blue, red and NIR regions while the correlations to the high N treatment weakened considerably. In the green region correlations for all N treatments weakened, but the relationship remained negative for low and high N. This corroborates previous studies which categorized the 400 – 720 nm region as greatly influenced by N stress in maize (Zhao et al., 2003). Additionally, the shape of the correlation curves for pN in which a dip occurs into negative correlations around 530 nm and then dips again around 705 nm was very similar to the pattern of correlations found for N concentration in wheat by Hansen et al. (2018) for hyperspectral bands. In summary, our data showed similar relationships between mid-season imaging and end-season pN as other researchers found for mid-season imaging and immediate sampling of pN.

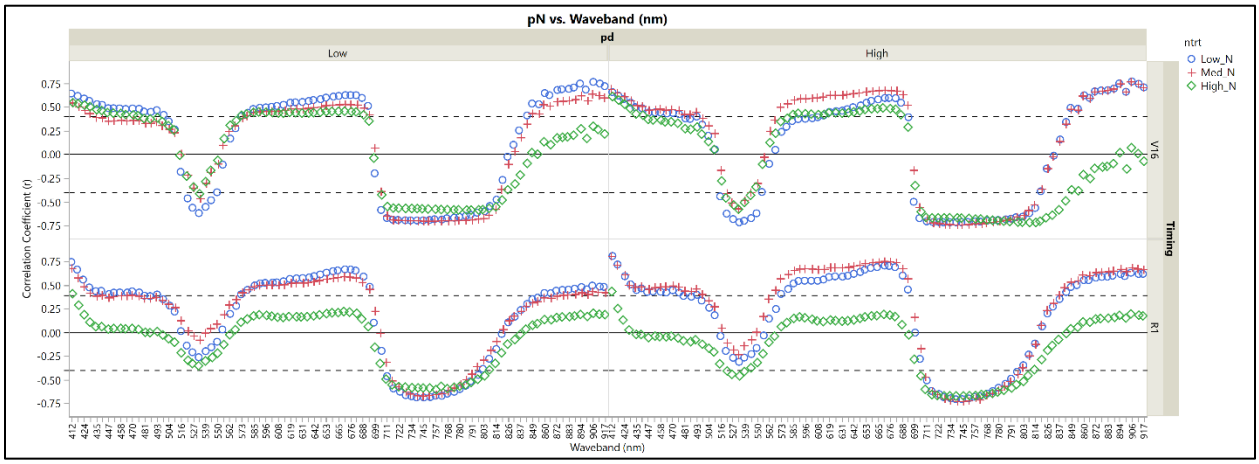

Figure 4.4. Pearson product-moment correlations (r) for N concentration (pN, %) at R6 by waveband (nm) from images at V16 (upper block) or R1 (lower block) for low and high planting density (pd) colored by N treatment (Low N = blue circle, Med N = red plus, High N = green diamond). Black lines are for reference only: solid line is at r = 0 and dashed lines at r = |0.4|.

The regions of strong correlations between reflectance and NCE were the same as those for pN except negatively instead of positively correlated (Figure 4.5). At V16, there was a difference in N treatment correlations only in the upper NIR region as correlation strength increased (i.e. more negative) with the low N rate than high N. By R1, there were clear differences in the correlations between N treatments in the blue, green, red, and upper NIR regions indicating changing reflectance levels likely due to plant response to N treatment. For the blue and red regions, correlations became less negative at high N while in the green region correlations decreased in strength and significance at low N. The similarity of the regions with strong correlations between pN and NCE confirmed our hypothesis that end-season NCE would show responses similar to that seen for pN since total plant N content (TNC) is an NCE component.

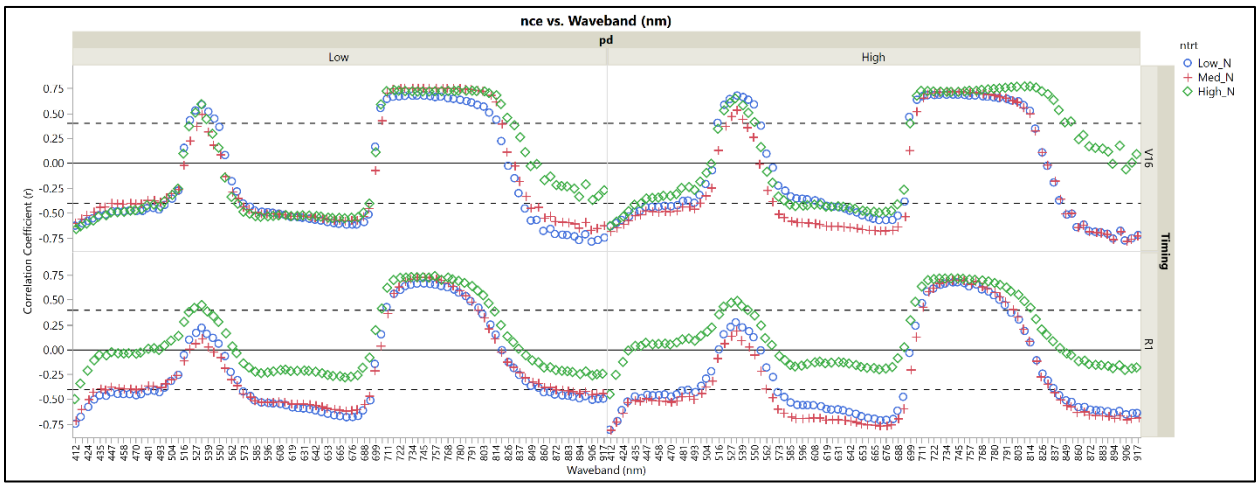

Figure 4.5. Pearson product-moment correlations (r) for NCE at R6 (kg/kg N) by waveband (nm) from images at V16 (upper block) or R1 (lower block) for low and high planting density (pd) colored shape by N treatment (Low N = blue circle, Med N = red plus, High N = green diamond). Black lines are for reference only: solid line is at r = 0 and dashed lines at r = |0.4|.

The differentiation between high N and low N plots for the correlations in the spectral range of 500 – 700 nm (Figure 4.5) is likely due to the effects of photosynthetic pigments, as identified by Zhao et al. (2003). They documented high correlation levels for chlorophyll *a* and *b*, carotenoids, and leaf N concentration and content in that same waveband region. Under low N conditions reflectance in this band region increases resulting in potentially higher correlation levels. In this study correlation levels between reflectance at R1 and NCE at R6 increased. This suggests that pigment loss at R1 was already occurring and would impact the future NCE outcome. The correlation pattern between mid-season reflectance and NCE at R6 in this study was quite similar

to that between biomass and reflectance of corn and soybean when measured simultaneously (Thenkabail et al., 2000). This finding substantiated our hypothesis that important spectral regions for NCE would be similar to those for biomass. The similarity also hints at the relationship between R1 biomass and R6 NCE suggesting that the relationship between R1 reflectance and R6 NCE is impacted less by TNC at R1 than biomass at R1.

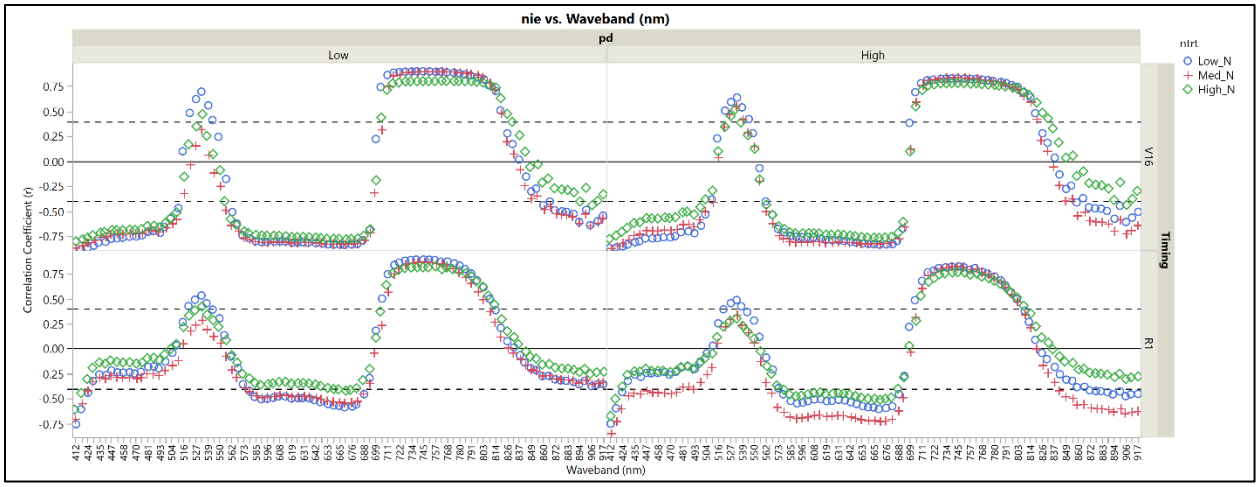

Figure 4.6. Pearson product-moment correlations (r) for NIE (kg/kg N) at R6 by waveband (nm) from images at V16 (upper block) or R1 (lower block) for low and high planting density (pd) colored by N treatment (Low N = blue circle, Med N = red plus, High N = green diamond). Black lines are for reference only: solid line is at r = 0 and dashed lines at r = |0.4|.

The N treatment effect on the correlations between reflectance and NIE was small at V16 (Figure 4.6). By R1, correlations were more strongly negative under low N in the red and NIR regions than for the high N treatment. Correlations at the bands studied for NIE (Figure 4.6) were more similar in pattern to correlations with NCE (Figure 4.5) than with pN (Figure 4.4). The overall shape of the correlations for NIE and NCE, in which a peak occurs around 530 nm and then a significant increase into positive correlations occurs around 710 nm, was similar to the correlation pattern found by Hansen and Schjoerring (2003) for leaf area index (LAI) and biomass in wheat.

Correlations with NIE at V16 were quite high in magnitude (Figure 4.5), higher than correlations to NCE (Figure 4.6), especially at the blue and red regions which were negatively correlated for all three N treatments. By R1 the correlations in those regions decreased in magnitude, while there was no change in correlation strength in the lower NIR zone of 715 – 800 nm. As found for NCE, the correlations between reflectance and NIE for the high N plots decreased even more than the

other N treatments in the blue, red, and upper NIR waveband areas. However, the difference in correlation between high and low N was less pronounced for NIE than NCE.

Overall, correlations to imaging were stronger for NIE (Figure 4.6) than NCE (Figure 4.5). This was especially true from the V16 images. Clear N treatment differences were most evident at R1, especially in the NIR region. These findings indicate that pigment changes during the vegetative stages impacted both (NIE and NCE) end-of-season measures. We hypothesize that by R1 plant health, intercellular plant cavity, and canopy changes sensed in the NIR region are more likely to impact grain production than total biomass at R6 (stover and grain). This suggests additional avenues for further research for breeding improvements in NIE such as: 1) In NIE it may be important to focus on plant health and monitoring/controlling structural leaf and canopy changes instead of pursuing pigment improvements; 2) Focus on post-silking changes such as remobilization of N and C in order to better predict grain increase and improve NIE; and 3) Develop NIR based spectral features to track and predict phenotypic traits that improve NIE selection in breeding programs.

In conclusion, end-season pN, NCE and NIE were correlated to in-season reflectance at varying degrees (of magnitude and directionality) through the portion of the electromagnetic spectrum studied here (400 – 917 nm). This is the first documentation of a linear relationship between in-season maize reflectance and end-season NCE and NIE. These results indicate that as N parameters change, plant reflectance changes; treatment effects on the N parameters were also apparent in changing reflectance; and specific portions of the spectrum were more important to the N parameters. Specifically, for end-season pN the blue, red, and NIR regions were important. Much of the VNIR responded to changes in NCE and for NIE the green (~530 nm) and the low NIR regions were most strongly related.

4.4.4 PLSR Model Development

Model tuning: Ten-fold cross-validation of the models, with all 91 predictors or a reduced number of bands, resulted in models with a range of latent factors. The number of parameters and factors in each model are shown in Figure 4.7. The cross-validation pattern was relatively similar for all N parameters. One example is shown below (Figure 4.7). In general, the models' ability to

account for variability in the predictors increased sharply to greater than 90% with ~3 factors while the dependent variable R^2 was more gradual, with an approximate maximum of 70%.

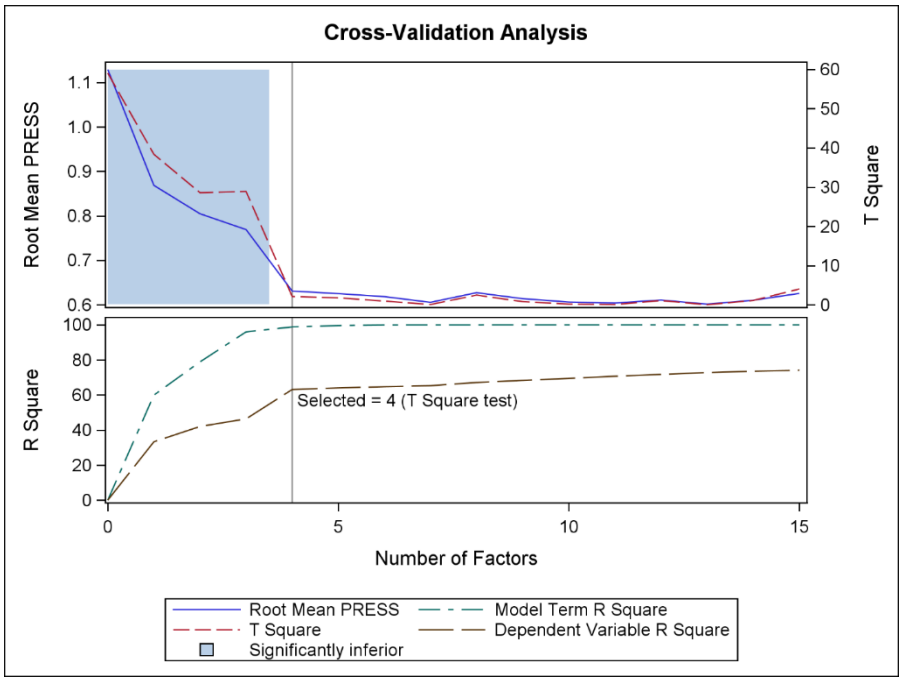

Figure 4.7. Cross-validation analysis plot for full PLSR model from V16 hyperspectral bands for predicting pN at R6

The plots of the VIP values show the band importance in fitting the models for the predictors and the response. The four plots for NCE and NIE are shown in Figure 4.8. The VIP plots for pN were very similar to those for NCE, thus are not shown. At V16 only two bands, at 694 and 699 nm (red) in the entire spectra examined were deemed unimportant to the pN model. Most important bands (VIP > 1.0) were found in the upper green region (533 – 579 nm), the RE region (711 – 740 nm) and the NIR region (803 – 917 nm). The number of important bands in the R1 pN model was smaller as many regions were deemed unimportant: the lower green portion of the spectrum (516 – 539 nm), the upper red region (694 – 705 nm) and a portion of the NIR area (808 – 854 nm). The lower blue region (412 – 447 nm) and the lower NIR region (745 – 791 nm) increased in importance in the R1 model for predicting pN.

In prior research, blue/green regions of the spectrum were found to be predictive of photosynthetic processes from leaf or canopy level images captured immediately before destructive sampling

(Meacham-Hensold et al., 2019; Yendrek et al., 2017). The RE band at 724 nm was correlated to leaf N concentration at V7-V10 (Fan et al., 2019). Furthermore, the NIR region was found to be important for current leaf N concentration predictions (Meacham-Hensold et al., 2019). Our results at V16 uniquely confirmed the relevance of the upper green, RE and NIR regions for in-field pN measurements approximately two months after canopy imaging. Because the lower blue and lower NIR regions increased in importance in the R1 model, our results suggest that by R1 other aspects are playing a larger role in the model for prediction of end-season pN measures. We infer that canopy level aspects (e.g. the vertical distribution of the canopy or foliage density) are impacting final pN more than leaf level processes such as photosynthesis. The importance of the RE and *upper* NIR region for both time-points in predicting end-season N evident in this study confirms findings by Osborne et al. (2002c) who developed a stepwise regression model for pN predictions separated in timing from imaging by 1 to 2 months. Their model based on canopy level imaging with bands in the RE (715 nm), upper NIR (935 nm), and several mid-IR bands predicted pN quite well ($R^2 = 0.95$).

For predicting NCE at maturity the most important bands (VIP > 1.0) were those in the upper green portion (533 – 579 nm), the RE (705 – 711 nm), and a large section of the upper NIR region (808 – 917 nm) (Figure 4.8). The importance of the NIR region (867 – 879 nm) for N uptake from V6 to V14 was previously identified by Nigon et al. (2020). Our results showed the importance of these N related bands for prediction of NCE at R6 from V16 imaging. The VIP changed considerably for the model based on the R1 images. A larger portion of the green region (516 – 539 nm), a few red bands (694 – 705 nm) and the mid-section of the NIR (803 – 849 nm) were deemed unimportant to the model for NCE. Conversely, the blue and upper green and lower red portions of the spectrum (585 – 613 nm) increased in importance. The RE and NIR regions (717 – 780 nm) also were more prominent.

Since NCE is the amount of biomass per unit N at R6, we hypothesized that regions previously identified to N-related processes such as photosynthesis and biomass formation would be important. The negative effect of N limitation on photosynthetic processes is well documented. Under N deficiency plant N concentration will decrease while growth can remain steady (Lemaire et al., 1997). Eventually, however, photosynthesis is down-regulated since photosynthetic mechanisms account for >50% of leaf N (Lambers et al., 2008). C-fixation decreases and plant

growth rate decreases (Lambers et al., 2008; Plénet & Lemaire, 2000). Regions identified as critical for photosynthetic processes (554 and 719 nm) (Yendrek et al., 2017) and maize biomass estimation (490, 605, 700 and 751 nm) (Ma et al., 2020) were found to be important in our models for prediction of future NCE. Thus, these results confirmed our hypothesis.

The VIP for NIE (Figure 4.8) were quite different than those for NCE. At V16, the unimportant bands were predominantly in the green region (510 – 521 and 539 – 556 nm) and in the NIR region (820 – 889, 900, and 917 nm). The important regions at V16 were the blue (412 – 476 nm and 493 nm), the upper green/red (573 – 688 nm) and RE/NIR (711 – 808 nm) sections. By R1, the predominance of the blue region (430 – 499 nm) decreased appreciably as did a large portion of the green region in the VIP plots for NIE (Figure 4.8). The RE (from 711 – 740 nm) and lower NIR region (745 – 803 nm) were still quite important for the R1 NIE model.

Yendrek et al. (2017) found the green band at 554 nm to be important in PLSR models for predicting leaf chlorophyll, photosynthetic rate (V_{max}) and specific leaf area during the early vegetative portion of the season (V7-V10). However, this region was not important for either of our NIE models. The most important band in their PLSR models was found to be the RE band at 719 (Yendrek et al., 2017). In other research spectral bands from the RE region (735 – 744 nm) were identified as prominent for N uptake detection in maize during the vegetative stage by Nigon et al. (2020). Our results showed the importance of the RE region for prediction of end-season NIE. We hypothesize the importance of this region in our models is likely due to the photosynthetic processes integrated into NIE through crop growth rates and ultimately, in grain yield.

The NIR region was found to be important for all three responses (pN, NCE and NIE) in this study though chlorophyll and related pigments are nearly transparent in that portion (Lambers et al., 2008; Sahoo et al., 2015). The NIR region is also impacted by canopy reflectance changes in light scattering within the leaves and stems (Ollinger, 2011). Chivasa et al. (2019) identified three bands in this region (765, 840, and 895 nm) as a subset of the 10 ideal bands for discriminating maize varieties differing by maturity group and leaf angle (i.e. erectophile vs. planophile) confirming the relationship between NIR reflectance and maize architecture. It is known that N stress results in architectural changes of reduced leaf area and early senescence of older leaf tissue (Banziger et

al., 2000), conditions expected during N research. Our results suggest physiological effects due to N stress were occurring at V16 and R1 though leaf or canopy changes were not readily visible. Instead, these changes were detectable with hyperspectral remote sensing and predictive of the future N parameters. Because the NIR region between 803 – 849 nm was not important by R1, we infer that these physiological changes are invisible in this spectral region. We recommend further study of the upper NIR region (> 850 nm) to understand the changes occurring at this mid-growth stage.

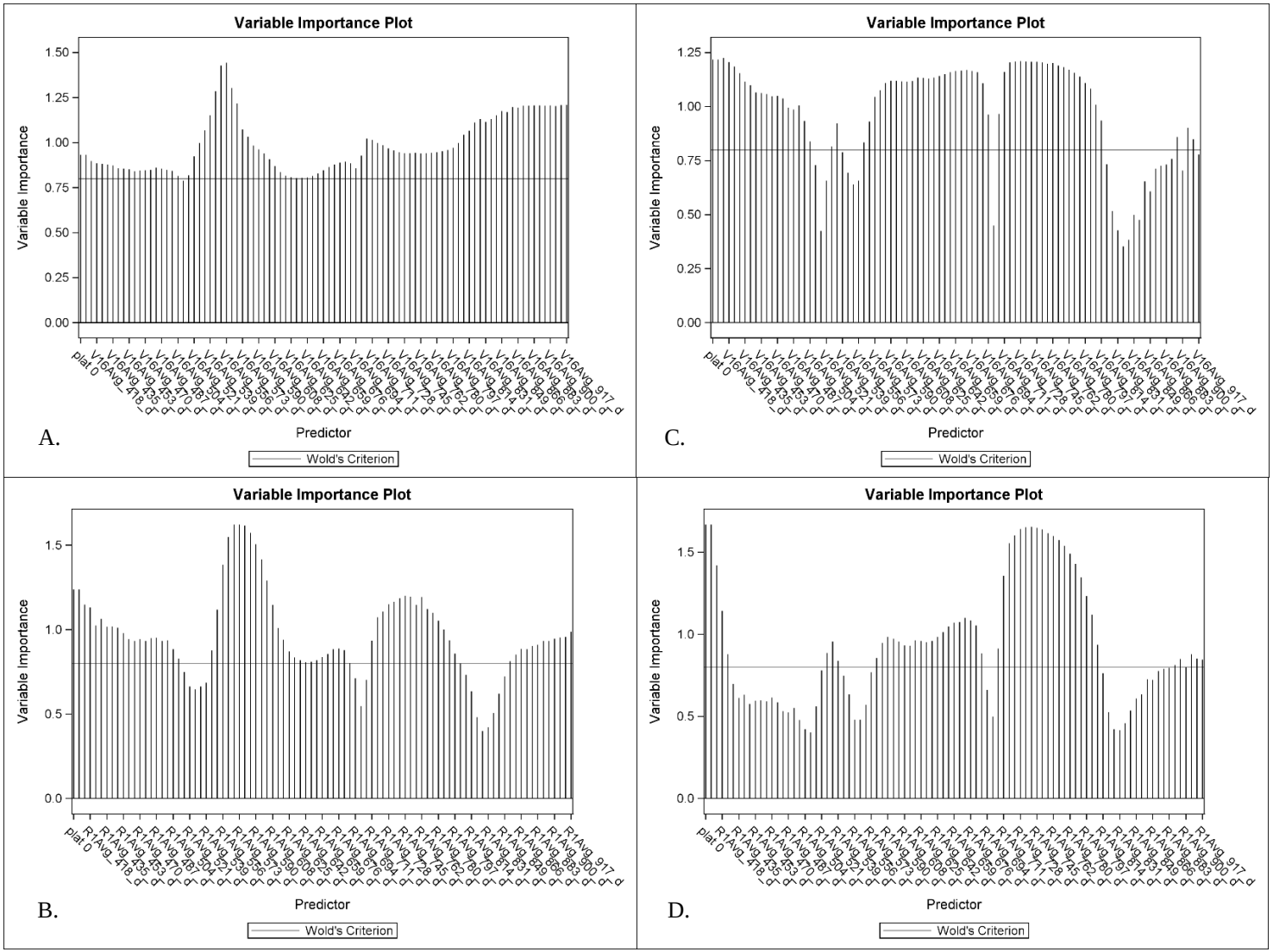

Figure 4.8. Plots of Variable Importance for Projection (VIP) values for NCE at V16 (A), NCE at R1 (B), NIE at V16 (C) and NIE at R1 (D). Predictors for each model are shown on the x axis. Line is at reference value of 0.8; values less than 0.8 are deemed not important as per Wold (1994).

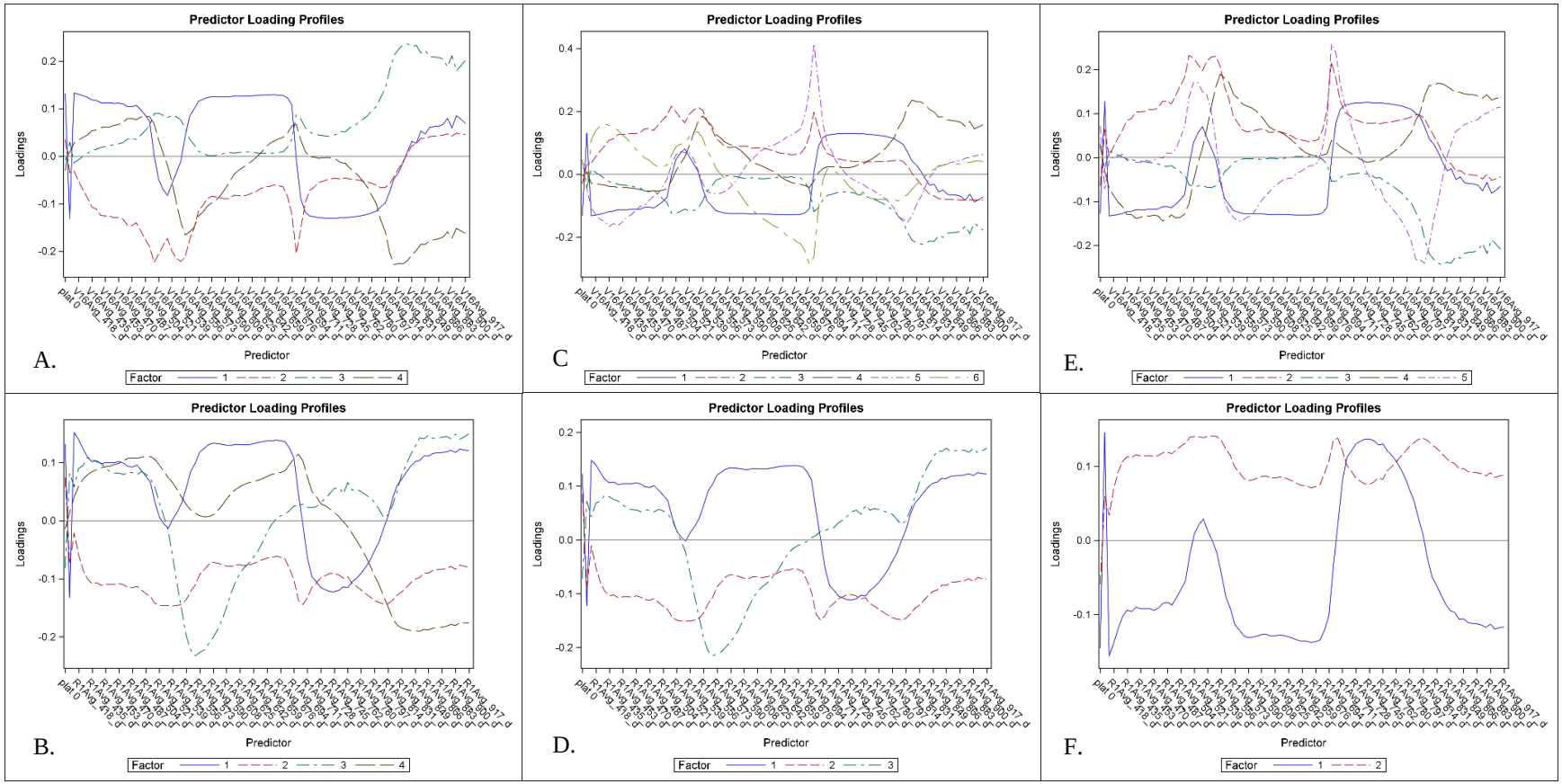

Figure 4.9. Factor loading profiles for PLSR models with all 91 predictors based on images at V16 and R1 for predicting pN (A & B), NCE (C & D), and NIE (E and F).

4.4.5 Comparison of Various Approaches for Spectral Assessment of N Parameters

Model performance for training and test data sets: Ten-fold cross-validation of the models for factor selection described in the previous section, as well as development of the final model regression coefficients, was performed using the training data set. In these experiments, the R^2 values for the test data set were often similar to the training data set (Table 4.1) but with some slight variation depending on the response being predicted. For example, the V16 full pN model had an R^2 value of 0.63 for the training set which increased to 0.73 for the test set. In contrast, the R^2 for the R1 pN train and test models were similar.

Full versus reduced models: For each response of pN, NCE or NIE, four models were evaluated. At each imaging time point (V16 and R1) two types of models were built – a full model with 91 predictors of 89 spectral bands or a reduced model with fewer bands. The number of bands in the reduced models differed considerably depending on the response being predicted and the imaging time point (Table 4.1). For the models predicting pN, the reduced model from the V16 data had 2 fewer spectral bands than the full model, while the model based on the R1 data used 73 predictors (71 bands). Similarly, the reduced NCE model from the V16 data used most of the bands, while the R1 model used fewer. The reduced models for NIE were based on an even smaller portion of the spectrum.

The purpose of developing the reduced models is to carefully tune the models by removing unimportant predictors to increase the model's ability to predict the response for the test set (i.e. higher R^2), while still maintaining the model's ability to explain the variation in the predictors. Consequently, the evaluation for the full vs. reduced models was focused on the models' ability to account for variation in the predictors of the training set while also accounting for the variability in the response (R^2) from the test set.

The percent of variability in the predictors of the training data set explained by the models, either full or reduced, was always greater than or equal to 95%, regardless of the type of model used (Table 4.1). The amount of variability in the dependent variable explained for the test set did not differ greatly between full vs. reduced models based on the V16 imaging. For example, both the full and reduced models at V16 predicted 73% of the variability in pN, 71% in NCE and 63% for the NIE response. Similarly, the models for pN and NIE from the R1 imaging data did not differ

greatly between the full and reduced models (Table 4.1). The R1 models for NCE differed slightly more. These results were not surprising as most of the reduced models had few eliminated bands. Because there was no increase in the R^2 values of the reduced models and reduction of the predictors did not improve the interpretation of the model, no benefit was found for the reduced models. Further discussion will focus on the full models with all measured spectra.

Factor loadings: The factor loadings shown in Figure 4.9 are plots of the frequency of the predictors present in each of the factors in order to provide a visual interpretation of the factors. The pN model from the V16 data contains 4 factors (Figure 4.9A). Factor 1 is largely affected by spectra in the blue region and the red region while factor 3 is mostly a weighted sum of the upper blue/lower green region and the NIR region. The loadings for the V16 NCE model (Figure 4.9C) show that for all 6 factors the RE region is a point of transition. The factors are largely impacted by the RE region as all have a peak or valley in that region (factors 2, 3, 5, and 6) or cross the 0 value (factors 1 and 4). An interesting point to note is that the pattern for factor 1 of the NCE V16 model in Figure 4.9C is a clear inverse of the pattern for factor 1 of the pN V16 model in Figure 4.9A. Also, the factors of the V16 NIE model (Figure 4.9E) are very similar to the NCE factor patterns, though the NIE model contains one less factor.

4.4.6 Comparative Model Performance & Selection

In order to select the final models between imaging time points (V16 vs. R1), model statistics for the test set were compared (Table 4.1). The model for pN at V16 explained more of the variability in the test data set than the R1 model (73% vs. 68%) with no difference in the RMSE or SEP between V16 and R1 models. Examination of the measured by predicted plots for pN in Figure 4.10 showed there was no significant bias and the variance of the residuals was relatively constant.

A distinct demarcation between the IN and CA data were observed around the 0.9% predicted value, especially for the V16 model. For the measured values $\geq$ 1.0% in IN, the model consistently underestimated those to ~0.9%. However, this pattern was not noted for the CA data. The difference may be due to the range of the pN between locations as the CA median value was 1.0% while IN had a lower median value of 0.7%. Response differences in pN between CA and IN could also be environmental, (e.g. soil-type or weather since CA locations were tested in 2014 and the IN location was tested in 2017). Other potential reasons for the disparity between CA and IN

are management differences (irrigation vs. rain-fed) or remote sensing scale differences (plane vs. drone).

Since the difference in pN between the 0N and HN treatment at the Gorman location was observed to be much less pronounced than at Rominger or IN, further investigation was conducted into potential differences between Gorman and Rominger. The California SWRCB (2020) lists 4 closed water wells within approximately 10 – 25 km of the two experiment locations due to excessive nitrate levels (> 45 mg/L NO_3) as defined by the state (SWRCB, 2017). This suggests a high potential of nitrates in the irrigation water in our experiment. Also, according to a study conducted for and in conjunction with the Yolo County Flood Control and Water Conservation District (2012) the Rominger location was closest to a region generalized to have wells with less than 20 mg/L NO_3 while Gorman was closer to a study area with higher N levels (20 – 40 mg/L NO_3). Measured values related to this study in Chapter 3 show pre-plant soil N at Gorman substantially higher than at Rominger. The clear evidence of nitrates in CA well water, higher early-season soil N at Gorman, plus the potential for higher nitrates at Gorman may be contributing factors to the models' apparent location bias and thus its inability to accurately predict high pN at IN. Generally, however, both V16 and R1 PLSR models provided reasonable pN predictions based on the reflectance data.

Statistics for the NCE models in Table 4.1 show that the V16 PLSR model accounted for 71% of the variability in NCE for the test set, but 73% when based on the R1 data. However, the RMSE, CV, and SEP of the V16 model was less than the R1 model. Examination of the measured by predicted plots (Figure 4.10) reveals three data points for the R1 model with measured values of 130 to 160 kg $kg^{-1}N$ yet predicted values greater than 175 kg $kg^{-1}N$. These outliers explained the poor statistics (RMSE and SEP) for the R1 vs. the V16 model. Due to non-constant variance in the residuals of the R1 NCE model, the PLSR was run on a transformed response. The transformation is a likely reason for the outliers, as no outliers were evident on the transformed predictions.

The previously mentioned disparity between the CA and IN data for the pN models is also evident in the NCE models. Again, this is likely due to environmental or agronomic differences between locations, some of which were described above. In the case of NCE the median value for CA (97

kg kg^{-1}N) was below the 1st quartile of data in IN (109 kg/kg N). Thus, there was an even greater dissimilarity between NCE values across general locations.

An additional factor complicating predictions of NCE at R6 from imaging at V16 or R1 is the parameter itself. NCE at R6 is based on the amount of biomass (stover + grain) per unit N. Therefore, total N, plant matter, and grain yield are all components in the parameter. However, grain is completely unformed at V16/18 and kernels are established from R1 through R3 (Abendroth et al., 2011). Consequently, the PLSR model based on the mid-season imaging is missing an entire component of the "equation" (i.e. grain) likely leading to its poorer predictability for NCE in comparison to pN.

When working with hyperspectral PLSR models for predicting wheat biomass, Pimstein et al. (2007) found inter-annual variability in weather had a very large impact on the PLSR models. A model based on a year with ideal weather conditions (2004/05) and thus high biomass levels was a poor predictor for a year with drier conditions (2003/04 data, $R^2 = 0.05$). However, the reverse model (poor weather year to predict good weather year) which had a broader distribution of biomass provided better predictions (Pimstein et al., 2007). These results highlight the importance of ensuring a balance in the training and test data sets such that the training data are representative of the conditions in the test set. It also underscores the negative effect of non-overlapping distributions on PLSR model predictions which may also be factors in this analysis.

The statistics for the models in this study based on imaging during the growing season for the future NCE outcome ($R^2 > 0.70$ and CV = 10-12%) were much better than those found by Osborne et al. (2002c) ($R^2 = 0.45$) and Quemada et al. (2014) ($r \leq 0.63$) who probed a similar separation in timing with hyperspectral imaging for predicting biomass at R6. Due to the greater variance of the error in the R1 NCE model, the V16 model was selected as best for predicting NCE. However, both models meet the criteria set for acceptable models ($R^2 > 0.65$ and CV < 20%).

Examination of the PLSR models for NIE indicated that both V16 and R1 models accounted for less than 65% of the variability in NIE (Figure 4.10), yet the CV was less than 15% (Table 4.1). The RMSE for the V16 model was 5.4 kg kg^{-1}N while the R1 model had a slightly higher RMSE (Table 4.1). The SEP values for the V16 and R1 models were quite similar. The plots of measured vs. predicted values for the NIE models in Figure 4.10 revealed an extreme difference in the

predictions for the general locations of CA and IN. A partial explanation for the separation between locations may be the large proportion of non-overlapping NIE values at the two locations compared to the other two N parameters. For NIE all CA data from the minimum value to the 3rd quartile (28 kg kg kg^{-1}N to 49 kg kg^{-1}N, respectively) were lower than the range of IN data which had a minimum value of 48 kg kg^{-1}N and 1st quartile of 62 kg kg^{-1}N. However, the poor NIE model results suggested that other factors may be at play. Investigation of the VIP plots (Figure 4.8) and factor loadings (Figure 4.9) showed that the RE/NIR region was especially important for both NIE PLSR models. An examination of the residuals for the NIE models by the predictors (i.e. bands) showed that in the RE/NIR region (717 – 774 nm) the assumption of constant variance was violated. Further investigation into the reflectance data at those bands showed a large divergence in the reflectance data between the 2 general locations. The difference is apparent in Figure 4.3 in which RE region, the inflection point at which plant reflectance increases (Horler et al., 1983), is shifted "leftward" in IN with higher reflectance values at lower wavelengths than in CA. These observations suggest the NIE models were more highly influenced by the shift in the spectral signatures than the other N parameters thus resulting in less predictive models.

Another potential cause for the lack of predictability for NIE with these models is the parameter itself. The parameter of NIE is based on grain yield and total N. As discussed previously, grain has not formed at V16/V18 and is only beginning to form by R1/R2. Overall, grain weight generally accounts for approximately 50% of final dry matter, a harvest index (HI, ratio of GY/TDM_R6) of 0.50 (Abendroth et al., 2011; Duvick et al., 2004) or higher for modern hybrids (Mueller et al., 2019). In this experiment the mean harvest index across N rates and locations was a relatively low 0.47. Thus, a full 47% of the final plant mass still needed to be formed at R1. More specifically, depending on N rate and location the change in total mass from PDM at R1 to TDM at R6 ranged from 5.1 to 14.5 Mg ha^{-1}. This was a change of approximately 21 to 60% in total matter from R1 to R6. Therefore, the PLSR NIE model was attempting to predict a variable very different from that being imaged. However, the hyperspectral index (HSI) models described in Chapter 3, also based on this reflectance data, predicted NIE very well. A potential reason for the inability to predict NIE based on PLSR models is that the few bands important for NIE prediction and used in the HSI are masked by all the other bands in the data set. The PLSR models are unable to put enough emphasis on those critical bands to result in predictive models.

Due to the large general location effect, especially evident for NIE, individual PLSR models were built and investigated for each of the general locations (IN or CA). These models were compared to the global models (those with all three site-years) and found to be much less predictive of all N parameters. Thus, no further discussion will be presented here on that analysis. In conclusion, these findings showed that in-season reflectance based PLSR models were effective in estimating the future pN and NCE values, but not NIE. Though correlations between reflectance and NIE were higher than for NCE, model predictions for NIE were the least accurate.

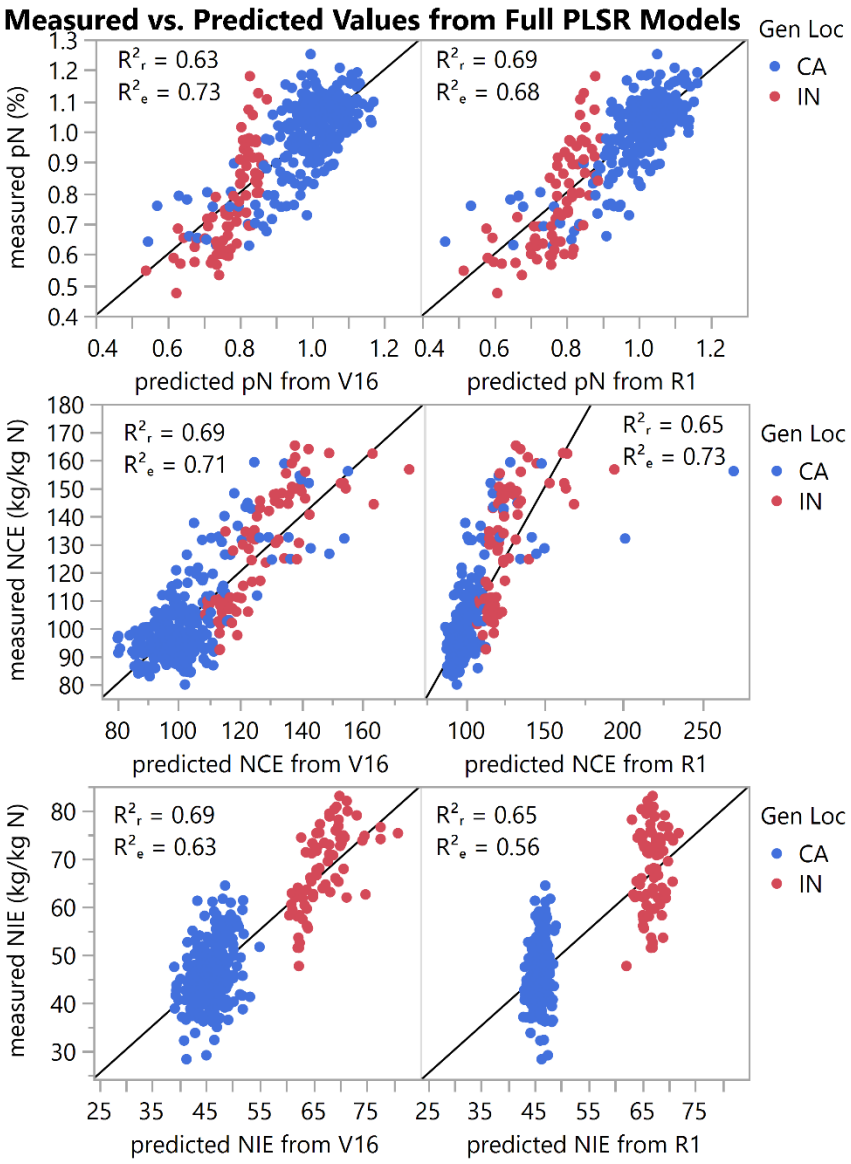

Figure 4.10. Measured by predicted plots for full PLSR models based on spectral data at V16/18 or R1/R2 for training and test data sets. R2r = Rsquare for training data set; R2e = Rsquare for test data set; pN = nitrogen concentration (%); NCE = nitrogen conversion efficiency (kg kg-1N); NIE = nitrogen internal efficiency (kg kg-1N); Gen Loc = general location; CA = California, blue dots (Gorman and Rominger locations); IN = Indiana, red dots (ACRE location). Black line is 1:1 reference line.

Table 4.1. PLSR models based on imaging obtained at V16 or R1 for predicting end-season %N, NCE or NIE in maize using models with all 91 predictors [including 89 hyperspectral bands] ("Full") or a reduced number of bands ("Reduced"). %N = Percent N (N Concentration); NCE = Nitrogen Conversion Efficiency (kg $kg^{-1}N$); NIE = Nitrogen Internal Efficiency (kg $kg^{-1}N$); N Obs = Number of Observations; N Pred Parm = Number of predictor parameters; N factor = Number of latent factors; % Pred = Percent of Variability for the Predictor Variables explained by the model; % Dep (R^2) = Percent of Variability for the Dependent Variable explained by the model or the R^2 value calculated for the Test data; RMSE = Root Mean Square Error; CV = Coefficient of Variance; SEP = Standard Error of the Predictor.

Image Time	Data set	Y var	N Obs	Full Models							Reduced Models						
				N Pred Parm	N factor	% Pred	% Dep (R^2)	RMSE	CV (%)	SEP	N Pred Parm	N factor	% Pred	% Dep (R^2)	RMSE	CV (%)	SEP
V16	Train	%N	254	91	4	98.8	63.1	0.10	10	0.13	89	4	99.0	63.4	0.10	10	0.13
		NCE	254	91	6	99.9	68.5	10.8	10	15.9	90	6	99.9	68.5	10.8	10	15.9
		NIE	254	91	5	99.0	68.8	6.1	12	9.0	68	5	99.1	69.0	6.0	12	9.0
	Test	%N	109				72.9	0.09	10	0.14				73.4	0.09	10	0.14
		NCE	109				70.8	10.7	10	17.3				70.9	10.7	10	17.3
		NIE	109				62.7	5.4	11	9.2				63.2	5.4	11	9.2
R1	Train	%N	241	91	4	99.5	68.6	0.09	9	0.13	73	3	97.1	67.6	0.09	10	0.13
		NCE	241	91	3	96.5	65.3	13.5	13	18.9	74	3	97.2	64.0	12.5	12	17.7
		NIE	241	91	2	95.8	65.3	6.4	13	8.9	52	2	97.3	65.0	6.5	13	8.9
	Test	%N	103				67.8	0.09	10	0.14				67.5	0.09	9	0.14
		NCE	103				72.6	13.1	12	18.0				67.2	12.5	12	17.3
		NIE	103				55.8	6.2	12	8.9				55.6	6.2	12	8.9

4.4.7 Hybrid Differentiation: Numerical Predictions

To determine whether the PLSR model predictions differentiated hybrids correctly we examined the strength of the linear relationship between the measured and predicted variables grouping by hybrid. The Pearson correlation coefficients (r) were determined and shown in Table 4.2. Hybrid differentiation for the NIE models was not assessed due to the poor fit of the NIE PLSR models. Both pN models had very strong correlation levels of 0.80 or greater for most of the hybrids indicating high similarity between the hybrid measured and predicted values. Hybrids DAS01, DAS07, and DAS08 had the weakest correlations (< 0.80) for at least one model. In general, the post-silking TNC gain for these three hybrids varied by location and N rate more drastically than for the other hybrids. DAS08 had minimal post-silking gain in TNC for all three N treatments at Rominger. Similarly, the low N treatment at Gorman only had a minimal gain in TNC from R1 to R6, yet the high N treatment had a notable TNC gain. For DAS01 a moderate TNC post-silking gain occurred for all N treatments at Gorman, however at Rominger the TNC post-silking gain for the high N treatment was quite pronounced. This suggests that the prediction strength of the imaging data collected at R1 is affected by inconsistent hybrid responses at the different locations. Also, it indicates that hybrids with greater flexibility to increase post-silking TNC may not be well predicted.

Though all correlations were significant for both pN models, the highest correlations between the measured and predicted values occurred for the full R1 PLSR model. The plots for these are shown in Figure 4.12. For some of the hybrids (e.g. DAS01, DAS02, and DAS03), the lower measured N concentrations were often overestimated, while the higher N levels were closer to the 1:1 line. All hybrids were consistently similar in pattern around the 1:1 line with none having greater scatter than the others; thus, there was no clear evidence of a notable hybrid bias.

Table 4.2. Pearson correlation coefficients (r) between measured and predicted values for each PLSR model by hybrid. Correlation probabilities: P < 0.0001 = ***; P < 0.01 = **; P < 0.05 = *. V16f = Full PLSR model based on imaging at V16/V18. R1f = Full PLSR model based on imaging at R1/R2. Hybrids marked to indicate whether hybrids tested across two(θ) or three site years.

Hybrids	**Predicted pN**		**Predicted NCE**	
	V16f	R1f	V16f	R1f
DAS01[θ]	0.68***	0.79***	0.79***	0.78***
DAS02	0.83***	0.83***	0.89***	0.87***
DAS03	0.87***	0.92***	0.89***	0.89***
DAS04	0.84***	0.80***	0.90***	0.72***
DAS05	0.80***	0.80***	0.85***	0.71***
DAS06[θ]	0.82***	0.77***	0.85***	0.77***
DAS07[θ]	0.66***	0.82**	0.67***	0.84*
DAS08[θ]	0.75***	0.78***	0.76***	0.77***
DAS09	0.81***	0.84***	0.88***	0.85***

The NCE predictions were more highly correlated to the measured values when generated by the full V16 PLSR model than the R1 model (Table 4.2). This indicates the V16 model hybrid predictions were more similar to the measured outcomes. All hybrids, except DAS07, had similar or stronger correlations values based on imaging at the earlier time point. The difference in the correlations between the NCE V16 and R1 models was much greater than the difference between the pN models. Only three of the nine hybrids had weak hybrid correlations (< 0.80) based on the V16 model. In contrast, the R1 NCE model provided poorer predictions for multiple hybrids. The hybrids with lower correlations with either one of the models (i.e. poorer predictions) tended to have inconsistent post-silking TNC or TDM gain across the locations and N rates. This suggests that the poorer predictions from the models are likely due to a genotype effect instead of an image timing effect. Interestingly, predictions from the V16 model for DAS07 were less accurate than those from the R1 model while the inverse was true for DAS04 and DAS05. However, both NCE models underestimated the predictions for DAS01 and DAS08, specifically for the higher in-situ NCE values such as those greater than 120 kg kg^{-1}N (data not shown).

Based on the best pN (R1) and NCE (V16) PLSR models, the highest correlation for a hybrid was for DAS03. In response to N treatment, DAS03 had similar incremental PDM gains from V12 to R1 to R6, with slightly higher gains under high N. DAS03 TNC levels increased considerably at high N at late vegetative growth (V12 to R1) but post-silking TNC gains were minimal at all N levels. No other hybrid was as well predicted (r > 0.90). Since the correlation values were below 0.9 and varied considerably by hybrid, hybrid rankings based on the predicted measures were not expected to match the measured hybrid rankings.

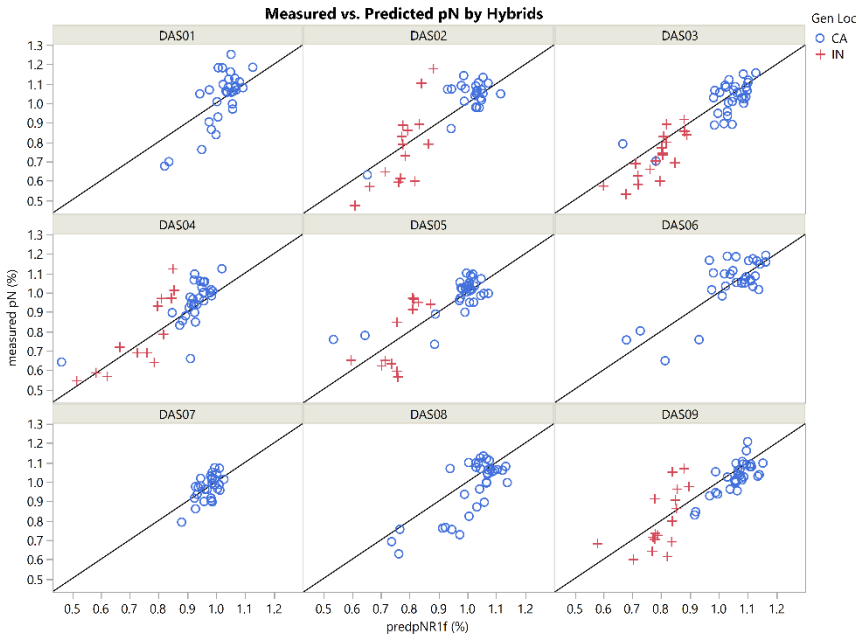

Figure 4.11. Measured by predicted plot for Full R1 PLSR model for predicting N concentration (pN, %) separated out by hybrid with general location indicated by color and marker shape. Black line is 1:1 reference line.

4.4.8 Hybrid Differentiation: Hybrid Rankings

Mixed model analysis of the predicted N parameters indicated that hybrid and N treatment were significant effects only for the R1 pN PLSR model. The full R1 PLSR model for NCE specified that hybrid was a significant effect, but N treatment was not ($P = 0.11$). Due to the proximity of this effect to our criteria ($P \leq 0.10$), the hybrid differentiation of the R1 PLSR NCE model was investigated and discussed here. All results are shown in Table 4.3. Based on the ground reference model for pN, the top two hybrids were DAS06 and DAS09. The PLSR R1 pN model designated the bottom three hybrids as DAS04, DAS05, and DAS07 and the top hybrids as DAS06 and DAS09. Removal of the bottom 33% of the hybrids based on the PLSR pN model resulted in a genotype pool containing the top 25% of the best hybrids thus meeting our criteria for effective hybrid selection. The ground reference NCE model designated DAS04 and DAS07 as the two best hybrids. The PLSR R1 model for NCE assigned 5 hybrids to the bottom tier based on letters (DAS01, DAS03, DAS06, DAS08 and DAS09) with the lowest numerical means to DAS06, DAS08, and a tie between DAS01 and DAS09. Elimination of the worst 4 or 5 hybrids from the pool resulted in a hybrid selection still containing the top 25% of the best hybrids. Accordingly, the NCE R1 PLSR model also met the criteria for efficient hybrid selection.

Table 4.3. Comparison of hybrid differentiation results for ground reference models and Full PLSR models based on R1 image for predicting N concentration (pN, %) or NCE at R6 (NCE, kg kg^{-1}N). Tukey Kramer least square means and letter differences shown. Means with the same letter are not different. Hybrids marked to indicate whether hybrids tested across two(θ) or three site years.

Hybrids	Ground Reference Agronomic Model (N, %)		Predicted pN from Full PLSR Model at R1 (%)		Ground Reference Agronomic Model (NCE, kg kg^{-1}N)		Predicted NCE from Full PLSR Model at R1 (kg kg^{-1}N)	
DAS01$^{\theta}$	0.97	ABC	0.93	ABC	102.7	ABC	104.3	A
DAS02	0.96	ABC	0.90	ABC	104.4	BCD	109.1	B
DAS03	0.92	BC	0.92	ABC	106.7	DE	105.4	A
DAS04	0.91	BC	0.85	C	109.5	EF	114.0	C
DAS05	0.93	ABC	0.89	BC	105.9	CDE	108.5	B
DAS06$^{\theta}$	1.01	A	0.96	AB	98.8	A	102.6	A
DAS07$^{\theta}$	0.89	C	0.87	BC	111.1	F	114.0	C
DAS08$^{\theta}$	0.94	ABC	0.93	ABC	106.6	CDEF	103.7	A
DAS09	0.97	AB	0.96	A	102.2	AB	104.3	A

4.4.9 Final Discussion

In this study we employed the nearly continuous spectral range inherent to hyperspectral data to study the future predictions of pN, NCE and NIE using PLSR. High spectral resolution provides an enhanced ability to distinguish materials with only subtle differences between them. This enhanced separability appeared useful for complex traits such as the N parameters studied here. An additional benefit to the hyperspectral data and the PLSR technique used in this trial was accurate estimations for pN and NCE even with broadly contrasting environments. An additional strength of the analysis shown here was the ability to accurately estimate pN and NCE from broadly contrasting environments.

One of the disadvantages to PLSR is the requirement for continuous predictors. This prevented inclusion of experimental design factors (e.g. N treatment [low, medium, high] or plot location [pass, range]) in the model which would likely improve predictions. We suggest investigations into models encompassing both reflectance data and agronomic factors. Another avenue is incorporation of grain yield data with the reflectance data of the hyperspectral bands. Grain yield data routinely collected by plot combines are readily available in breeding research. Incorporation of yield data may inform and substantially improve the model predictions, especially those for NIE. However, this would only be applicable to retrospective studies. An alternative for forward-predictive studies is incorporation of weather data into the model (such as GDD or precipitation) to generalize model outputs to wider geographic areas and multiple growing seasons, yet still provide in-season predictions. Another possible avenue for further research is the use of mixed

models with the traditional genotype and environment factors (i.e. hybrid, treatment, etc.) in addition to principle components (PCs) derived from the hyperspectral reflectance data. One caution in this approach is the potential multicollinearity between the PCs and model factors. Finally, since yield to N response in maize is complex and follows a quadratic plus plateau or Gompertz curve as the response, non-linear analysis methods such as support vector machines and kernel PLSR are encouraged for studying the complex interactions inherent to N efficiency research with the goal of accurately predicting the critical N parameters.

Resource limitations of this study impacted consistent testing of all nine hybrids across all three site-years as well as multi-year testing of the same sites. Ideally the pN and biomass would have been sampled throughout the season, especially at all imaging points (V16 and R1), for *all* plots. In addition, supplemental images at R3 and R6 would have allowed a more intense study of the in-situ N remobilization and corresponding spectral measurements. Furthermore, ensuring lower 0N levels at Gorman for a wider N response distribution may have resulted in PLSR models with enhanced predictive abilities. These constraints and the impact on the PLSR models were especially evident for the NIE models which were faced with ground reference data with highly divergent distributions. Therefore, ensuring greater overlap of the response distributions across locations and site-years is imperative. Further studies into the potential of remote sensing for predictions of N use efficiency parameters is highly encouraged in order to facilitate N efficiency advancements through development of new hybrids and a better scientific understanding of the ongoing physiological mechanisms.

4.5 Conclusion

This was the first known attempt to relate in-season canopy level hyperspectral characteristics to final N use efficiency parameters, NCE and NIE, using PLSR. With the PLSR technique all the spectral information gathered from the remote imaging was employed while managing the high dimensionality and multicollinearity inherent to hyperspectral data. This study demonstrated that the blue, red, and NIR (720 – 920 nm) regions of the spectrum were most strongly related to future pN while the blue, green and red regions were found to be strongly related to NCE. Relationships between spectral data and NIE were weaker, though the green and low NIR (720 – 810 nm) regions were most prominent. Stronger correlation differences amongst N treatments were observed

between N parameters and in-season reflectance levels at R1 than V16. PLSR models based on reflectance at V16 and R1 were found to accurately account for the variability in the response (R^2 > 0.65 and CV < 20%) of pN or NCE at R6 for previously unseen data. However, the models developed for NIE predictions had poor fit. Lastly, individual hybrids were more consistently estimated based on the R1 PLSR model for pN and the V16 PLSR model for NCE. Comparison of the PLSR based hybrid differentiation to the ground reference ranking revealed that both pN and NCE models from the R1 images provided accurate designation of the top and bottom hybrids, meeting the goal for efficient selection of genotypes as a screening method in early breeding stages. Therefore, the utility of mid-season PLSR models was evident for accurately predicting the future pN and NCE at R6 in maize hybrids grown at multiple densities in widely varied environments.

Acknowledgements

The authors want to acknowledge all field station support, especially at Gorman and Rominger locations. Financial backing from Dow AgroSciences and Corteva Agriscience is appreciated.

4.6 References

Abendroth, L. J., Elmore, R. W., Boyer, M. J., & Marlay, S. K. (2011). *Corn growth and development*. PMR.

Araus, J. L., & Cairns, J. E. (2014). Field high-throughput phenotyping: the new crop breeding frontier. *Trends Plant Sci*, *19*(1), 52-61. https://doi.org/10.1016/j.tplants.2013.09.008

Bajwa, S., & Kulkarni, S. (2011). Hyperspectral data mining. In P. Thenkabail, J. G. Lyon, & A. Huete (Eds.), *Hyperspectral remote sensing of vegetation and agricultural crops* (pp. 93-137). CRC Press, New York.

Banziger, M., Edmeades, G., Beck, D., & Bellón, M. (2000). Breeding for drought and nitrogen stress tolerance in maize: From theory to practice.

Bioucas-Dias, J. M., Plaza, A., Camps-Valls, G., Scheunders, P., Nasrabadi, N., & Chanussot, J. (2013). Hyperspectral remote sensing data analysis and future challenges. *IEEE Geoscience and Remote Sensing Magazine*, *1*(2), 6-36. https://doi.org/10.1109/mgrs.2013.2244672

Blackmer, T. M., Schepers, J. S., Varvel, G. E., & Walter-Shea, E. A. (1996). Nitrogen deficiency detection using reflected shortwave radiation from irrigated corn canopies. *Agronomy Journal*, *88*(1), 1-5.

Campbell, J. B., & Wynne, R. H. (2011). *Introduction to Remote Sensing*. Guilford Press.

Cassman, K. G., Dobermann, A., & Walters, D. T. (2002). Agroecosystems, nitrogen-use efficiency, and nitrogen management. *AMBIO: A Journal of the Human Environment*, *31*(2), 132-140.

Chen, K., & Vyn, T. J. (2017). Post-silking factor consequences for N efficiency changes over 38 years of commercial maize hybrids. *Front Plant Sci*, *8*, 1737. https://doi.org/10.3389/fpls.2017.01737

Chivasa, W., Mutanga, O., & Biradar, C. (2019). Phenology-based discrimination of maize (Zea mays L.) varieties using multitemporal hyperspectral data. *Journal of Applied Remote Sensing*, *13*(1), 017504.

Ciampitti, I. A., & Vyn, T. J. (2011). A comprehensive study of plant density consequences on nitrogen uptake dynamics of maize plants from vegetative to reproductive stages. *Field Crops Research*, *121*(1), 2-18. https://doi.org/10.1016/j.fcr.2010.10.009

Curran, P. J. (1989). Remote sensing of foliar chemistry. *Remote Sensing of Environment*, *30*(3), 271-278. https://doi.org/10.1016/0034-4257(89)90069-2

Dobermann, A. R. (2005). Nitrogen use efficiency-state of the art. *Agronomy--Faculty Publications*, 316.

Doering, O., Galloway, J., Theis, T., Aneja, V., Boyer, E., Cassman, K., Cowling, E., Dickerson, R., Herz, W., & Hey, D. (2011). Reactive nitrogen in the United States: an analysis of inputs, flows, consequences, and management options. *United States Environmental Protection Agency*.

Duvick, D., Smith, J., & Cooper, M. (2004). Long-term selection in a commercial hybrid maize breeding program. *Plant Breeding Reviews*, *24*(2), 109-152.

Duvick, D. N. (2005). The contribution of breeding to yield advances in maize (Zea mays L.). *Advances in Agronomy*, *86*, 83-145.

Fan, L., Zhao, J., Xu, X., Liang, D., Yang, G., Feng, H., Yang, H., Wang, Y., Chen, G., & Wei, P. (2019). Hyperspectral-based estimation of leaf nitrogen content in corn using optimal selection of multiple spectral variables. *Sensors (Basel)*, *19*(13), 2898. https://doi.org/10.3390/s19132898

FAO. (2017). *The future of food and agriculture : trends and challenges* (9789251095515). http://www.fao.org/3/a-i6583e.pdf

Gausman, H. W. (1977). Reflectance of leaf components. *Remote Sensing of Environment*, *6*(1), 1-9. https://doi.org/https://doi.org/10.1016/0034-4257(77)90015-3

Gausman, H. W., & Allen, W. A. (1973). Optical parameters of leaves of 30 plant species. *Plant Physiology*, *52*(1), 57-62. https://doi.org/10.1104/pp.52.1.57

Gautam, R., & Panigrahi, S. (2007). Leaf nitrogen determination of corn plant using aerial images and artificial neural networks. *Canadian Biosystems Engineering*, *49*, 7.

Goel, P. K., Prasher, S. O., Landry, J. A., Patel, R. M., Viau, A. A., & Miller, J. R. (2003). Estimation of crop biophysical parameters through airborne and field hyperspectral remote sensing. *Transactions of the ASAE*, *46*(4), 1235-1246.

Haegele, J. W., Cook, K. A., Nichols, D. M., & Below, F. E. (2013). Changes in nitrogen use traits associated with genetic improvement for grain yield of maize hybrids released in different decades. *Crop Science*, *53*(4), 1256. https://doi.org/10.2135/cropsci2012.07.0429

Hansen, N. J. S., Plett, D., Berger, B., & Garnett, T. (2018). *Tackling Nitrogen Use Efficiency in Cereal Crops Using High-Throughput Phenotyping*. https://doi.org/10.1007/978-3-319-92958-3_7

Hansen, P. M., & Schjoerring, J. K. (2003). Reflectance measurement of canopy biomass and nitrogen status in wheat crops using normalized difference vegetation indices and partial least squares regression. *Remote Sensing of Environment*, *86*(4), 542-553. https://doi.org/10.1016/s0034-4257(03)00131-7

Hatfield, J. L., Gitelson, A. A., Schepers, J. S., & Walthall, C. L. (2008). Application of spectral remote Ssnsing for agronomic decisions. *Agronomy Journal*, *100*(S3). https://doi.org/10.2134/agronj2006.0370c

Horler, D. N. H., Dockray, M., & Barber, J. (1983). The red edge of plant leaf reflectance. *International Journal of Remote Sensing*, *4*(2), 273-288. https://doi.org/10.1080/01431168308948546

Jin, X., Zarco-Tejada, P., Schmidhalter, U., Reynolds, M. P., Hawkesford, M. J., Varshney, R. K., Yang, T., Nie, C., Li, Z., & Ming, B. (2020). High-throughput estimation of crop traits: A review of ground and aerial phenotyping platforms. *IEEE Geoscience and Remote Sensing Magazine*, 1-33.

Karimi, Y., Prasher, S., Madani, A., & Kim, S. (2008). Application of support vector machine technology for the estimation of crop biophysical parameters using aerial hyperspectral observations. *Canadian Biosystems Engineering*, *50*(7), 13-20.

Kruse, J. K., Christians, N. E., & Chaplin, M. H. (2006). Remote sensing of nitrogen stress in creeping bentgrass. *Agronomy Journal*, *98*(6), 1640-1645.

Lambers, H., Chapin III, F. S., & Pons, T. L. (2008). *Plant Physiological Ecology*. Springer Science & Business Media.

Lassaletta, L., Billen, G., Grizzetti, B., Anglade, J., & Garnier, J. (2014). 50 year trends in nitrogen use efficiency of world cropping systems: the relationship between yield and nitrogen input to cropland. *Environmental Research Letters*, *9*(10), 105011. https://doi.org/10.1088/1748-9326/9/10/105011

Lemaire, G., Plénet, D., & Grindlay, D. (1997). Leaf N content as an indicator of crop N nutrition status. In G. Lemaire (Ed.), *Diagnosis of the Nitrogen Status in Crops* (pp. 189-199). Springer Berlin Heidelberg. https://doi.org/10.1007/978-3-642-60684-7_11

Li, F., Miao, Y., Feng, G., Yuan, F., Yue, S., Gao, X., Liu, Y., Liu, B., Ustin, S. L., & Chen, X. (2014). Improving estimation of summer maize nitrogen status with red edge-based spectral vegetation indices. *Field Crops Research*, *157*, 111-123. https://doi.org/10.1016/j.fcr.2013.12.018

Lillesand, T., Kiefer, R. W., & Chipman, J. (2014). *Remote sensing and image interpretation*. John Wiley & Sons.

Ma, D., Maki, H., Neeno, S., Zhang, L., Wang, L., & Jin, J. (2020). Application of non-linear partial least squares analysis on prediction of biomass of maize plants using hyperspectral images. *Biosystems Engineering*, *200*, 40-54. https://doi.org/https://doi.org/10.1016/j.biosystemseng.2020.09.002

Meacham-Hensold, K., Montes, C. M., Wu, J., Guan, K., Fu, P., Ainsworth, E. A., Pederson, T., Moore, C. E., Brown, K. L., Raines, C., & Bernacchi, C. J. (2019). High-throughput field phenotyping using hyperspectral reflectance and partial least squares regression (PLSR) reveals genetic modifications to photosynthetic capacity. *Remote Sensing of Environment*, *231*, 111176. https://doi.org/https://doi.org/10.1016/j.rse.2019.04.029

Moll, R. H., Kamprath, E. J., & Jackson, W. A. (1982). Analysis and interpretation of factors which contribute to efficiency of nitrogen utilization. *Agronomy Journal*, *74*, 562-564. https://doi.org/10.2134/agronj1982.00021962007400030037x

Mueller, S. M., Messina, C. D., & Vyn, T. J. (2019). Simultaneous gains in grain yield and nitrogen efficiency over 70 years of maize genetic improvement. *Sci Rep*, *9*(1), 1-8.

Muñoz-Huerta, R. F., Guevara-Gonzalez, R. G., Contreras-Medina, L. M., Torres-Pacheco, I., Prado-Olivarez, J., & Ocampo-Velazquez, R. V. (2013). A review of methods for sensing the nitrogen status in plants: advantages, disadvantages and recent advances. *Sensors*, *13*(8), 10823-10843. https://doi.org/10.3390/s130810823

Nigon, T. J., Yang, C., Dias Paiao, G., Mulla, D. J., Knight, J. F., & Fernández, F. G. (2020). Prediction of early season nitrogen uptake in maize using high-resolution aerial hyperspectral imagery. *Remote Sensing*, *12*(8), 1234.

Ollinger, S. V. (2011). Sources of variability in canopy reflectance and the convergent properties of plants. *New Phytologist*, *189*(2), 375-394.

Osborne, S. L., Schepers, J. S., Francis, D. D., & Schlemmer, M. R. (2002a). Detection of phosphorus and nitrogen deficiencies in corn using spectral radiance measurements. *Agronomy Journal*, *94*(6), 1215-1221.

Osborne, S. L., Schepers, J. S., Francis, D. D., & Schlemmer, M. R. (2002b). Use of spectral radiance to estimate in-season biomass and grain yield in nitrogen- and water- stressed corn. *Crop Science*, *42*(1), 165-171.

Peterson, H., Williams, M., Frankenberger, J., King, K., McGrath, J., Moody, L., Ribaudo, M., Strock, J., Johnson, K., & Nelson, N. (2019). Reducing the impacts of agricultural nutrients on

water quality across a changing landscape. *Issue Paper-Council for Agricultural Science and Technology* (64).

Pimstein, A., Karnieli, A., & Bonfil, D. J. (2007). Wheat and maize monitoring based on ground spectral measurements and multivariate data analysis. *Journal of Applied Remote Sensing*, *1*(1), 013530-0135316. https://doi.org/10.1117/1.2784799

Plénet, D., & Lemaire, G. (2000). Relationships between dynamics of nitrogen uptake and dry matter accumulation in maize crops. Determination of critical N concentration. *Plant and Soil*, *216*(1-2), 65-82.

Quemada, M., Gabriel, J., & Zarco-Tejada, P. (2014). Airborne hyperspectral images and ground-level optical sensors as assessment tools for maize nitrogen fertilization. *Remote Sensing*, *6*(4), 2940-2962. https://doi.org/10.3390/rs6042940

Sadras, V. O., & Calderini, D. F. (2015). *Crop physiology: Applications for genetic improvement and agronomy* (V. O. Sadras & D. F. Calderini, Eds. 2nd ed.). Academic Press.

Sahoo, R. N., Ray, S. S., & Manjunath, K. R. (2015). Hyperspectral remote sensing of agriculture. *Current Science*, *108*(5), 848-859. http://search.ebscohost.com/login.aspx?direct=true&db=aph&AN=101659167&site=ehost-live

Salvagiotti, F., Castellarín, J. M., Miralles, D. J., & Pedrol, H. M. (2009). Sulfur fertilization improves nitrogen use efficiency in wheat by increasing nitrogen uptake. *Field Crops Research*, *113*(2), 170-177. https://doi.org/10.1016/j.fcr.2009.05.003

SAS Institute Inc. (2013). The PLS Procedure. In *SAS/STAT 13.1 User's Guide* (pp. 6247-6304). SAS Institute Inc.

Sawatsky, M. L., Clyde, M., & Meek, F. (2015). Partial least squares regression in the social sciences. *The Quantitative Methods for Psychology*, *11*(2), 52-62.

Schlemmer, M., Gitelson, A., Schepers, J., Ferguson, R., Peng, Y., Shanahan, J., & Rundquist, D. (2013). Remote estimation of nitrogen and chlorophyll contents in maize at leaf and canopy levels. *International Journal of Applied Earth Observation and Geoinformation*, *25*, 47-54. https://doi.org/10.1016/j.jag.2013.04.003

Shanahan, J. F., Schepers, J. S., Francis, D. D., Varvel, G. E., Wilhelm, W. W., Tringe, J. M., Schlemmer, M. R., & Major, D. J. (2001). Use of remote-sensing imagery to estimate corn grain yield. *Agronomy Journal*, *93*(3), 583-589.

Smil, V. (2001). *Enriching the earth: Fritz Haber, Carl Bosch, and the transformation of world food production*. MIT press.

SWRCB. (2017). *Nitrate Groundwater Information Sheet*.

SWRCB. (2020). *Nitrate Impacted Wells*. State of California. Retrieved 11/7/2020 from https://gispublic.waterboards.ca.gov/portal/apps/MapSeries/index.html?appid=a884c5cc81844b289b666f15fad3dc7d

Thenkabail, P. S., Gumma, M. K., Teluguntla, P., & Mohammed, I. A. (2014). Hyperspectral remote sensing of vegetation and agricultural crops. *Photogrammetric Engineering & Remote Sensing (PE&RS), 80*(8), 697-723.

Thenkabail, P. S., Smith, R. B., & De Pauw, E. (2000). Hyperspectral vegetation indices and their relationships with agricultural crop characteristics. *Remote Sensing of Environment, 71*(2), 158-182.

Tobias, R. D. (1995). An introduction to partial least squares regression. Proceedings of the twentieth annual SAS users group international conference,

Umetrics. (1995). *Multivariate Analysis* Winchester, MA, Umetrics.

Uno, Y., Prasher, S. O., Lacroix, R., Goel, P. K., Karimi, Y., Viau, A., & Patel, R. M. (2005). Artificial neural networks to predict corn yield from Compact Airborne Spectrographic Imager data. *Computers and Electronics in Agriculture*, *47*(2), 149-161. https://doi.org/10.1016/j.compag.2004.11.014

Walburg, G., Bauer, M. E., Daughtry, C., & Housley, T. (1982). Effects of nitrogen nutrition on the growth, yield, and reflectance characteristics of corn canopies. *Agronomy Journal*, *74*(4), 677-683.

Wen, P.-F., Wang, R., Shi, Z.-J., Ning, F., Wang, S.-L., Zhang, Y.-J., Zhang, Y.-H., Wang, Q., & Li, J. (2018). Effects of N application rate on N remobilization and accumulation in maize (Zea mays L.) and estimating of vegetative N remobilization using hyperspectral measurements. *Computers and Electronics in Agriculture*, *152*, 166-181.

Wold, H. (1966). Estimation of principal components and related models by iterative least squares. *Multivariate analysis*, 391-420.

Wold, S. (1994). PLS for multivariate linear modeling. . In H. van de Waterbeernd (Ed.), *QSAR: chemometric methods in molecular design methods and principles in medicinal chemistry* (pp. 195-218). Verlag-Chemie.

Wold, S., Sjöström, M., & Eriksson, L. (2001). PLS-regression: a basic tool of chemometrics. *Chemometrics and intelligent laboratory systems*, *58*(2), 109-130.

Yendrek, C. R., Tomaz, T., Montes, C. M., Cao, Y., Morse, A. M., Brown, P. J., McIntyre, L. M., Leakey, A. D., & Ainsworth, E. A. (2017). High-throughput phenotyping of maize leaf physiological and biochemical traits using hyperspectral reflectance. *Plant Physiol*, *173*(1), 614-626. https://doi.org/10.1104/pp.16.01447

Yolo County Flood Control and Water Conservation District. (2012). *Regional Conjunctive Use Enhancement: Nitrate Fingerprinting and Groundwater Age Determination Study*.

Zhao, D., Raja Reddy, K., Kakani, V. G., Read, J. J., & Carter, G. A. (2003). Corn (Zea mays L.) growth, leaf pigment concentration, photosynthesis and leaf hyperspectral reflectance properties as affected by nitrogen supply. *Plant and Soil*, *257*(1), 205-218. https://doi.org/10.1023/a:1026233732507

Zhou, K., Cheng, T., Zhu, Y., Cao, W., Ustin, S. L., Zheng, H., Yao, X., & Tian, Y. (2018). Assessing the impact of spatial resolution on the estimation of leaf nitrogen concentration over the full season of paddy rice using near-surface imaging spectroscopy data. *Frontiers in Plant Science*, *9*, 964-964. https://doi.org/10.3389/fpls.2018.00964

CHAPTER 5. GENERAL DISCUSSION

5.1 Research Summary and Contributions to Science

The overall focus of this research was estimation or prediction of nitrogen use efficiency (NUE) in maize through non-traditional methods. Traditional NUE parameters are dependent on field collection and subsequent laboratory sampling which are very time and labor intensive. Chapter 1 of this research consisted of an overview of current literature with a focus on remote sensing specific to maize and detection of various physiological components such as biomass, leaf chlorophyll, whole-plant N content, and grain yield. Because the imaging conducted in this research was hyperspectral, the literature review emphasized two methods used to cope with the large dimensionality of such data: hyperspectral vegetation indices (HSI) and partial least squares regression (PLSR). Chapter 2 focused on Nitrogen Internal Efficiency (NIE) measurement of nearly 300 genotypes and various surrogate techniques for detection of this N parameter with a single low N rate at one location. Chapter 3 focused on end-season (R6) prediction of N concentration, Nitrogen Conversion Efficiency (NCE) and NIE with HSI from mid-season images using a smaller set of 9 hybrids grown at three N rates in three site-years. Chapter 4 subsequently applied PLSR techniques for feature extraction (400 – 900 nm) of the same images taken at V16 or R1 for prediction of the aforementioned N parameters for the same set of 9 hybrids.

The focus of Chapter 2 was evaluating the NIE (grain yield per unit of accumulated plant N) of hundreds of genotypes. Additionally, an investigation was conducted into comparisons of in-season field-based physiological measurements or remote sensing as surrogate measurements for evaluating N metrics such as total plant N at R6 or final NIE. The intense assessment of the numerous hybrids was successful in determining the top 10 and bottom 10 hybrids for each maturity group (early and late) in both NIE or grain yield. However, high levels of variance resulted in only a few hybrids being significantly different from each other. Interestingly, five hybrids (DAS039, DAS026, DAS136, DAS130, and DAS131) appeared as top performers for both NIE and yield. This discovery points to the genetic potential present in maize for improving N efficiency through breeding.

The investigation into secondary traits (plant height, stalk diameter, LAI, green leaf counts, and SPAD measurements) as a substitute for field measurement showed that only leaf SPAD (at R1 and R2/3) was strongly correlated to grain yield or total plant N at R6. No in-field measurements were found to be strongly related to NIE for use as a surrogate. Similarly, the attempt to use vegetation indices (NDVI and SR) from aerial imagery at R1 and R3/4 for prediction of grain yield or total plant N was unsuccessful. However, the aerial imagery results are likely due to calibration and pre-processing limitations which negatively affected the data quality rather than the indices themselves (Chapter 2).

In Chapter 3 the focus of the research was on imaging for prediction of agronomic parameters related to N use efficiency. High quality hyperspectral imaging by manned aircraft and UAVs was obtained of maize hybrids grown under N stress conditions over three site-years. Subsequently, 20 HSI were extracted from each in-season image (at V16/V18 and R1/R2) to predict the end season (R6) N parameters of NCE and NIE. Both parameters are measures of the plant's ability to produce biomass or grain yield for each unit of N taken up, respectively.

Analysis of the 40 HSI using mixed models showed that two indices, $HBSI1_{682,855}$ and $HBS2_{682,910}$, were predictive of NCE, and two indices, $HBCI8_{515,550}$ and $HBCI9_{490,550}$ were predictive of NIE for actual data collected at R6 from nine hybrids at multiple N rates. With the HSI models, the greatest prediction accuracy was achieved for NIE. However, statistical differentiation of hybrids for both NCE and NIE was possible based on the HSI models. The indices predictive of NCE were NIR:red indices developed for studying structural plant components. Those predictive of NIE were indices based on the green or green:blue portions of the spectrum initially established for studying biochemical plant components. These portions of the electromagnetic spectrum are closely related to the absorbance and reflectance characteristics of plant pigments, such as carotenoids and chlorophyll, which might explain the relationship discovered between these HSI and the N parameters.

Our findings were quite novel because none of these indices have been previously studied for prediction of future N efficiency parameters. Additionally, the ability to predict end season parameters based off in-season imaging was unexpected due to the prevalence of literature showing greater accuracy in model predictions with short timeframe between imaging and field

collection. Remarkable, too, was the accuracy of the NIE predictions since the imaging was conducted prior to any substantial grain formation.

The final portion of Chapter 3 focused on the resampling of the 2017 images and its effect on the conclusions from the data. In this step, the spatial resolution of the images was decreased from 4 cm to 50 cm resulting in loss of fine detail. Resampling of the high resolution images led to higher index values which were significantly different from the lower resolution index values. The hybrid rankings for NCE or NIE were not affected significantly by the spatial resolution change. However, the hybrid rankings were not accurately predicted from the imaging with either high or low resolution. This conflicting result is likely due to the smaller dataset used in the analysis. It indicates further investigation into this research question is needed.

Chapter 4 continued the investigations of the hyperspectral images captured in 2014 and 2017. In this analysis we studied the use of PLSR models for prediction of end-season N concentration (pN), NCE, and NIE. This statistical method can handle multi-correlated data by projecting the predicted and observed variables to a new latent space. PLSR models for unseen test data resulted in accurate predictions for pN and NCE at R6 for both imaging times. Neither timepoint resulted in accurate predictions for NIE. Additionally, the PLSR models based on the R1 images accurately distinguished the top and bottom hybrids for pN and NCE.

5.2 Implications for Agriculture

The findings from these investigations can contribute to agriculture in multiple manners. Firstly, the discovery of 5 hybrids having both top grain yields and NIE exposes the potential in maize genetics for breeding improvement for NUE. Not only does this discovery urge initiation of breeding efforts with these hybrids, but it also spurs future investigations into the genetic variability for N efficiency of other available maize germplasm. It also suggests that physiological investigations into these hybrids may be useful to determine what mechanisms resulted in the combination of high grain yields and the high NIE.

The most positive impact on agriculture from this research was the identification of the four HSIs gathered in-season which were predictive of final NCE or NIE. None of these HSIs have been previously correlated to either of these N parameters. The utility of the PLSR models for

accurately predicting pN or NCE also holds immense potential. Confirmation of these HSIs and PLSR models with other locations, genotypes, and remote sensing platforms would provide an in-season method to accurately predict end-season N efficiency parameters. Specifically, the HSIs are convenient to use since the index calculations only require imaging data from a few spectral bands. Thus, the targeted HSI approaches are easy to implement in terms of cost, availability of technological equipment, and technical expertise.

These discoveries have high potential for practical application in an early stage breeding program in which hundreds or thousands of hybrids are evaluated. The HSIs or PLSR models could be used for early identification of the best and worst hybrids providing a data-based decision for culling or selecting specific genotypes. As an example, hybrids with low pN levels could be identified using PLSR models in order to remove them from the breeding pool thus selecting for high N hybrids. At the next stage, HSI for predicting NCE or NIE could be used to identify the poor performing hybrids, again allowing a focus of efforts on the more N efficient hybrids. Savings would be achieved in both in-season and end-season sampling as well as for breeding resources in the next growing season. N research is very labor intensive thus difficult to implement regularly into a breeding program. Consequently, our findings could facilitate N research and enhance the potential for significant advancements in the development of N efficient maize hybrids positively impacting N use in agriculture.

Spatial resolution is an important consideration in remote sensing since higher resolution provides greater image detail, but also results in dramatically greater processing times due to higher image complexity. The results documented in Chapters 3 and 4 demonstrated the utility of low resolution (50 cm) data for predicting N parameters. However, our direct assessment into the effect of downgrading the data provided conflicting results and an inability to accurately rank hybrids equivalent to measured data. Greater clarity on spatial resolution is needed and should prove useful in designing future imaging research.

5.3 Limitations of Research

In any research effort, manpower, time, and money, must always be balanced with the perfect experimental design necessary for addressing project goals. The large number of hybrids evaluated in Chapter 2 led to the decision to use only one N rate in that experiment. It also led to

limitations on plant sampling and N measurements. Only the critical end-of-season sampling time points were possible. These decisions limited the potential conclusions attained from this study. Multiple N rates and biomass and nutrient content sampling throughout the season would have provided an understanding of the N uptake, remobilization, and utility of a broad genetic pool. In addition, the lack of 0N treatment in this experiment resulted in the inability to normalize results to actual soil N levels which can fluctuate depending on environmental conditions and agronomic management.

Large amounts of variance were evident in our NIE analysis of the nearly 300 hybrids. This variance resulted in the inability to statistically differentiate many of the hybrids from one another. Methods to minimize variance include using fields dedicated to low N research managed agronomically to limit and control N. An example of such agronomic management is the planting of non-leguminous crops the previous year and removing all stover immediately after harvest. If maize or other cereal crops had been grown previously, our experiment may have experienced lower mineralized N.

The imaging research for Chapter 2 was limited by several factors and could be improved using ground control points and reference panels for calibration of the equipment and subsequent data. During the spectral pre-processing each band was normalized individually for brightness to maximize the visual quality of each image. Though this provided greater visual contrast it also skewed the pixel values possibly distorting the index calculations based on those pixel values. This may be a reason imaging results were in apparent opposition to the field collected data. Appropriate imaging methodology for equipment calibration and pre and post processing of data have large impacts on the quality. These recommended changes are likely to significantly improve the imaging data and subsequent conclusions.

Finally, due to time limitations the N parameter of NCE was not analyzed for the 285 hybrids evaluated in Chapter 2. Exploration and analysis into the relationship between NIE and NCE of these hybrids, as well as the individual yield components (kernel weight and number) is recommended. Such study may provide further understanding into the overall N use efficiency of these hybrids.

The general design of the experiment used for Chapters 3 and 4 included 3 site-years (2 locations in CA in 2014 and 1 location in IN in 2017) with different imaging platforms each year. The lack of replication of sites across years due to a lack of resources resulted in several confounding factors in both the physiological and imaging components. These effects left many unanswered questions and complicated analysis. A potential consequence on the imaging data in Chapter 3 was the low amount of overlap in HSI distribution and large differences in scale for some HSI. In such cases Simpson's paradox was often observed, resulting in reversal or disappearance of trends depending on how data were grouped (by or across location). Replication of locations would have removed this as a confounding factor. Other limitations in the experimental design were that in 2017 only 5 of the original 9 hybrids were grown due to a lack of seed availability. This led to a loss of power and an unbalanced design complicating statistical analysis.

This research focused on detection of maize response to N stress through imaging. However, in 2014 soil N tests only measured NO_3^- levels and not NH_4^+ levels. Plants use both forms of N from soil for growth (Connor et al., 2011). Additional soil sampling at the beginning of the season would have provided greater detail of the pre-plant N status. Furthermore, in-season soil testing and N testing of irrigation and rain water was not conducted at any location. These would have provided a better understanding of the N dynamics in this research – especially the poor N response at Gorman which potentially impacted the results in Chapter 4.

Imaging in 2017 was conducted throughout the season (V5, V8, V16/17, R1, R3/4, R5, and R5/6), but in 2014 only two time points (V18 and R1/2) were captured due to resourcing constraints. Such limitation restricted our ability to obtain a more complete picture of the maize response throughout the growing season. Imaging later in the season may have shown a greater contrast between the low and high N treatments as N stress intensifies over the growing season. Imaging during mid-grain fill is recommended as large genetic differences in leaf senescence may assist in N efficiency predictions. With such data other HSI or PLSR models may be found to be (more) predictive of the N parameters.

The 2014 images were collected from a plane and thus had lower spatial resolution than those collected from a drone in 2017. This difference in resolution was compensated for by resampling the 2017 images. However, the analysis showed that the change in resolution had a statistical

effect on the index values, though not specifically on the hybrid rankings. Because the analysis could only be conducted on the higher resolution data, this conclusion was reached based on only 1/3 of the entire data set. If there had been resourcing for higher spatial resolution imaging in 2014, we would have a clearer picture of the effect of resolution difference on hybrid rankings.

All remote imaging of vegetation must manage the interference of soil pixels. In Chapter 3 the soil pixels were removed through thresholding. Drawbacks to this method were observed later in the growing season as the index values of the stressed plants resembled those of soil. In Chapter 4 soil pixels were removed based on supervised classification using a kernel-based support vector machine. This resulted in a more granular assessment of soil pixels. However, in general the lower spatial resolution from 2014 resulted in more mixed pixels in the analysis (pixels containing both soil and vegetation) regardless of soil pixel removal method. Higher spatial resolution in 2014 would have resulted in images with more clearly separated plots, avoidance of alleyways and plot edges, and greater ability to bypass in-season plant sampling areas. Higher spatial resolution would have also impacted in-field experiment design by necessitating 4-row plots (instead of 6 rows) thus requiring less land.

Mixed linear models were used to analyze the ability of HSI to predict the N parameters in Chapter 3. However, constant variance of the residuals is a critical statistical assumption many HSI did not meet even upon transformation of the data. Use of non-linear mixed models could have complemented our results potentially allowing analysis of a greater number of HSI.

Along the same vein of statistical analysis, the HSI models studied in Chapter 3 included no agronomic effects such as N rate or plant density. Inclusion of such factors may have improved predictions due to the large amount of experiment information in these factors. However, in our case this led to errors in the statistical analysis due to the multicollinearity between the HSI and these agronomic elements. In Chapter 4, the method chosen for analysis of the imaging data, PLSR, is uniquely suited to analysis of multicollinear data. Unfortunately, such agronomic features were not included in the analysis of Chapter 4 because PLSR requires continuous factors as predictors.

5.4 Future Research Suggestions

In Chapter 2, we identified 5 top performing hybrids in both yield and NIE. Additionally, the 285 hybrids were sorted into the top and bottom 10 hybrids for each maturity group. Future investigations are recommended using the top and bottom hybrids to better determine the NUE potential of these specific genotypes under lower and higher N rates. The ideal hybrid yields well under low N conditions yet is capable of increasing yields considerably under high N conditions. Only research at multiple N rates can reveal those characteristics. Additionally, including a 0N control allows analysis of NRE (plant N per unit fertilizer N), an important N uptake measure. Before a plant can utilize N efficiently it must be capable of sufficient N uptake. Future in-depth inquiries should focus on investigating the physiological differences and N uptake and remobilization patterns throughout the growing season of the 40 hybrids identified in this research in order to realize the goal of maximizing yield while minimizing surplus N used.

Under limited funding however, the focus should be on a limited number of top hybrids for yield and NIE. This may be a rare event. As a result, the goal of such research would be to understand what physiological characteristics and mechanisms are unique about these hybrids which produce high yields and efficient N use. Based on the statistical importance of location identified here we recommend these studies be conducted at multiple (3+) locations.

Due to the extremely accurate predictions of NIE and NCE from the identified models (i.e. biochemical HSIs or PLSR, respectively) we encourage confirmation of these results at additional locations and various genotypes. This would provide a better understanding of these methods' utility for predicting hybrid rankings in N efficiency research across a variety of environments. For practical application, methods must be robust enough for accurate predictions across genotypes and locations.

Furthermore, future remote imaging should consist of additional time-points, not just at R1 and R3/R4 as investigated in Chapter 2 or at V16/V18 and R1/R2 as studied in Chapters 3 and 4. Obtaining both earlier and later images during the growing season would provide greater ability to monitor relative maize hybrid development and response to N stress.

The relationship between leaf SPAD, Total N at R6, and NIE should be examined further by gathering additional leaf SPAD time points or leaf positions. These may optimize the SPAD measurements to allow for use as a surrogate measurement for accurate NIE rankings.

The strong link between SPAD at R1 or R2/R3 to Total N suggests that further analysis should be conducted into NIE and vegetation indices containing bands in those regions. Indices focused on NIR:R are many; these include MSAVI, OSAVI and a multitude of SR indices. However, additional support for expanded research on bands in those regions are the findings from Chapter 3. Due to the importance of NIR:R indices for NCE prediction and G:G or G:B indices for NIE we suggest investigation of other similar indices. Many NIR:R indices exist such as $PSSR_a$ or $PSSR_b$ (Blackburn, 1998) or NLI (Goel & Qin, 1994). We did not investigate multiple lower range HSI although many have been developed such as variations of Photochemical Reflectance Index ($PRI_{528,587}$ or $PRI_{531,570}$) or Blue Green Pigment Index ($BGI_{450,550}$)) (Gamon et al., 1990; Gamon et al., 1992; Metternicht, 2003; Peñuelas et al., 1995; Zarco-Tejada et al., 2005).

The spatial resolution analysis in Chapter 3 was made on a subset of the data; thus, we suggest additional research into this aspect of imaging. High resolution imaging has its own data handling complexities. Such imaging can always be resampled and the spatial resolution degraded to allow for this analysis. Low resolution imaging cannot be increased.

During our analysis in Chapter 3 it was noted that many HSI models had to be castoff because the data did not fit the statistical assumptions of linear regression thus rendering any interpretation of those models invalid. Similarly, in Chapter 4 analysis complexities were encountered due to the non-linear response of the N parameters being studied. We advise exploration of other statistical methods such as principle component analysis or non-linear PLSR analysis to determine whether those methods provide better estimation of NCE and NIE than the linear HSI mixed models or linear PLSR investigated here.

Finally, in Chapter 4 we found that PLSR predictions for NCE were much more accurate than those for NIE. To further inform these models, we suggest including grain yield as an additional continuous predictor with the hyperspectral bands. This variable is always and easily field collected in maize breeding research; thus it poses no additional burden. Though this method would not improve in-season model predictions it is possible that it would allow easy culling of

the poorest hybrids saving breeding resources for the next growing season. Prediction improvements may also be gained through the inclusion of weather data (e.g. precipitation or GDD) into the models. Such data may generalize the models to geographic area providing better predictions across localities.

5.5 References

Blackburn, G. A. (1998). Quantifying Chlorophylls and Caroteniods at Leaf and Canopy Scales: An Evaluation of Some Hyperspectral Approaches. *Remote Sensing of Environment*, *66*(3), 273-285. https://doi.org/10.1016/S0034-4257(98)00059-5

Connor, D. J., Loomis, R. S., & Cassman, K. G. (2011). *Crop Ecology: Productivity and Management in Agricultural Systems*. Cambridge University Press.

Gamon, J., Field, C., Bilger, W., Björkman, O., Fredeen, A., & Peñuelas, J. (1990). Remote Sensing of the Xanthophyll Cycle and Chlorophyll Fluorescence in Sunflower Leaves and Canopies. *Oecologia*, *85*(1), 1-7.

Gamon, J. A., Peñuelas, J., & Field, C. B. (1992). A Narrow-Waveband Spectral Index That Tracks Diurnal Changes in Photosynthetic Efficiency. *Remote Sensing of Environment*, *41*(1), 35-44. https://doi.org/https://doi.org/10.1016/0034-4257(92)90059-S

Goel, N. S., & Qin, W. (1994). Influences of Canopy Architecture on Relationships between Various Vegetation Indices and Lai and Fpar: A Computer Simulation. *Remote Sensing Reviews*, *10*(4), 309-347. https://doi.org/10.1080/02757259409532252

Metternicht, G. (2003). Vegetation Indices Derived from High-Resolution Airborne Videography for Precision Crop Management. *International Journal of Remote Sensing*, *24*(14), 2855-2877.

Peñuelas, J., Peck, E. A., Fillela, I., & Gamon, J. A. (1995). Assessment of Photosynthetic Radiation-Use Efficiency with Spectral Reflectance. *New Phytologist*, *131*(3), 291-296. https://doi.org/10.1111/j.1469-8137.1995.tb03064.x

Zarco-Tejada, P. J., Berjón, A., López-Lozano, R., Miller, J. R., Martín, P., Cachorro, V., González, M., & De Frutos, A. (2005). Assessing Vineyard Condition with Hyperspectral Indices: Leaf and Canopy Reflectance Simulation in a Row-Structured Discontinuous Canopy. *Remote Sensing of Environment*, *99*(3), 271-287.